THE ROLE OF NUTRITIONAL VIRULENCE IN *FRANCISELLA TULARENSIS* PATHOGENESIS

Shaun Steele

A dissertation submitted to the faculty at the University of North Carolina at Chapel Hill in partial fulfillment of the requirements for the degree of Doctor of Philosophy in the department of Microbiology and Immunology in the School of Medicine.

Chapel Hill
2015

Approved by:

Tom Kawula

Nathaniel Moorman

William Goldman

Ed Miao

Miriam Braunstein

ABSTRACT

Shaun Steele: The Role of Nutritional Virulence in *Francisella tularensis* Pathogenesis
(Under the direction of Thomas Kawula)

Intracellular pathogens and infected host cells compete with each other for survival and limited resources, such as nutrients. To limit infections, host cells have evolved a multitude of overlapping innate defense mechanisms; but, intracellular pathogens evade or exploit these defenses to replicate within cells. The bacterial pathogen *Francisella tularensis* manipulates several host defense mechanisms to proliferate within cells. *F. tularensis* replicates to extremely high densities within host cells and transfers to uninfected cells without inducing significant host cell death. The efficiency of *F. tularensis* intracellular replication and spread raises two fundamental questions that form the core of my dissertation work: how does *F. tularensis* acquire enough nutrients from the host cell to sustain rapid proliferation and how does *F. tularensis* infect new cells while maintaining the viability of infected host cells? Here I show that *F. tularensis* exploits novel host defense mechanisms to acquire intracellular nutrients and to transfer between cells. *F. tularensis* harvests autophagy-derived amino acids from the host to sustain rapid intracellular proliferation. These amino acids are used by *F. tularensis* to build proteins and as a carbon source to build other molecules, such as nucleic acids. Additionally, I found that *F. tularensis* transfers to macrophages when the macrophage ingests a portion of cytosol from a live, infected neighboring cell, a process that we have termed metadosis. My dissertation work contributed to our understanding of how pathogens interact with host cells. My work on autophagy helped to lay the groundwork for a paradigm of ‘nutritional virulence’ and

my work has translated well in other intracellular pathogens. I anticipate that my work on metadosis will lay the foundation for future studies on how bacteria spread within the host and how antigen presenting cells acquire antigen to interact with the adaptive immune system.

ACKNOWLEDGEMENTS

My research has only been possible through the contributions of dozens of people who have mentored, assisted, and guided me. Tom and Jeff have been the greatest contributors to my research career. In addition to all of their scientific mentorship, I would not have been successful without the confidence and independence they instilled in me.

Jason, Sharon and Cheryl have helped me develop and filter my research for years. In addition to working with me on experiments, they have been instrumental in helping me develop and shape my research. Our impromptu lab meetings that led to many of my experiments were inspired by or came directly from them.

Finally, I don't know where I would be without Lydia. There is nobody I trust more to work side by side with. We have always worked in sync; teaching each other, helping design experiments and finishing projects together. I would not have been comfortable venturing so far from my lab's expertise without her knowledge.

TABLE OF CONTENTS

LIST OF TABLES

LIST OF FIGURES

LIST OF ABBREVIATIONS

AIM2	Absent in Melanoma 2
AMP	Adenosine monophosphate
AMPK	AMP-activated protein kinase
APC	Antigen presenting cell
ATP	Adenosine triphosphate
EBV	Epstein Barr Virus
FACS	Fluorescence activated cell sorting
FCV	*Francisella* containing vacuole
FDA	Food and Drug Administration
FPI	*Francisella* pathogenicity island
GAS	Group A *Streptococcus*
GFP	Green Fluorescent protein
ggt	gamma-glutamyl transpeptidase
GSH	Glutathione
HBV	Hepatitis B virus
HCMV	Human cytomegalovirus
HCV	Hepatitis C virus
hMDM	Human monocyte derived macrophage
HIV	Human immunodeficiency virus
HSV	Herpes Simplex Virus
IFNγ	Interferon gamma
IL-12	Interleukin-12

IL-18	Interleukin-18
IL-1B	Interleukin-1β
IL-6	Interleukin-6
IRES	Internal ribosome entry site
J774	J774A.1 macrophage-like cell
KSHV	Kaposis sarcoma herpesvirus
LC3	Microtubule associated light chain 3
LPS	Lipopolysaccharide
Lux	Luciferase
LVS	Live vaccine strain
mBMDM	Mouse bone marrow derived macrophages
MEF	Mouse embryonic fibroblasts
MHC-I	Major histocompatibility complex- I
MHC-II	Major histocompatibility complex- II
MOI	Multiplicity of infection
mRNA	Messenger ribonucleic acid
mTOR	Mammalian target of rapamycin
NLR	Nucleotide-binding domain, leucine-rich repeat containing proteins
PI3K	Phosphoinositide-3-kinase
PolyI:C	Polyinosinic: polycytidylic acid
RVFV	Rift Valley Fever virus
SD	Standard deviation
SEM	Standard error of the mean

SV40	Simian virus 40
T6SS	Type VI secretion system
TCA	Trichloroacetic acid
TEM	Transmission electron microscopy
TGF-B	Transforming growth factor B
Th	T helper
TLR	Toll like receptor
U112	Utah 112
UPR	Unfolded protein response

CHAPTER 1: INTRODUCTION

Intracellular pathogens and infected host cells compete with each other for survival and limited resources, such as nutrients. To limit infections, host cells have evolved a multitude of overlapping innate defense mechanisms; but, intracellular pathogens evade these defenses to replicate within cells. In many instances, microbes even co-opt host innate immune defenses to enhance microbial survival or replication. For example, host immune cells ingest microbes via phagocytosis. Phagocytosis destroys the vast majority of ingested microbes; however, intracellular bacterial pathogens must overcome phagocytosis to proliferate within cells. The strategies to nullify phagocytosis vary between different bacterial pathogens but generally they either escape from the phagosome to enter the cell cytosol or co-opt the phagosome to form a replicative niche. By modifying the phagosome, certain bacterial pathogens incorporate an anti-microbial host defense into a crucial step in their intracellular replication and virulence within the host. Manipulating host defenses to benefit the pathogen is a recurrent theme in pathogenesis. As a result, intracellular bacteria are frequently used as a tool to characterize many different host immune and cell biology pathways. My dissertation work focused on identifying and characterizing host anti-microbial pathways that bacterial pathogens exploit to enhance intracellular survival or replication.

For my dissertation work, I used the model organism *Francisella tularensis*. *F. tularensis* is a Gram-negative, facultative intracellular bacterium and the causative agent of the disease tularemia. *F. tularensis* is primarily an intracellular pathogen and may be undergoing genome

decay to become an obligate intracellular pathogen [1]. *F. tularensis* replicates within virtually every cell type tested, but macrophages are the major replicative niche [2]. *F. tularensis* is an excellent model organism for characterizing host-pathogen interactions because it is a 'stealth pathogen' that replicates to high densities in the cytosol without eliciting a substantial host response. Cells infected with dozens or hundreds of *F. tularensis* bacteria will even undergo cell division at the same rate as uninfected cells (unpublished data). Despite inhibiting cell death, *F. tularensis* rapidly disseminates to new cells at the site of infection and systemically [2-4]. Moreover, *F. tularensis* replicates quickly within cells, often 100 to 1000-fold within 24 hours [5]. In comparison, most intracellular pathogens, such as *Listeria monocytogenes* and *Salmonella typhimurium,* replicate approximately 10-fold within cells [6,7]. The efficiency of *F. tularensis* intracellular replication and spread raises two fundamental questions that formed the core of my dissertation work: how does *F. tularensis* acquire enough nutrients from the host cell to sustain rapid proliferation and how does *F. tularensis* infect new cells despite inhibiting cell death?

F. tularensis **Cytosolic Replication**

F. tularensis replicates extremely rapidly and to high densities inside the host cell cytosol. *F. tularensis* even has a faster doubling time in macrophages than in Chamberlains defined media (unpublished data). This is unusual because only a few bacterial pathogens replicate within the host cell cytosol due to the scarcity of readily available nutrients and a multitude of host defense mechanisms designed to destroy intracellular bacteria. But *F. tularensis* thrives within the cell cytosol, making *F. tularensis* an ideal model organism to study both immune evasion and nutrient acquisition strategies that other pathogens may also employ. To this end, I identified a process whereby *F. tularensis* exploits the host degradative process of

autophagy for nutrients while evading the anti-microbial form of autophagy, a process termed xenophagy.

Nutrient Deprivation in the Host Cell Cytosol

During infection, the host cell and intracellular pathogen compete for the same nutrients. When the bacteria invade the cell, most cellular nutrients are sequestered within macromolecular structures. Cells have some free amino acids to build new proteins, but the majority of amino acids within the cell are already incorporated into proteins. To secure a large amount of amino acids for replication, intracellular bacteria must either increase host cell amino acid import or degrade host proteins to acquire amino acids.

The nutrients that *F. tularensis* requires for replication are known. *F. tularensis* requires several salts and metals such as iron as well as pantothenate, spermine, thiamine, 13 amino acids that *F. tularensis* cannot synthesize, and a carbon source such as glucose or excess amino acids [8]. During infections, *F. tularensis* must acquire each of these nutrients from the host cell. Several groups have assessed how *F. tularensis* acquires iron and select amino acids from the host, and we focused our effort on determining the major source of carbon that *F. tularensis* uses for replication.

Iron

Iron is a critical metal that is available in very low abundances within host cells. Iron acquisition is well studied in many bacteria, but there are still several unknown factors in *F. tularensis* iron acquisition.

F. tularensis synthesizes siderophores to acquire exogenous iron [9]. Iron siderophores are required for virulence in the less pathogenic *F. novicida* and the live vaccine strain of *F. tularensis*, but not in the highly virulent Schu S4 strain [10]. Instead, FupA is required for iron uptake in Schu S4. The mechanism of FupA iron acquisition is unknown, but does not involve siderophores [10]. An interesting quirk of *F. tularensis* iron acquisition is that unlike many other Gram-negative bacteria, *F. tularensis* does not transport iron via TonB [11].*F. tularensis* still transports the iron bound molecules through its membranes via proton motive force, but via a different mechanism than other bacteria.

Amino acid uptake

Another characterized nutrient acquisition mechanism in *F. tularensis* is amino acid uptake. *F. tularensis* cannot synthesize 13 amino acids and must acquire these from the host cell. Additionally, we found that amino acids are a major carbon source for *F. tularensis* [5]. *F. tularensis* uses a number of synergistic mechanisms to acquire these amino acids. *F. tularensis* degrades glutathione, increases host amino acid transport, and harvests autophagy by-products [5,12,13].

Glutathione degradation

Glutathione (GSH) is tripeptide that is synthesized from glutamic acid, cysteine, and glycine. GSH is a highly conserved antioxidant that is critical for detoxifying the cytotoxic and carcinogenic material within the cytosol [14]. Importantly, GSH is highly abundant in the cytosol of mammalian cells [15].

F. tularensis can synthesize glycine and glutamic acid, but is auxotrophic for cysteine [8]. *F. tularensis* degrades GSH for its constituent amino acids via a gamma-glutamyl transpeptidase (*ggt*). Deletion mutants of *ggt* are highly attenuated for replication in cells, but can be functionally complemented with exogenous cysteine [13]. Although *F. tularensis* may also import glycine or glutamic acids, cysteine is the only required nutrient that *F. tularensis* obtains from GSH.

Amino Acid transporters

The eukaryotic amino acid transporter SLC1A5 (also called ASCT2) imports neutral amino acids. *F. tularensis* infection increases both SLC1A5 mRNA and protein levels in infected cells [12]. SCL1A5 works with SLC7A5 (LAT1), another amino acid transporter, to balance the cytoplasmic pool of amino acids [16]. While SLC1A5 levels are increased during infection, SLC7A5 has decreased mRNA expression and protein levels during *F. tularensis* infection [12]. Altering the ratio of SCL1A5 and SLC7A5 may functionally increase the intracellular level of glutamine during *F. tularensis* infections [12].

Autophagy

Macroautophagy (hereafter autophagy) is a constitutive process that degrades long lived-proteins, organelles, and aggregates into their base constituents. Autophagy is a critical, constitutive process for nutrient generation and maintenance of cellular homeostasis. In mouse embryonic fibroblasts (MEFs), a common cell line used for autophagy research, approximately 1-2% of the cytosolic volume of the cell is engulfed by autophagosomes at any given time [17]. A wide range of stimuli increase autophagy. Two major signaling pathways for autophagy induction are the activation of the energy sensing protein AMP-activated protein kinase (AMPK)

and inhibition of the mammalian target of rapamycin (mTOR). AMPK is activated in response to a low ATP to AMP ratio, such as during glucose deprivation [18,19]. AMPK induces autophagy directly by phosphorylating ULK1 or indirectly through mTOR inhibition [20]. mTOR is inhibited by several other stress factors besides AMPK, such as amino acid starvation or hypoxia [21].

The initiation of autophagy results in a complex signaling cascade with several intricacies and permutations. In canonical autophagy, AMPK activation or mTOR inhibition result in ULK1 activation [20]. ULK1 phosphorylates Beclin-1 and activates the kinase VPS34. ULK1, Beclin-1, and VPS34 as well as their associated complexes localize to an open, double membrane structure termed the phagophore. The phagophore is elongated by the ATG5-ATG12-ATG16L complex [22]. The phagophore expands to engulf cytoplasmic material while forming a double membrane vacuole termed the autophagosome. Molecules targeted for autophagic degradation are anchored to the autophagosome by microtubule associated light chain 3 (LC3). Unprocessed LC3 is cytosolic (LC3-I), but LC3 is cleaved, lipidated with phosphatidylethanolamine (LC3-II), and embedded into the autophagic membrane upon the initiation of autophagy [23]. Molecules targeted for autophagic degradation are polyubiquitinated and adaptor proteins including p62, OPTINEURIN, or NDP52 bind to both LC3-II and ubiquitinated molecules [24-26]. The autophagosome then fuses with a lysosome to become an autolysosome. The adaptor molecule NDP52 was recently shown to also regulate the fusion of a subset of bacteria containing autophagosomes to lysosomes by mediating binding between LC3 (which is embedded in the autophagosome), Myosin VI (a myosin motor protein that moves toward the minus end of actin) and Tom-1 (which associates with lysosomes) [27]. The contents within the autolysosome are degraded into their components and exported to the cytosol through an undefined process.

Canonical autophagy is the best characterized type of autophagy, but there are several versions of non-canonical autophagy. These non-canonical forms also generate double membrane, degradative vacuoles with the same basic maturation process (phagophore to autophagosome to autolysosome). However, non-canonical autophagosomes are formed through different signaling cascades and do not use all of the proteins or protein complexes required for canonical autophagy. One recurrent form of non-canonical autophagy in pathogenesis is ATG5-independent autophagy. ATG5-independent autophagy uses some of the same machinery as canonical autophagy, such as ULK1 and Beclin-1, but does not require ATG5, ATG7, or LC3 [17]. LC3 cleavage and ATG5 knockouts are the best characterized autophagy tools that are commonly used to assay for xenophagy, a version of autophagy that targets intracellular microbes for degradation. Pathogens may preferentially induce ATG5-independent autophagy to avoid xenophagy.

ATG5-independent autophagy is induced by starvation and correlates with mTOR inhibition, but mTOR inhibition alone is not sufficient to induce this form of autophagy [5,17]. ATG5-independent autophagy is critical for *Brucella abortus* to infect neighboring cells [28]. *Mycobacterium marinum* enters autophagosome-like vacuoles in an ATG5-independent manner although the function of this vacuole is unknown [29]. The differences between ATG5-independent autophagy and other forms of autophagy in pathogenesis are not known. It is also unclear how ATG5-independent autophagy is preferentially induced during these infections.

In summary, autophagy generates nutrients for the host cell. This seems like an excellent process for pathogens to exploit for nutrients, but autophagy is also a host defense mechanism against intracellular microbes. In addition to the previous autophagy induction mechanisms, the anti-microbial form of autophagy (xenophagy) is up-regulated by numerous immune stimuli.

F. tularensis Immune suppression

F. tularensis is often referred to as a 'stealth pathogen' because infection by this organism does not stimulate a robust immune response. *F. tularensis* evades identification and cytokine production in response to infection while resisting innate host cell anti-microbial defenses. It is important to note that the closely related *F. novicida* strain (often referred to as *F. tularensis novicida* in older literature) is highly pro-inflammatory, synthesizes a different LPS structure, and has different immune evasion characteristics and interactions with the inflammasome [30-32].

Immune suppression during infection is an important aspect of *F. tularensis* pathogenesis. In addition to transcriptional changes within the cell to destroy microbes, the activation of Toll-like receptors (TLRs), the inflammasome, and other changes to cellular homeostasis induce xenophagy [33-35]. For *F. tularensis* to successfully harvest autophagy derived nutrients, *F. tularensis* must evade xenophagy.

Toll-like receptors

TLRs identify extracellular microbes or microbes within endosomes. 13 different TLRs have been identified in mice and humans, although certain TLRs are species specific. TLRs recognize conserved microbial features such as lipopolysaccharide (LPS), peptidoglycan, and flagella [36].

TLR signaling occurs through two major pathways. TRIF-dependent TLR signaling is specific to TLR3 and TLR4. *F. tularensis* does not stimulate TRIF signaling. Treating infected cells with the TLR3 agonist polyI:C inhibits bacterial replication, presumably because *F. tularensis* does not inhibit the TRIF pathway [37]. The other major TLR signaling pathway is

through Myd88. Myd88 is an adapter molecule that interacts with all of the TLRs except TLR3 to initiate downstream signaling. TLR signaling through Myd88 eventually leads to stimulation of several pro-inflammatory transcription factors including NF-kB, IRF3, and IRF7 [36]. These transcription factors lead to transcription of a range of chemokines, cytokines, and the up-regulation of a number of anti-microbial factors [36].

TLRs are stimulated in response to most pathogens, but *F. tularensis* evades and suppresses TLR stimulation [38]. TLRs are pattern recognition receptors, but the typical bacterial agonists that stimulate the various TLRs are structurally different in *F. tularensis*. For example, Gram-negative bacteria typically stimulate TLR4 with lipopolysaccharide (LPS), but *F. tularensis* LPS is structurally different than LPS from other bacteria and does not stimulate TLR4 [39]. Instead, *F. tularensis* LPS primarily stimulates TLR2, although induction is relatively weak [40]. In addition to poor stimulation of TLRs, *F. tularensis* dampens artificial TLR stimulation by secreting an uncharacterized lipid [41,42].

Inflammasome

The inflammasome is a multimeric complex involved in detecting conserved microbial factors within the cytosol. The specific inflammasome complex formed depends on the microbial stimuli that are detected. In a simplified model, the inflammasome is composed of an inflammasome sensor such as a nucleotide-binding domain, leucine-rich repeat containing proteins (NLR), the adaptor molecule ASC, and caspase-1 [43]. Activation of the sensor molecule in this system leads to inflammasome formation and caspase-1 maturation [43]. Mature caspase-1 processes pro- interleukin-1 Beta (IL-1B) and pro-interleukin-18 (IL-18) into their mature forms

[44]. The mature cytokines are then secreted. Robust IL-1B secretion also requires TLR stimulation to increase IL-1B transcription [45].

F. tularensis infection results in negligible caspase-1 processing and IL-1B secretion, suggesting that *F. tularensis* does not induce caspase-1 inflammasome activation [46]. Likewise, *F. tularensis* does not stimulate caspase-11 due to its non-canonical LPS structure [47]. Instead, *F. tularensis* suppresses inflammasome activation, even in the presence of strong artificial inflammasome stimulation [48]. The closely related *F. novicida* has a very different interaction with the inflammasome. *F. novicida* activates the inflammasome when bacterial DNA binds to absent in melanoma 2 (AIM2) [49].

Xenophagy

Xenophagy is a form of selective autophagy that sequesters and degrades intracellular pathogens. Briefly, bacteria are polyubiquitinated and the polyubiquitin binds to an adaptor molecule. The adaptor molecule can be p62/sequestosome 1, NBR1, or opineurin. The adaptor molecule recruits LC3 to isolate the bacteria within a phagosome. The targeted bacteria are then degraded and antigens from the bacteria are presented via the major histocompatibility complex II (MHC-II) [50].

Xenophagy degrades most microbes that enter the cytosol, so successful intracellular pathogens must avoid xenophagy. For example, several serotypes of Group A *Streptococcus* (GAS) are efficiently cleared from the cytosol by xenophagy [51,52]. But the GAS protein speB degrades the xenophagy adaptor molecule p62 and NBR1 [53]. GAS strains that normally are destroyed in the cytosol can be rescued for intracellular replication when they express speB [53].

Not surprisingly, GAS strains that encode speB are much more likely to cause disease than strains that lack speB [53].

Xenophagy has many overlapping and redundant surveillance mechanisms that pathogens must avoid. Xenophagy is induced in response to extracellular or phagocytosed microbes through the activation of TLRs. TLRs initiate xenophagy when Myd88 or TRIF interact with Beclin-1 [33,34]. Cell to cell signaling can also induce autophagy. IFN-γ activates xenophagy through IRGM1 in human cells while CD40 ligation stimulates xenophagy through phosphoinositide-3-kinase (PI3K) and Rab7; priming cells to resist microbes [54,55].

After phagocytosis, certain pathogens escape the phagosome and replicate within the cytosol. The host cell mounts a xenophagic response to the membrane damage that occurs during phagosomal escape [56]. Once microbes reach the cytosol, they can be targeted for xenophagy through immune surveillance or by causing cell stress. Several molecules identify microbial components within the cytosol and target microbes for xenophagy, such as Nod-1 and Nod-2. Nod-1 and Nod-2 induce xenophagy and microbial antigen processing in response to bacterial peptidoglycan [57,58]. Microbes can also induce xenophagy through a number of cell stress mechanisms, such as the unfolded protein response (UPR) or changes in intracellular calcium levels [59-61]. Lastly, xenophagy can also be directly induced by bacterial proteins. For example, *Shigella flexneri* exports VirG to polymerize actin and propel the bacteria through the cytosol [62]. ATG5 binds directly to VirG and initiates autophagosome formation without upstream autophagy signaling [63]. *S. flexneri* secretes the effector protein IcsB to block ATG5 from binding to VirG, which inhibits autophagy [63].

Although *F. tularensis* does not stimulate TLRs or the inflammasome, *F. tularensis* infection still activates several signals that typically lead to xenophagy. *F. tularensis* escapes the

phagosome which initiates xenophagy [56]. Likewise, *F. tularensis* infection results in mTOR inhibition immediately after late during infection [5]. Additionally, *F. tularensis* uses amino acids as a carbon source, which should induce autophagy when ammonium by-products of amino acid catabolism are secreted into the cytosol [5,64]. Despite the appropriate signals to induce xenophagy, *F. tularensis* does not induce xenophagy or co-localize with xenophagy markers [5,65]. *F. tularensis* LPS and O-antigen contribute to resistance to xenophagy, but there is also an active, unidentified factor that contributes to xenophagy evasion [65,66]. Together, these results suggest that *F. tularensis* both suppresses and resists xenophagy.

F. tularensis Exocytosis

The final step in the intracellular life cycle of *F. tularensis* is exocytosis. The mechanism for *F. tularensis* egress is unclear, but is well defined in many other intracellular bacterial pathogens. Several bacterial pathogens transfer from cell to cell via actin polymerization or syncytia formation. For example, *L. monocytogenes* secretes ActA to polymerize actin so that protrusions containing bacteria propel into and are engulfed by neighboring cells, thereby infecting the neighboring cell [67,68]. *F. tularensis* does not contain any homologs to known actin polymerization proteins and does not co-localize with actin as determined by fluorescence and transmission electron microscopy (unpublished results). Additionally, *F. tularensis* infected cells do not form giant multi-nucleated cells characteristic of syncytia formation (unpublished results). As a result, it was assumed that *F. tularensis* does not transfer directly from infected to uninfected cells.

However, *F. tularensis* infects 10-fold more cells than initial inoculum by 24 hours post inoculation and rapidly infects new cell types *in vivo* while eliciting very little cell death [2,69].

Although *F. tularensis* does not polymerize actin or form multi-nucleated syncytia, these results suggest that *F. tularensis* transfers between cells via an alternate mechanism.

F. tularensis Suppression of Cell Death

Host cells use several pathways to induce cell death upon infection. This is a highly efficient way to ensure that intracellular pathogens cannot survive within a host during infection. For optimal intracellular replication, *F. tularensis* must suppress host cell death. *F. tularensis* mutants lacking *FTT1236, FTT1237,* or *FTT1238* are disrupted for capsule or O-antigen production [70,71]. These mutants replicate within the cytosol as a similar rate as wild type bacteria, but they are significantly more cytotoxic. As a result, these mutants only replicate for approximately 12 to 18 hours in cells compared to the 24 hours replication cycle typical of wild type bacteria [70]. As a result, these mutants are significantly less virulent in mice [71].

F. tularensis inhibits infected host cell death. *F. tularensis* uses a TolC-dependent mechanism to inhibit apoptosis [72,73]. TolC is an outer membrane channel involved in the export of bacterial virulence factors and is likely not the effector protein inhibiting apoptosis [72]. Caspase-11 induced pyroptosis is another common cell death mechanism in response to infection, but *F. tularensis* does not stimulate caspase-11 [47].

F. tularensis Cell to Cell Transfer

We were interested in how *F. tularensis* infects new cells while inducing minimal infected cell death. We found that *F. tularensis* transfers directly from one cell to another by live cell imaging and part of my dissertation research was to characterize how *F. tularensis* transferred between cells. Other bacterial species use active processes to transfer between cells,

but *F. tularensis* does transfer between cells via homologous mechanisms. Mammalian cells routinely transfer cytosolic components, and we investigated if *F. tularensis* and other intracellular bacteria are transferred via a passive transfer mechanism.

Francisella containing vacuoles

F. tularensis enters autophagic vacuoles termed *Francisella* containing vacuoles (FCVs) late during infection [74]. *Brucella abortus* enters an autophagic vacuole late in infection for non-lytic exocytosis [28], and FCVs have been proposed as a potential mechanism for *F. tularensis* cell to cell transfer. However, FCVs did not affect *F. tularensis* cell to cell transfer (unpublished data). These results prompted us to investigate other potential cell to cell transfer mechanisms.

Cytosolic exchange

Cells communicate with one another through a wide variety of mechanisms including cytokines, chemokines, hormones, surface proteins, pyroptosis, exosomes, and through the exchange of cytosolic material. The exchange of cytosolic material is best studied in the context of pore formation between the cells, such as gap junctions [75]. But several groups have also found that immune cells exchange intracellular proteins, polystyrene beads, and live mitochondria [76-78]. Cytosolic transfer requires cell to cell contact but the molecular mechanism of cytosolic exchange is unknown. There are at least 2 different forms of cytosolic exchange: the formation of nanotubules and the phagocytosis of live cells by macrophages [78,79]. Human immunodeficiency virus (HIV) transfers between cells via nanotubules, but *F. tularensis* bacteria appear to transfer via phagocytosis by macrophages [80]. Cytosolic transfer of pathogens is an important phenomenon because it is both a mechanism for pathogens to infect new cells and for

non-antigen presenting cells (APCs) to transfer antigen to professional APCs to mount an adaptive immune response [77,80-82].

Phagocytosis of Live Cells

Macrophages are phagocytic cells that are commonly associated with ingesting extracellular particles and dead cells. But macrophages also ingest portions of live cells. For example, macrophages acquire lipid droplets from live adipocytes without killing the adipocytes [79]. The ingested material can then stimulate an immune response. Macrophage ingestion of adipocytes can lead to through NF-KB, leading to interleukin-6 (IL-6) production [79]. *F. tularensis* is primarily found within macrophages *in vivo* and phagocytosis of live cells by macrophages is a potential mechanism for *F. tularensis* to transfer between cells.

Trogocytosis

Trogocytosis is a mechanism for cells to exchange proteins embedded in the plasma membrane. The intercellular exchange of membrane bound proteins is a cellular communication strategy that has been conserved from bacteria to mammalian cells [83,84]. Although trogocytosis was described several decades ago, trogocytosis is not well understood and there is no described molecular mechanism to induce or execute this process. The exchange of plasma membrane proteins benefits the host by passing along immune signals [85]. One example is the exchange of peptide bound major histocompatibility complex I (MHC-I), which presents antigen to $CD8^+$ T cells. MHC-I transfers from one cell to an APC via trogocytosis to stimulate a $CD8^+$ T cell response [86]. Trogocytosis has been implicated in macrophage phagocytosis of adipocytes and

Entamoeba histolytica ingestion of human cells [79,87]. Our work indicates that cytosolic material also transfers during trogocytosis and that this is a mechanism for bacterial spread.

Other Research Related to My Dissertation

My dissertation research primarily focused on how *F. tularensis* exploits host defense mechanisms. In addition to my primary research articles, I have helped to write reviews on how pathogens interact with the host to acquire nutrients (Appendix 1 and 2). My interest in these types of interactions was piqued by a project characterizing how the innate and adaptive immune response interacted in response to pathogens, and how pathogens altered this interaction (Appendix 3). Although I began this research prior to beginning my dissertation, shaping and completing this project in my dissertation lab was instrumental for me to develop as an independent scientist. This work was the foundation and inspiration for my research on bacterial cell to cell transfer and provided me with the requisite background and skills to complete the project. Lastly, I developed several tools and protocols for my lab to assess how *F. tularensis* interacts with the host. The most extensive method I developed and characterized is included in Chapter 2.

An important question we wanted to address is whether one of the secretion systems in *F. tularensis* induces autophagy or contributes to *F. tularensis* nutrient acquisition. *F. tularensis* encodes a putative secretion system termed the *Francisella* pathogenicity island (FPI), which resembles a Type VI secretion system (T6SS) [88]. There are no proteins that are known to be exported via the FPI, and the only known function of the FPI is for phagosomal escape [88]. We postulated that the FPI also contributed to cytosolic replication, but we needed to develop a method to test this hypothesis. Part of my dissertation research focused on building a method to

bypass the phagosome via intracellular trans-complementation and assess if the FPI played a role in intracellular survival and/or replication in the cytosol. We are currently assessing if the FPI affects autophagy induction, in part using intracellular trans-complementation.

CHAPTER 2: A METHOD FOR FUNCTIONAL TRANS-COMPLEMENTATION OF INTRACELLULAR *FRANCISELLA TULARENSIS*[1]

Overview

Francisella tularensis is a highly infectious bacterial pathogen that invades and replicates within numerous host cell types. After uptake, *F. tularensis* bacteria escape the phagosome, replicate within the cytosol, and suppress cytokine responses. However, the mechanisms employed by *F. tularensis* to thrive within host cells are mostly unknown. Potential *F. tularensis* mutants involved in host-pathogen interactions are typically discovered by negative selection screens for intracellular replication or virulence. Mutants that fulfill these criteria fall into two categories: mutants with intrinsic intracellular growth defects and mutants that fail to modify detrimental host cell processes. It is often difficult and time consuming to discriminate between these two possibilities. We devised a method to functionally trans-complement and thus identify mutants that fail to modify the host response. In this assay, host cells are consistently and reproducibly infected with two different *F. tularensis* strains by physically tethering the bacteria to antibody-coated beads. To examine the efficacy of this protocol, we tested phagosomal escape, cytokine suppression, and intracellular replication for *F. tularensis* Δ*ripA* and Δ*pdpC*. Δ*ripA* has an intracellular growth defect that is likely due to an intrinsic defect and fails to suppress IL-1β secretion. In the co-infection model, Δ*ripA* was unable to replicate in the host cell

[1]This chapter was previously published as an article in PLOS One. The citation is: Steele S, Taft-Benz S, Kawula T. A method for functional trans-complementation of intracellular *Francisella tularensis*. *PLoS One*. 2014;9(2):e88194. doi: 10.1371/journal.pone.0088194

when wild-type bacteria infected the same cell, but cytokine suppression was rescued. Therefore, Δ*ripA* intracellular growth is due to an intrinsic bacterial defect while cytokine secretion results from a failed host-pathogen interaction. Likewise, Δ*pdpC* is deficient for phagosomal escape, intracellular survival and suppression of IL-1β secretion. Wild-type bacteria that entered through the same phagosome as Δ*pdpC* rescued all of these phenotypes, indicating that Δ*pdpC* failed to properly manipulate the host. In summary, functional trans-complementation using bead-bound bacteria co-infections is a method to rapidly identify mutants that fail to modify a host response.

Introduction

Francisella tularensis is a facultative intracellular bacterial pathogen and is the causative agent of the disease tularemia. *F. tularensis* enters host cells through phagocytosis, escapes the phagosome, and replicates in the host cell cytosol while suppressing cytokine secretion [89-92]. Although substantial progress has been made in understanding the intracellular life cycle of *F. tularensis*, the *F. tularensis* proteins responsible for manipulating many host cell pathways are unknown. Identifying novel host-pathogen effector proteins is difficult because there is no rapid method to reliably distinguish between bacterial proteins that modify host processes and proteins that are involved in bacterial processes that are required for the bacteria to survive or replicate in the intracellular environment. The ability to identify mutants that are deficient for host-pathogen interactions is important because it can aid in prioritizing the investigation of genes of interest and in downstream experimental design. Moreover, certain mutant phenotypes, such as decreased phagosomal escape, hinder investigation of other potential phenotypes. A method to specifically complement these phenotypes would allow for further characterizations of certain *F.*

tularensis mutants. Thus we sought to develop a method to easily identify and functionally complement mutants that are deficient for interactions with the host.

In order to distinguish whether a phenotype results from a host-pathogen interaction or an intrinsic bacterial defect, we devised a method to functionally complement and thus identify host-pathogen interactions *in trans*. Wild-type and a mutant strain were tethered to the same magnetic bead to ensure that both bacteria enter the same eukaryotic cell. Since cells are consistently infected with both strains of bacteria via the same phagosome, the wild-type bacteria functionally complement the host-pathogen interactions that the neighboring mutant strain fails to initiate. For example, a mutant deficient for phagosomal escape that co-infects a host cell with wild-type bacteria will escape the phagosome because the wild-type bacteria secrete the effectors required for phagosomal escape. Bacterial mutants that exhibit a phenotype caused by intrinsic deficiencies such as defective metabolite production or acquisition will not be functionally complemented by this method since intrinsic defects cannot be trans-complemented by neighboring bacteria.

To demonstrate the efficacy of this protocol, we functionally complemented cytokine suppression, phagosomal escape, and intracellular survival in *F. tularensis* subsp. *holartica* live vaccine strain (LVS) Δ*pdpC* and Δ*ripA*. The *pdpC* gene is located in the *Francisella* pathogenicity island (FPI), which is proposed to encode a secretion and effector system that facilitates phagosomal escape [93-101]. PdpC contributes to phagosomal escape, intracellular survival and cytokine suppression [93,101]. We therefore used Δ*pdpC* as a model of a mutant that contributes to a host-pathogen interaction.

ΔripA can escape the phagosome but is defective for intracellular growth and cytokine suppression [90,102]. *ΔripA* replication is reduced in defined media at a pH of 7.5 compared to a pH

of 6.5, which implies that cytosolic pH, rather than a host-pathogen interaction, is responsible for decreased intracellular proliferation [103]. Furthermore, RipA regulates the activity of LpxA, a protein required for *F. tularensis* lipid A synthesis (our unpublished data). The *ΔripA* strain does not proliferate within host cells, but *ΔripA* strains encoding *lpxA* suppressors are able to replicate within host cells (our unpublished data). These data imply that *ΔripA* fails to replicate inside of host cells due to irregular regulation of lipid A synthesis and therefore intracellular proliferation of this mutant should not be restored by co-infection with wild-type organisms.

Results

Two bacterial strains consistently bind to the same bead

Reliable functional complementation of mutants within infected cells requires that both the mutant and complementing strain consistently enter host cells together. To achieve this result we tethered two different *F. tularensis* strains to individual magnetic beads. To test if the two different strains consistently bound to the same bead, we combined anti- *F. tularensis* lipopolysaccharide (LPS) antibody coated beads with a 1:1 mixture of *F. tularensis* expressing either GFP or DsRed. By microscopy, virtually every observed bead had GFP and DsRed bacteria bound to it (Figure 2.1 A-C). We quantified the amount of beads that bound to both GFP and Cell Trace Far Red labeled *F. tularensis* by flow cytometry and found that 97.3 +/- 0.7% (mean +/- SD) of the beads bound to both GFP and Cell Trace Far Red labeled bacteria (Figure 2.1 D-F). This indicates that in infection experiments where wild-type and mutant bacteria are bound to beads, the majority of cells will be infected with both bacterial strains.

Although this method requires multiple bacteria to be present on each bead, too many bacteria infecting the same cell may skew results or phenotypes compared to a normal infection.

To quantify the number of bacteria per bead, *F. tularensis* LVS containing a luciferase plasmid was bound to beads and the amount of luminescence per bead was compared to a standard curve. The median bacteria per bead was 3.43 (SEM = 6.69, 4 independent experiments). Additionally, 6.66 +/- 2.52 intracellular wild-type bacteria per cell were present at 4 hours post inoculation (average +/- SEM, n=23 from 9 independent experiments, assumptions described in materials and methods). Taken together, we estimate that the average cell is infected with 3 to 8 bacteria using bead co-infections.

F. tularensis is transiently linked to the bead

Tethering the bacteria to the same bead ensures that cells are co-infected with different strains, but irreversible binding of *F. tularensis* to the bead could affect the intracellular life cycle of *F. tularensis*. Thus, we took advantage of a binding mechanism that should allow the bacteria to detach from the bead over time by linking the bacteria to beads coated with antibodies to *F. tularensis* LPS. Each bacterium should initially link to the bead by binding to several anti-LPS antibodies, which should create a high avidity between the bead and the bacterium. The advantage of binding *F. tularensis* to the bead by an anti- LPS antibody is that Gram-negative bacteria, including *F. tularensis*, shed LPS. Thus, viable *F. tularensis* should detach from the bead over time. Indeed, the majority of bacteria were bound to beads immediately prior to infection as determine by flow cytometry (Figure 2.2A). Intracellular bacteria dissociated from beads within 2 hours during an infection of J774A.1 macrophage-like (J774) cells, presumably due to the bacteria shedding LPS (Figure 2.2A). Furthermore, microscopy of cells infected with GFP LVS bound to beads shows that some bacteria are spatially separated from the bead by 4 hours post inoculation (Figure 2.2B). These data demonstrate that the described methodology

results in bacteria bound to beads upon initial infection, but that the bacteria detach from the bead following host cell entry. The bacteria also released from beads at similar rates when left in PBS for 2 hours, suggesting that bacterial release from the bead is not mediated by infection (data not shown).

Bead co-infections functionally complement cytokine suppression

F. tularensis suppresses host cell production or secretion of several different cytokines, including interleukin 1β (IL-1β) by both active (such as MAPK inhibition) and passive mechanisms (such as via LPS modifications) [90,92,93,104-106]. Since wild-type *F. tularensis* actively suppresses inflammatory responses, co-infection of cells with wild-type bacteria should complement a mutant that fails to suppress the immune response. To test the efficacy of bead co-infections on rescuing immune suppression, we co-infected murine bone marrow derived macrophages (mBMDM) with wild-type *F. tularensis* bound to beads with either *ΔpdpC* or *ΔripA* and measured IL-1β secretion.

Infections of mBMDMs with *ΔripA* results in increased IL-1β secretion compared to wild-type [90]. Similarly, cells infected with *ΔripA* bound to beads also induced increased IL-1β secretion compared to cells infected with bead-bound wild-type *F. tularensis* (Figure 2.3). However, co-infecting cells with wild-type bacteria and *ΔripA* resulted in reduced IL-1β secretion compared to *ΔripA* alone (Figure 2.3). *ΔripA* bound to beads and typical *ΔripA* infections elicit similar levels of IL-1β, even though the cells infected with beads should contain more bacteria initially (data not shown). Thus the decrease of IL-1β secretion during co-infections was not due to fewer *ΔripA* infecting each cell. Together, these data demonstrate that

active immune suppression mechanisms expressed by wild-type *F. tularensis* was sufficient to inhibit the inflammatory response induced by *ΔripA*.

We also measured IL-1β secretion of *ΔpdpC* infected mBMDMs and found that cells infected with *ΔpdpC* bound to beads also had slightly increased IL-1β secretion when compared to wild-type infected cells (Figure 2.3). Co-infecting cells with wild-type and *ΔpdpC* bacteria resulted in decreased IL-1β secretion compared to *ΔpdpC* bacteria alone (Figure 2.3). Thus, *ΔpdpC* failed to entirely suppress the host immune response but suppression could be rescued by the presence of wild-type bacteria. Wild-type bacteria fully complemented suppression of IL-1β secretion during mixed infections of wild-type and *ΔpdpC* ($p=0.77$) but there was a slight increase in the wild-type and *ΔripA* mixed infection when compared to wild-type infections alone ($p=0.01$). We hypothesize that the observed increase in IL-1β secretion during co-infections with *ΔripA* is due to a small subset of cells that are infected by beads bound only to *ΔripA* bacteria combined with the increased magnitude of IL-1β secretion observed during *ΔripA* infections compared to *ΔpdpC* infections. However, we cannot rule out the possibility that *ΔripA* may stimulate the immune response via a pathway that cannot be entirely suppressed by wild-type bacteria. In summary, co-infections of mutant and wild-type bacteria can rescue a phenotype caused by the inability of the mutant to properly modify the host cell.

Phagosomal escape is functionally complemented during bead co-infections

Several FPI mutants, including *ΔpdpC,* as well as killed *F. tularensis* do not effectively escape the phagosome [93-101]. Therefore, *F. tularensis* phagosomal escape is a *F. tularensis* mediated process. As a result, wild-type bacteria should facilitate release of escape-defective mutants so long as the mutant and wild-type bacteria are within the same phagosome. To test this

hypothesis, we bound *ΔpdpC* containing a GFP-expressing plasmid (GFP*ΔpdpC)* to beads and quantified the amount of GFP*ΔpdpC* present in the cytosol of J774 cells. We found that GFP*ΔpdpC* had reduced phagosomal escape at 2 hours post inoculation compared to GFP expressing wild-type bacteria and GFP*ΔpdpC* phagosomal escape was rescued by the presence of wild-type bacteria within the same phagosome (Figure 2.4). This result is consistent with other published analyses of *ΔpdpC* mutant phenotypes and indicates that PdpC contributes to, but is not absolutely required for, *F. tularensis* LVS phagosomal escape [93,101]. More importantly, wild-type bacteria export the necessary effector protein(s) to allow both wild-type and *ΔpdpC* to escape the phagosome.

Bead co-infections achieve functional complementation of phagosomal escape across an entire population. This allows for the further characterization of phagosomal escape deficient mutants in the cytoplasmic environment. One caveat to using wild-type bacteria for complementation is that wild-type bacteria may out-compete certain mutants in the cytosol or obscure additional host-pathogen interactions. We hypothesized that any mutant strain that escapes the phagosome can be used to complement phagosomal escape of escape deficient mutants. To test this hypothesis, we co-infected cells with GFP*ΔpdpC* and *ΔripA*. The *ΔripA* strain escapes the phagosome with similar kinetics as wild-type bacteria, but does not replicate inside the host cell [102]. Indeed, *ΔripA* functionally complemented GFP*ΔpdpC* phagosomal escape when GFP*ΔpdpC* entered through the same phagosome as *ΔripA* (Figure 2.4). Our data demonstrate that infecting cells with *ΔpdpC* and a phagosome escape competent *F. tularensis* bacterium results in phagosomal escape of both bacteria. Thus, pairing a phagosomal escape deficient mutant with an escape competent mutant will allow for further characterization of cytoplasmic phenotypes associated with the phagosomal escape deficient mutant.

Bead co-infections complement intracellular survival

F. tularensis mutants can be deficient for intracellular survival or replication due to the inability of the mutant to perform a required interaction with the host or due to an intrinsic intracellular survival or replication defect. Co-infections with both mutant and wild-type bacteria can be used to determine whether the mutant fails to properly control a host-pathogen interaction

The *ripA* gene encodes a hypothetical protein of unknown function that is required for *F. tularensis* intracellular proliferation, likely through regulation of lipid A synthesis [102] (our unpublished data). We found that co-infecting J774 cells infected with wild-type *F. tularensis* did not complement *ΔripA* intracellular growth (Figure 2.5A). Likewise, individual cells had similar numbers of *ΔripA* expressing GFP regardless of whether or not wild-type *F. tularensis* was present in the same cell (Figure 2.5D, 2.5E). These data further indicate that *ripA* is involved in an intrinsic bacterial process essential for intracellular bacterial proliferation.

The PdpC protein is encoded on the FPI and *ΔpdpC* bacteria are deficient for intracellular proliferation [93,101]. Intracellular proliferation of *ΔpdpC* is not consistent across the entire population, as this strain replicates to high numbers in a small subset of cells [101]. Since the FPI is proposed to encode a secretion system, the failure of FPI gene deletion strains to replicate in the host cell is likely due to the inability to initiate host-pathogen interactions [107]. Thus *ΔpdpC* replication may be rescued by the presence of wild-type bacteria. Consistent with previous reports, the amount of viable intracellular LVS *ΔpdpC* bacteria decreased over time (Figure 2.5B) [93,101]. On average, the number of *ΔpdpC* organisms decreased over 2 orders of magnitude between 4 and 22 hours post inoculation (9 independent experiments). However, when J774 cells were co-infected with a mixture of wild-type and *ΔpdpC* bound to beads, *ΔpdpC* survival was functionally complemented by the wild-type bacteria (Figure 2.5B). Specifically, we observed a

slight increase in *ΔpdpC* replication during co-infections with wild type between 4 and 22 hours (2.0 +/- 0.3 fold, n=7 independent experiments, p=0.0014) (Figure 2.5B, 2.5D, 2.5E). We conclude that wild-type bacteria complemented the defect of *ΔpdpC* by secreting the effector(s) necessary to manipulate the host cell into being permissive for *F. tularensis* survival. Thus, *F. tularensis* LVS *ΔpdpC* does not survive inside of J774 cells due to its inability to properly manipulate an interaction(s) with the host that *F. tularensis* requires for intracellular survival.

Although *ΔpdpC* replicated slightly when wild-type bacteria were present in the same cell, *ΔpdpC* replication did not achieve wild-type levels. This is interesting because *ΔpdpC* escaped the phagosome, albeit at lower levels than wild-type, but was still inhibited by the host cell during individual infections (Figure 2.4, 2.5B) [93,101]. Thus, wild-type bacteria may promote *ΔpdpC* survival in the host cytosol (Figure 2.5B) but wild-type *F. tularensis* either out-competes *ΔpdpC* or *pdpC* is also required for a cell intrinsic process to fully restore intracellular replication. To distinguish between these possibilities, we co-infected cells with *ΔpdpC* and *ΔripA.* The *ΔripA* strain has an intact FPI and rescues *ΔpdpC* phagosomal escape, but since *ΔripA* does not replicate, it should not out-compete *ΔpdpC*. We found that co-infections with *ΔripA* and *ΔpdpC* resulted in *ΔpdpC* survival but proliferation did not increase to wild-type levels (Figure 2.5C). Thus, we conclude that PdpC is required for intracellular survival through a host-mediated process but has a secondary function that enhances bacterial proliferation.

Together, the *ΔpdpC* and *ΔripA* intracellular replication data demonstrate that co-infecting cells with wild-type and mutant bacteria can differentiate between mutants that fail to replicate due to defective host-pathogen interactions and mutants that are defective for growth due to intrinsic replication defects.

Discussion

We developed and optimized a method to reliably deliver two distinct *F. tularensis* bacteria into the same host cell. Co-infection of cells with bacteria bound to beads allows for functional complementation of host-pathogen interactions, which can be used to identify mutants that fail to induce a host-pathogen interaction or to complement a specific host-pathogen interaction.

The *ΔripA* strain fails to replicate inside of cells and induces IL-1β secretion [90,102,103]. With the described co-infection method, neighboring wild-type bacteria functionally complement IL-1β suppression in *ΔripA* infected cells but not *ΔripA* intracellular proliferation. The *Francisella novicida ΔripA* strain has also been shown to have increased intracellular lysis compared to wild-type *F. novicida* bacteria, which leads to increased cytokine secretion via the AIM2 inflammasome [108]. Herein we show that wild-type *F. tularensis* LVS bacteria can suppress cytokine secretion in cells infected with *ΔripA* bacteria. Assuming that RipA has an identical function between the different *Francisella* species, these data indicate that wild-type LVS bacteria, but not *ΔripA,* suppress the AIM2 inflammasome.

Interestingly, wild-type *F. tularensis* bacteria replicated in cells that contained *ΔripA* bacteria, which indicates that the cell cytosol remains permissive for *F. tularensis* replication and that the proliferation defect is specific to *ΔripA* bacteria. These data also indicate that increased cytokine secretion and intracellular proliferation phenotypes seen in *ΔripA* infections occur through different mechanisms because one phenotype is functionally complemented while the other is not. Additionally, we were able to genetically distinguish between *ΔripA* cytokine suppression and intracellular replication. A chromosomal *ripA* N21A point mutant of LVS proliferated in the cytosol at a rate comparable to wild-type bacteria, but failed to suppress IL-1β

secretion (data not shown). Taken together, the described co-infection method indicates that RipA is involved in cytokine suppression (a host-pathogen interaction) and a separate, intrinsic bacterial process for intracellular replication.

The *ΔpdpC* strain was functionally complemented for phagosomal escape, intracellular survival, and IL-1β suppression. Thus, PdpC contributes to those host-pathogen interactions. Interestingly, *ΔpdpC* replication never reached the same level as wild-type bacteria during co-infections even though *ΔpdpC* escaped the initial phagosome with the wild-type bacteria. These data hint that PdpC is involved in an intrinsic bacterial replication process that is required for optimal growth. It is also possible that a local host-pathogen interaction is required that is not reliably complemented by neighboring bacteria. Further investigation is needed to determine if the intracellular growth defect is specific to *ΔpdpC* or if other FPI genes are required for replication in the host cell cytosol.

The antibody used throughout these experiments has been used to identify *F. tularensis* Schu S4 by microscopy and for purifying Schu S4 from infected cell lysates [5,109]. As described, this method should be compatible with a range of *F. tularensis* species with O-antigen structures similar to *F. tularensis* LVS. More importantly, the described co-infection method is compatible with any biotinylated antibody, so antibodies specific to surface molecules of *F. tularensis* novicida or other bacterial species can be used to link bacterial cells to beads.

Binding bacteria to beads does alter some aspects of infection that must be taken into consideration when designing experiments. The beads are dense and sink to the bottom of the well, allowing for a substantially lower multiplicity of infection (MOI) while maintaining a high infection frequency. More bacteria are phagocytosed per cell when bacteria are bound to beads compared to a typical infection. This may require time points to be taken earlier than a typical

infection and the magnitude of certain phenotypes, particularly intracellular proliferation, are slightly different. Lastly, we expect that phagocytosis of beads coated in bacteria will primarily occur through typical phagocytic routes of a given bacteria because bacteria on the bead surface still interact with the cell. But phagocytosis may occasionally occur through a different mechanism than in a typical infection. For example, some Fc receptor mediated phagocytosis likely occurs in some cells due to antibodies bound to the beads. Despite these potential pitfalls, our individual infection controls for IL-1β secretion, phagosomal escape, and intracellular proliferation resulting from infection with bead-bound bacteria are consistent with previously published data based on infection by free bacterial cells [90,93,101,102].

Bead co-infections provide a consistent method of functionally complementing most intracellular bacterial manipulations of the host cell. However, there are a few specialized cases in which further characterization beyond bead co-infections is necessary. We expect that some gain of function mutants and host-pathogen interactions that require local manipulation will not be reliably complemented. For example, immune signaling phenotypes that are not complemented by wild-type bacteria are likely gain of function mutations because the mutants stimulate the immune system in a manner that wild-type bacteria cannot suppress. Likewise, xenophagy evasion and re-entry into *Francisella* containing vacuoles likely requires local host-pathogen interactions. As a result, a lack of complementation for mutants that are strongly suspected of manipulating the host cell can also narrow down potential functions for a given protein. Altogether, bead co-infections are a reliable method to gain insight into the function of a gene of interest, identify mutants that fail to initiate a host-pathogen interaction, and to aid in downstream experimental design.

Materials and Methods

Bacteria and plasmids

Francisella tularensis subsp *holartica* LVS was obtained from the CDC Atlanta, GA. A *pdpC* deletion construct was made by splice overlap extension (SOE) PCR as described previously [102]. Primers were used to delete all but the first five amino acid (MNDKY) and the last five codons (KISS stop) while keeping the deletion in frame. After blunt end cloning into pCR BLUNT II (Invitrogen), the SOED *pdpC* fragment was removed by BamHI-Not I digest and cloned into suicide vector pMP812 [110]. Integrants were selected on kanamycin (10 ug/ml). Resolved integrants were selected by growth overnight in brain heart infusion (BHI) broth (BD Biosciences) supplemented with isovitalex followed by plating on chocolate containing 10% sucrose. Resolved integrants were sequenced to confirm in-frame deletion of *pdpC* and integrity of the flanking sequence. Deletion of both *pdpC* genes was verified by PCR. Genetic complementation of *pdpC* by constitutively expressing the *pdpC* gene on pMP822 restored intracellular proliferation (Supplemental Figure 1) [111]. The *ΔripA* in-frame deletion and GFP*ΔripA* strains were previously generated [112].

GFP wild-type LVS (GFP-wt) was generated by Hall et al [2] and GFP-Δ*pdpC* was generated using the same GFP plasmid. DsRed LVS and luciferase expressing LVS were generated with the plasmids from DsRed Schu S4 and luciferase expressing Schu S4 respectively [5]. Hygromycin B resistant *ΔpdpC* and *ΔripA* were generated by transforming the deletion mutant bacteria with the hygromycin B resistance plasmid pMP831 [111]. The kanamycin resistant wild-type strain was generated by transforming wild-type bacteria with the kanamycin resistance plasmid pMP828 and kanamycin resistant *ΔripA* with the pkkMCS plasmid [102,111].

Cell Culture

J774A.1 Macrophage like cells were obtained from ATCC and grown in DMEM with 4.5 g/L glucose and supplemented with 10% FBS, L-glutamine and sodium pyruvate (all from Gibco). Mouse bone marrow derived macrophages were generated from a C57Bl/6 as previously described [113]. All animal studies were conducted according to the Institutional Animal Care and Use Committee guidelines of the University of North Carolina- Chapel Hill (IACUC ID 13-213).

Binding *F. tularensis* to the magnetic beads

800 nm streptavidin coated magnetic beads (Solulink) were blocked with sterile filtered Tris buffered saline (TBS) containing 0.1% casein for 20 minutes. The beads were washed 4 times with antibody wash buffer (100 mM Tris, 150 mM NaCl and 0.05% tween 20 in distilled water, pH 8.0). For every 10 ug of beads, we added 2.5 μg of anti-*Francisella tularensis* LPS antibody (US Biological) that was previously biotinylated using a FluoReporter Mini-Biotin-XX Protein Labeling Kit (Invitrogen) following the manufacturer's instructions. The antibody was suspended in antibody wash. After 30 minutes of rocking at 4°C, the beads were washed twice in antibody wash buffer and twice in PBS. 10 μg of magnetic beads coated with anti- LPS antibody were mixed with $8x10^8$ bacteria for 20 minutes. Each sample was then washed twice in PBS to remove unbound *F. tularensis*. After the final wash, the beads were suspended in cell culture media and ready to use for the given experiment. All washes were performed by placing a 12 x 75 mm round bottom tube containing the sample on a BD IMagnet (BD biosciences) and waiting approximately 2 minutes for the beads to move toward the magnet. After all wash steps, approximately $1x10^7$ beads bound to bacteria were present for every 10 ug of beads initially added (based on plating bacteria bound to beads on chocolate agar). The amount varied up to 4 x

10^6 beads between experiments. All experiments were inoculated assuming $1x10^7$ bacteria bound to beads per 10 ug of starting beads.

For samples where multiple strains were added together, $4x10^8$ of each strain was added. For all mixed infections, the inoculum of each type of bacteria was plated and compared to ensure both types of bacteria were equally represented. Typically the ratio of one type of bacteria to the other was between 1: 0.8 and 1: 1.2 (data not shown). Infecting cells at a MOI higher than 1 can result in each cell taking up a substantial number of beads, which may impact results (data not shown). Bead aggregates can form over time which may impact the number of bacteria that enter each cell.

Microscopy

For micrographs of bacteria on beads, GFP-LVS and/or DsRed labeled LVS were coated onto the beads as described above. The bacteria bound beads were fixed in 4% paraformaldehyde and were placed into an 8 well chamber slide (Nunc). The beads were allowed to settle and the fixative was carefully removed.

For images of infected cells, beads were prepared as above with the indicated bacteria. J774 cells were inoculated for 2 hours and then the media was removed and replaced with media containing 25 μg/ml of gentamicin. The cells were washed and fixed with 4% paraformaldehyde at 4 or 22 hours post inoculation. Cells were treated with 50 mM ammonium chloride for 10 minutes and then stained with 10 μg/ml of AF647 wheat germ agglutinin (Invitrogen) where indicated.

All samples were mounted using a DAPI containing mounting media (Vector Shield). Images were acquired using a Zeiss 700 confocal laser scanning microscope (Zeiss) using Zen

image acquisition software (Zeiss) or an Olympus FV500 confocal scanning laser microscope (Olympus). Images were cropped and scale bars were added using ImageJ [114].

Flow Cytometry

To assess the frequency of both types of bacteria binding to a single bead, beads were prepared as above with GFP-LVS and/or Cell Trace Far Red DDAO-SE (Invitrogen) labeled wild-type LVS. Immediately following the final wash, the beads were stained with pacific blue conjugated anti- *F. tularensis* LPS antibody (US biological) (Pacific blue antibody labeling kit [Invitrogen] following the manufacturers protocol). The beads were washed once more and then immediately fixed using 4% paraformaldehyde. The event trigger on the flow cytometer was set to only record Pacific Blue positive events.

Phagosomal escape assays were performed as previously described [74]. Briefly, J774 cells were inoculated with beads coated with the indicated wild-type or deletion mutants bacteria (prepared as above). 2 hours post inoculation, the cells were suspended and stained with pacific blue conjugated anti- *Francisella tularensis* LPS antibody to label extracellular bacteria. After the antibody was washed away with KHM buffer, the cells were permeabilized with 100 ul of 10 μg/ml digitonin and the cells were stained with AF647 conjugated anti- *Francisella tularensis* LPS antibody to stain cytosolic bacteria. The cells were lysed and the samples were then analyzed by flow cytometry. We compared the ratio of intracellular cytosolic bacteria (GFP+ AF647+ Pac Blue-) to bacteria in the phagosome (GFP+ AF647- Pac Blue-). The data from these experiments includes both bacteria bound to beads and unattached bacteria. No significant difference in localization was seen between *F. tularensis* attached to beads and unbound bacteria, although bacteria bound to beads tended to escape the phagosome at higher rates. Control cells

were stained with calnexin to assay the percentage of cells that were permeabilized. The percentage of permeabilized cells was used to determine the total percentage of bacteria that escaped the phagosome.

To assay for bacterial dissociation from the beads prior to inoculation, GFP-LVS was bound to beads as previously described and stained with pacific blue conjugated anti- *F. tularensis* LPS antibody. The fixed sample was then analyzed for the percentage of bacteria bound to beads. To assess the amount of dissociation from beads inside of cells, GFP-LVS was bound to beads as previously described. The cells were removed from the plate, washed in KHM buffer [74], and permeabilized with digitonin 2 hours post inoculation. The permeabilized cells were stained with an AF647 conjugated anti- *F. tularensis* LPS antibody (US biological). The antibody was washed away and then the infected cells were lysed by vortexing the cells in distilled water. AF647+, GFP+ events were analyzed for attachment to a bead based on size.

All samples were analyzed using a Cyan Flow Cytometer (Dako) with the event trigger set to record only pacific blue positive events or GFP positive events depending on the experiment. All histograms were pre-gated so that only single events were analyzed.

Intracellular bacterial proliferation assay

The indicated LVS mutants were coated on beads as previously described. J774 cells were seeded at approximately $2.5x10^5$ cells per well the night before infection and were infected with an approximate multiplicity of infection (MOI) of 1 bead per cell (assuming $5x10^5$cells prior to infection). The media was replaced with media containing 25 μg/ml of gentamicin 2 hours post inoculation. At 4 and 22 hours post inoculation, the cells were scraped off the plate, lysed, serially diluted and plated on chocolate agar containing isovitalex and either kanamycin or

hygromycin to assess bacterial proliferation. As expected, hygromycin resistant colonies did not form under kanamycin selection and vice versa (data not shown).

Quantification of bacteria per bead

F. tularensis LVS containing a luciferase –expressing plasmid was bound to beads following the previously described method. Half of the sample was plated on chocolate agar to assay for the number of beads bound to bacteria and the other half was placed into an Infinite M200 Pro plate reader (Tecan) and the amount of light produced was quantified and compared to a standard curve consisting of know quantities of *F. tularensis* LVS containing the luciferase plasmid.

The number of bacteria per cell was determined based on the results at 4 hours post inoculation of the wild-type bacteria from the intracellular proliferation assay described previously. We assumed that 60% of the cells were infected based on flow cytometry of similar samples examined 2 hours post inoculation. Since gentamicin is added 2 hours post inoculation, additional cells should not be infected. We also assumed that the J774 cells doubled overnight, resulting in $5x10^5$ cells, that each cell was infected with 1 bead, that 100% of bacteria were bound to beads and no bacterial death or replication occurred between 0 and 4 hours post inoculation.

IL-1β ELISA

Murine bone marrow derived macrophages were seeded at $5x10^5$ cells per well in 24-well plates. Beads coated with the appropriate bacterial strains and were used to inoculate the cells at an MOI of approximately 1 bead per cell. The cell supernatant was collected 22 hours post

inoculation and the amount of IL-1β was measured using a BD OptEIA mouse IL-1β ELISA set (BD biosciences) following the manufacturers protocol.

Statistics

All statistics were performed using an unpaired Student t-test using the compiled data from all experiments performed. Intracellular proliferation assays were $\log_{10}$ transformed prior to statistical analysis.

Figures

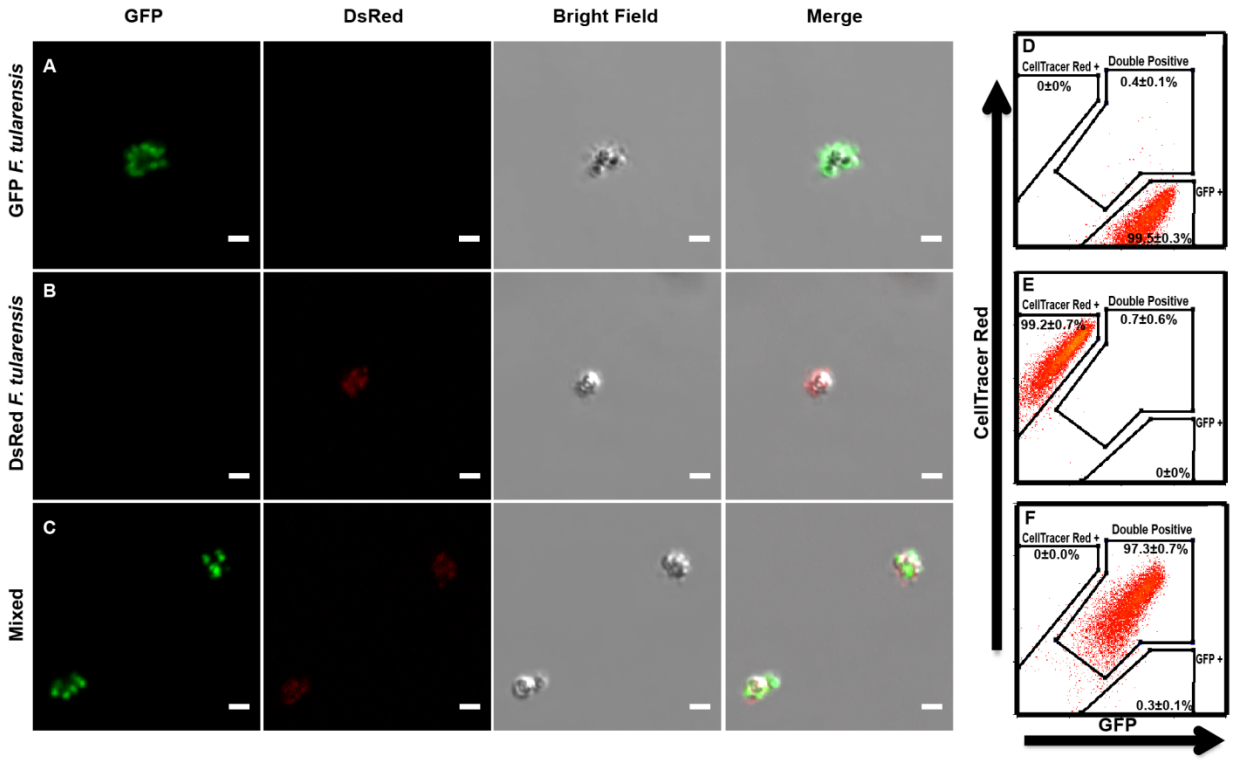

Figure 2.1: Multiple *F. tularensis* bacteria reliably bind to the same bead.

Representative flourecence micrographs of beads bound to (A) GFP LVS, (B) DsRed LVS, or (C) a mixture of GFP LVS and DsRed LVS. All scale bars represent 2 μm. Representative flow cytometry histograms of three independent experiments depicting beads bound to (D) GFP LVS, (E) CellTrace Far Red labeled LVS, or (F) a one to one mixture of GFP LVS and CellTrace Far Red labelled LVS. Histograms were pregated on size to exclude aggregates and non-specific events. Quantification was compiled from all 3 experiments and represents the mean +/- the standard deviation.

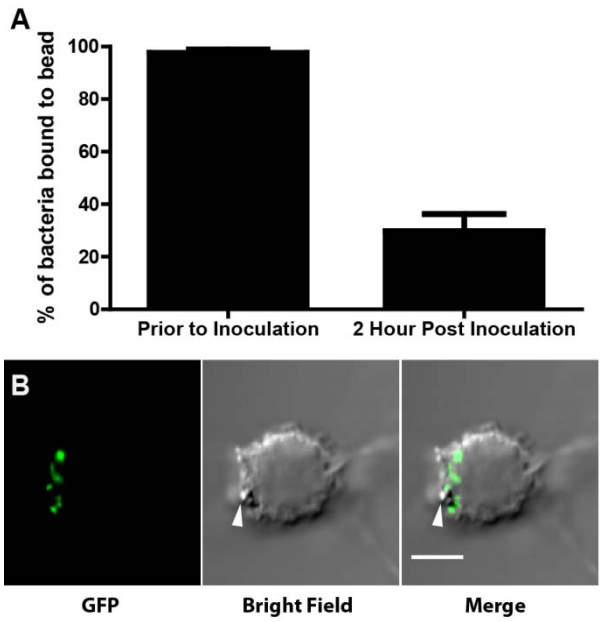

Figure 2.2: *F. tularensis* separates from the beads inside host cells.

(A) Percentage of events representing bacteria that were bound to a bead prior to infection (n=3) and the percentage of events representing intracellular bacteria bound to a bead 2 hours post inoculation (n=9), as quantified by flow cytometry. Bar graph represents the mean +/- the standard deviation. (B) Representative fluorscence micrograph of a cell infected with beads bound to GFP (green) expressing LVS. The white arrow indicates the location of the bead. The image was taken 4 hours post inoculation. The scale bar represents 5 uM.

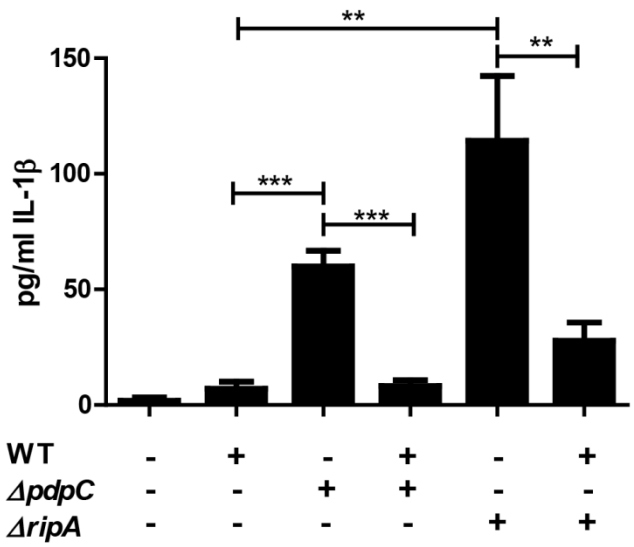

Figure 2.3: Functional trans-complementation via bead-bound bacteria complements suppression of cytokine secretion.

IL-1β ELISA of murine bone marrow derived macrophages that were inoculated with single or mixed inoculations of wild-type, *ΔpdpC* or *ΔripA* LVS (triplicates, n=3). All samples were bound to beads prior to infection. Bar graph represents the mean +/- SEM. **p<.01, ***p<.001

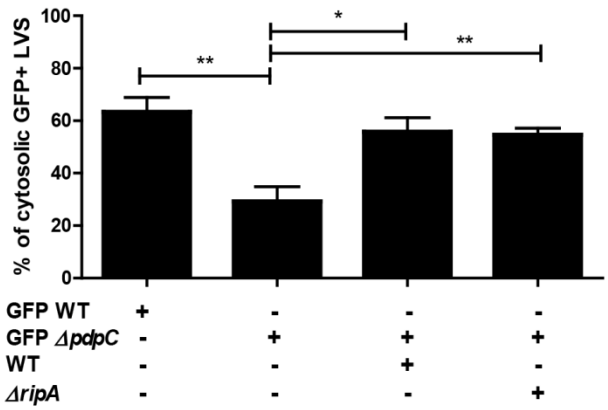

Figure 2.4: Functional trans-complementation via bead-bound bacteria complements phagosomal escape.

J774 cells were inoculated with either GFP wild-type LVS or mixtures of GFP *ΔpdpC*, wild-type LVS, or *ΔripA* (n=4 independent experiments). The amount of cytosolic GFP positive bacteria was quantified by flow cytometry and normalized based on the amount of permeabilized cells, as determine by calnexin staining controls. All samples were bound to beads prior to infection. Data includes bacteria attached and detached from beads in the same sample. Bar graph represents the mean +/- SEM. * p<.05, **p<.01

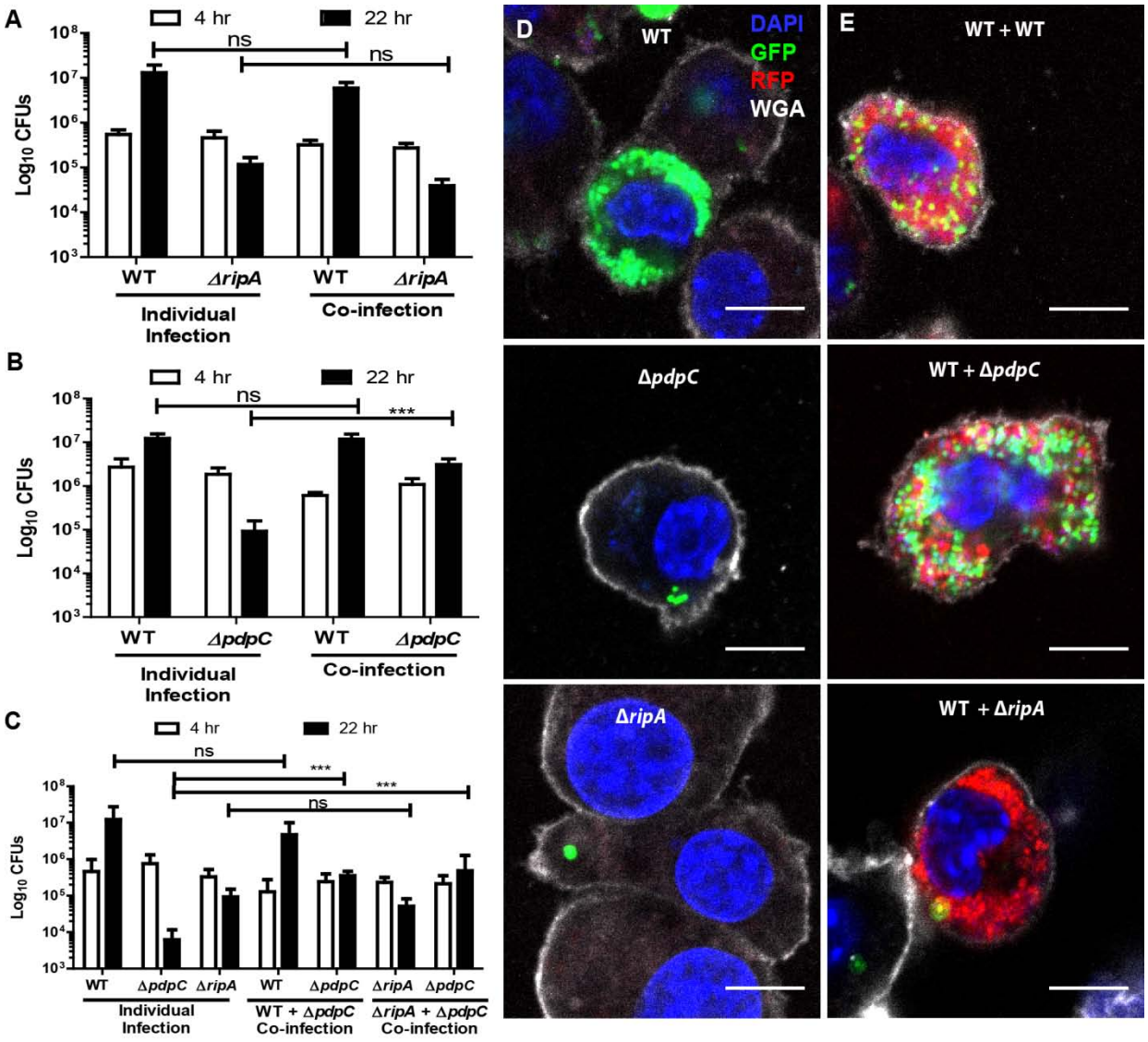

Figure 2.5: Functional trans-complementation via bead-bound bacteria complements intracellular proliferation of ΔpdpC but not ΔripA.

(A) Kanamycin resistant wild-type LVS or hygromycin resistant ΔripA were individually or co-inoculated into J774 cells and assayed for intracellular proliferation at 4 and 22 hours post inoculation. (B) Kanamycin resistant wild-type LVS or hygromycin resistant ΔpdpC were individually or co-inoculated into J774 cells and assayed for intracellular proliferation at 4 and 22 hours post inoculation. (C) Kanamycin resistant wild-type LVS, kanamycin resistant ΔripA or

hygromycin resistant ΔpdpC were individually or co-inoculated into J774 cells and assayed for intracellular proliferation at 4 and 22 hours post inoculation. Results are from 3 independent experiments performed in duplicate or triplicate. Bar graphs represent the mean +/- the standard deviation. (D) Representative fluorescence micrographs of J774 cells inoculated for 22 hours with GFP wild-type, GFPΔpdpC or GFPΔripA bacteria attached to beads. (E) Representative fluorescence micrographs of J774 cells inoculated with beads bound to DsRed LVS and either GFP WT, GFPΔpdpC or GFPΔripA. Blue represents the nucleus (DAPI), green represents the indicated GFP LVS mutants, red represents DsRed wild-type LVS, and white represents the plasma membrane stain wheat germ agglutinin (WGA). All scale bars represent 10 μm. All samples were bound to beads prior to infection. Not significant (ns), $p>.05$, * $p<0.05$, ***$p<0.005$

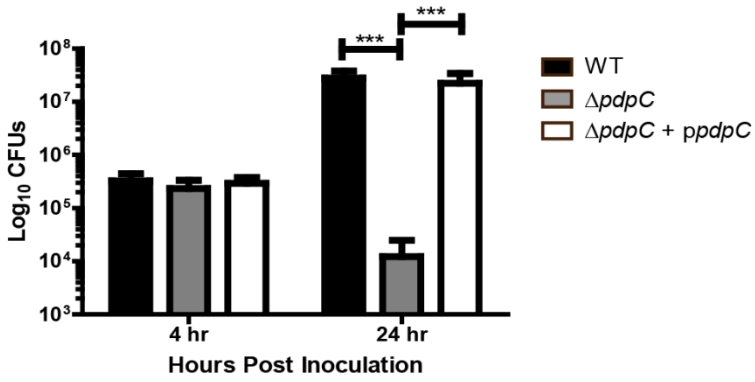

Figure 2.6: Genetic complementation of ΔpdpC intracellular proliferation.

Supplemental figure 1

Intracellular proliferation assay of J774 cells infected with wild-type, Δ*pdpC* or Δ*pdpC* with a complementation plasmid containing the *pdpC* gene. The bar graph represents the mean +/- the standard deviation. Data is a compilation of 3 independent experiments performed in triplicate. ***p<0.005

CHAPTER 3: *FRANCISELLA TULARENSIS* HARVESTS NUTRIENTS DERIVED VIA ATG5-INDEPENDENT AUTOPHAGY TO SUPPORT INTRACELLULAR GROWTH[2]

Overview

Francisella tularensis is a highly virulent intracellular pathogen that invades and replicates within numerous host cell types including macrophages, hepatocytes and pneumocytes. By 24 hours post invasion *F. tularensis* replicates up to 1000-fold in the cytoplasm of infected cells. To achieve such rapid intracellular proliferation, *F. tularensis* must scavenge large quantities of essential carbon and energy sources from the host cell while evading anti-microbial immune responses. We found that macroautophagy, a eukaryotic cell process that primarily degrades host cell proteins and organelles as well as intracellular pathogens, was induced in *F. tularensis* infected cells. *F. tularensis* not only survived macroautophagy, but optimal intracellular bacterial growth was found to require macroautophagy. Intracellular growth upon macroautophagy inhibition was rescued by supplying excess nonessential amino acids or pyruvate, demonstrating that autophagy derived nutrients provide carbon and energy sources that support *F. tularensis* proliferation. Furthermore, *F. tularensis* did not require canonical, ATG5-dependent autophagy pathway induction but instead induced an ATG5-independent autophagy pathway. ATG5-independent autophagy induction caused the degradation of cellular constituents

[2]This chapter was previously published as an article in PLOS Pathogens. The citation is: Steele S, Brunton J, Ziehr B, Taft-Benz S, Moorman N, Kawula T. *Francisella tularensis* harvests nutrients derived via ATG5-independent autophagy to support intracellular growth. *PLoS Pathog*. 2013;9(8):e1003562. doi: 10.1371/journal.ppat.1003562; 10.1371/journal.ppat.1003562.

resulting in the release of nutrients that the bacteria harvested to support bacterial replication. Canonical macroautophagy limits the growth of several different bacterial species. However, our data demonstrate that ATG5-independent macroautophagy may be beneficial to some cytoplasmic bacteria by supplying nutrients to support bacterial growth.

Author Summary

Francisella tularensis is a highly virulent bacterial pathogen that infects hundreds of different animal species including humans. During infection *F. tularensis* bacteria invade and rapidly multiply inside host cells. Within the host cell environment basic nutrients that bacteria require for growth are in limited supply, and the majority of nutrients are tied up in complex molecules that are not readily available in forms that can be used by bacteria. In this study we asked and answered a very simple question; how does *F. tularensis* harvest sufficient carbon and energy sources from the host cell to support rapid intracellular growth? We found that *F. tularensis* induces a host recycling pathway in infected cells. Thus the host cell degrades nonessential proteins and releases amino acids. *F. tularensis* harvests the host-derived amino acids to generate energy and build its own more complex molecules. When we inhibited the host recycling pathway, growth of the intracellular bacteria was limited. Therefore, manipulation of host cell metabolism may be a means by which we can control the growth of intracellular bacterial pathogens during infection.

Introduction

When intracellular bacterial pathogens invade host cells, the bacteria must scavenge energy sources and anabolic substrates from the nutrient-limited intracellular environment. Most

of the potential nutrient sources inside a host cell are stored within complex structures such as lipid droplets, glycogen and proteins that are not immediately available to intracellular pathogens. To obtain nutrients for proliferation, intracellular bacteria must degrade these complex structures into their constituents (fatty acids, carbohydrates and amino acids respectively) or increase nutrient import. The strategies that bacteria use to acquire nutrients could potentially have widespread effects on the host cell. For example, pathogens that import amino acids from the host cell cytoplasm may starve the cell. Host cell amino acid starvation leads to mammalian target of rapamycin (mTOR) inhibition, thereby inhibiting mRNA transcription and other critical cellular homeostatic processes [115]. Thus, nutrient acquisition is an important step in the pathogenesis of intracellular bacteria and is critical to understand how a pathogen interacts with the host.

Autophagy is a highly conserved eukaryotic cell process that can be initiated by a variety of factors such as amino acid starvation, energy depletion, mTOR inhibition and immune signaling [116,117]. Autophagy is a process by which multi-membranous vesicles called autophagosomes surround and degrade cellular constituents (during starvation) or cytoplasmic bacteria (during infection through a related innate immune response termed xenophagy [118]). The autophagosomes fuse with lysosomes to become autolysosomes, which then degrade the engulfed material. During starvation, autophagy can degrade nonessential proteins, thereby releasing free amino acids that are recycled into new proteins and organelles. Current studies of the interactions between host autophagy and intracellular bacterial pathogens are primarily focused on xenophagy [119-121]. However, a few intracellular pathogens are known to benefit from autophagy [122-124]. Autophagosome formation is induced during infection with *Anaplasma phagocytophilum* and the autophagy derived nutrients are harvested and used by *A.*

phagocytophilum to enhance intracellular replication [9]. Likewise, dengue virus uses autophagic byproducts to acquire lipids for viral replication [123,124]. Pathogens such as *Listeria monocytogenes* express active mechanisms that prevent bacterial degradation via xenophagy, yet autophagy still occurs in the infected cell and has the potential to provide nutrient sources for the bacteria [125]. These and other recent studies highlight the potential role of autophagy in providing nutrients or other benefits for intracellular pathogens.

Francisella tularensis is a facultative intracellular bacterium that infects over 200 different species (from amoeba to humans) [126]. The highly virulent *F. tularensis* subsp. *tularensis* Schu S4 strain has an infectious dose of fewer than 25 bacteria and a mortality rate of 30-60% in untreated pneumonic infections [127,128]. *F. tularensis* infects a diverse range of cell types including macrophages, which are a key replicative niche for *F. tularensis* in humans and other susceptible mammals. *F. tularensis* also invades and replicates within several other cell types including epithelial cells and endothelial cells [2,126]. *F. tularensis* enters the host cell through phagocytosis and proceeds to escape the phagosome and replicate in the host cell cytoplasm. By 24 hours post inoculation, *F. tularensis* replicates up to 1000-fold inside host cells. This rapid intracellular replication plays a major role in *F. tularensis* pathogenesis but the mechanisms by which this organism acquires nutrients are not well characterized. Therefore, we sought to determine how these nutrients become available to support efficient *F. tularensis* intracellular replication.

In primary murine macrophages, *F. tularensis* induces the formation of a multi-membranous, autophagosome-like structure termed the Francisella containing vacuole (FCV) through an autophagy related process [74]. FCV formation occurs between 20 and 36 hours post inoculation, after the majority of *F. tularensis* replication has taken place. Blocking FCV formation late during infection does not increase *F. tularensis* proliferation, suggesting that FCV

formation does not play a role in controlling intracellular *F. tularensis* replication [74]. However, the formation of FCVs hints that autophagy may be induced during *F. tularensis* infection. Additionally, replication deficient and chloramphenicol treated *F. tularensis* bacteria, but not wild type *F. tularensis* bacteria, are degraded via canonical autophagy [129]. This observation implies that *F. tularensis* avoids xenophagy. Lastly, treating *F. tularensis* infected macrophages 2 hours post inoculation with chloroquine or autophagy- inhibiting levels of ammonium chloride impairs *F. tularensis* intracellular replication [130-132]. Although chloroquine and ammonium chloride inhibit acidification of cellular compartments and have broad effects on the host cell, these data raise the intriguing possibility that autophagy may contribute to *F. tularensis* intracellular replication.

Taken together these observations suggest that intracellular *F. tularensis* avoids xenophagy yet induces autophagy or an autophagy-like process that contributes to *F. tularensis* proliferation. We therefore examined the potential role of autophagy in aiding *F. tularensis* intracellular growth.

Results

Host cell constituents are sufficient to support F. tularensis intracellular proliferation.

F. tularensis replicates efficiently and rapidly in host cells. Indeed, transmission electron microscopy analysis showed that *F. tularensis* consumed over half of the area of the cell cytoplasm of infected mouse embryonic fibroblasts (MEFs) by 16 hours post inoculation (Figure S1). *F. tularensis* cannot make all of the nutrients it needs *de novo* and must interact with the host to acquire certain metabolites to support rapid proliferation. In particular, *F. tularensis* is auxotrophic for 13 amino acids, some of which mammalian cells also do not synthesize. Thus,

for sustained proliferation within infected cells, the bacteria must either take up amino acids imported by the host cell or degrade host proteins and reuse the resulting amino acids. To distinguish between these possibilities, we determined if decreasing the availability of free amino acids limited *F. tularensis* intracellular growth. We replaced the media on infected MEFs with media lacking amino acids at 3 hours post inoculation. *F. tularensis* replicated to similar numbers with or without amino acids present in the tissue culture media (Figure 3.1A). This result demonstrates that *F. tularensis* can acquire the amino acids it needs to sustain growth directly from the host cell. Since the majority of host amino acids are typically sequestered in proteins inside the cell, protein degradation likely occurs to provide sufficient amino acids to support *F. tularensis* intracellular growth. Additionally, amino acid depletion results in starvation induced autophagy [133]. Starvation induced autophagy will degrade proteins to produce amino acids. Thus, *F. tularensis* may take advantage of host cell autophagy to acquire free amino acids.

Autophagy supplies energy and anabolic substrates that support *F. tularensis* growth in Fibroblasts.

To determine if autophagy had any impact on *F. tularensis* intracellular growth we measured bacterial replication inside cells treated with several different autophagy inhibitors. MEFs were treated with 3-methyladenine (3MA), which inhibits autophagosome formation, thereby blocking autophagy. *F. tularensis* replication inside 3MA treated MEFs was significantly reduced (Figure 3.1B), suggesting that intracellular *F. tularensis* benefit from host cell autophagy. Since autophagy is both a starvation response and a process by which damaged organelles and non-essential proteins are degraded we considered the possibility that *F. tularensis* may scavenge and utilize amino acids released by this process. We therefore wanted to

determine if exogenous amino acid supplementation would rescue *F. tularensis* growth in MEFs that have impaired autophagy function. Indeed, *F. tularensis* intracellular growth in the presence of 3MA was restored by the addition of excess amino acids to the culture media (Figure 3.1B). These results, which were corroborated using confocal fluorescence microscopy of cells infected with GFP-expressing *F. tularensis* Schu S4 (Figure 3.1C) indicate that autophagy provides a source of nutrients that support *F. tularensis* replication.

To determine if degradative autophagy was responsible for optimal bacterial growth, we quantified *F. tularensis* intracellular growth in the presence of Bafimoycin A(1) (Baf) or chloroquine (CQ), each of which inhibits autophagy by blocking functional autolysosome formation. We tested the effect of these drugs on *F. tularensis* replication kinetics by infecting MEFs with *F. tularensis* containing a bioluminescence reporter plasmid (Schu S4-LUX) [134]and measuring luminescence every 30 minutes to determine the bacterial growth kinetics. The limit of detection for this assay was approximately 50 relative light units (RLUs) or approximately 10^5 bacteria in a 96 well format (data not shown). We verified this technique by treating *F. tularensis* infected cells with 3MA or 3MA supplemented with amino acids and saw similar results to the standard intracellular proliferation assays (Figure S2A, S2B). Additionally, CQ significantly reduced *F. tularensis* growth and amino acid supplementation rescued bacterial growth in CQ treated cells (Figure S2C, S2D). Similar to 3MA and CQ, treating MEFs with Baf also significantly reduced *F. tularensis* intracellular growth and growth was rescued with amino acid supplementation (Figure S2E, S2F). None of the inhibitors affected *F. tularensis* growth in broth culture. Although 3MA, CQ, and Baf were each cytotoxic to MEFs, viability was comparable between treatments with and without amino acid supplementation (Figure S3A, S3B). Thus, the

observed rescue was not due to increased eukaryotic cell viability upon amino acid supplementation.

Since all chemical inhibitors have the potential to confer off-target or non-specific effects on host cell processes we wanted to confirm the inhibitor results using genetic approaches. Beclin-1 is required for autophagosome formation in most autophagy pathways [135]. We therefore reasoned that depletion of Beclin-1 should limit bacterial replication if autophagy is required for *F. tularensis* growth. We created two Beclin-1 knock down MEF cell lines, Beclin-1 KD-1 and KD-2 that expressed 63.8% (+/- 14.4%) and 59.2% (+/- 12.9%) of the scrambled shRNA control Beclin-1 mRNA, respectively (Figure S4). Despite the relatively modest reduction of Beclin-1 mRNA *F. tularensis* replication was significantly reduced in the knockdown cell lines compared to the scrambled control (Figure 3.1D); supporting the conclusion that autophagy may have a pro-bacterial role in *F. tularensis* infected cells. Interestingly, the infection frequency of the knock down cell lines was approximately 2-fold higher than the scrambled control (data not shown) suggesting that Beclin-1 activity may modestly impair *F. tularensis* infection of host cells.

Autophagy supports *F. tularensis* replication in primary human monocyte derived macrophages.

During the course of infection *F. tularensis* invade and replicate within many different cell lineages and types. Intracellular growth properties of *F. tularensis* vary depending on host cell type. For example, *F. tularensis* infects monocytes at a significantly higher frequency than epithelial cells or fibroblasts. On the other hand, *F. tularensis* intracellular growth is more prolonged, and achieves nearly 10-fold higher peak numbers in MEFs as compared to

monocytes. Growth within monocytes is a property that is fundamental to *F. tularensis* virulence. *F. tularensis* is also a human pathogen; we therefore wanted to determine the relevance of autophagy in supporting *F. tularensis* growth within human macrophages. Inhibition of autophagy with 3MA significantly decreased *F. tularensis* growth in hMDMs, and growth was rescued in 3MA treated hMDMs by supplementing the media with excess amino acids (Figure 3.1E). Therefore, autophagy provides amino acids that support *F. tularensis* intracellular growth in primary human monocytes, a property that is crucial to *F. tularensis* pathogenesis.

***F. tularensis* infection increases autophagic flux.**

We compared the rate of degradation of long-lived proteins in uninfected and infected cells to determine if *F. tularensis* infection impacted autophagic flux. Since we were attempting to quantify a specific infected host cell response we performed this analysis in the J774 monocyte cell line where the *F. tularensis* infection frequency is much greater than the infection frequency in MEFs (data not shown). We first labeled cellular proteins by incubating J774 cells in media containing ^{35}S methionine and cysteine for 18 hours and chased for 2 hours to remove any remaining labeled free amino acids. The labeled cells were inoculated with *F. tularensis* and incubated for 16 hours. Following infection, infected cells had a 49.5% +/- 7.9% (Average +/- SEM) decrease of ^{35}S label in the TCA insoluble fraction of the cytoplasm (which will primarily contain proteins) compared to uninfected J774 cells (Figure 3.2A). Thus, infected cells had increased turnover of long lived proteins than uninfected cells. This result is consistent with autophagy induction in *F. tularensis* infected J774 cells. The decrease of total ^{35}S label in both host and bacterial proteins in infected cells is also consistent with *F. tularensis* using the majority

of amino acids for energy rather than for protein synthesis, but may indicate that the transfer of amino acids from the host to the bacteria is inefficient. Uninfected and infected J774 cells had similar levels of cytotoxicity at 16 hours post inoculation, indicating that the loss of label in infected compared to uninfected cells was not due to cell lysis (Figure S3D).

Autophagy derived amino acids are transferred from host proteins to *F. tularensis*

To confirm that *F. tularensis* imports amino acids derived from host proteins, we monitored transfer of radiolabeled amino acids from host proteins into bacterial proteins. MEFs were first metabolically labeled with ^{35}S-labeled methionine and cysteine for 18 hours to fully label all host proteins. Then the radiolabel was removed and the cells were incubated in unlabeled media for two hours prior to infection with *F. tularensis* to remove ^{35}S that was not incorporated into protein. At 16 hours post infection (18 hours after the radiolabel was removed) we lysed the MEFs and purified *F. tularensis* by mixing cell lysate from either uninfected or infected cells with magnetic beads linked to an anti- *F. tularensis* lipopolysaccharide (LPS) antibody. We then determined if *F. tularensis* proteins contained radiolabeled amino acids by examining the trichloroacetic acid (TCA) insoluble fraction of purified *F. tularensis*. There was a significant increase of radiolabel in the TCA insoluble, *F. tularensis* bead purified fraction from infected MEFs as compared to uninfected control samples (Figure 3.2B). Indeed, 6.22% +/- 4.15% (average +/- SEM, n=5 samples) of the TCA insoluble radiolabel present prior to infection transferred to the bacteria during the 16 hour infection. To control for possible direct transfer of labeled amino acids that were not incorporated into host proteins we analyzed infected MEFs that were treated with cycloheximide during ^{35}S labeling prior to infection. There were negligible amounts of radiolabel present in the bead purified fraction of cycloheximide treated

cells (Figure 3.2B). *F. tularensis* survived and replicated within cycloheximide pre-treated cells and *F. tularensis* was present in the bacterial purified fraction (data not shown). Thus, host cell lysis due to the cycloheximide treatment was not solely responsible for the lack of radiolabel in the bacterial fraction. ^{35}S radiolabel was primarily incorporated into host proteins, rather than as free ^{35}S labeled amino acids. Taken together, these data demonstrate that *F. tularensis* synthesized proteins using amino acids derived from host cell proteins.

Treating the radiolabeled cells with either Baf or 3-MA resulted in significantly decreased incorporation of the radiolabel by *F. tularensis* (Figure 3.2C). Since *F. tularensis* proliferation is reduced in 3MA and Baf treated MEFs, several fold fewer bacteria were present in the bacteria purified fraction of the treated MEFs (data not shown). Nevertheless, the median ^{35}S counts per bacteria were significantly lower in the 3MA or Baf treated samples compared to untreated samples (untreated: 0.016 CPM/bacteria, 3MA: 0.000 CPM/bacteria, Baf: 0.000 CPM/bacteria [n= 3 experiments done in duplicate]). Therefore, transfer of radiolabeled amino acids to bacterial proteins was reduced by both 3MA and Baf treatment, indicating that under normal culture conditions, amino acids derived by the degradation of host cell proteins via autophagy were used by *F. tularensis*.

F. tularensis uses autophagy by- products primarily for energy.

F. tularensis is capable of using amino acids as an energy source when simple carbohydrates such as glucose are not available (Figure 3.3A). Thus, autophagy derived amino acids could conceivably be used by intracellular *F. tularensis* for either the synthesis of new proteins or to provide energy for other bacterial processes. Although we found that *F. tularensis* uses host-derived amino acids for protein synthesis (Figure 3.2B), the proportion of amino acids

used for protein synthesis as opposed to energy is unknown. To determine if *F. tularensis* uses autophagy-derived amino acids primarily as anabolic precursors or as an energy source, we supplemented autophagy inhibited, *F. tularensis* infected MEFs with either serine or the metabolite pyruvate. Annotation of the *F. tularensis* genome indicates that *F. tularensis* encodes the protein L-serine dehydratase, which degrades serine directly into pyruvate. The addition of either pyruvate or serine alone rescued *F. tularensis* intracellular growth in Baf treated cells (Figure 3B). Fibroblasts cannot convert serine or pyruvate into all of 13 of the amino acids required to fulfill *F. tularensis* auxotrophies. Thus, host autophagy-derived nutrients are used by *F. tularensis* primarily as a source of energy. Although *F. tularensis* can incorporate autophagy derived amino acids into bacterial proteins (Figure 3.2B), these data indicate that energy, rather than amino acids for protein synthesis, was the limiting factor for *F. tularensis* proliferation in autophagy-deficient cells cultured in tissue culture media.

ATG5 is not required for autophagy in *Francisella* infected cells.

Canonical autophagy is typically induced by the inhibition of mammalian target of rapamycin (mTOR) during starvation or upon treatment with either rapamycin or Torin1. Thus, monitoring mTOR activity through downstream substrates such as S6 kinase is likely to correlate well with canonical autophagy induction. To determine if *F. tularensis* infection activates the autophagy signaling cascade, we assessed mTOR activity in infected J774 cells by measuring phosphorylation of the mTOR substrate S6 ribosomal protein. The ratio of phospho- S6 ribosomal protein to unphosporylated S6 ribosomal protein decreased progressively over the course of infection, which is consistent with mTOR inhibition and thus autophagy induction (Figure 3.4A, 3.4B) [136]. However, loss of phospho - S6 ribosomal protein was not evident before

8 hours post inoculation suggesting that mTOR inhibition occurred after some bacterial replication had already taken place.

In the canonical autophagy pathway the protein ATG5 is essential for autophagosome formation. Thus, we would predict that ATG5 expression would be required for autophagic degradation of host proteins to amino acids that support *F. tularensis* intracellular growth. However, it was recently shown that *F. tularensis* replicates efficiently within ATG5$^{-/-}$ macrophages [129]. We also found that F. tularensis replication was not impaired in ATG5-/- MEFs (Figure 3.5A). In fact, there was a slight but statistically significant increase in bacterial replication in ATG5$^{-/-}$ MEFs compared to wild type MEFs (Figure 3.5A). Therefore, ATG5 is not required for efficient *F. tularensis* intracellular proliferation. Treatment of ATG5$^{-/-}$ MEFs with 3MA resulted in decreased bacterial proliferation and bacterial growth was rescued by supplementing treated cells with amino acids (Figure 3.5B). Taken together, these data suggest that *F. tularensis* intracellular growth is supported by nutrients generated by an ATG5-independent autophagy pathway.

Unlike canonical autophagy, ATG5-independent autophagy generates autophagosomes from the trans-Golgi apparatus [17]. Brefeldin A (Bref A) inhibits ATG5-independent autophagosome formation but does not affect canonical autophagosome formation [17]. To determine if ATG5-independent autophagy provides metabolites for *F. tularensis* in macrophages, we measured *F. tularensis* replication in J774A.1 macrophage-like cells (J774 cells) in the presence and absence of Bref A. Cells were infected with Schu S4-LUX and growth was monitored by measuring luminescence every 30 minutes. We found that *F. tularensis* replication was significantly reduced in Bref A-treated J774 cells (Figure 3.5C, D), and growth was significantly rescued in Bref A treated cells by the addition of amino acids (Figure 3.5C,

3.5D). Bref A cytotoxicity was comparable regardless of amino acid supplementation, indicating that the increase in bacterial replication was not due to decreased eukaryotic cell cytotoxicity in amino acid treated cells (Figure S3C). The ability of amino acids to rescue bacterial replication in Bref A-treated cultures indicates that Bref A affects *F. tularensis* nutrient availability. This result is consistent with the conclusion that ATG5-independent autophagy provides nutrients that support F. tularensis growth in macrophages as well as in MEFs.

We wanted to determine the extent to which autophagosomes are formed during *F. tularensis* infection, and the spatial relationship between the bacteria and autolysosomes in $ATG5^{-/-}$ cells. Analysis of transmission electron microscopy (TEM) micrographs revealed that autophagic vacuoles constituted a greater percentage of the cytoplasm in *F. tularensis* infected as compared to uninfected $ATG5^{-/-}$ MEFs (Figure 3.6A-D) confirming that autophagy is induced in $ATG5^{-/-}$ MEFs.

Since morphological analysis of autophagic structures by TEM is inexact, we used fluorescence confocal microscopy as a secondary means to identify acidified autophagic vacuoles in infected MEFs. We stained and quantified the number of LysoTracker Red positive acidic vacuoles in infected and uninfected $ATG5^{-/-}$ MEFs. There were significantly more acidic vacuoles in the infected $ATG5^{-/-}$ MEFs as compared to uninfected $ATG5^{-/-}$ MEFs (Figure 3.6E). LysoTracker Red can also stain other acidic vacuoles including lysosomes and phagosomes. However, the increased number of acidic vacuoles found in infected wild type and $ATG5^{-/-}$ MEFs as compared to uninfected and 3MA treated infected control cells strongly argues that the increase in acidic vacuoles was an increase in autophagic vacuoles. Combined with the morphological analysis of the infected-cell vacuoles by TEM this data demonstrates that *F. tularensis* induced ATG5-independent autophagy in infected cells.

Neither canonical autophagy nor xenophagy are induced during *F. tularensis* intracellular replication.

The slight but statistically significant increase in *F. tularensis* growth observed in ATG5 $^{-/-}$ MEFs suggested that canonical autophagy may be induced in infected cells and exert some control over bacterial growth. It is also possible that in addition to destroying the bacteria, canonical autophagy could serve as a redundant mechanism for nutrient acquisition. To determine if canonical autophagy was induced in addition to ATG5-independent autophagy during infection with *F. tularensis*, we analyzed infected MEFs that were transiently transfected with a GFP-LC3 plasmid for an increase in GFP-LC3 puncta. LC3 puncta formation is stimulated by canonical autophagy; however, ATG5-independent autophagy does not induce LC3 puncta formation [17,137]. LC3 puncta levels were unchanged in infected compared to uninfected MEFs at 16 hours post inoculation, whereas both the amino acid starvation and Torin1 controls conferred an increase in LC3 puncta (Figure 3.7A, B). Thus, it appears that canonical autophagy remained at basal levels in *F. tularensis* infected cells during late stages of infection.

To determine if induction of canonical autophagy would either increase bacterial clearance or generate additional nutrients that support bacterial replication, we artificially induced autophagy throughout infection with the mTOR inhibitor Torin1. Torin1 treatment throughout infection had no impact on *F. tularensis* intracellular survival or growth in MEFs (Figure 3.7C). Thus, *F. tularensis* evades destruction by canonical autophagy and increased canonical autophagy did not benefit *F. tularensis* intracellular replication.

F. tularensis induces ATG5-independent autophagy while canonical autophagy remains at basal levels during infection. Little is known about the functional differences between canonical and ATG5-independent autophagy. However, xenophagy is known to occur via canonical autophagy whereas xenophagy via ATG5-independent autophagy has not been addressed. In canonical autophagy, cytosolic pathogens including chloramphenicol treated *F. tularensis* are targeted for xenophagy when bound to p62/SQSTM1 and polyubiquitin [129,138-140]. We therefore investigated the role of polyubiquitin and p62/SQSTM1 in ATG5 independent autophagy induction in *F. tularensis* infected cells.

There was a significant decrease in the number of polyubiquitin puncta in the cytoplasm of infected wild type and $ATG5^{-/-}$ MEFs as compared to uninfected MEFs (Figure 8A). If polyubiquitin was degraded upon ATG5-independent autophagy induction, we would expect a corresponding increase in co-localization between polyubiquitin and acidic vacuoles in infected cells. However, the number of acidic vacuoles co-localizing with polyubiquitin in uninfected cells (15.2 % +/- 2.2%) and infected cells (20.0% +/- 3.5%) was not significantly different (n >25 cells, mean +/- SEM) (Figure 3.8B). These data indicate that the decrease in polyubiquitin aggregates in infected cells was independent of autophagy.

In addition, there were similar numbers of p62/SQSTM1 puncta in infected MEFs compared to uninfected MEFs (Figure 3.8C, S5C-S5E). Interestingly, although there were similar total numbers of p62/SQSTM1 puncta, there was increased co-localization of p62/SQSTM1 with acidic vacuoles in infected wild type MEFs. However, there was no difference in p62/SQSTM1 co-localization between uninfected and infected $ATG5^{-/-}$ MEFs (Figure 3.8D). The increased co-localization of p62/SQSTM1 with acidic vacuoles may indicate that some basal level of xenophagy is occurring in an ATG5-dependent manner, which is

consistent with the increase in bacterial replication that we observed in ATG5$^{-/-}$ MEFs. Taken together, these data indicate that *F. tularensis* induced ATG5-independent autophagy is not associated with polyubiquitin, LC3B, or p62/SQSTM1.

F. tularensis is adjacent to autophagic vacuoles.

A recent study demonstrated that *Salmonella enterica* associates with ubiquitinated aggregates that are degraded by autophagy [141]. Although these aggregates likely target *S. enterica* for degradation rather than supplying nutrients, these data suggest that mechanisms exist which target autophagosomes to bacteria or vice versa. We hypothesized that *F. tularensis* may recruit autophagic vacuoles putting them in close proximity to facilitate nutrient acquisition. *F. tularensis* was frequently found within 250 nm of autophagic vacuoles in both ATG5$^{-/-}$ MEFs and J774 cells as determined by TEM (Figure S6A, S6B). Indeed, 25.8 +/- 4.0% (average +/- SEM) of the autophagic vacuoles in ATG5$^{-/-}$ MEFs were also within 250 nm of a bacterium. We confirmed the TEM results using confocal microscopy. Since ATG5-independent autophagy does not appear to require ubiquitination or any known target marker, we were limited to examining the relationship between bacteria and acidified vacuoles. Infected cells were stained with LysoTracker Red and Z-stacks from infected cells were analyzed by confocal microscopy. 28.0% +/- 3.7% of bacteria in wild type MEFs and 35.1% +/- 5.1% of bacteria in ATG5 $^{-/-}$ MEFs were within 250 nm of an acidic vacuole (Average +/- SEM, n>10 cells) (Figure S6 C-H). At least 1 bacterium was within 250 nm of an acidic vacuole in every cell. The number of bacteria within 250 nm of an acidic vacuole was significantly lower in 3MA treated MEFs compared to the untreated MEFs (p=.01) (Figure S3 H). These data suggest that *F. tularensis* may recruit or traffic to autophagic vacuoles. Further investigation may reveal that not only autophagy

induction, but also proximity to an autophagic vacuole contributes to *F. tularensis* nutrient acquisition.

Discussion

Intracellular pathogens have evolved to thrive within the hostile nutrient-limited host cell environment. Successful pathogens disarm or avoid innate and adaptive immune responses while simultaneously extracting carbon and energy sources to support their proliferation. Autophagy is a highly conserved degradation process that serves a multitude of functions including cell development, stress response and resistance to cytoplasmic pathogens. Herein we investigated the interaction between *F. tularensis* and the host cell autophagy response. Our results demonstrate that ATG5-independent autophagy is triggered in *F. tularensis* infected cells and that intracellular bacterial replication was enhanced by this process. Furthermore, *F. tularensis* can replicate in cells when there are no amino acids present in the media, indicating that *F. tularensis* obtains all of the amino acids necessary to fulfill its 13 amino acid auxotrophies from the host cell through processes such as autophagy. *F. tularensis* acquires amino acids, and possibly other nutrients, via autophagy. These nutrients are then used for both energy and protein synthesis, although decreased bacterial replication in ATG5-independent autophagy deficient cells is primarily due to a lack of available energy. Autophagy derived nutrients are necessary for optimal *F. tularensis* replication, but *F. tularensis* still replicated in ATG5-independent autophagy deficient MEFs. This indicates that *F. tularensis* uses other nutrient acquisition strategies in conjunction with ATG5-independent autophagy to supply nutrients for rapid and efficient proliferation.

Rapid bacterial proliferation requires readily available and abundant carbon and energy sources, commodities that are typically limited in the eukaryotic cell environment. Intracellular pathogens must acquire all required nutrients from the host cell, but the strategies that these pathogens employ to accomplish this task are only beginning to be characterized and vary widely between pathogens [123,124,142-144]. For example, *Legionella pneumophila* uses the byproducts of host proteosomal degradation rather than autophagy to obtain amino acids for energy [142]. Dengue virus growth is supported by autophagy mediated release of lipids while autophagosome formation increases nutrient availability for *Anaplasma phagocytophilum* [123,124]. It is likely that other intracellular pathogens that successfully avoid autophagic destruction benefit from the nutrients that are released by this process. Thus, autophagy subversion through various means may be a more common strategy for pathogens to acquire nutrients from the host than previously thought.

The conclusion that autophagy derived amino acids were sufficient to rescue intracellular growth was supported by the fact that the absence of amino acids in tissue culture media did not appreciably affect *F. tularensis* intracellular replication. Thus, host cell amino acid import was not required to support bacterial growth. This result would seem to contradict the recent observation that knocking down expression of the amino acid transporter SLC1A5 decreases *F. tularensis* LVS growth approximately 2-fold [143]. LVS is an attenuated *F. tularensis* vaccine strain that, like fully virulent *F. tularensis*, grows within macrophages and other cell types, but is significantly less virulent than *F. tularensis* and other wild type *F. tularensis* strains in humans and animal models of infection. Unlike *F. tularensis* Schu S4, we found that LVS intracellular growth was significantly impaired in ATG5$^{-/-}$ MEFs and growth in these cells was restored by supplying excess amino acids, implying that LVS harvests nutrients via ATG5-dependent

autophagy or another ATG5-dependent mechanism (data not shown). It is therefore likely that LVS is less reliant on ATG5-independent autophagy to support efficient intracellular growth. It is also possible that SLC1A5 contributes to the export of free amino acids out of autolysosomes thereby making autophagy derived amino acids available to the cytoplasmic bacteria. Amino acid transporters export amino acids from autolysosomes to the cytosol in *Saccharomyces cerevisiae*, and a similar system likely exists in mammalian cells [145]. This latter possibility highlights the fact that currently little is known about how free amino acids derived from autophagic degradation of host proteins are transported within eukaryotic cells.

Canonical autophagy destroys several different pathogens, including replication deficient and chloramphenicol treated *F. tularensis* [129]. The slight increase in bacterial replication in ATG5 $^{-/-}$ MEFs compared to wild type MEFs supports the notion that canonical autophagy can degrade wild type bacteria in MEFs, although this may be cell type specific as there is no difference in *F. tularensis* replication between wild type and ATG5 $^{-/-}$ bone marrow derived macrophages [129]. Also, induction of autophagy by starvation or Torin1 treatment did not reduce bacterial replication. Surprisingly, although we saw mTOR inhibition in J774 cells and autophagy induction in ATG5 $^{-/-}$ MEFs, our results suggest that canonical autophagy is either at or close to basal levels 16 hours post inoculation. Our results suggest that *F. tularensis* suppresses canonical autophagy downstream of mTOR or that mTOR is inhibited in ATG5-independent autophagy and other signals help determine which autophagy pathway is induced.

In contrast to xenophagy via canonical autophagy, ATG5-independent autophagy is involved in the lifecycle of two other intracellular bacterial pathogens. *Mycobacterium marinum* and *Brucella abortus* are each sequestered into an autophagosome-like structure via an ATG5-independent pathway as part of their intracellular lifecycles [122,146]. It is unclear why *M. marinum*

is sequestered, but bacterial sequestration by autophagy appears to be part of the *B. abortus* intracellular lifecycle and may benefit the bacteria by increasing cell to cell spread rather than providing nutrients [122,146]. Both of these interactions with ATG5-independent autophagy are different from that of *F. tularensis*. What remains to be determined is if this difference is due to bacterial manipulation, if there are multiple ATG5-independent autophagy pathways, or if there are different functions for the same ATG5-independent autophagy pathway. Unfortunately, there is little information about how the various autophagy pathways are functionally different. We found that ATG5-indepdendent autophagy, unlike canonical autophagy, does not appear to use two proteins associated with xenophagy during infection. Further characterization of how xenophagy and ATG5-independent autophagy are associated may reveal why certain pathogens induce ATG5-independent autophagy.

Little is known about how ATG5-independent autophagy is induced or the role that it plays in a healthy eukaryotic cell, let alone during pathogenesis. However, there appears to be distinct benefits for certain pathogens to induce ATG5-independent autophagy over the canonical autophagy pathway. Determining how this pathway is induced in *F. tularensis* infected cells will give us insight as to how different autophagy pathways are initiated and how these pathways differentially impact intracellular pathogen survival and growth.

Materials and Methods

Bacteria and Plasmids

Francisella tularensis subsp. *tularensis* Schu S4 was obtained from Biodefense and Emerging Infections Research Resources Repository. For inoculation of eukaryotic cells Schu S4, Schu DsRed, Schu S4-GFP [2] and Schu S4 – LUX (plasmid from [134]) were each grown initially on

chocolate agar supplemented with 1% isovitalex then overnight in Chamberlain's defined broth media (CDM).

Cell Culture

J774A.1 (J774) cells were maintained in 4.5 g/L glucose Dulbecco's minimal essential media (DMEM) with 10% FBS and supplemented with L-glutamine and sodium pyruvate. Mouse embryonic fibroblasts (MEFs) were maintained in 4.5 g/L glucose DMEM with 10% FBS. For treatment of MEFs without amino acids, DMEM with 4.5 g/L glucose was made following the ATCC DMEM protocol without adding amino acids and supplemented with 10% dialyzed FBS.

Human monocyte derived macrophages (hMDMs) were obtained by isolating peripheral blood mononuclear cells (PBMCs) from blood via ficoll gradient centrifugation. PBMCs were cultured for 2 hours in RPMI with 10% FBS and then washed to remove non-adherent cells. The adherent cells were cultured for 2 weeks in RPMI containing 10% FBS and 3ng/ml GM-CSF (Biolegend). The media was replaced every 2 days. Experiments were performed using PBMCs isolated from peripheral blood from 2 healthy volunteers who gave informed, written consent following a protocol approved by the Institutional Review Board for human volunteers at University of North Carolina at Chapel Hill. Peripheral blood was obtained specifically for these experiments.

Stable Beclin-1 knockdown (TRCN0000087291 or TRCN0000087291) and scramble cell lines were generated by transducing MEFs with lentivirus encoding each shRNA. Cells were propagated in media containing 1 μg/ml puromycin for 2 weeks prior to the first experiment to select for transduced cells. Concurrent with the first experiment and last intracellular bacterial

proliferation assay in the knockdown cell lines, mRNA was harvested from the transduced cells, subjected to reverse transcription, and was analyzed by quantitative RT-PCR to determine the amount of Beclin-1 mRNA present in each sample. The results were normalized to a GAPDH control. Primer sequences in Supplemental Table 1.

Drug Treatments

3-methyladenine (10 mM) (Sigma), bafilomycin A(1) (200 nM) (Sigma), and chloroquine (160 μM) (Sigma) were each added with 25 μg/ml of gentamicin to the MEFs 3 hours post bacterial inoculation. Brefeldin A (17 μM) (Sigma) was added to J774 cells 3 hours post inoculation. Torin1 (250 nM) (Tocris Biosciences) was added overnight prior to inoculation and maintained throughout the infection. The excess amino acid mixture (12 mM L-amino acids containing aspartic acid, arginine, cysteine, histidine, isoleucine, leucine, lysine, methionine, proline, serine, threonine, tyrosine, and valine), L- serine (15 mM) or pyruvate (18 mM) were added at the same time as the inhibitors. All media was brought to a pH of 7.5.

Inhibitor cytotoxicity in MEFs was determined using a Live/Dead Fixable Green Dead Cell Stain kit (Invitrogen) following the manufacturer's instructions. Drugs were placed on cells for the same duration they would be on cells during infection (21 hours for Baf and CQ, 29 hours for 3MA). Percent cytotoxicity by flow cytometry was determined by gating. Cytotoxicity of *F. tularensis* in J774 cells 16 hours post inoculation was determined by testing the amount of lactate dehydrogenase (LDH) in the supernatant with a CytoTox-Glo cytotoxicity kit (Promega) following the manufacturer's instructions. Percent cytotoxicity was determined based on media and digitonin treated controls. Brefeldin A cytotoxicity was determined 21 hours post treatment using an *In vitro* Toxicology Assay Kit (Sigma) to measure LDH release from J774 cells.

Intracellular Growth Assays

MEFs were plated at $2x10^5$ cells per well in 24 well tissue culture treated plates and grown overnight. MEFs were inoculated with a multiplicity of infection (MOI) of 100 with wild type Schu S4. The media was removed 3 hours post inoculation and replaced with media containing 25 µg/ml of gentamicin to inhibit the growth of any remaining extracellular bacteria. MEFs were lysed by vortexing for 1 minute and the lysates were serially diluted and plated on chocolate agar to calculate the number of intracellular bacterial cells at the indicated times. hMDM cells were inoculated with an MOI of 100 wild type Schu S4 in RPMI containing 10% FBS. At 2 hours post inoculation, the media was replaced with media containing 10 µg/ml of gentamicin. At 4 hours post inoculation, the media was replaced with media that did not contain gentamicin. Intracellular bacteria were quantified as described previously.

Bacterial intracellular growth kinetics was calculated by measuring luminescence of Schu S4 – LUX infected MEFs or J774 cells. MEFs and J774 cells were plated at $5x10^4$ cells per well in 96 well black wall clear bottom polystyrene plates (Corning) the night before infection. Each well was inoculated at an MOI of 100 with Schu S4- LUX and treated with gentamicin and inhibitors as described above. Luminescence was measured every 30 minutes using an Infinite M200 Pro plate reader (Tecan) maintaining constant 37°C temperature and 5% carbon dioxide. All intracellular growth assays were performed in triplicate for each independent experiment. All of the inhibitors were added 3 hours post inoculation to reduce the impact of the inhibitors on *F. tularensis* phagosomal escape.

Growth Curves

Bacterial growth curves of broth cultures were generated by measuring the optical density at 600 nm (OD600 every 15 minutes) using an Infinite M200 Pro plate reader (Tecan) maintaining constant temperature (37°C). To test toxicity of each drug on Schu S4, the bacteria were grown in CDM overnight, and then diluted to an OD600 of 0.05 in CDM containing the indicated inhibitors. CDM glucose substitution media were made without added glucose and 30 mM of the defined amino acid or carbon source. 50 mM MES buffer was added to all CDM media in the glucose substitution experiments.

Fluorescence Microscopy

For confocal fluorescent microscopy images depicting the number of bacteria in drug treated cells, MEFs were plated at $1x10^4$ cells per well in an 8 well chamber slide (Nunc) and grown overnight. MEFs were inoculated at a MOI of 100 with Schu S4-GFP or Schu S4- DsRed and treated with 25 µg/ml of gentamicin as described above. At the indicated time post inoculation, the MEFs were washed and fixed with 4% paraformaldehyde for 15 minutes and then washed again in PBS. To stain the plasma membrane, 10 µg/ml of AF647 conjugated wheat germ agglutinin (Invitrogen) was added to the fixed cells for 5 minutes and then washed away. DAPI containing mounting media (Vector Shield) was added to the slides to identify the nucleus. Infection frequency was determined by fixing GFP infected MEFs 5 or 6 hours post inoculation and comparing the number of cells containing green puncta to the total number of cells completely within the field of view.

To quantify LC3B puncta, GFP-LC3 MEFs were generated by transfecting MEFs attached to an 8 well chamber slide (Nunc) with an eGFP-LC3 plasmid (Addgene plasmid

21073) [137]. 18 hours after transfection, the media was replaced with fresh media for one hour. After one hour, the cells were either infected with Schu-DsRed or placed in fresh media. 3 hours post inoculation, the media in all wells was replaced with media containing 25μg/ml gentamicin. 14 hours post inoculation, Torin1 or media lacking amino acids was added to the appropriate wells. The cells were fixed as above and stained with a mouse anti-GFP antibody (1:250 dilution, Millipore) followed by an AF488 anti-mouse secondary antibody (Invitrogen) as previously described.

To quantify acidic vacuoles and determine co-localization with polyubiquitin and p62, MEFs were initially prepared as described above but were incubated for 2 hours in the presence of 150 ng/ml of LysoTracker red (Invitrogen) beginning at 14 hours post inoculation. The cells were washed and MEF media was added for an additional 10 minutes at 16 hours post inoculation. The cells were fixed in 4% paraformaldehyde and treated with 10 mM ammonium chloride following fixation. The MEFs were incubated with a polyubiquitin antibody (1:1000 dilution, Enzo Life Sciences) or a p62/SQSTM1 primary antibody (1:250 dilution, Abnova) followed by an AF647 conjugated anti-mouse secondary antibody (Invitrogen). DAPI containing mounting media (Vector Shield) was added to the slides to identify the nucleus. Images were acquired using a Zeiss 700 confocal laser scanning microscope (Carl Zeiss SMT, Inc.). Image acquisition, contrast adjustments, and cropping were all performed using Zen 2011 (Carl Zeiss SMT, Inc.).

Acidic vacuoles, p62, and polyubiquitin puncta were quantified by setting thresholds using ImageJ [114]. Only polyubiquitin puncta outside of the nucleus were counted. Co-localization of p62 or ubiquitin puncta with acidic vacuoles was determined by manual counting overlap.

Any acidic vacuole or bacteria that overlapped any portion of the puncta was considered to co-localize.

To determine the distance between acidic vacuoles and *F. tularensis*, Z-stacks of LysoTracker red stained cells were taken using a Flow View 500 confocal laser scanning microscope (Olympus America). The distance between the bacteria and the acidic vacuoles was determined using ImageJ [114]and Corsen [147], following the protocols described in Jourdren et al. Additional protocol information and ImageJ plug-ins were available at http://transcriptome.ens.fr/corsen. The distance between objects was measured from the surface of the bacteria to the closest surface of the nearest acidic vacuole. To decrease the impact of noise, acidic vacuoles and bacteria with a volume of less than 0.05 µm (as determined by the Corsen program) were not included in the analysis.

Radiolabel Experiments

To monitor transfer of amino acids from the host cell to *F. tularensis*, $4x10^5$ MEFs were incubated in cysteine and methionine free DMEM containing 10% dialyzed FBS and 0.125 mC of S^{35} radiolabeled cysteine and methionine (EasyTag Express ^{35}S, Perkin-Elmer) for 18 hours. 10 ug/ml of cycloheximide was added with the radiolabel in the indicated sample. The MEFs were then washed once and then incubated with DMEM containing 10% FBS for 2 hours. DMEM contains in excess of 100,000 times more cysteine and methionine than the initial radiolabel. The MEFs were then inoculated with *F. tularensis* Schu S4 at an MOI of 100 for 3 hours in fresh media. At 3 hours post inoculation, the media was replaced with media containing 25 ug/ml of gentamicin and either Baf or 3MA, as indicated, and supplemented with either a 12 mM amino acid mixture or 18 mM serine. The cells were washed in PBS, scraped from the plate,

and lysed by vortexing the in PBS 16 hours post inoculation. The cell lysates were mixed with streptavidin coated magnetic beads (Solulink) that were pre-bound to biotinylated anti-*F. tularensis* lipopolysaccharide antibody (US biological). The anti-*F. tularensis* LPS antibody was biotinylated using a Biotin-xx protein labeling kit following the manufacturer's instructions (Invitrogen). The bead lysate mixture was incubated at room temperature for 20 minutes and then washed three times on a magnet. After the final wash, an equal volume of beads was added to 20% trichloroacetic acid (TCA) to make a final concentration of 10% TCA. The TCA mixture was mixed with an equal volume of 5% BSA and spun to pellet the TCA insoluble fraction. The TCA soluble fraction was removed and the TCA insoluble fraction was resuspended in PBS, added to scintillation fluid, and the number of counts was measured. An aliquot of the sample after the final wash was plated on chocolate agar to determine the number of bacteria present. The percent of radiolabel that was incorporated into *F. tularensis* was calculated by dividing the radiolabel counts from samples taken immediately prior to infection by the difference between the infected and uninfected samples.

To evaluate host protein degradation, J774 cells were radiolabeled for 24 hours, chased with non-radioactive media, inoculated and treated with gentamicin as described above. At 16 hours post inoculation, the cells were washed in PBS and lysed in RIPA buffer. The lysate was spun immediately to pellet the insoluble fraction. The soluble fraction was harvested and added to an equal volume of 20% TCA. The TCA insoluble fraction was then prepared and quantified as above.

Electron Microscopy

Uninfected and Schu S4 infected J774 cells or ATG5 $^{-/-}$ MEFs were maintained on small plastic tissue culture dishes. 25 µg/ml of gentamicin was added 2 hours post inoculation for J774 cells and 3 hours post inoculation for MEFs. 16 hours post inoculation the cells were fixed for 1 hour at room temperature in 2% paraformaldehyde, 0.5% glutaraldehyde in 0.15 M sodium phosphate buffer at pH 7.4. The cells were then rinsed in buffer and post-fixed with 0.5% osmium tetroxide/0.15 M sodium phosphate buffer, pH 7.4, for 10 minutes.

TEM samples for J774 cells were prepared similarly, although the cells were post-fixed for 1 hour in 1% osmium tetroxidein 0.15 M sodium phosphate buffer at pH 7.4 and then stained *en bloc* with 2% aqueous uranyl acetate for 20 minutes.

Both fixed samples were dehydrated in ethanol (30%, 50%, 75%, 100%, 5 minutes each step) and infiltrated and embedded in L.R. White Resin (Electron Microscopy Sciences). The dehydrated samples were sectioned en face (parallel to the substrate) at 70 nm, mounted on 200 mesh nickel grids, and post-stained with 4% uranyl acetate followed by Reynolds' lead citrate. Samples were observed with a LEO EM910 transmission electron microscope operating at 80 kV (Carl Zeiss SMT, Inc.) and digital images were acquired using a Gatan Orius SC1000 CCD Digital Camera with Digital Micrograph 3.11.0 (Gatan).

Western Blot Analysis

For the phospho- S6 ribosomal protein western blots, J774 cells were inoculated with Schu S4 at an MOI of 100 and treated with 25 µg/ml gentamicin 2 hours post inoculation. The uninfected sample had media replaced and media containing gentamicin added at the same times as infected samples. The uninfected samples were harvested 24 hours post inoculation. At the

indicated times, cells were lysed by adding water containing phosphatase (Roche) and protease inhibitor cocktails (Pierce) and vortexing. The lysates were filtered through two 0.22 μm filters, separated on an SDS-PAGE gel under reducing conditions and then transferred to a nitrocellulose membrane. The membranes were probed with rabbit anti- S6 ribosomal protein or rabbit anti- phospho S6 ribosomal protein (Ser 235/236). All primary antibodies were obtained from Cell Signaling Technologies. Membranes were then probed with a horse radish peroxidase conjugated goat anti-Rabbit IgG (KPL) and bands were detected using an ECL Western Blotting Detection Kit (GE Life Sciences). Densitometry analysis was performed using ImageJ and comparing the amount of phosphor S6 ribosomal protein to the total amount of S6 ribosomal protein at the same time point [114]. The densities were then normalized to the uninfected sample.

Data Analysis

Fold change was determined by subtracting each sample from the average of 3 samples taken at 5 hours post inoculation and a Mann-Whitney test was used to determine significance. The rest of the bacterial proliferation assays were pooled across experiments, $\log_{10}$ transformed, and then analyzed by a two-tailed Student's t-test were used to measure statistical significance. Significance for bacterial kinetic experiments was performed by pooling the maximum luminescence of each replicate for each experiment and performing a Mann-Whitney test. Statistical significance for the distance measurement between *F. tularensis* and acidic vacuoles was performed using a two tailed Student's t-test on the pooled distance measurements across all 3 experiments for each sample. Significance for radiolabel incorporation into *F. tularensis* was determined by a Mann-Whitney test. All data represents data pooled from 3 independent experiments unless otherwise stated.

Morphology analysis was performed on the transmission electron micrographs by outlining the whole cell, nucleus, and each bacteria or autophagic vacuole in ImageJ to determine the area of each [114]. Morphology was determined with the aid of the following references [148-150]. Any rips in the slice were excluded from this analysis. Each micrograph depicted the nucleus and all infected cells had at least one bacteria present in the slice. The area of cytoplasm was determined by subtracting the area of the nucleus and bacteria from the area of the whole cell. At least 20 cells of each sample were examined and significance was determined by a two tailed Student's t-test.

Figures

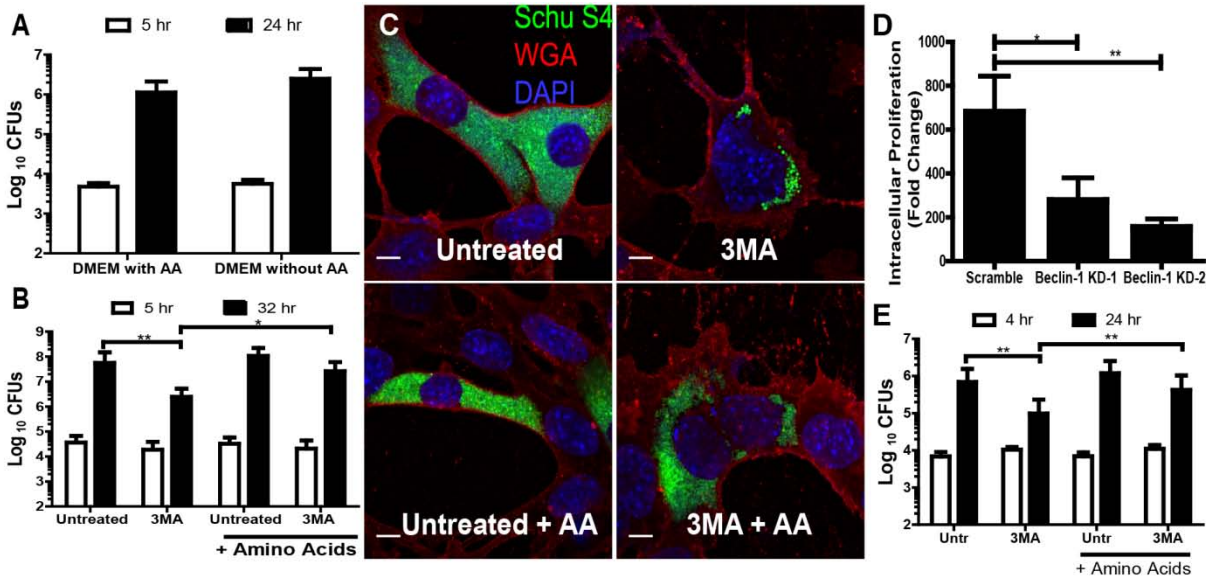

Figure 3.1: Autophagy derived nutrients enhance F. tularensis intracellular growth.

(A) Intracellular bacterial proliferation was measured in MEFs cultured in DMEM with or without amino acids (mean +/- SD, 4 independent experiments). **(B)** Intracellular bacterial proliferation in untreated and 3MA (10 mM) treated MEFs with or without amino acid supplementation (AA) (mean +/- SD, 3 independent experiments) (* $p<0.05$, **$p<0.01$ by Student's t-test). **(C)** Representative confocal microscopy images of infected MEFs 24 hours post inoculation that were untreated, 3MA treated or each treatment with amino acid supplementation. Each scale bar represents 10 µm. GFP- Schu S4 bacteria are depicted in green, DAPI in blue, and wheat germ agglutinin (WGA) in red. **(D)** Intracellular bacterial proliferation in MEFs transduced with a scrambled control or one of two different shRNA's to Beclin-1 (mean +/- SD, 5 independent experiments). (* $p<0.05$, **$p<0.01$ by Mann-Whitney test).

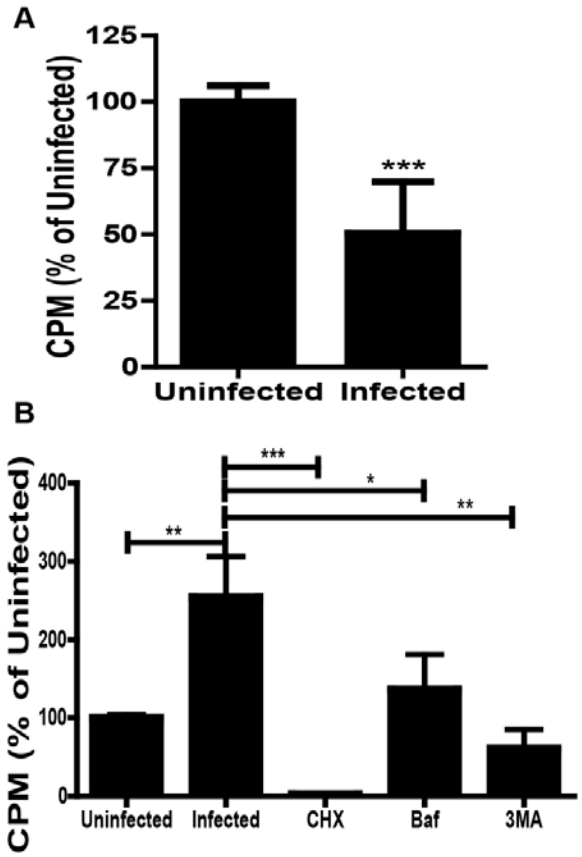

Figure 3.2: F. tularensis harvests amino acids via host cell autophagy.

(A) S35 counts in the TCA insoluble fraction of uninfected or infected J774 cells 16 hours post inoculation (mean +/− SEM, 3 independent experiments). **(B)** S35 counts in the bead purified F. tularensis fraction that was TCA insoluble from either uninfected MEFs or F. tularensis infected MEFs exposed to the indicated treatments (mean +/− SEM, 6 independent experiments) (* $p<0.05$, ** $p<0.01$, *** <0.001).

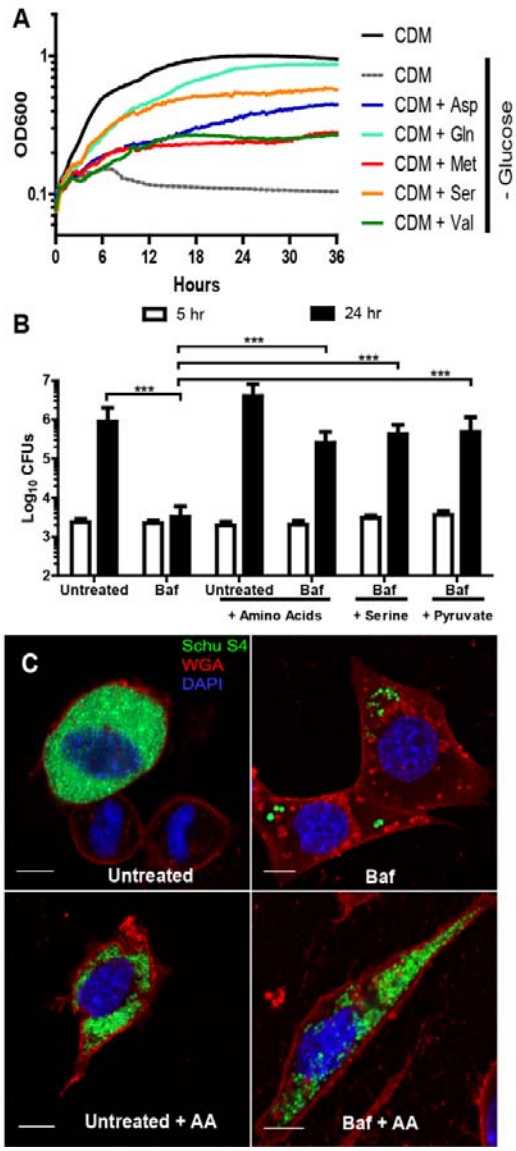

Figure 3.3: F. tularensis uses autophagy derived nutrients for energy and anabolic substrates.

(A) Representative experiment of *F. tularensis* growth in Chamberlin's defined media (CDM) without glucose supplemented with 30mM of a specific amino acid or carbon source (each point represents an average of triplicate wells, 3 independent experiments). **(B)** Intracellular proliferation assay of untreated or Baf (200 nM) treated MEFs. MEFs were supplemented with a 12 mM amino acid mixture, 15 mM serine, or 18 mM pyruvate (mean +/- SD, 3 independent

experiments). **(C)** Representative confocal microscopy images of infected MEFs 24 hours post inoculation that were untreated, Baf treated or each treatment with amino acid supplementation. Each scale bar represents 10 μm. GFP- Schu S4 bacteria are depicted in green, DAPI in blue, and wheat germ agglutinin (WGA) in red. (***$p<0.001$ by Student's t-test)

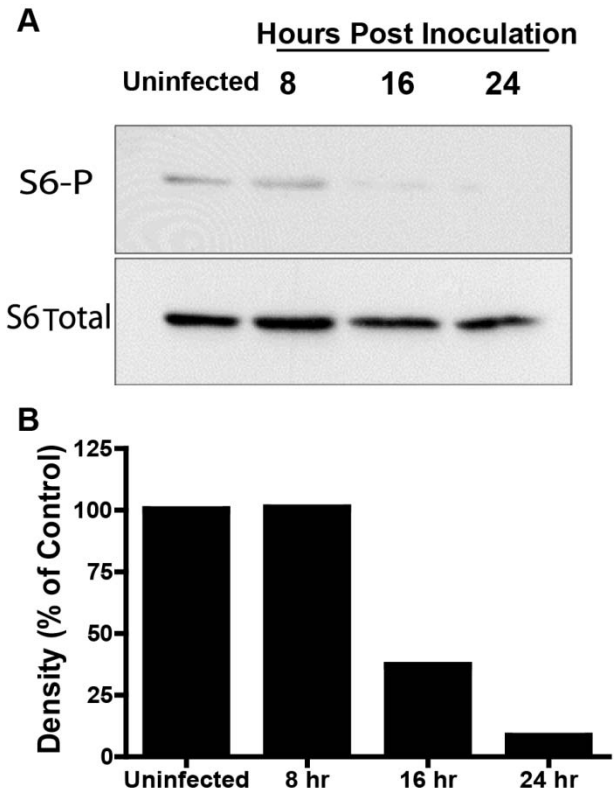

Figure 3.4: S6-P is reduced in F. tularensis infected cells.

(**A**) A representative immunoblot of S6 ribosomal protein phosphorylation states from J774 cells uninfected and over the course of infection (3 independent experiments). (**B**) The ratio of phosphorylated ribosomal S6 to total ribosomal S6 as determined by densitometry from panel B. Densities were normalized to total ribosomal S6 protein using ImageJ and expressed as a percentage of the uninfected control.

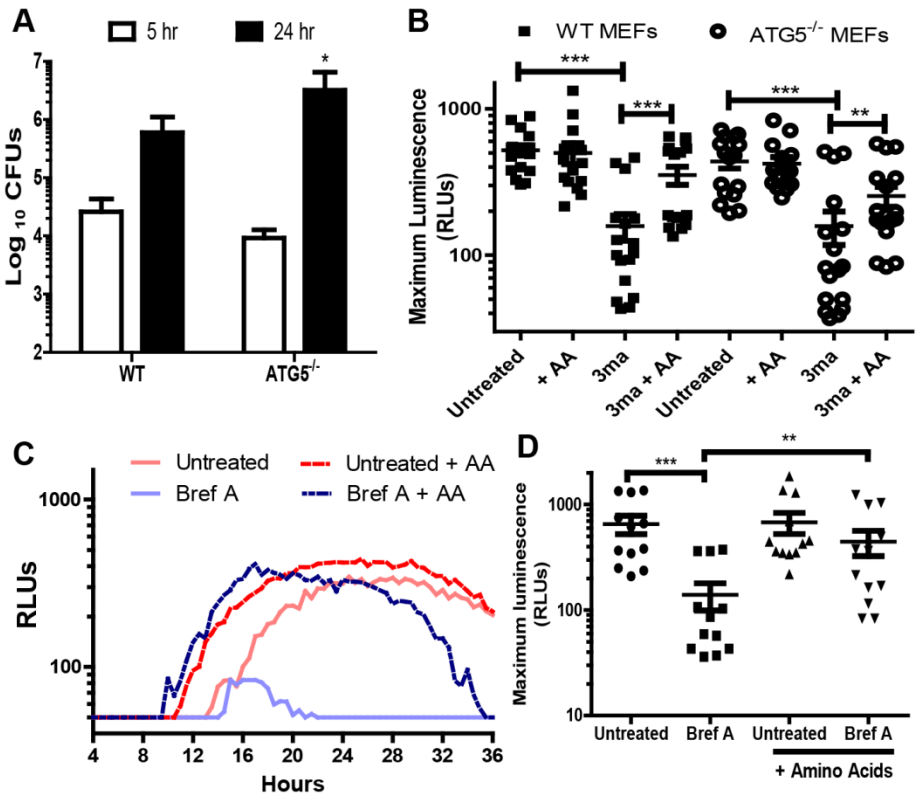

Figure 3.5: ATG5 is not required for efficient F. tularensis intracellular replication.

(**A**) Number of intracellular *F. tularensis* 5 and 24 hours post inoculation of wild type and ATG5$^{-/-}$ MEFs (mean +/− SD, 3 independent experiments). (**B**) Maximum luminescence values expressed in relative light units (RLUs) from kinetic growth assays for Schu S4 –LUX infected wild type or ATG5$^{-/-}$ MEFs treated with 3MA and supplemented with amino acids as indicated (mean +/− SEM, 6 independent experiments). (**C**) Representative intracellular bacterial growth kinetics of *F. tularensis* Schu S4 LUX in untreated and brefeldin A treated J774 cells with or without amino acid supplementation (each point represents an average of triplicate wells) as measured by luminescence (3 independent experiments). (**D**) Maximum luminescence values expressed in relative light units (RLUs) from kinetic growth assays for Schu S4 LUX infected J774 cells untreated and treated with brefeldin A (4 independent experiments). (* $p<0.05$, ** $p<.01$, *** $p<0.001$).

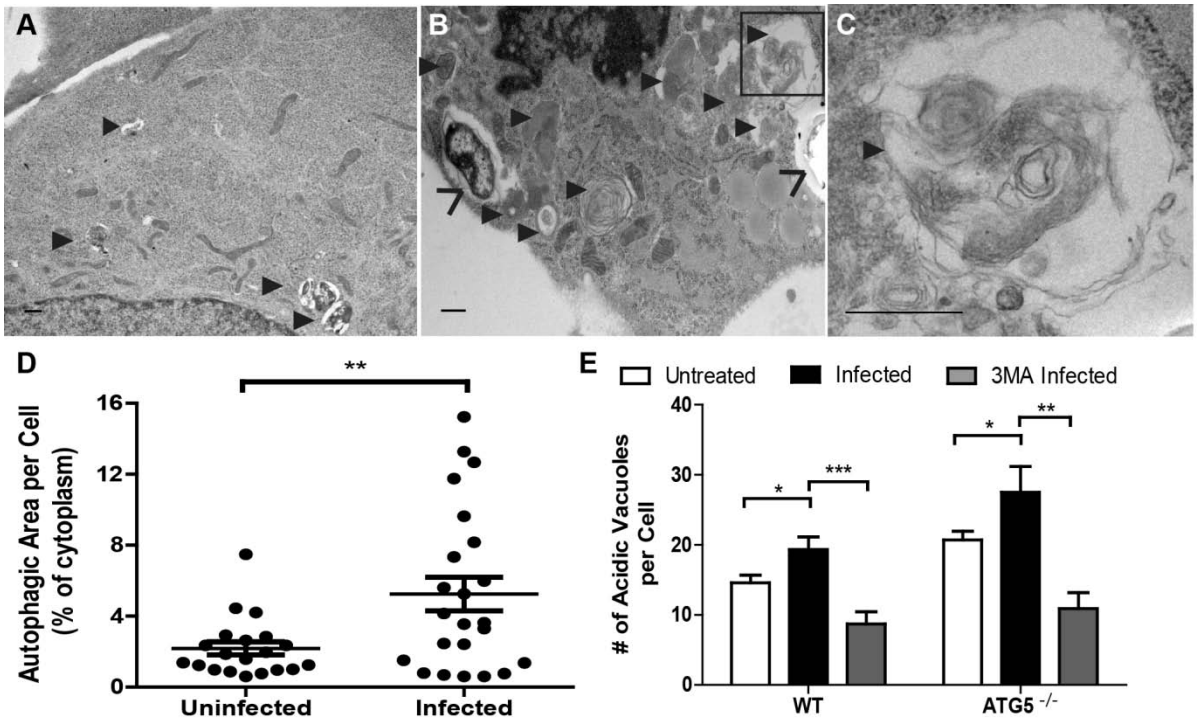

Figure 3.6: F. tularensis induces ATG5-independent autophagy in late logarithmic growth. Representative transmission electron micrographs of **(A)** uninfected and **(B)** infected ATG5 $^{-/-}$ MEFs. **(C)** Higher magnification of representative infected MEF. *F. tularensis* is depicted with open faced arrows (>) and autophagosomes with solid arrows (►).All scale bars represent 0.5 um. **(D)** The percentage of cytoplasm that is autophagic in ATG5 $^{-/-}$ MEFs in uninfected and infected cells (• represents 1 cell, n ≥20 per sample). **(E)** The number of acidic vacuoles per cell in wild type and ATG5 -/- MEFs. MEFs were uninfected, infected, or infected and treated with 10 mM 3MA (mean +/- SEM, n>30 cells per sample). (* $p<0.05$, ** $p<0.01$, *** $p<0.001$ by Student's t-test)

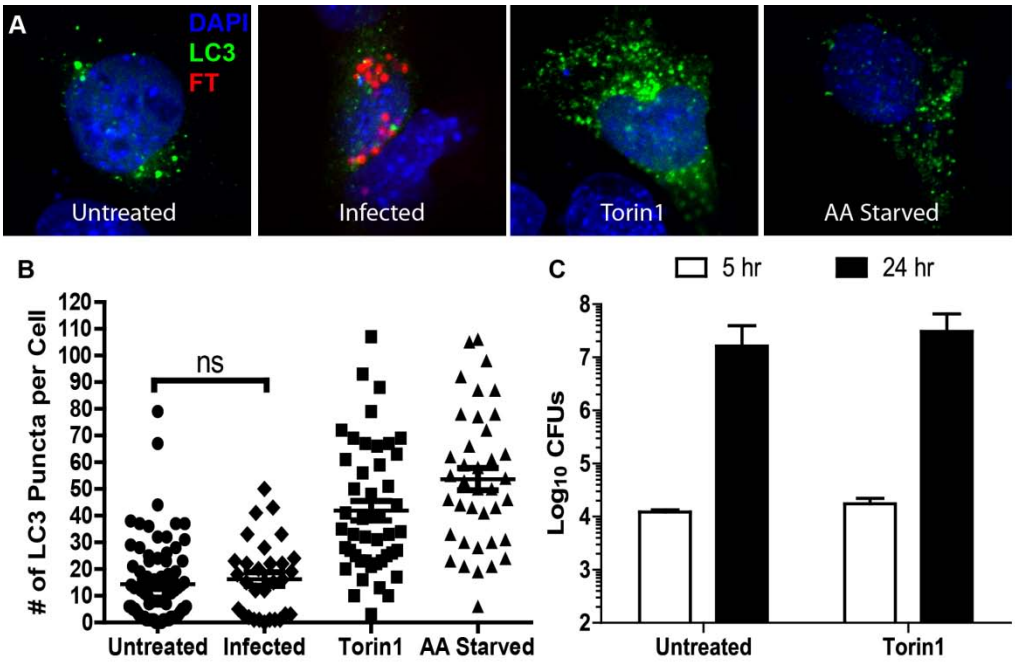

Figure 3.7: F. tularensis does not induce canonical autophagy during late logarithmic phase of intracellular growth.

(**A**) Representative confocal microscopy images depicting LC3-GFP transfected MEFs with the indicated treatments. DAPI is represented in blue, LC3 in green, and *F. tularensis* in red. (**B**) The number of GFP puncta in LC3-GFP transfected MEFs that were untreated, infected for 16 hours, Torin1 treated for 2 hours, or amino acid starved for 2 hours (mean +/− SEM, n>30 cells per sample, 4 independent experiments). (**C**) Number of intracellular *F. tularensis* 5 and 24 hours post inoculation of untreated or Torin1 treated MEFs (mean +/− SD, 3 independent experiments). (ns $p>0.05$).

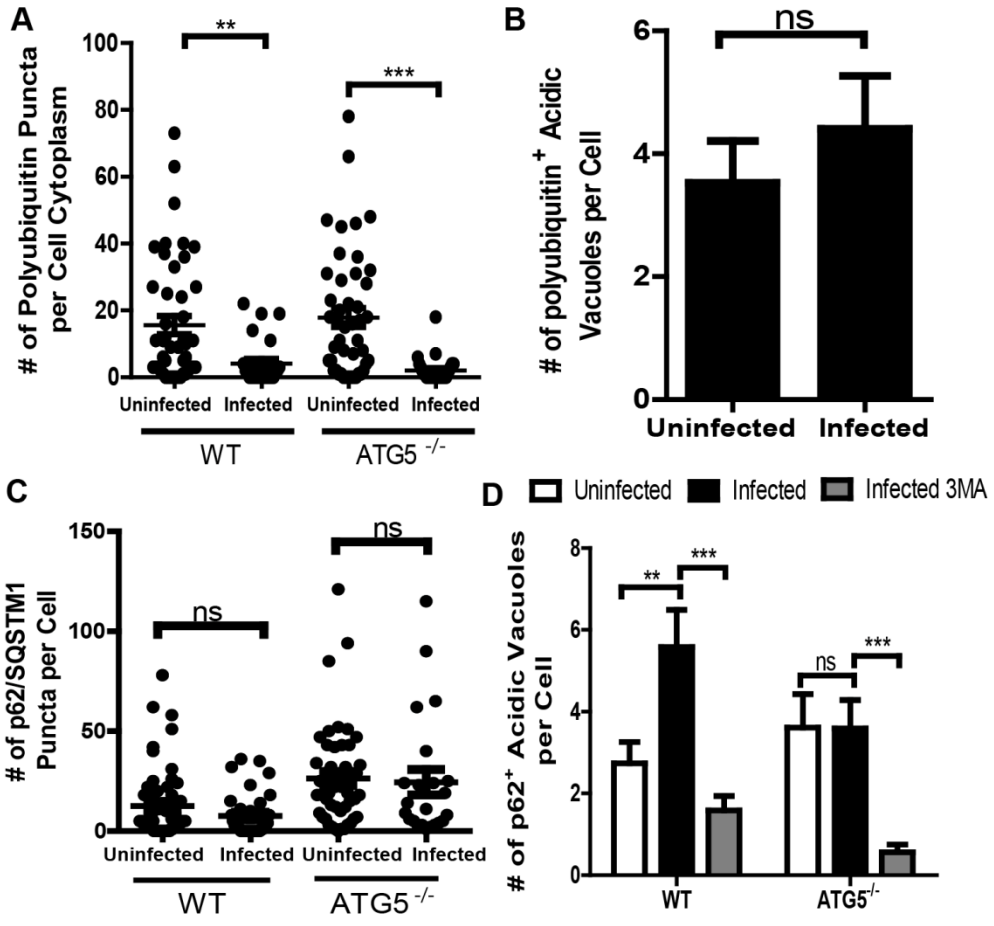

Figure 3.8: p62/SQSTM1 and polyubiquitin are not required for F. tularensis induced ATG5-independent autophagy

(**A**) The number of polyubiquitin puncta in the cytoplasm of uninfected and *F. tularensis* infected wild type and ATG5$^{-/-}$ cells 16 hours post inoculation (• represents 1 cell, n≥25 per sample, 3 independent experiments). (**B**) The number of acidic vacuoles that co-localized with a polyubiquitin puncta per cell in uninfected and *F. tularensis* infected wild type MEFs 16 hours post inoculation (mean +/− SEM, n>25 cells per sample, 3 independent experiments). (**C**) The numbers of p62/SQSTM1 puncta per cell in uninfected and *F. tularensis* infected wild type and ATG5$^{-/-}$ cells 16 hours post inoculation (• represents 1 cell, n≥35 per sample, 3 independent experiments). (**D**) The numbers of p62 positive acidic vacuoles in wild type or ATG5$^{-/-}$ MEFs

that were untreated, infected, or infected and treated with 3MA where infected samples were enumerated16 hours post inoculation (mean +/− SEM, n>30 cells per sample, 3 independent experiments). (ns $p>0.05$, * $p<0.05$, ** $p<0.01$, *** $p<0.001$).

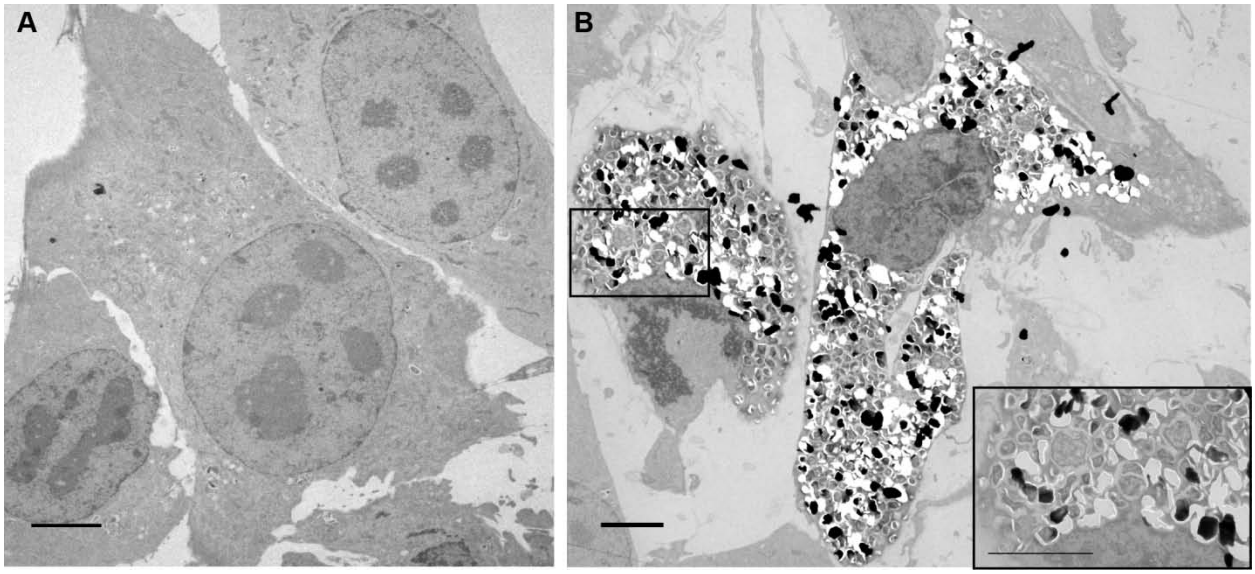

Figure 3.9: F. tularensis replicates to high densities in the host cell cytoplasm.

Supplemental Figure 1.

Representative transmission electron micrographs depicting **(A)** uninfected or **(B)** infected MEFs at 16 hours post inoculation. The scale bars represent 5 um.

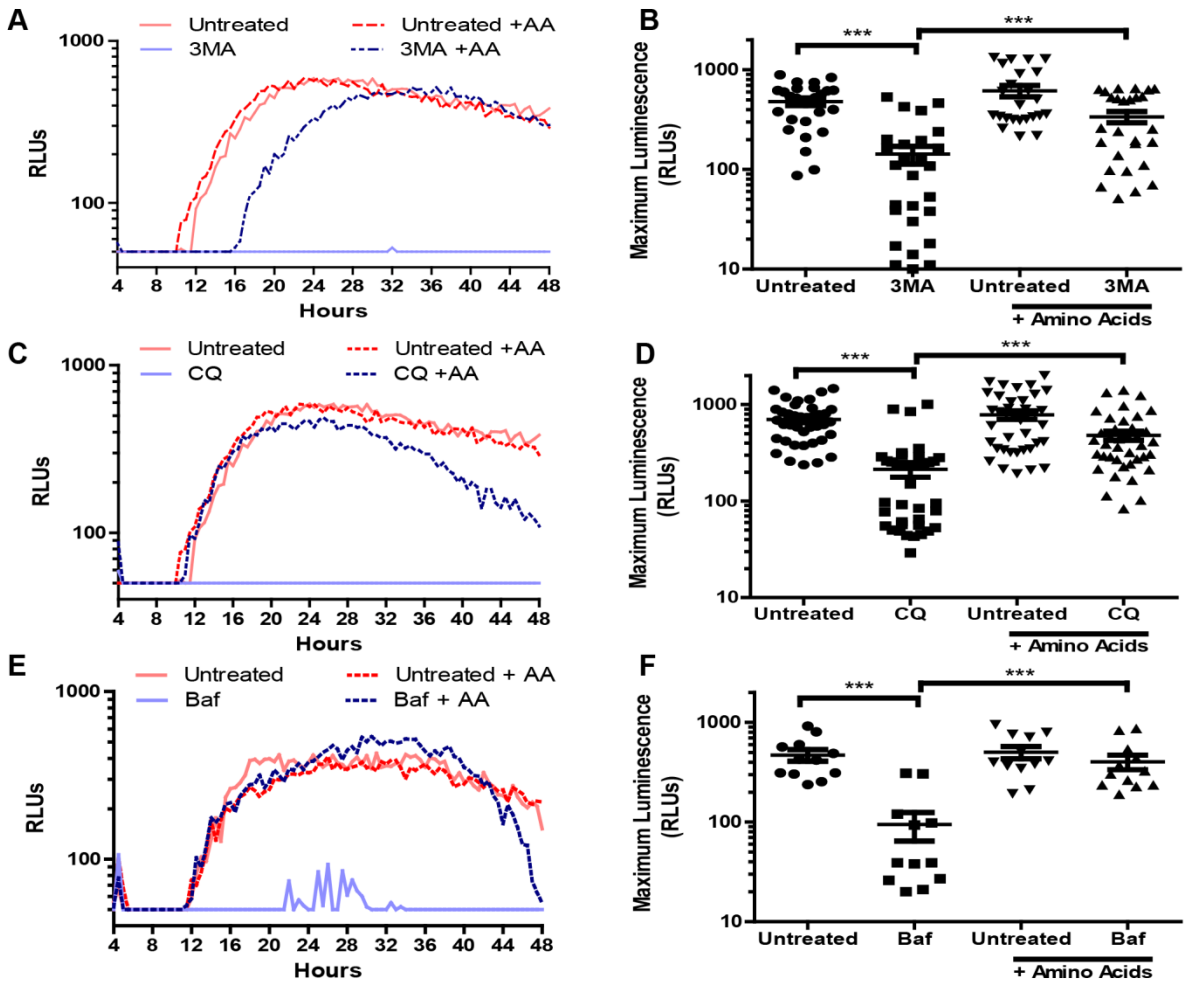

Figure 3.10: Autophagy derived nutrients enhance F. tularensis intracellular growth.

Supplemental Figure 2.

Representative intracellular bacterial growth kinetics of *F. tularensis* intracellular growth in untreated and (A) 3MA, (C) CQ, or (E) Baf treated MEFs with or without amino acid supplementation (each point represents an average of triplicate wells). Maximum luminescence values from kinetic growth assays for Schu S4 –LUX infected J774 cells treated with (B) 3MA (10 independent experiments), (D) CQ (13 independent experiments), or (F) Baf (4 independent experiments). Error bars represent the mean +/- SEM.

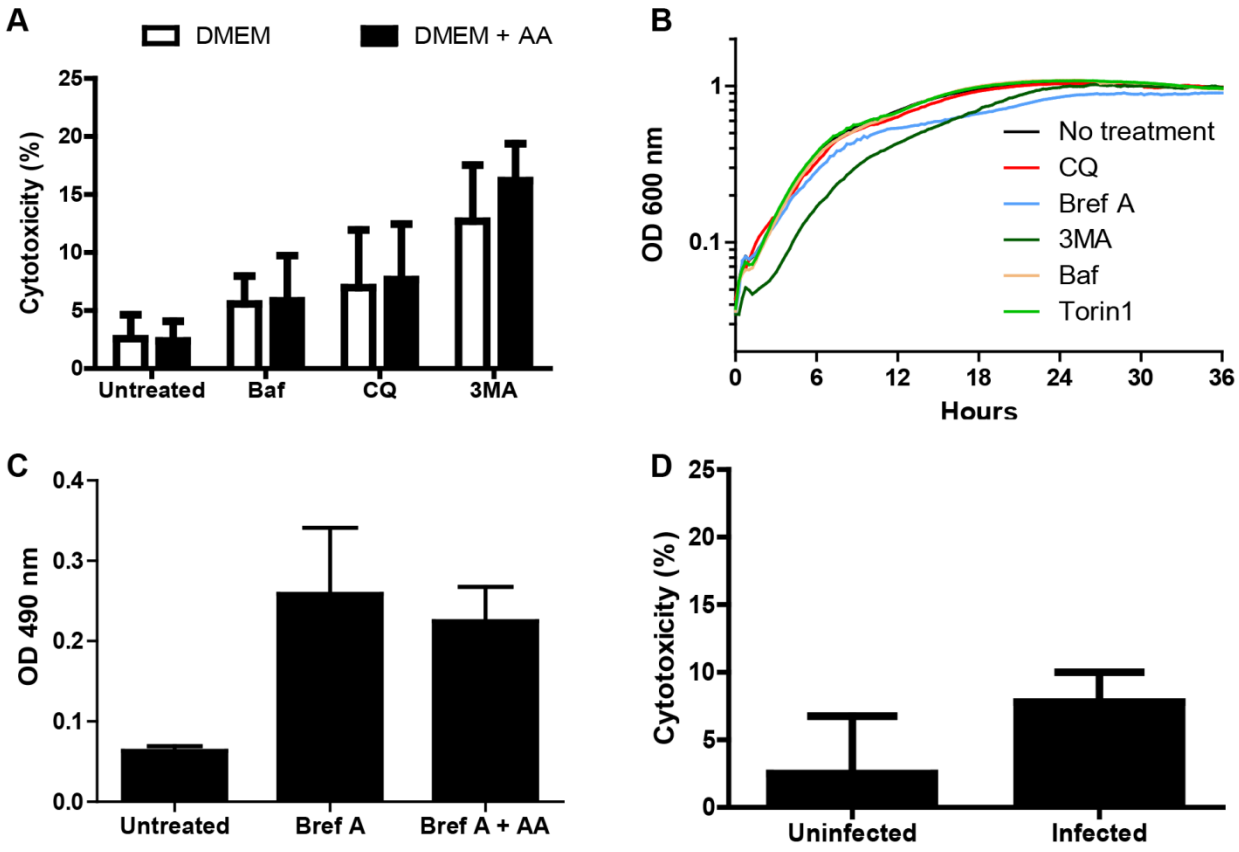

Figure 3.11: Autophagy inhibitor cytotoxicity.

Supplemental Figure 3.

(A) Cytotoxicity of the indicated drugs in MEFs with and without amino acid supplementation (AA) (3 independent experiments, mean +/- SD). (B) Representative *F. tularensis* growth curve in Chamberlin's defined media (CDM) containing the indicated drug (curve represents the average of triplicates in a single experiment, 3 independent experiments). (C) Cytotoxicity of Brefeldin A in J774 cells with and without amino acid supplementation (AA) (4 independent experiments, mean +/- SD). (D) Cytotoxicity of *F. tularensis* in J774 cells at 16 hours post inoculation (3 independent experiments, mean +/- SD).

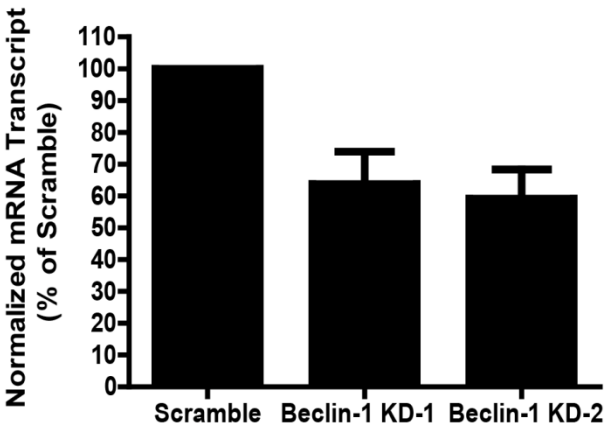

Figure 3.12: Beclin-1 shRNA depletes Beclin-1 mRNA in MEFS.

Supplemental Figure 4.

qRT-PCR analysis of the amount of Beclin-1 mRNA in MEFs transduced with a lentivirus encoding a Beclin-1 or scramble shRNA. Results were normalized to GAPDH and expressed as a percent of the scramble control.

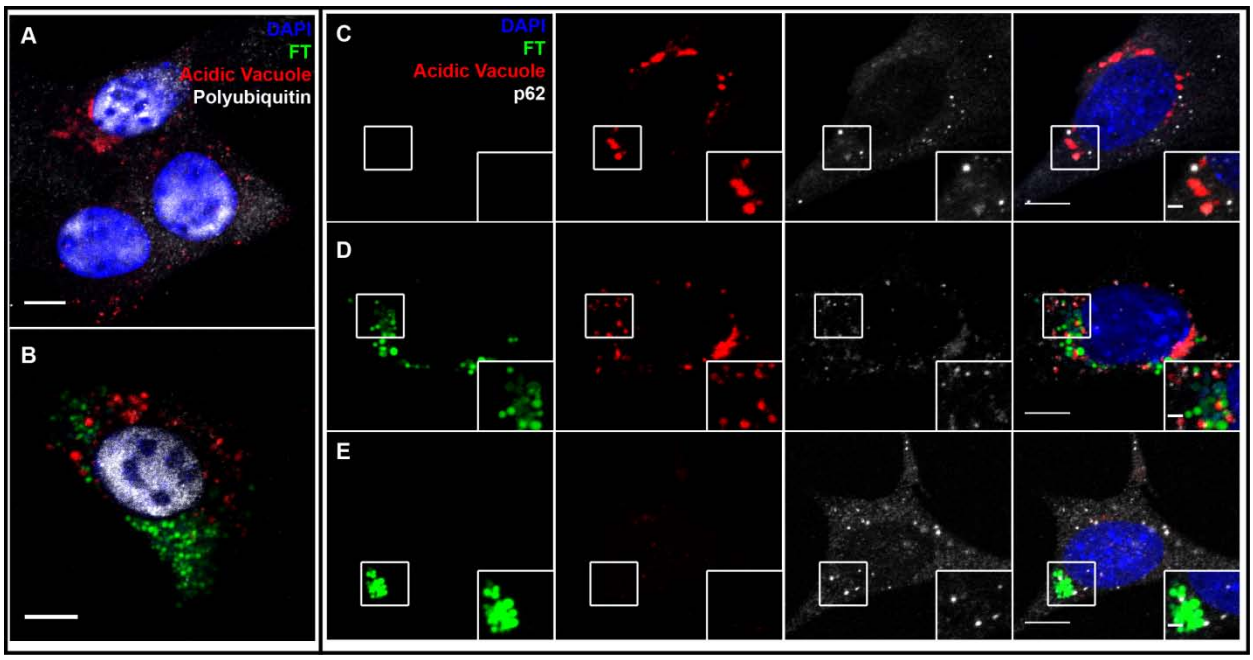

Figure 3.13: F. tularensis infection decreases polyubiquitin puncta but increases the number of p62+ acidic vacuoles.

Supplemental Figure 5.

Representative fluorescent confocal micrographs of (A) uninfected and (B) infected wild type MEFs depicting polyubiquitin. Representative fluorescent confocal micrographs of (C) uninfected, (D) infected, or (E) infected 3MA treated wild type MEFs stained for p62/SQSTM1. Scale bars represent 10 um at the low magnification and 2 um for the higher magnification inset. DAPI is depicted in blue, GFP-Schu is depicted in green, acidic vacuoles are depicted in red, and polyubiquitin or p62/SQSTM1 are depicted in white.

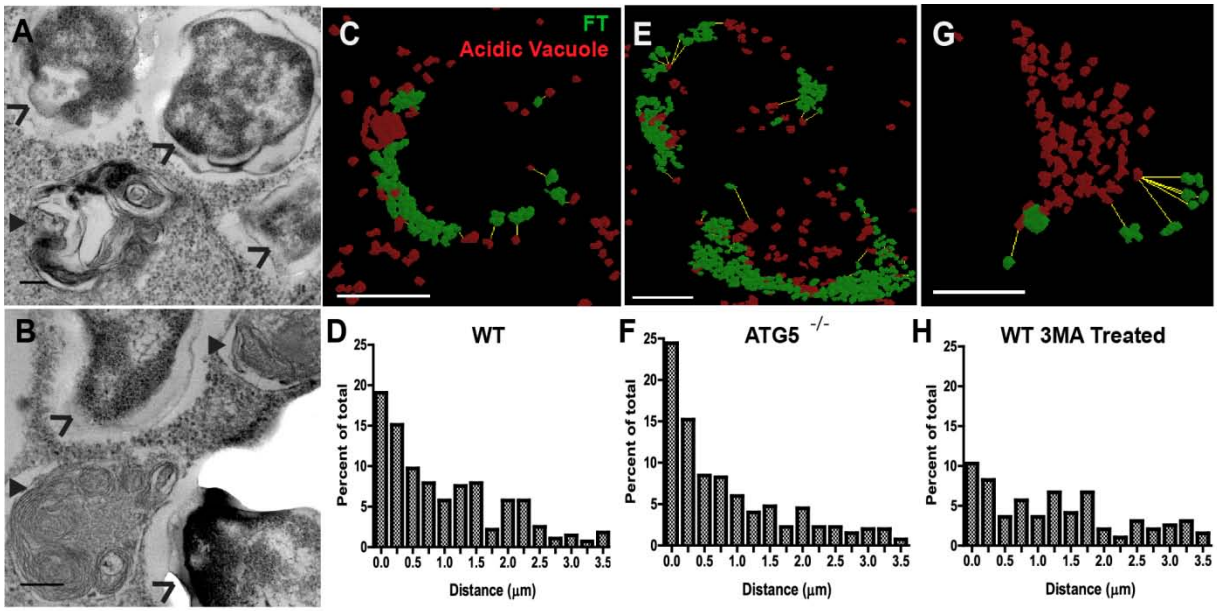

Figure 3.14: *F. tularensis* localizes adjacent to autolysosomes.

Supplemental Figure 6.

Representative transmission electron (TEM) micrograph of Schu S4 (open faced arrows [>]) adjacent to an autophagosome (solid arrows [►]) in **(A)** J774 cells or **(B)** ATG5 $^{-/-}$ MEFs 16 hours post inoculation. The scale bar for the TEM micrograph represents 200 nm. Representative compiled Z-stack images showing the distance (yellow line) between Schu S4 (green) and acidic vacuoles (red) in **(C)** wild type untreated, **(E)** ATG5 $^{-/-}$ untreated or **(G)** wild type 3MA treated MEFs 16 hours post inoculation. Scale bars for the 3D images represent 10 μm. The distance between Schu S4 and the closest acidic vacuole in **(D)** untreated (n=342 bacteria), **(F)** ATG5 $^{-/-}$ (n=401 bacteria) or **(H)** 3MA treated (n=194 bacteria) MEFs. The distribution histograms are pooled from 3 independent experiments

Primer	Sequence (5’ to 3’)
Beclin-1 Forward	CAGCCTCTGAAACTGGACACGA
Beclin-1 Reverse	CTCTCCTGAGTTAGCCTCTTCC
GAPDH Forward	CATCACTGCCACCCAGAAGACTG
GAPDH Reverse	ATGCCAGTGAGCTTCCCGTTCAG

Table 3.1: Quantitative RT-PCR primer sequences.

Supplemental Table 1.

Primer sequences for assaying the amount of Beclin-1 or GAPDH mRNA in lentiviral transduced MEFs by qRTPCR.

CHAPTER 4: TROGOCYTOSIS-ASSOCIATED TRANSFER OF INTRACELLULAR PATHOGENS

Overview

Macrophages are myeloid-derived phagocytic cells and one of the first immune cell types to respond to microbial infections. However, a number of bacterial intracellular pathogens are resistant to the antimicrobial activities of macrophages and can actively grow within these cells. Macrophages also have other immune surveillance roles within the host that include the acquisition of cytosolic components from multiple types of host cells. We hypothesized that intracellular pathogens that can replicate within macrophages exploit cytosolic transfer to facilitate bacterial spread. Here we show that viable *Francisella tularensis* bacteria transfer from infected cells to uninfected macrophages along with other cytosolic material through a transient, contact dependent mechanism. Bacterial transfer occurs when the host cells exchange plasma membrane proteins and cytosol via a trogocytosis related process that leaves both donor and recipient cells intact and viable. Trogocytosis was strongly associated with infection in a mouse infection model, suggesting that direct bacterial transfer occurs by this process *in vivo*. Furthermore *Salmonella enterica* serovar *Typhimurium* bacteria or fluorescent beads also transfer via this same process demonstrating that trogocytosis-associated cell to cell spread is not limited to *Francisella*. Our results demonstrate that macrophages can become infected with live intracellular bacteria upon contact with infected cells.

Introduction

Mammalian cells routinely exchange cytosolic components such as antigens, lipid droplets and mitochondria [78,79,151]. The exchange of cytosolic components has been described in over 40 reports across a wide range of distinct cells types [152]. Importantly, foreign material can also transfer between cells during cytosolic exchange. Both bacteria and polystyrene beads transfer directly between macrophages without entering the extracellular space when macrophages phagocytose a portion of the neighboring cell [78]. However, the prevalence of bacterial transfer during cytosolic exchange and the effects of this process on bacterial pathogenesis are unknown. We hypothesized that macrophage-tropic intracellular bacteria exploit cytosolic exchange to facilitate infection of new cells and sustain infection without entering the extracellular space.

To define how macrophages and bacteria interact during cytosolic exchange, we used the macrophage-tropic, facultative intracellular bacterium *Francisella tularensis*. *F. tularensis* rapidly infects new cells and cell types during infections despite inducing minimal cell death in infected cells [2,3,70]. Although these data suggest that bacterial transfer may occur, *F. tularensis* does not encode homologs of any proteins that other bacterial species use for cell to cell spread. As such, the transfer of live bacteria during cytosolic exchange and trogocytosis is a potential explanation for the rapid increase in the number of newly infected cells in murine tularemia.

Results and Discussion

Francisella tularensis transfers between macrophages during cytosolic exchange.

Macrophages phagocytose portions of neighboring cells to acquire cytosolic material, such as lipid droplets from adipocytes [79]. The macrophages can then generate a cytokine response to the ingested material [79]. It is likely that macrophages undergo a related process to acquire bacteria from infected cells. By live cell imaging, we observed GFP-expressing *F. tularensis* bacteria transfer from infected to uninfected macrophages upon cell to cell contact (Figure 1A, Supplemental Video 1, 2). After bacterial transfer, both macrophages were typically motile suggesting that both the donor and recipient macrophages remained viable after bacterial transfer (Figure 1A). These data are consistent with macrophages ingesting a portion of an infected cell without killing the infected cell. When the ingested portion contains bacteria, they can infect the recipient macrophage. Our data further indicates that nanotube formation is not required for bacterial transfer [78].

We quantified bacterial transfer in several macrophage cell lines using flow cytometry. In these experiments, we infected the macrophage with *F. tularensis*, added the antibiotic gentamicin to destroy extracellular bacteria, and then co-incubated the infected macrophages with uninfected, Cell Trace Red labeled macrophages. *F. tularensis* transferred from infected to uninfected recipient J774A.1 macrophage-like cells (J774s), mouse bone marrow derived macrophages (BMDMs) and primary human monocyte derived macrophages (hMDMs) (Figure 1B). *F. tularensis* replicates within the host cell cytosol. Thus, *F. tularensis* transfer suggests that portions of the cytosol also transfer between cells. As predicted, *F. tularensis* transfer strongly correlated with the transfer of the cytosolic dye calcein between cells (Figure 1C, 1D). These

data suggest that *F. tularensis* transferred between cells during the exchange of other cytosolic material.

Bacterial transfer requires cell to cell contact.

The concurrent transfer of cytosol with bacteria indicates that the bacteria transferred to the previously uninfected cell without first exiting the initially infected cell. We verified that cell contact was the predominant method of intercellular transfer through several experiments. First, direct cell to cell contact significantly increased bacterial transfer to uninfected cells (Figure 1E, Experimental Design in Supplemental Figure 1). Additionally, the number of cells infected over time was significantly higher than the number of extracellular bacteria (Supplemental Figure 2A, B). Further decreasing the number of extracellular bacteria by inhibiting cell lysis through apoptosis or necrosis had no detectable effect on the number of cells infected (Supplemental Figure 2C). Taken together, these data demonstrate that *F. tularensis* bacteria primarily transfer between cells in a host cell contact dependent manner.

Viable bacteria transfer between cells to propagate infection.

F. tularensis bacteria transferred between cells, but it is unclear if the transferred bacteria were viable or sustain an infection. To assess bacterial viability after transfer, we permeabilized the host cell and measured bacterial viability by propidium iodide exclusion. The percent of viable bacteria was similar between the donor and recipient populations, indicating that bacteria were not killed during transfer between cells (Figure 2A, B). To test if the transferred bacteria could propagate infection, we infected approximately 1% of the BMDMs then inhibited cell to cell contact dependent bacterial transfer with soy lecithin (Figure 2C) and monitored bacterial

viability over 3 days. Both treated and untreated cells reached peak infection at 24 hours post inoculation, but the lecithin treated samples had significantly fewer viable bacteria compared to untreated samples at 48 and 72 hours post inoculation (Figure 2D). In the soy lecithin treated samples, the majority of bacteria should be within the initially infected cells. As such, the bacterial death observed at the later time points is likely due to gentamicin entering the initially infected cells when they lose membrane integrity. Thus, bacterial transfer enhances bacterial survival. *F. tularensis* exploits cell to cell transfer to extend infection by invading previously uninfected cells without entering the extracellular space.

Lecithin treatment almost completely blocks bacterial transfer (Figure 2C), but we were unable to ascertain the mechanism behind this inhibition. Treating infected cells with individual phospholipid components of soy lecithin did not affect bacterial transfer (data not shown). Other complex phospholipid mixtures such as bovine lung surfactants (Survanta) also decreased bacterial transfer, likely through a related mechanism (data not shown).

Bacterial transfer is cell type specific.

Many bacterial species transfer from cell to cell through bacterial mediated processes, such as actin based motility. Since these transfer mechanisms are driven by bacterial effectors, transfer occurs across a diverse range of cell types [62,153,154]. In contrast, cytosolic transfer varies widely between cell types [152]. We assessed bacterial transfer in different cell types to test if *F. tularensis* transferred between cells via a host or bacterial mediated process. Macrophages and epithelial cells are both well documented for organelle transfer [152], so we evaluated *F. tularensis* transfer in TC-1 epithelial cells compared to macrophages. Although *F. tularensis* replicates well in TC-1 epithelial cells [112](data not shown), *F. tularensis* did not transfer between these epithelial

cells (Figure 3A, B). However, we tested and found that *Francisella* transferred from infected epithelial cells to macrophages (Figure 3C). These data indicate that bacterial transfer only occurs when the uninfected recipient cell is a specific cell type. As such, *F. tularensis* transfer is likely a host mediated process.

***F. tularensis* does not transfer via previously described bacterial transfer mechanisms.**

Recipient cell type specificity suggests that *F. tularensis* does not use similar transfer mechanisms of cell to cell spread as other bacterial pathogens. *F. tularensis* did not form actin tails that are characteristic of bacterial pathogens such as *Listeria monocytogenes*, further suggesting that *F. tularensis* does not use actin based motility (Supplemental Figure 3 7A-C). Likewise, actin based motility requires continual bacterial protein synthesis [153]; but, bacterial protein synthesis was not required for *F. tularensis* transfer (Supplemental figure 3D). A proposed alternative form of *F. tularensis* spread is through an autophagy related mechanism [74,122], but inhibiting autophagy with 3-methyladenine (3MA) or using ATG5 knockout BMDMs did not block bacterial transfer (Supplemental figure 3E, data not shown). Altogether these data are consistent with *F. tularensis* exploiting host-mediated cytosolic transfer for cell to cell spread.

These results raise the question of why certain bacterial species require a bacterial driven transfer mechanism for optimal virulence rather than exploiting cytosolic exchange. Only 5-10% of macrophages became infected with *F. tularensis* via trogocytosis-associated transfer in a 6 hour interval (Figure 3B). Bacteria that encode mechanisms such as actin based motility likely increase the rate of cell to cell spread. Separately, certain bacterial species that use actin based transfer between epithelial and endothelial cells [62,154,155]. It is possible these transfer mechanisms

evolved so that these bacteria can transfer between cells types other than macrophages. As such, bacterial mediated transfer likely evolved to enhance bacterial spread and allow for spread between cell types that do not undergo trogocytosis-associated bacterial transfer.

Bacterial transfer correlates with trogocytosis.

One mechanism for cytosolic exchange observed in cytotoxic T cells (CTL) occurs when pores connecting the cytosol form between CTL with the target cell [156]. During this cytosolic intermingling, the cells also exchange specific plasma membrane proteins [156]. The cell to cell exchange of intact and functional plasma membrane proteins that retain their orientation is termed trogocytosis [81]. We noted a similar phenomenon during bacterial transfer. Newly infected recipient BMDMs frequently acquired plasma membrane proteins as well as cytosolic material from the initially infected cell (Figure 4A, B). Transferred plasma membrane proteins retained their orientation; so membrane proteins that were surface exposed on the initially infected cell were also surface exposed on the newly infected recipient cell (Figure 4A, 4B). These data are consistent with trogocytosis and imply that trogocytosis occurs at the same time as bacterial transfer. Importantly, trogocytosis can be used as a marker for bacterial transfer and differentiate direct bacterial transfer from more conventional mechanisms such as infection via extracellular bacteria.

To quantify how often bacterial transfer resulted in detectable levels of trogocytosis, we monitored major histocompatibility complex I (MHC-I) transfer between infected donor and uninfected recipient BMDMs [86,157]. We infected C57BL/6 (B6) BMDMs (MHC-I H2-Kb) and added uninfected Balb/c BMDMs (MHC-I H2-Kd) to the infected B6 cells. After 6 hours of co-incubation, we assayed the Balb/c BMDMs for both *F. tularensis* infection and the acquisition of

B6 MHC-I. We found that infection increased the amount of Balb/c BMDMs that acquired B6 MHC-I (Supplemental Figure 4A). Newly infected Balb/c cells were significantly more likely to acquire B6 MHC-I than neighboring Balb/c cells that did not become infected (Figure 4C). As with bacterial transfer, MHC-I transfer did not require *de novo* host or bacterial protein synthesis (Supplemental Figure 5). We also observed MHC-I exchange during bacterial transfer when monitoring hMDMs (Figure 4D). Additionally, the surface exposed MHC-I likely remained functional after transfer because it was capable of binding the ovalbumin derived peptide SIINFEKL (Figure 4E). Taken together, these data confirmed that trogocytosis occurs concurrent with bacterial transfer.

Infected cells undergo increased levels of trogocytosis in a mouse infection model.

Because trogocytosis is a marker for cell to cell transfer, we assessed the exchange of plasma membrane proteins in infected splenocytes as a surrogate for bacterial transfer *in vivo*. We generated chimeric mice by injecting irradiated F1 B6 and Balb/c mice with wild type Balb/c and transgenic CD45.1^{+} B6 bone marrow. In these mice, no cells encode both CD45.1 and the MHC-I H2-Kd. Thus, cells must undergo trogocytosis if both CD45.1 and H2-Kd are present on the surface of an individual cell. We infected these mice for 3 days and assayed their splenocytes for trogocytosis. Consistent with our *in vitro* data, *F. tularensis* infection increased trogocytosis and infected cells were significantly more likely to transfer plasma membrane proteins than uninfected splenocytes from the same mouse (Figure 4F, Supplemental Figure 4B). Indeed, the majority of infected splenocytes had undergone detectable levels of trogocytosis. Combined with our *in vitro* data, these results suggest that cell to cell bacterial transfer occurs in a mouse infection model.

The percent of cells that underwent trogocytosis varied widely between different cell types. Of the cell types we tested, macrophages and monocytes underwent significantly more trogocytosis than dendritic cells or a compilation of all of the other cell types (Supplemental Figure 6) ($p<.05$ for both cell types from raw data). These data further indicate that the rate of trogocytosis, and likely bacterial transfer, are cell type specific.

Trogocytosis-associated bacterial transfer is a general phenomenon.

Recipient cell type specificity suggests that trogocytosis-associated bacterial transfer is a host mediated event. As a result, we should observed similar results in other bacterial species. We therefore assessed bacterial transfer and trogocytosis with *Salmonella enterica serovar Typhimurium* (*S. typhimurium*) infected cells. Similar to *F. tularensis* cell to cell transfer, *S. typhimurium* infection increased trogocytosis and bacterial transfer correlated with the exchange of MHC-I (Figure 5A, Supplemental Figure 4C). We also measured the transfer of beads between cells to test if transfer was specific to bacterial infections. Unlike infections, beads did not increase the level of trogocytosis above the basal level (Supplemental Figure 4D). However, the Balb/c macrophages that acquired beads also acquired B6 MHC-I (Figure 5B). Taken together, our data demonstrate that macrophages acquire cytosolic material and plasma membrane proteins from neighboring cells at a basal rate that is enhanced during infection.

An unexpected observation from our work was that the rate of trogocytosis increased during infection. Trogocytosis is an important immunological process with broad consequences on host engraftment, vaccine efficacy, immune regulation and tumor recognition [158-161]. Our results indicate that a bacterial stimulus triggers trogocytosis. Future efforts to discern the

bacterial products or processes responsible for trogocytosis up-regulation may lead to a specific tool to manipulate trogocytosis.

Interestingly, cells infected with *F. tularensis* or *S. typhimurium* participated in trogocytosis more frequently than uninfected cells (Supplemental Figure 4A-C). These results suggest that infected cells expressed a signal of some kind that initiated, enhanced, or stabilized trogocytosis. This signal is likely not soluble or generalizable because the frequency of trogocytosis does not increase in the uninfected cells neighboring infected cells. The molecular mechanism for trogocytosis is unknown, but an infection model could be exploited to determine the factors responsible for initiating trogocytosis.

Concluding remarks

Our study demonstrates that intracellular bacteria can exploit a host cell cytosolic exchange mechanism to transfer directly from infected cells to macrophages. The bacteria are viable after transfer and can sustain infection without entering the extracellular space. During infections, trogocytosis-associated transfer is a likely mechanism for *F. tularensis* to disseminate. Shortly after infection, *F. tularensis* infects dendritic cells and then traffics to the draining lymph node within these infected dendritic cells [4]. But alveolar macrophages are the primary cell type initially infected by *F. tularensis* following inoculation [3]. Direct cell to cell transfer is a likely mechanism for the bacteria to transfer from alveolar macrophages to dendritic cells because the kinetics of *F. tularensis* infected cell death are typically longer than for dissemination [70]. *F. tularensis* may then use analogous mechanisms to transfer systemically from the lymph node.

Bacterial transfer via trogocytosis requires the recipient cell to be a specific cell type, suggesting that this transfer mechanism is a host mediated event. The spread of bacteria aids in

expanding the replicative niche and possibly dissemination, but could intercellular transfer of live bacteria also benefit the host? In cancer biology, trogocytosis of pMHC-I and pMHC-II results in a cytotoxic T cell response to the tumor [159,162]. The immune system may use a similar tactic during infection. The transfer of plasma membrane proteins such as MHC-I during infection may initiate or amplify a cytotoxic T cell response that ultimately aids in pathogen clearance. Trogocytosis-associated transfer may spread antigen between antigen presenting cells to improve the likelihood of stimulating a specific T cell receptor. In other cell types such as epithelial cells, trogocytosis-associated transfer may result in trafficking pMHC-I to cells capable of initiating a cytotoxic T cell response. Separately, epithelial cells transfer whole antigen to macrophages and dendritic cells to initiate a T cell response via a cytosolic mechanism [151]. As such, bacterial transfer could be a mechanism for cells to transfer an antigen source to antigen presenting cells.

Trogocytosis-associated bacterial transfer is likely beneficial to the host or bacteria depending on the context and the microbe. Future studies on how this process impacts pathogenesis will likely improve our understanding of how bacteria spread in the host and how the innate immune system acquires antigen to initiate the adaptive immune response.

Materials and Methods

Bacterial growth

Francisella tularensis subsp. *tularensis* Schu S4 was obtained from Biodefense and Emerging Infectious Research Resources Repository (BEI Resources) and *Francisella tularensis* subsp. *holartica* live vaccine strain (LVS) expressing GFP was generated as described [2]. Schu S4 was used for all experiments shown except live cell imaging. Prior to infection, *F. tularensis* was

grown overnight in Chamberlin's defined media. *L. monocytogenes* and *S. typhimurium* were grown overnight in Luria broth.

Antibodies and Critical Reagents

The clone numbers for the antibodies used in these experiments: *F. tularensis* lipopolysaccharide (1.B.288, US Biologicals), MHC I H2-Kd (SF1-1.1.1, eBioscience), MHC I H2-Kb (AF6-88.5.5.3, eBioscience), MHC I HLA-A2 (BB7.2, eBioscience), CD45.1 (A20, eBioscience), CD45 (30-F11, eBioscience), MHC I H2-Kb-SIINFEKL (25-D1.16, eBioscience).

The catalog number and company for critical reagents used in these experiments: Cell Trace Red DDAO-SE (C34553, Life Technologies), Calcein-AM (C3099, Life Technologies), Soy Lecithin (Cas number 8002-43-5, Acros), phalloidin (A22287, Life Technologies), 3 um pore Transwells (3402 Costar), gentamicin (15750-060, Gibco)

The beads (M-1002-010, Solulink) used in these experiments were labelled with AF488 succinimidyl ester (A-20100, Life Technologies) to make fluorescent beads.

Cell Culture

TC-1 lung epithelial cells (ATCC CRL-2785) were maintained in RPMI supplemented with sodium pyruvate, L-glutamine and non-essential amino acids in 10% fetal bovine serum (FBS). J774A.1 macrophage-like cells (ATCC TIB-67) were maintained in DMEM containing 10% FBS supplemented with sodium pyruvate and L-glutamine. All cell types were kept at 37°C and 5% CO2. All cell types were checked for proper morphology prior to every experiment and consistently monitored for changes in cell replication that might indicate *Mycoplasma* contamination.

For the BMDM, TC-1 and J774 transfer experiments, cells were seeded the night before the experiment at 250,000 cells per well in non-tissue culture treated 12 well dishes or 500,000 cells per well in a 6 well dish on coverslips for microscopy. BMDMs were generated as previously described [163]. Unless otherwise indicated, cells were infected with *F. tularensis* at a multiplicity of infection (MOI) of 100 bacteria, *S. typhimurium* at an MOI of 10 or beads at an MOI of approximately 1. 10 ug/ml of gentamicin was added at 2 hours post inoculation when BMDMs or J774s were infected or 3 hours post inoculation for TC-1 cells. For co-incubation experiments, the indicated recipient cell type was added to the infected cells at 18 hours post inoculation unless otherwise indicated for *F. tularensis.*

Primary human monocyte derived macrophages were generated by acquiring human blood in heparin tubes and isolating the peripheral blood mononuclear cells (PBMC) and serum on a ficoll gradient. The cells were plated in Iscove's modified Dulbecco's medium (IMDM) for 2 hours. The non-adherent cells were washed away and the media was replaced with IMDM containing 5% autologous human serum. Primary human cells were cultured for 7 days prior to infection. The blood was isolated from several healthy volunteers who gave informed, written consent following an approved protocol by the Institutional Review Board for human volunteers at the University of North Carolina at Chapel Hill. Blood was obtained specifically for these experiments. Different donors were used for each experiment.

The infected cells were seeded onto a coverslip for all experiments involving primary human cells. The coverslip was inverted in a well of uninfected cells so that the infected cells were in contact with the uninfected cells. The reciprocal setup was used for TC-1 to BMDM transfer experiments. Other methods to transfer the cells resulted in large amounts of cell lysis.

Bacterial transfer inhibition assay

BMDMs were seeded at 500,000 cells the night before infection. Cells were infected with an MOI of 0.5 bacteria and 10 ug/ml of gentamicin was added at 2 hours post inoculation. 0.5 mg/ml of soy lecithin (Acros) was added with gentamicin at 6 hours post inoculation. 50% of each sample was used for viable bacteria quantification through serial dilutions and plating on chocolate agar. The remaining 50% of the sample was used to determine the number of cells infected as previously described. Soy lecithin is composed of phospholipids, but treatment of cells with the major phospholipid components of soy lecithin, such as phosphatidylcholine, did not block bacterial transfer (data not shown).

Live Cell Imaging

For live cell imaging, J774 cells were infected at an MOI of 500 with GFP-expressing LVS bacteria in a synchronous infection. Briefly, the J774 cells were chilled on ice for 30 minutes, the media was exchanged with media containing the bacteria, centrifuged for 5 minutes and then the bottom of the plate was placed in a 37°C water bath for 2 minutes. The cells were incubated for 15 minutes in an incubator at 37°C and 5% carbon dioxide and then the media was replaced with media containing gentamicin. The cells were then imaged every 5 minutes for 24 hours using a 40x objective on an Olympus IX70 microscope in a temperature and carbon dioxide contained chamber. All data were analyzed using ImageJ [114].

Flow Cytometry Assays

When analyzing surface markers (CD45, H2-KD, H2-KB, or H2-KB-SIINFEKL), cells were stained in the wells in which they were infected. We added 2.4G2 cell supernatant (Fc

blocking buffer) to infected cells for 5 minutes. The 2.4G2 was removed and antibodies were added. After 5 minutes, the cells were washed twice in PBS containing 2% fetal bovine serum (FBS) then fixed in 4% paraformaldehyde.

F. tularensis within infected cells were detected by permeabilizing the plasma membrane with 0.1% saponin (Millipore) in PBS and 2% FBS (Gibco). The cells were stained with an anti-*F. tularensis* lipopolysaccharide antibody (US biological) conjugated to either Pacific blue, AF488, or AF647 by combining the antibody with a succinimidyl ester of the dye. The conjugated antibody was separated from unbound dye by a 30,000 molecular weight filter and repeated washes with PBS and glycine. Conjugation efficiency was then assayed for each batch.

All mouse plasma membrane protein transfer experiments included a doublet control. Uninfected cells from both populations were each stained with all antibodies. Each population was removed from the plate and combined in 4% paraformaldehyde. We were able to detect bacteria at 1 hour post-inoculation when as few bacteria as 1 bacteria per cell were present (data not shown).

We stained for both extracellular and intracellular bacteria and found that 1% or less of the infected BMDMs were positive due to surface bound extracellular bacteria (data not shown). Due to the low number of false-positive events, we did not stain specifically for extracellular bacteria in the majority of assays so that we could minimize spectral overlap of our panel.

Transfer of cytosolic dyes

BMDMs were infected for 18 hours and then stained with calcein-AM following the manufacturer's protocol (Invitrogen). Uninfected BMDMs were concurrently stained with Cell Trace Red (Invitrogen) following the same protocol. The different populations were either fixed

immediately for controls or combined and co-incubated for 6 hours. The cells were then stained for *F. tularensis* as described above.

Transwell assay

The day before infection, BMDMs were seeded either in a 12 well plate or in the chamber of 12 mm, 3.0 uM pore transwell. Each chamber (transwell and plate) was kept separate. One chamber per pair was infected and 10 ug/ml of gentamicin was added at 2 hours post inoculation to kill any extracellular bacteria. At 6 hours post-inoculation, the gentamicin was removed and the infected and uninfected chambers were combined. We then separated and harvested each chamber at either 6 or 18 hours post inoculation.

To test for bacteria traversing the membrane, we combined the chambers, added bacteria directly to the media of the indicated chamber (MOI 100) and tested for the number of infected cells in each chamber 2 hours later (Supp 1B).

Extracellular bacterial enumeration

BMDMs were infected for two hours and then gentamicin was added. At 6 hours post inoculation, the media was exchanged for media with or without gentamicin. At 6 hour intervals, the cells were harvested and stained for intracellular *F. tularensis* and the media was serially diluted and plated on chocolate agar. To approximate the number of cells infected every 6 hours, we used the change in infection percentage between intervals and assumed the number of BMDMs doubled overnight.

Cell Death and Autophagy Inhibition

BMDMs were infected and gentamicin was added at 2 hours post inoculation. At 6 hours post inoculation, the media was exchanged for media containing gentamicin and the indicated treatment. Z-Vad(OMe)-FMK (Cayman Chemicals) was used at 20 uM and Necrostain-1 (Cayman Chemicals) at 10 uM. At 6 or 24 hours, samples were harvested and analyzed for intracellular bacteria.

Autophagy inhibition experiments were performed in the same manner, with 10 uM 3-methyladenine (Cayman Chemicals) added at 18 hours post inoculation.

Saponin Permeabilization

Cell Trace Red BMDMs were added to infected BMDMs 18 hours post inoculation. At 24 hours post inoculation, the cells were treated with 0.1% saponin in PBS and 2% FBS for 15 minutes at room temperature (wash buffer). 3 uM propidium iodide was added to the cell for 12 minutes in wash buffer. The cells were washed 3 times and then fixed in paraformaldehyde.

Epithelial to BMDM transfer

TC-1 epithelial cells were infected for 6 hours as described above. A cover slip seeded with BMDMs was inverted on top of the infected TC-1 cells and the cells were co-incubated for 18 hours in media containing gentamicin. At 24 hours post inoculation, the slide was removed and the TC-1 and BMDM cells that migrated from the cover slip to the bottom of the plate were stained for CD45 to determine cell type, fixed, and then stained with *F. tularensis* LPS as described above. The 0 hour co-incubation represents TC-1 cells that were infected for 24 hours but did not have BMDMs added to the well.

Mice

All mice were obtained from Jackson Laboratory (Bar Harbor, ME) and were housed in specific pathogen free housing at the University of North Carolina- Chapel Hill. All mouse experiments were performed under approved protocols from the University of North Carolina-Chapel Hill Institutional Animal Care and Use Committee. All mice used were female. The age of mice for bone marrow macrophage production varied widely (6 weeks to 6 months old). All mice used to generate chimeric mice were 6 weeks old at the time of irradiation or bone marrow harvest.

Bone Marrow Chimera Mouse Experiment

F1 mice from a mating of C57Bl/6 and Balb/c mice were irradiated with 1000 cGY using an X-ray irradiator. About 5 hours after irradiation, the irradiated mice were reconstituted by intravenous injection of 10 million T cell depleted bone marrow cells per mouse (T cells depleted using Miltenyi CD3e Microbead Kit following the manufacturers protocol). The bone marrow cells were approximately a 1:1 mixture of cells from wild-type Balb/c mice and CD45.1 C57bl/6 mice (B6.SJL-PTprc^{a} Pepc^{b}/ BojJ). No blinding was performed in these studies.

5-7 weeks after irradiation, half of the bone marrow chimera mice in each irradiation group were infected intranasally with approximately 500 colony forming units of GFP-expressing *F. tularensis* Schu S4. Mice were randomly assigned to each group. At 3 days post inoculation, the spleens were harvested and made into a single cell suspension. The cells were treated with ammonium chloride lysing buffer to removed red blood cells. The splenocytes were then stained with anti CD45.1 and H2-KD (Balb/c MHC I) antibodies, washed, fixed in 4% paraformaldehyde, stained for intracellular *F. tularensis* and analyzed by flow cytometry.

Plasma Membrane Protein Transfer (Trogocytosis) Assays

C57BL/6 BMDMs were infected and gentamicin was added at 2 hours post inoculation. At 18 hours post inoculation, Balb/c BMDMs were added to the infected B6 cells in the presence of gentamicin. For select experiments, 0.5 ug of the ovalbumin peptide SIINFEKL (ova 257-264) (AnaSpec Inc) was also added at 18 hours post inoculation. At 24 hours, the cells were stained and harvested for flow cytometry. All flow cytometry experiments included a doublet control, where stained and paraformaldehyde fixed B6 and Balb/c cells were mixed at approximately a 1 to 1 ratio with a similar cell concentration as the rest of the samples. The doublet control sample represents the background level of false positives for plasma membrane protein transfer due to doublets.

Experiments with *S. typhimurium* or magnetic beads were performed by infecting B6 BMDMs with an MOI of 10 GFP expressing *S. typhimurium* bacteria or an MOI of 1 streptavidin coated magnetic bead (Solulink) conjugated to AF488. At 2 hours post inoculation, the cells were washed and media containing 25 ug/ml of gentamicin was added. At 10 hours, Balb/c BMDMs were added and the samples were harvested at 16 hours. The samples were surface stained as previously described.

For microscopy, infected BMDMs were biotinylated at 18 hours post inoculation (Thermo Scientific; EZ-Link Sulfo-NHS-LC-biotin following the manufacturer's protocol). Cell Trace Red labeled BMDMs were added to the infected cells immediately following biotinylation. 1 to 2 hours later, the samples were stained with AF568 or PE conjugated streptavidin, fixed in 4% paraformaldehyde, and mounted using DAPI containing mounting media. Images were acquired using the 63x objective on a Zeiss CLSM 700 Confocal Laser Scanning Microscope.

Images were acquired using Zen software (Zeiss). All data were analyzed using ImageJ [114]. 3D images were generated using Imaris software (Bitplane).

For human samples, HLA-A2 negative, biotinylated MDMs were added to infected HLA-A2+ MDMs at 18 hours post inoculation. The cells were co-incubated for 6 hours and then the recipient cell population was stained with biotin and HLA-A2 to assess plasma membrane protein transfer.

Protein synthesis inhibition

Recipient BMDMs and the indicated treatment (0.1 ng/ml cycloheximide or 50 ug/ml chloramphenicol) were added to infected BMDMs at 18 hours post inoculation. The samples were assessed as described above. At these concentrations, cycloheximide increased the basal rate of plasma membrane protein transfer while chloramphenicol decreased the basal rate of plasma membrane protein transfer.

Actin localization

Cells were infected with an MOI of 1 for *L. monocytogenes* or 100 for *F. tularensis*. Cells were harvested at 16 hours post inoculation, fixed, permeabilized and stained with AF647 conjugated phalloidin.

Data Analysis

All statistics were performed by a 2 tailed, unpaired Student t-tests using raw data values. Confocal microscopy experiments represent all cells from 100 total fields of view from 2 independent experiments. For statistics, each field of view was treated as an independent sample.

Chimeric mouse experiments were performed with 2 mice per group in 4 independent experiments. We estimated the size for these animal studies based on our results in tissue culture. All other experiments were performed in triplicate for each group in at least 3 independent experiments unless otherwise indicated.

Figures

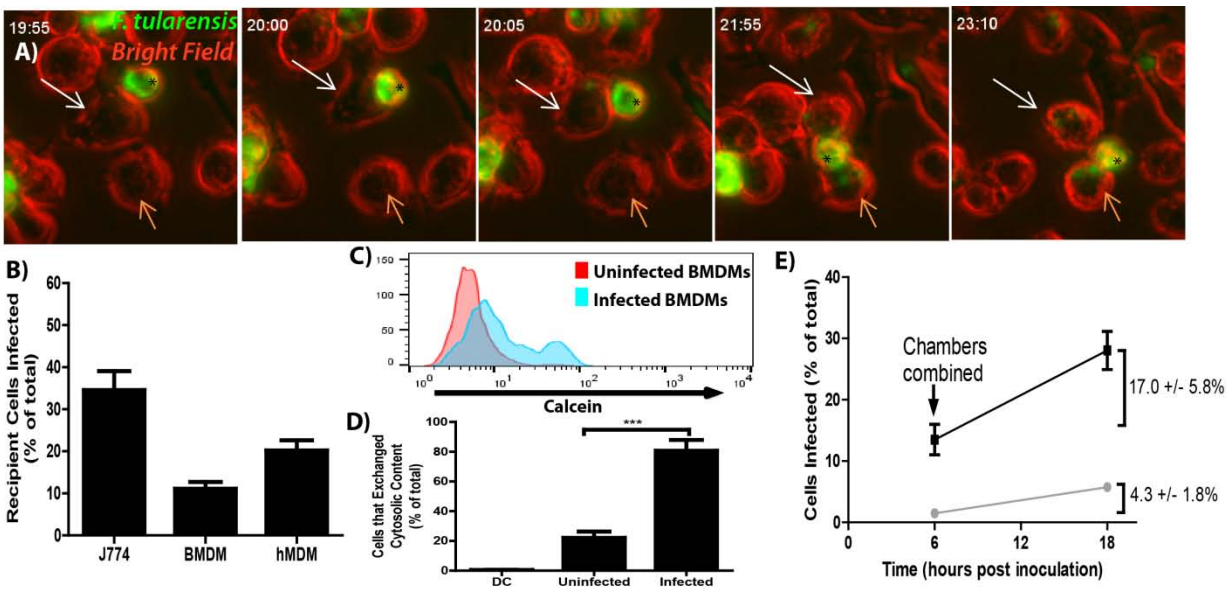

Figure 4.1: *F. tularensis* transfers between macrophages during cytosolic transfer.

A) Representative live cell imaging micrographs of *F. tularensis* infected J774 cells transferring bacteria. Time- hour: minutes post inoculation; * - initially infected cell; White arrow- first bacterial transfer event; Orange arrow- second bacterial transfer event. Movie available as Supplemental Video 1. **B)** The amount of recipient macrophages infected after a 6 hour co-incubation between the indicated macrophage cell types (3 independent experiments performed in triplicate). **C)** A representative histogram of the amount of calcein that transferred to recipient cells (log_{10} fluorescence). **D)** The percent of infected or uninfected cells that exchanged cytosolic content (positive for both Cell Trace Red and calcein). The uninfected population represents cells in the infected well that did not become infected. DC refers to a doublet control (2 independent experiments performed in triplicate) **E)** The percent of BMDMs infected in each transwell chamber. ■ Transwell (initially infected). ● Bottom. The percentages indicate the change in infected BMDMs over time. The difference in the number of BMDMs infected over time was

significant (p<0.001) (3 independent experiments performed in triplicate). (Mean +/- SEM). (***p<0.001)

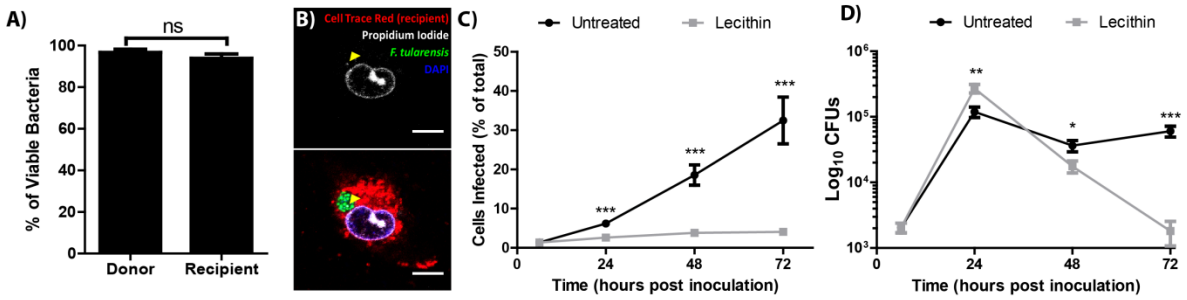

Figure 4.2 Live bacteria transfer to macrophages during bacterial transfer.

A) The percent of viable bacteria (propidium iodide negative) in donor and recipient BMDMs (2 independent experiments, 50 fields of view each) **B)** Micrographs of permeabilized BMDMs. Arrow- propidium iodide positive bacterium. Scale bar- 10 uM. **C)** The number of cells infected in untreated or soy lecithin treated BMDMs. **D)** The number of viable bacteria in untreated or soy lecithin treated BMDMs. Lecithin was added at 6 hours post inoculation (All other results from 3 independent experiments performed in triplicate). (Mean +/- SEM). (ns p>0.05, * p<0.05, **p<0.01, ***p<0.001).

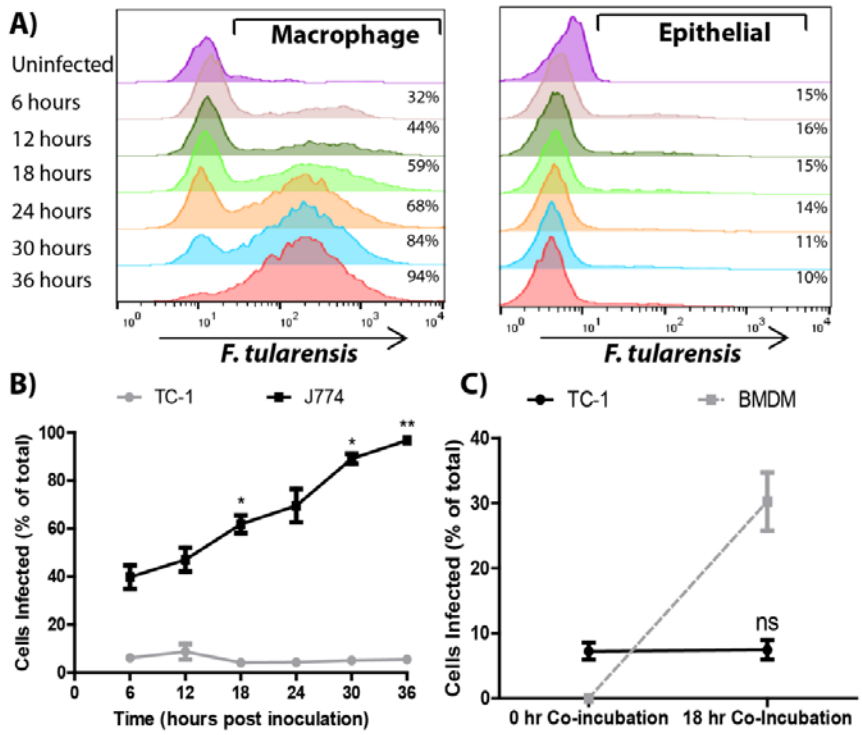

Figure 4.3: Bacterial transfer is cell type specific.

A) Percentage of infected J774 macrophages or TC-1 epithelial cells at the indicated time post inoculation for the represented histogram (log_{10} fluorescence). **B)** A compilation of the number of J774 or TC-1 cells infected over time. Statistics represent tested for a significant increase in the number of cells infected compared to the previous 6 hour time point. **C)** TC-1 to TC-1 transfer vs TC-1 to BMDM transfer after a 0 or 18 hour co-incubation. (All results from 3 independent experiments performed in triplicate) (Mean +/- SEM). (ns $p>0.05$, * $p<0.05$, **$p<0.01$).

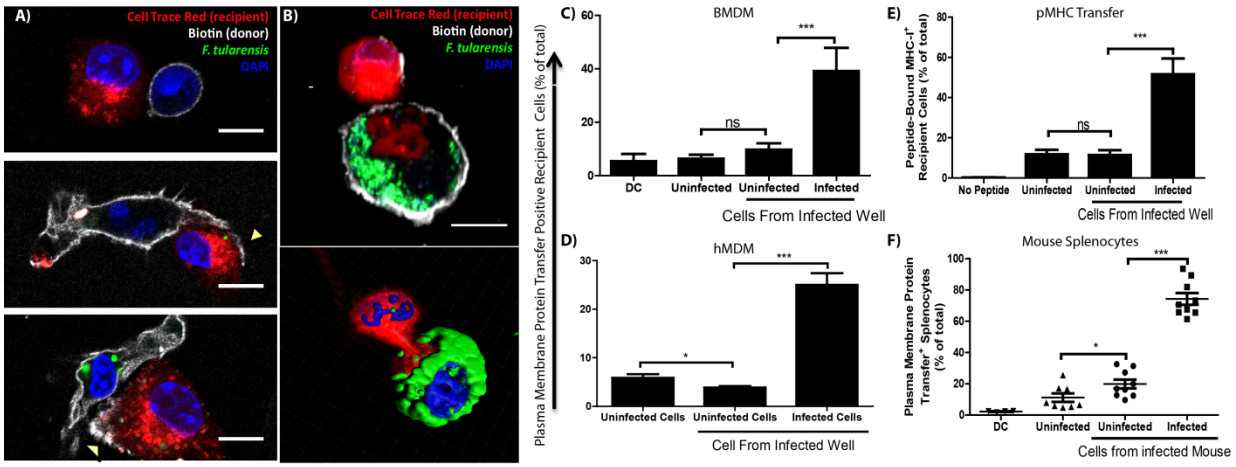

Figure 4.4: Plasma membrane protein transfer correlates with bacterial transfer.

A) Fluorescence micrographs of BMDMs before, during, and after trogocytosis. **B)** A donor [white plasma membrane] and trogocytosis positive recipient BMDM [red cell] exchanging cytosolic material and bacteria. The bottom panel is a 3D rendering of the Z-stack from the cells in the top panel. Percent of trogocytosis positive recipient cells that are in **C)** BMDMs or **D)** hMDMs. **E)** The percent of recipient macrophages that acquired SIINFEKL peptide bound MHC-I from B6 BMDMs. **F)** The percent of infected splenocytes that underwent trogocytosis in a mouse infection model (8 or 9 mice per group from 4 independent experiments). DC refers to a doublet control. (All other data are from 3-4 independent experiments performed in triplicate) (Scale bar- 10 um) (Mean +/- SEM). (ns $p>0.05$, * $p<0.05$, **$p<0.01$, ***$p<0.001$)

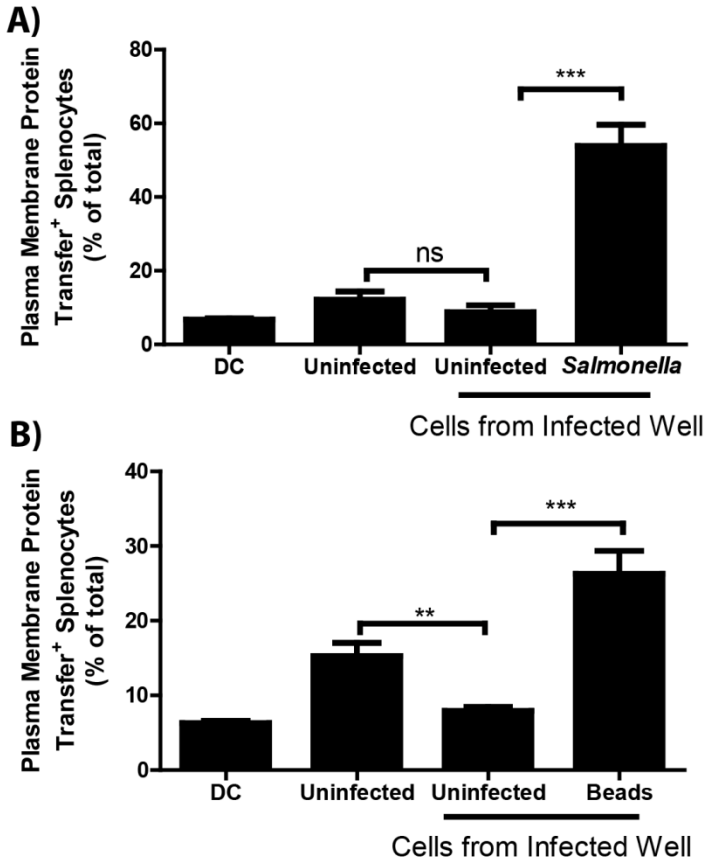

Figure 4.5: Bacterial transfer is a general phenomenon.

The percent of recipient cells that underwent PMP transfer in response to **A)** *Salmonella typhimurium* or **B)** fluorescent beads with the recipient BMDMs that acquired bacteria or beads grouped separately from recipient cells in the same well that did not acquire foreign material. DC refers to a doublet control. (All results from 3-4 independent experiments performed in triplicate) (Mean +/- SEM). (ns $p>0.05$, ** $p<0.01$, *** $p<0.001$)

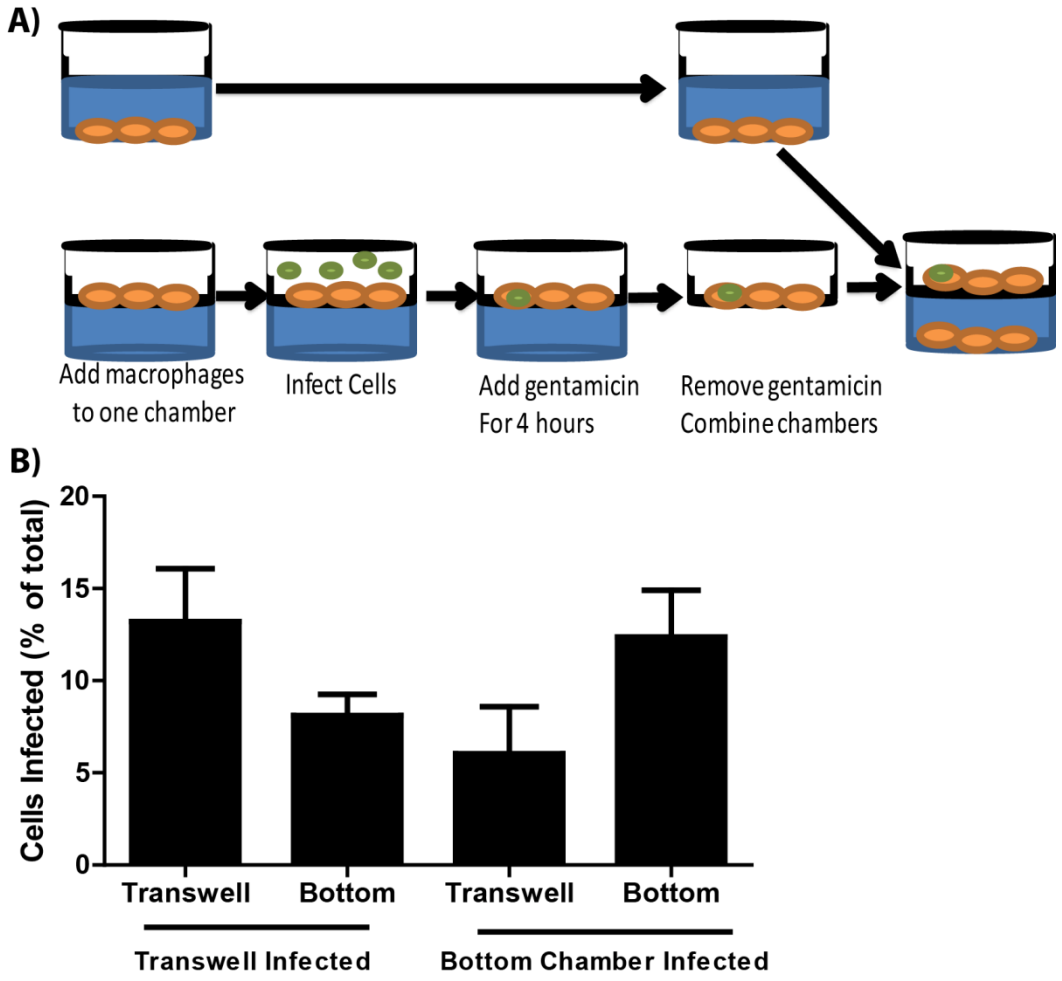

Figure 4.6: Experimental design and bacterial motility for transwell assay.

Supplemental Figure 1

A) An experimental design of the transwell assay performed in Figure 1. **B)** *F. tularensis* was added to the indicated chamber for 2 hours and both chambers were assessed for the number of BMDMs that became infected. (3 independent experiments performed with a single replicate) (Mean +/- SEM).

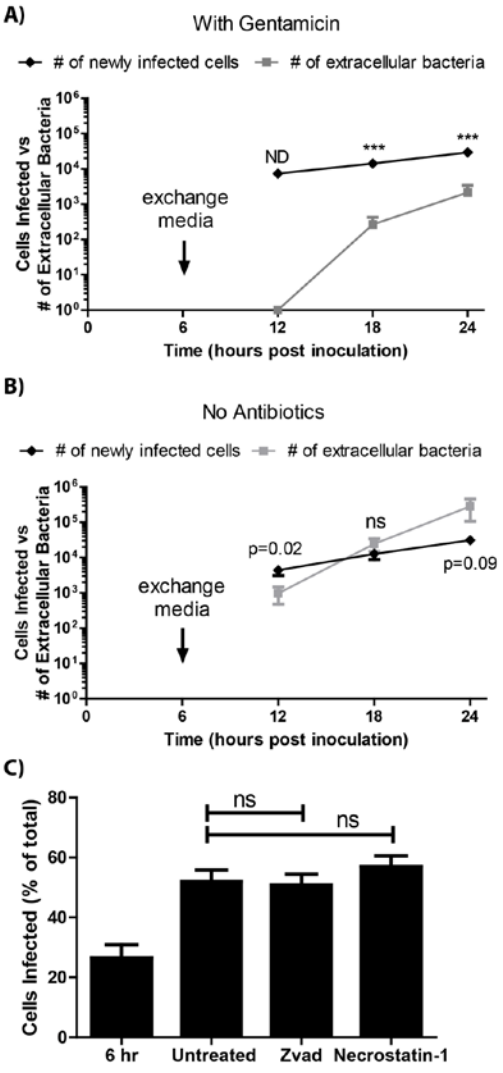

Figure 4.7: The extracellular space is not a major source of infectious bacteria.

Supplemental Figure 2

The total number of BMDMs infected per 6 hour interval compared to the number of extracellular bacteria in 1 milliliter of media either **A)** with or **B)** without gentamicin. All samples were treated with gentamicin between 2 and 6 hours post inoculation to destroy extracellular bacteria from the inoculum. **C)** BMDMs were assessed for the number of infected cells at 6 or 24 hours post inoculation. Z-Vad(OMe)-FMK or necrostatin-1 were added at 6 hours post inoculation. (All experiments from 3 independent experiments performed in triplicate)

(Mean +/- SEM). (ND- not determined, bacterial counts below limit of detection, ns $p>0.05$, **$p<0.05$,**$p<0.01$, ***$p<0.001$)

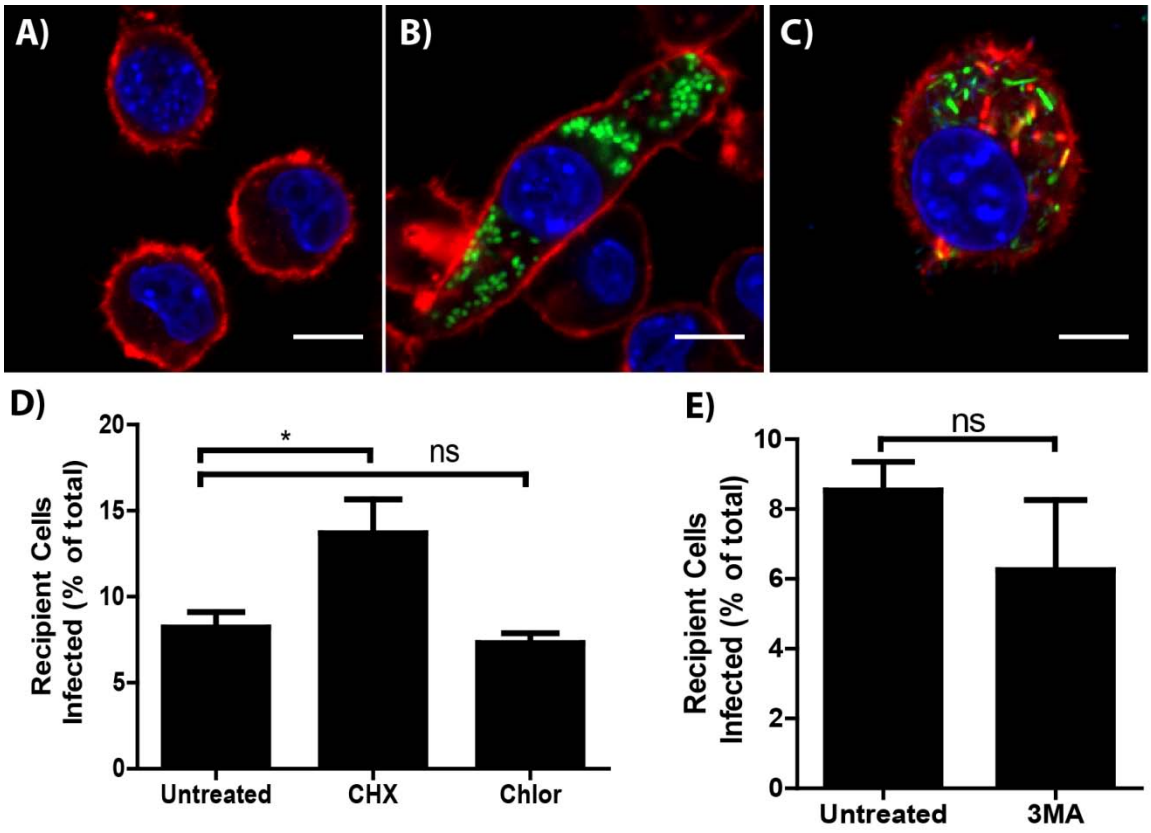

Figure 4.8: *F. tularensis* does not transfer via actin based motility or autophagy.

Supplemental Figure 3

Representative micrographs of **A)** uninfected, **B)** *F. tularensis* infected, or **C)** *Listeria monocytogenes* infected BMDMs 16 hours post inoculation. DAPI is depicted in blue, phalloidin (actin) in red and the bacteria in green. The scale bar represents 10 uM. **B)** Transfer of bacteria to recipient cells in the presence of host (cycloheximide [CHX]) or bacteria (chloramphenicol [Chlor]) protein synthesis inhibitors. **E)** *F. tularensis* transfer to recipient BMDMs after a 6 hour co-incubation in the presence or absence of 3-methyladenine. (All experiments from 3 independent experiments performed in triplicate) (Mean +/- SEM). (ns $p>0.05$, * $p<0.05$).

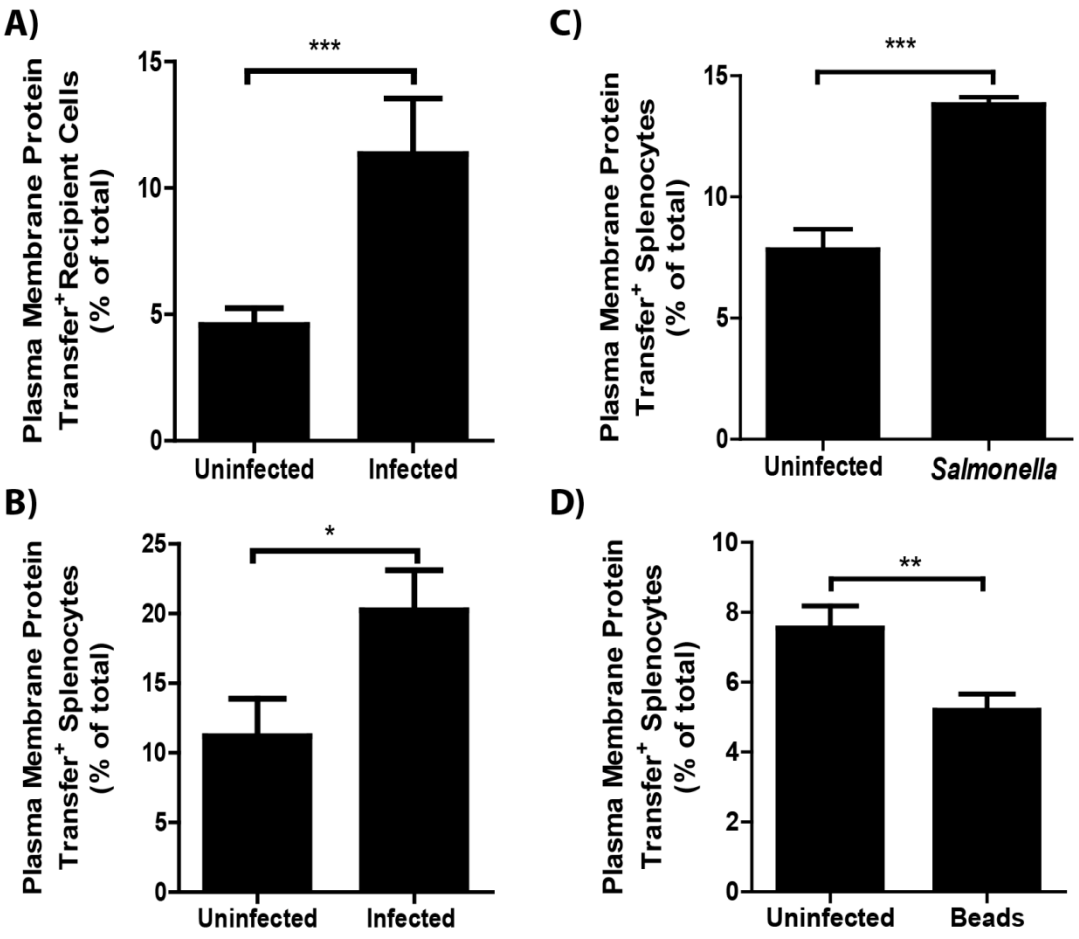

Figure 4.9: Plasma membrane protein exchange increases during infection.

Supplemental Figure 4

A) The percent of Balb/c recipient BMDMs that acquired B6 MHC-I from *F. tularensis* infected or uninfected donor B6 BMDMs. **B)** The percent of splenocytes that exchanged MHC-I in infected or uninfected mice (8 or 9 animals per group from 4 independent experiments). The percent of Balb/c recipient BMDMs that acquired B6 MHC-I from uninfected or **C)** *S. typhimurium* or **D)** bead infected donor B6 BMDMs. (Mean +/- SEM). (All other experiments from 3 independent experiments performed in triplicate) (* $p<0.05$, ** $p<0.01$, *** $p<0.001$)

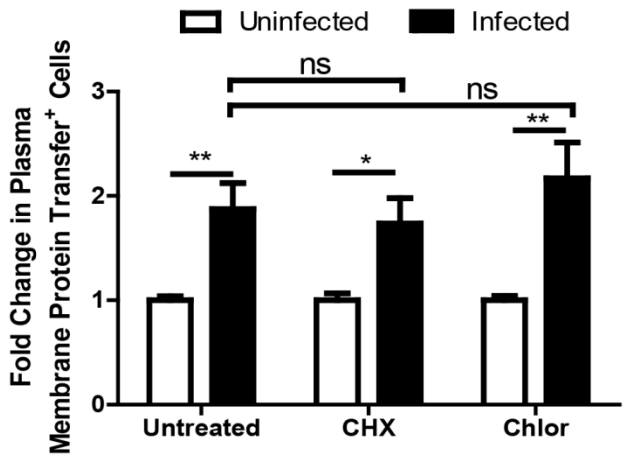

Figure 4.10: Plasma membrane protein transfer does not require *de novo* protein synthesis.

Supplemental Figure 5

The change in MHC-I transfer induced by infection when host (cycloheximide [CHX]) or bacteria (chloramphenicol [Chlor]) protein synthesis is inhibited. The uninfected cells were averaged for each experiment and each infected or uninfected sample was compared to this average because cycloheximide and chloramphenicol altered the basal level of MHC-I exchange. (Mean +/- SEM). (n=2 independent experiments performed in triplicate) (ns $p>0.05$, * $p<0.05$, ** $p<0.01$).

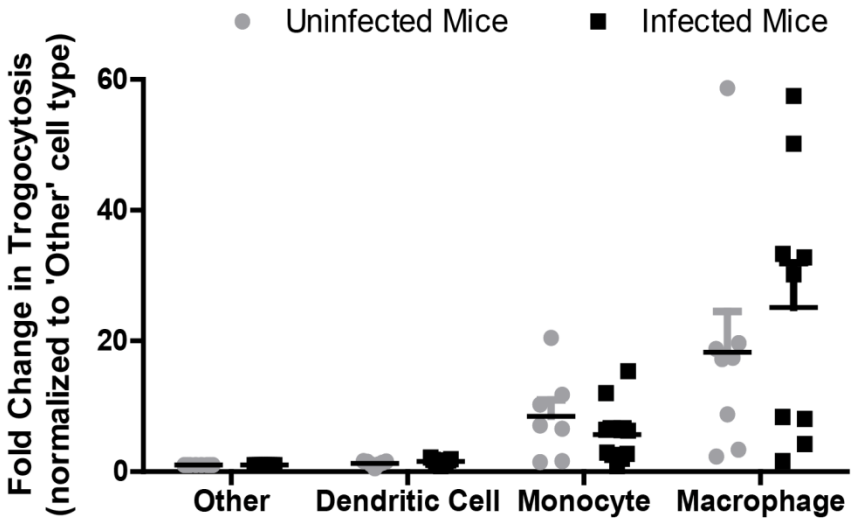

Figure 4.11: Trogocytosis in various cell types in mouse splenocytes.

Supplemental Figure 6

The percent of Balb/c H2-Kd positive cells that had surface exposed CD45.1 in each represented population. Macrophage: F4/80+; Monocyte: F4/80-, CD11b+; Dendritic Cell: F4/80-, CD11c+; Other: F4/80-, CD11b-, CD11c-. Results for each cell type were normalized to the 'Other' population. (8 or 9 animals per group from 4 independent experiments)

CHAPTER 5: DISCUSSION, FUTURE DIRECTION AND CONCLUSIONS

The characterization of a novel interaction between bacterial pathogens and autophagy.

Intracellular pathogens manipulate host defense mechanisms to enhance microbial proliferation. One such example is autophagy. Autophagy is a well characterized anti-microbial host defense that is manipulated by a wide range of pathogens for intracellular survival and replication. Autophagy induction inhibits cell death, increases the amount of intracellular nutrients by degrading macromolecules, and autophagosomes are a non-canonical secretion mechanism for select proteins, including the cytokine IL-1B [164-166]. Viral pathogens manipulate autophagy to maintain infected cell viability or exploit autophagy for non-lytic exocytosis (Table B.1). Prior to my dissertation, one important question was whether pathogens could out-compete the host for autophagy-derived nutrients. Cells infected with Dengue virus use autophagy derived triglycerides to increase intracellular ATP levels for the host cell, presumably to maintain host cell viability for Dengue virus replication [124]. But Dengue virus does not directly use autophagy by-products [124]. My work indicated that select pathogens are able to directly harvest autophagy by-products while evading xenophagy. These data were confirmed in *A. phagocytophilum* [123]. My dissertation research was one of the first to describe precisely how autophagy benefits a bacterial pathogen during infection.

How can pathogens benefit from autophagy induction?

My work on how *F. tularensis* harvests nutrients from ATG5-independent autophagy helped to change the model for how intracellular pathogens acquire nutrients from the host. Prior to this project, the paradigm for bacterial nutrient acquisition was that intracellular microbes simply scavenged the host cell cytosol for available nutrients. The rationale for this model was that bacteria acquire iron and a few other nutrients in this manner. Basically, iron acquisition generally relies on bacteria exporting iron chelating molecules (siderophores) or breaking down host iron containing compounds such as heme [167]. Both of these mechanisms are active bacterial processes and can function in the absence of a host cell. Since iron acquisition occurs through bacteria-mediated scavenging, many groups focused on bacterial scavenging to acquire other nutrients from the host. These investigations have been successful at characterizing certain individual nutrients. For example, *F. tularensis* degrades glutathione (GSH) for cysteine and *Mycobacterium tuberculosis* degrades cholesterol for lipids [13,168].

But bacterial nutrient scavenging requires the required nutrients to be present in structures that are conserved in each host the bacteria infect. GSH is important for enzyme detoxification in species ranging from aerobic amoebae to mammals and is likely present within each host that *F. tularensis* infects [13,169]. But certain nutrients are in complex macromolecules that vary widely between different hosts, such as amino acids being sequestered primarily within proteins or peptides. Instead of secreting effectors to degrade these macromolecules, we hypothesized that *F. tularensis* exploits host protein degradative mechanisms to increase intracellular amino acids levels.

We found that autophagy, a critical host degradative pathway, is a major source of nutrients for *F. tularensis*. Autophagy derived by-products are a source of the amino acids that *F.*

tularensis cannot synthesize and a major source of carbon that *F. tularensis* uses to synthesize amino acids, LPS, nucleic acids, and other critical molecules. Around the same time we published our results; two other groups confirmed that intracellular bacteria exploit autophagy or host cell proteosomal degradation for amino acids [123,142]. Collectively, our work shifted the paradigm for intracellular nutrient acquisition by bacteria. The current paradigm now focuses on pathogens exploiting host degradative pathways for nutrients, a process termed 'nutritional virulence' [170]. Nutrient scavenging is required for intracellular bacteria to acquire certain specific nutrients. But nutrients that are needed en masse, such as a primary carbon source, are likely generated by manipulating host degradative or import processes. Together, these processes work synergistically to provide the bacteria with host derived nutrients.

My research on the interactions between *F. tularensis* and autophagy characterized how *F. tularensis* acquires amino acids and carbon from host cells. Yet there are still several questions that need to be addressed. *F. tularensis* may acquire other nutrients from autophagy besides amino acids, such as carbohydrates or lipids. It is also not clear how *F. tularensis* induces autophagy or how *F. tularensis* biases the infected cell to promote ATG5-independent autophagy over canonical autophagy. Identifying how *F. tularensis* exploits this pathway should yield important information about how autophagy functions and host regulation of the different forms of autophagy.

The only bacteria that benefit from autophagy through known mechanisms are *F. tularensis, A. phagocytophilum*, and *B. abortus* [122,123]. Yet most bacterial pathogens induce autophagy and evade xenophagy (Table B.1). It is unclear if or how these pathogens benefit from autophagy induction. Autophagy is actively induced by and increases replication in *Coxiella burnetti* and *Burkholderia pseudomallei,* but the exact role of autophagy in these pathogens is

unclear [171-174]. It is likely that other bacterial pathogens that induce autophagy also benefit from autophagy.

There are several different ways that pathogens can benefit from autophagy. In contrast, pro-microbial benefits of autophagy have been well defined for many viral pathogens. Viruses promote viral replication, increase host cell survival, and for non-lytic exocytosis (Table). As previously mentioned, Dengue virus benefits from autophagy due to the increase in intracellular triglycerides [124]. Intracellular bacterial pathogens require nutrients, host cell viability, and a mechanism of escape. Yet very little is known about if or how bacteria manipulate autophagy to accomplish these goals, and these events may be linked (Table B.1). Even the bacterial pathogens that have a known benefit from autophagy may also exploit autophagy for other advantages, such as enhanced cell viability.

Finally, my research on autophagy also characterized how *F. tularensis* interacts with xenophagy. Until recently, autophagy induction was viewed as a critical anti-microbial process. But recent studies indicate that microbes intentionally stimulate autophagy and use separate mechanisms to evade xenophagy (Table B.1). *F. tularensis* is frequently located adjacent to autophagosomes in cells. These data suggest that *F. tularensis* recruits or moves to autophagosomes while avoiding engulfment by xenophagy. It is unclear how *F. tularensis* evades xenophagy except that it occurs through an active process and O-antigen passively contributes to xenophagy resistance [66,175]. Another important question is how *F. tularensis* localizes adjacent to autophagosomes without becoming engulfed by the autophagosome.

Why do we care that pathogens acquire nutrients via autophagy?

Nutritional virulence is an important area of study because the bacteria rely on host mechanisms for a fundamental part of their survival: nutrients. For example, autophagy inhibition is a potential therapeutic intervention for *F. tularensis*. Treating a *F. tularensis* infected patient with the FDA approved autophagy inhibitor chloroquine should decrease *F. tularensis* replication and help the patient clear the infection. Additionally, several drugs are in clinical trials for tumor treatment that inhibit autophagy [176-178]. *F. tularensis* cannot easily compensate for impaired autophagy and would need to evolve alternate nutrient acquisition mechanisms before this treatment became ineffective. At the moment, this method is impractical because chloroquine and other autophagy drugs inhibit a variety of host processes that will result in significant side effects and antibiotics are a safer treatment option. But future work on how *F. tularensis* induces autophagy may identify specific inhibitors for *F. tularensis* induced autophagy, leading to a viable host directed therapy. Admittedly, *F. tularensis* is not a highly relevant organism for this type of therapy because it is susceptible to several antibiotics; however, this example is relevant to other pathogens that induce autophagy or for *F. tularensis* bio-defense purposes.

In summary, my research on autophagy as a nutrient acquisition strategy is part of the foundation for the nutritional virulence paradigm. Future research on how pathogens interact with autophagy will hopefully lead to host directed therapies to inhibit microbial replication.

Macrophages acquire live bacteria from neighboring infected cells.

The second major finding of my dissertation research was that intracellular bacteria transfer from infected cells to macrophages through a host-mediated process. Unlike my work on

autophagy, there is very little background information on this project and previous research on this topic comes from a diverse set of fields. Several studies have demonstrated that macrophages can acquire intracellular material from neighboring cells, such as proteins for antigen presentation [76-78]. Unfortunately, this process has several different names, including trogocytosis and 'nibbling' [77,79,80,87].

It is important to note that trogocytosis has two different connotations. Historically, trogocytosis refers to the exchange of plasma membrane components between neighboring cells [81]. Antigen cross dressing refers to dendritic cell acquisition of peptide-bound MHC-I or MHC II via trogocytosis [86,179]. This is the definition I use for trogocytosis in my writing. However, trogocytosis has recently been used in reference to a cell ingesting part of another live cell. In these works, trogocytosis refers to macrophages that gnaw on adipocytes to acquire intracellular lipid droplets and *E. histolytica* gnawing on live human cells for nutrients [79,87].

My research explicitly links the exchange of intracellular material to the exchange of plasma membrane material. This is important because the implications of this link could have important ramifications on how immune cells interact with one another. When macrophages acquire portions of tumor cells, they are likely also acquiring intracellular antigens. This may impact antigen presentation or processing and could have important implications on cancer therapeutics. Conversely, when macrophages acquire intracellular content from adipocytes or other cell types, they may also acquire certain plasma membrane proteins that alter their function.

In addition to linking these two cell biology processes, my work demonstrated a novel mechanism for pathogen transfer. The consequences of this work are potentially vast. Briefly, this mechanism of bacterial transfer could impact bacterial dissemination, mounting an adaptive

immune response and provide a new mechanism of cell to cell communication during infection. This work is not only relevant to bacterial pathogenesis, but is also highly relevant for tissue engraftment, vaccine development, tumor biology, and the link between the innate and adaptive immune systems.

What are the implications of live cell phagocytosis by macrophages?

Macrophages ingest portions of living cells to generate immune responses upon cell to cell contact [79]. I found that when the ingested cell is infected, bacteria transfer to and infect the recipient macrophage. We have temporarily termed phagocytosis of live cell as metadosis (metadosi is Greek for 'transfer' or 'communicate'). Interestingly, bacterial infections increase the rate of metadosis by macrophages, suggesting that this is a protective mechanism for the host during infection. My work on bacterial transfer during metadosis should have far reaching implications on microbial dissemination, the adaptive immune response, and cell to cell communication during infections.

The benefits of direct cell to cell transfer of live bacteria in microbial pathogenesis are relatively straightforward. By transferring via metadosis, the bacteria can infect new cells and gain access to a new replicative niche without encountering extracellular anti-microbial factors such as antibodies or complement. The newly infected macrophage can also migrate from the site of infection to potentially disseminate the bacteria.

Macrophages enhance trogocytosis and bacterial transfer in response to infection, implying that this process is host mediated. But how does the host benefit when macrophages acquire live bacteria from other cells? Only select immune cell types can generate a systemic immune response to pathogens through antigen presentation. Metadosis may be a mechanism for

antigen presenting cells (APCs) to acquire antigen from non-APCs to generate a T cell response. Additionally, the newly infected macrophages may migrate away from the site of infection, but they will likely migrate to lymph nodes or other immunological strongholds. Thus, intracellular bacteria may benefit from transfer in the short term through dissemination and moving to new replicative niches, but metadosis is a potential mechanism to prime the adaptive immune response and eventually clear the pathogen.

Metadosis may also help macrophages limit bacterial replication immediately following transfer. Macrophages serially transfer *F. tularensis*, but the increase in infected cells did not result in an increase the total number of viable bacteria. Instead, the total number of viable bacteria significantly decreased after peak infection. These data indicate that the macrophages that become infected via metadosis are resistant to infection. As previously mentioned, *F. tularensis* infection does not lead to robust cytokine secretion. Other extracellular cell communication signals may occur, but a more likely explanation centers on the transfer of bulk cytosolic material with bacteria during metadosis. The newly infected macrophages may acquire anti-microbial signals in addition to live bacteria. For example, cytosolic DNA leads to the production of the second messenger cGAMP [180]. cGAMP binds to STING to activate the transcription factors IRF3 and NF-kB, leading to the transcription of type 1 interferon [181]. If cGAMP transfers to a newly infected cell along with the bacteria, the recipient macrophage may immediately shift its transcriptional profile to be anti-microbial. Several other immune sensing intermediates, RNA molecules, or other anti-microbial factors could also transfer with bacteria upon live cell phagocytosis. Importantly, we only tracked metadosis when bacteria transferred, but macrophages may frequently phagocytose portions of infected cells without becoming infected. Thus, macrophages may be primed to destroy the pathogen prior to becoming infected.

Why is enhancing macrophage trogocytosis important?

We also found that macrophages enhance the transfer of plasma membrane proteins in response to bacterial stimuli. Specifically, macrophages were more likely to exchange functional MHC-I. Trogocytosis is a constitutive immune cell process and the observed increase in MHC-I transfer during infection likely improves antigen transfer to stimulate an immune response. Artificial up-regulation of MHC-I trogocytosis may have several therapeutic applications. Trogocytosis is important for the generation of an immune response to recognition of tumors and foreign material. MHC-I trogocytosis is important for several clinically important fields, including vaccine efficacy, tumor identification, and tissue engraftment.

For tumor identification, dendritic cells acquire peptide bound MHC-I from tumor cells via trogocytosis and generate a cytotoxic T cell response solely from the acquired peptide-bound MHC-I [182]. Importantly, the amount of transferred peptide-bound MHC-I affected the CD8+ T cell response [182]. Artificially increasing trogocytosis by the addition of bacterial agonists should increase MHC-I trogocytosis between tumor cells and APCs to improve tumor clearance. Interestingly, infecting tumors with bacterial pathogens increases anti-tumor immune responses in human patients and has been used as a cancer therapy for over 100 years [183,184]. Pathogens have extremely broad effects on the immune response, but my data suggests that one benefit of infection is increased MHC-I trogocytosis. Further research into how bacterial pathogens enhance trogocytosis should make these procedures safer and more efficient.

Furthermore, MHC-I trogocytosis by dendritic cells enhances vaccine efficacy. Dendritic cells acquire antigen to stimulate T cells via trogocytosis [160]. Identifying how cells up-regulate trogocytosis in response to pathogens should improve adjuvant and/or vaccine design. Likewise,

trogocytosis is likely important in tissue engraftment. When mice are injected with human cells, the cells that acquire mouse CD45 via trogocytosis are far more likely to survive than human cells that do not acquire this protein [158]. Thus trogocytosis may enhance tissue engraftment. Taken together, future research into how trogocytosis is regulated or the mechanisms to manipulate trogocytosis is likely to have clinical benefits.

In summary, my work on cell to cell transfer of intracellular pathogens should further our understanding of how macrophages function in the immune response and describes a new mechanism for bacterial transfer. Future research into this phenomenon may have wide ranging clinical applications.

Conclusions

Host cells have evolved intricate innate immune defense mechanisms that are highly effective at destroying the overwhelming majority of microbes that cells encounter. But intracellular pathogens not only evade these defenses, they often manipulate these defenses to enhance intracellular survival and proliferation. Identifying how pathogens manipulate the host is important for several reasons. These host processes can be targeted for therapeutic intervention to enhance or replace antibiotic therapies. Secondly, pathogens, or specific microbial structures, stimulate a range of host defense pathways and are a tool to identify new host immune defenses. This identification strategy has been effective at finding a wide range of immunological and mammalian cell biology processes. We used *F. tularensis* to track metadosis and found that bacteria can transfer from cell to cell via this process. Further research into this phenomenon is likely to link metadosis to the interaction between the innate and adaptive immune responses.

Finally, the microbial proteins responsible for manipulating host defenses can be used as tools to better define cellular pathways and for therapeutic development [185,186].

My dissertation research improved our understanding of how intracellular pathogens manipulate the host to enhance bacterial replication or survival. Although my work has vast potential for future research directions, one important unresolved question for both of my dissertation topics is the molecular mechanisms for both microbial induction and host execution. Hopefully future work on these pathways will reveal the precise interactions necessary for these host-pathogen interactions to occur, allowing the translation of my research to clinical applications.

APPENDIX 1: FEEDING UNINVITED GUESTS: MTOR AND AMPK SET THE TABLE FOR INTRACELLULAR PATHOGENS[3]

Introduction

Most pathogenesis studies focus on pathogen virulence attributes that mediate host colonization, toxicity, or immune evasion. Some studies focus on how pathogens employ active mechanisms to acquire essential nutrients such as iron and vitamins from the host by producing siderophores or avidins. In order to prevent pathogen nutrient acquisition, host cells employ a process called nutritional immunity to sequester these nutrients, particularly iron, from invading pathogens [187]. However, relatively little attention has been paid to understanding the mechanisms by which pathogens parasitize energy and catabolic substrates from the host even though several host and pathogen metabolic genes, including those in central carbon metabolism, are regularly identified as required for growth in the host [188,189]. This issue is particularly important for intracellular pathogens that must compete with the host cell for energy and nutrient sources.

How and where do intracellular pathogens obtain sufficient amounts of energy and nutrients to support their replication? Pathogens may either parasitize existing energy stores or manipulate the host cell to create usable energy and anabolic precursor metabolites. Several recent studies have identified the host AMP-activated protein kinase (AMPK) and mammalian target of rapamycin (mTOR) kinases as two important regulators of cellular metabolism whose activities are often altered during infection. However, the AMPK/mTOR pathway also regulates autophagy, which can destroy cytosolic pathogens. While the evasion of autophagy by pathogens

[3]This article was previously published in PLOS Pathogens. The citation is: Brunton J, Steele S, Ziehr B, Moorman N, Kawula T. Feeding uninvited guests: mTOR and AMPK set the table for intracellular pathogens. *PLoS Pathog*. 2013;9(10):e1003552. doi: 10.1371/journal.ppat.1003552

is well appreciated, recent work suggests that both the AMPK/mTOR pathway and autophagy itself can provide intracellular metabolites that support intracellular pathogen replication.

AMPK and mTOR Regulate Energy Homeostasis

During times of limited nutrient availability, intracellular ATP levels fall, with a corresponding increase in AMP levels. Within eukaryotic cells the increased AMP:ATP ratio induces AMPK activity, which in turn initiates a series of signaling events that stimulate energy and nutrient acquisition [190]. For example, activated AMPK stimulates glycolytic flux, increases glucose uptake, and induces fatty acid oxidation (Figure A1.1). Together these events allow the cell to use its existing metabolic stores and also acquire new sources of energy. At the same time, activated AMPK limits energy consuming processes. Activated AMPK conserves energy by globally reducing protein synthesis, which perhaps is the most energy-intensive process in eukaryotic cells. AMPK limits protein synthesis by antagonizing the mTOR kinase, and mTOR kinase activity is necessary for formation of the elF4F complex, which is critical for translation initiation. In addition, mTOR and AMPK inversely regulate the recycling of existing intracellular metabolites through their effects on autophagy. Active AMPK stimulates autophagic breakdown of macromolecular complexes in the cell, thus producing energy and nutrients. In contrast, active mTOR suppresses autophagy to promote cell growth and proliferation. In a simplified view, when energy is low AMPK is active and mTOR is inhibited. This stimulates energy-producing processes and inhibits energy consumption thereby providing sufficient energy to support cell viability. Although AMPK and mTOR have additional roles outside of cellular metabolism, here we focus on the effects of AMPK and mTOR on cellular metabolism during infection by intracellular pathogens.

Manipulation of Both AMPK and mTOR by Intracellular Pathogens

In order to achieve optimal levels of proliferation, many pathogens must manipulate activity of AMPK and mTOR. Interestingly, several viral pathogens have evolved strategies that allow for the induction of both AMPK and mTOR activity. For example, infection with human cytomegalovirus (HCMV) increases both AMPK and mTOR activity [191]. To acquire sufficient energy for viral growth, HCMV infection increases glycolytic flux in an AMPK-dependent manner [189,192]. However, HCMV must strictly regulate AMPK activity during infection, as treatment of infected cells with chemicals that strongly activate or inhibit AMPK can limit viral replication [192,193]. Interestingly, HCMV replication also requires fatty acid synthesis, which should be inhibited when AMPK is activated. Yet fatty acid synthesis is maintained during HCMV infection through a mechanism that requires mTOR activation [194]. How does HCMV allow for the activation of both AMPK and mTOR? The answer lies in part in the activity of the HCMV UL38 protein (pUL38). pUL38 binds and inhibits the TSC1/2 complex, which is necessary for antagonism of mTOR by activated AMPK [195]. HCMV thus uncouples AMPK/mTOR signaling resulting in increased energy production and lipid synthesis, both of which contribute to virus replication.

Simian virus 40 (SV40) infection also stimulates both AMPK and mTOR activity. SV40 small T antigen is both necessary and sufficient for AMPK activation [196,197]. This function of small T antigen may provide critical nutrients needed for viral replication. mTOR activity is induced early in infection but inhibited as infection progresses. The mechanism driving the early induction of mTOR activity is unknown, but may be the result of Akt activation by the SV40 T antigens. However, the inhibition of mTOR activity during the late stage of infection is due to the effects of the SV40 small T antigen [197]. While activated AMPK would seemingly reduce

SV40 protein synthesis, the expression of SV40 late proteins is driven by an internal ribosome entry site (IRES) that allows for efficient late mRNA translation when mTOR is inhibited [196]. It is likely that other pathogens employ active mechanisms to balance AMPK and mTOR signaling to allow for both catabolic and anabolic processes essential for pathogen replication, similar to HCMV and SV40.

Inhibiting AMPK or Inducing mTOR Can Provide Essential Substrates for Pathogen Replication

Enveloped viruses require host lipids to generate the virion membrane. Activated mTOR stimulates fatty acid and lipid synthesis, and therefore could prove beneficial for virus assembly. In fact, host lipid metabolism is essential for the hepatitis C virus (HCV) life cycle and is highly regulated during infection [198,199]. HCV infection limits AMPK activity and chemical induction of AMPK suppresses viral replication and inhibits fatty acid synthesis in HCV-infected cells [200]. Consistent with AMPK suppression, mTOR activity is increased during HCV infection through increased Akt signaling and decreased TSC1/2 expression [201]. However, this raises the question of how HCV acquires significant energy sources for viral replication in an AMPK-inhibited, mTOR-activated metabolic state? The answer may be the temporal regulation of host signaling and nutrient usage. Glucose import is required for viral replication and glycolytic flux is induced early during HCV infection [199,202]. The products of glycolysis are likely diverted to fatty acid synthesis, as TCA flux and oxidative phosphorylation are reduced in HCV-infected cells [199,203]. Later during infection, glucose uptake is reduced, while β-oxidation and amino acid catabolism are increased [199]. It is therefore possible that HCV temporally regulates AMPK and mTOR activity to achieve significant viral protein translation and lipid production, yet still obtain

sufficient energy to support virus replication. Some bacterial pathogens may benefit from inhibiting AMPK and activating mTOR by inducing lipid synthesis, as *Mycobacterium tuberculosis* and *Chlamydia trachomatis* utilize fatty acids derived from lipid droplets [204,205]. However, it is unknown how these bacteria affect host metabolic signaling to acquire nutrients.

AMPK activation also inhibits the replication of several arboviruses, including Rift Valley fever virus (RVFV) [206]. RVFV replication can be rescued in the presence of activated AMPK by providing cells with excess palmitate [206]. This suggests that AMPK inhibition is required to provide lipids essential for viral replication. The HIV-1 Tat protein inhibits the host SIRT1 protein resulting in AMPK inhibition [207]. Interestingly, AMPK induction inhibits lytic HIV replication, but is involved in reactivation of latent HIV genomes suggesting that AMPK activity may have different roles in acute and persistent infection [208].

AMPK Activation May Benefit Replication of Diverse Pathogens

It takes a lot of energy to make hundreds, thousands, or potentially millions of new parasites, bacteria, or viruses. It seems logical that intracellular pathogens that undergo significant intracellular growth would activate AMPK due to the energetic demands placed on the infected cell. Activation of AMPK could provide several benefits for intracellular pathogens. The increased glucose uptake, glycolysis, and fatty acid breakdown would increase available intracellular energy and nutrient pools needed for pathogen replication. For example, *Leishmania donovani* amastigotes (the parasitic form that grows inside macrophages) preferentially generate energy through fatty acid oxidation and amino acid catabolism [209], suggesting *L. donovani* acquires fatty acids and amino acids from the infected host cell. Consistent with this finding, transcriptomic analysis of macrophages infected with the related parasite *Leishmania major*

suggests that infected cells increase glucose transport, glycolysis, and starch degradation [210]. While it is currently unknown how *Leishmania* alters host metabolic processes, a reasonable hypothesis is that intracellular *Leishmania* activates AMPK to benefit parasite replication. Activated AMPK could stimulate increased glucose utilization and autophagy, thus creating elevated levels of anabolic precursor pools for parasite growth. Parasite replication requires the *Leishmania* protein GP63, which cleaves and inactivates mTOR to reduce type I interferon production, thus AMPK activation could further benefit parasite replication by inhibiting mTOR [211]. Viral pathogens may also benefit from AMPK activation. Measles virus requires β-oxidation for replication [212], but it is unknown if the virus manipulates AMPK for energy generation. It would be interesting to determine if these intracellular pathogens and others induce AMPK to generate energy and nutrients for growth.

Autophagy Provides Intracellular Pathogens with Nutrients

Autophagy is an essential cellular process that recycles cellular constituents from macromolecular complexes under conditions of nutrient stress. As discussed above, autophagy is positively regulated by AMPK and negatively regulated by mTOR. However, autophagy also functions as a host defense mechanism that destroys intracellular pathogens through a process termed xenophagy. While generally viewed as detrimental for intracellular pathogens, some bacteria and viruses use autophagosomes as a replicative niche [213]. Whether these pathogens benefit or simply tolerate residing in autophagosomes remains unclear. However, it may be that replicating in a site where free nutrients are accumulating provides pathogens with a competitive edge for the acquisition of nutrients. This concept is supported by recent evidence that intracellular pathogens may use autophagy to acquire energy and nutrients for growth. Dengue

virus–induced autophagy degrades lipid droplets. This increases free fatty acids levels in the cell and stimulates β-oxidation, which is required for efficient dengue virus replication [124]. Similarly, we have found that *Francisella tularensis* growth is impaired in autophagy-deficient host cells. Bacterial growth was restored in autophagy-deficient cells by supplying the infected cells with excess pyruvate or amino acids. Since *F. tularensis* replicates within the cytosol of host cells, our results suggest that intracellular *F. tularensis* uses autophagy to increase cytosolic nutrient pools that support bacterial growth [5]. Interestingly, *F. tularensis* avoids engulfment by classical autophagosomes [129] and instead induces an alternative form of autophagy that is required for bacterial replication [5]. It is attractive to speculate that other intracellular pathogens manipulate autophagy to avoid xenophagic destruction, while simultaneously benefiting from autophagy-derived nutrients.

Conclusion

AMPK and mTOR are critical regulators of host cell metabolism making them logical targets for manipulation by invading pathogens. The energetic burden of the host cell to create hundreds or more pathogens should deplete cellular ATP levels, thus activating AMPK. AMPK induction stimulates host processes to produce energy and nutrients that the pathogen could then steal from the host. This idea suggests AMPK activation may be a common theme among infection by successful intracellular pathogens. On the other hand, mTOR signaling stimulates protein and lipid synthesis, which could be beneficial for many viral pathogens; whereas mTOR modulation is likely less important for free-living bacteria pathogens and parasites that supply their own biosynthetic and translation machinery. Identifying what nutrient sources are required for intracellular growth and how host metabolic signaling is manipulated by infection is being

investigated in viral pathogenesis, yet remains poorly understood in bacterial and parasitic pathogenesis.

Manipulating host metabolism is an attractive approach to controlling infection as targeting the host rather than the pathogen should considerably reduce the ability of pathogens to develop drug resistance. Several drugs already in clinical use target the AMPK or mTOR kinases to treat diseases such as cancer and diabetes. The studies described above suggest that these drugs may have additional uses in treating infections with intracellular pathogens. As our understanding of pathogen manipulation of host metabolism grows, it may also be possible to develop inhibitors of specific host metabolic pathways hijacked by intracellular pathogens. Identifying the essential nutrients required for intracellular pathogen proliferation and the host pathways manipulated to acquire these nutrients will be a significant step in understanding the requirements for viral, bacterial, and parasitic pathogenesis and identifying new targets for novel therapeutics.

Figures

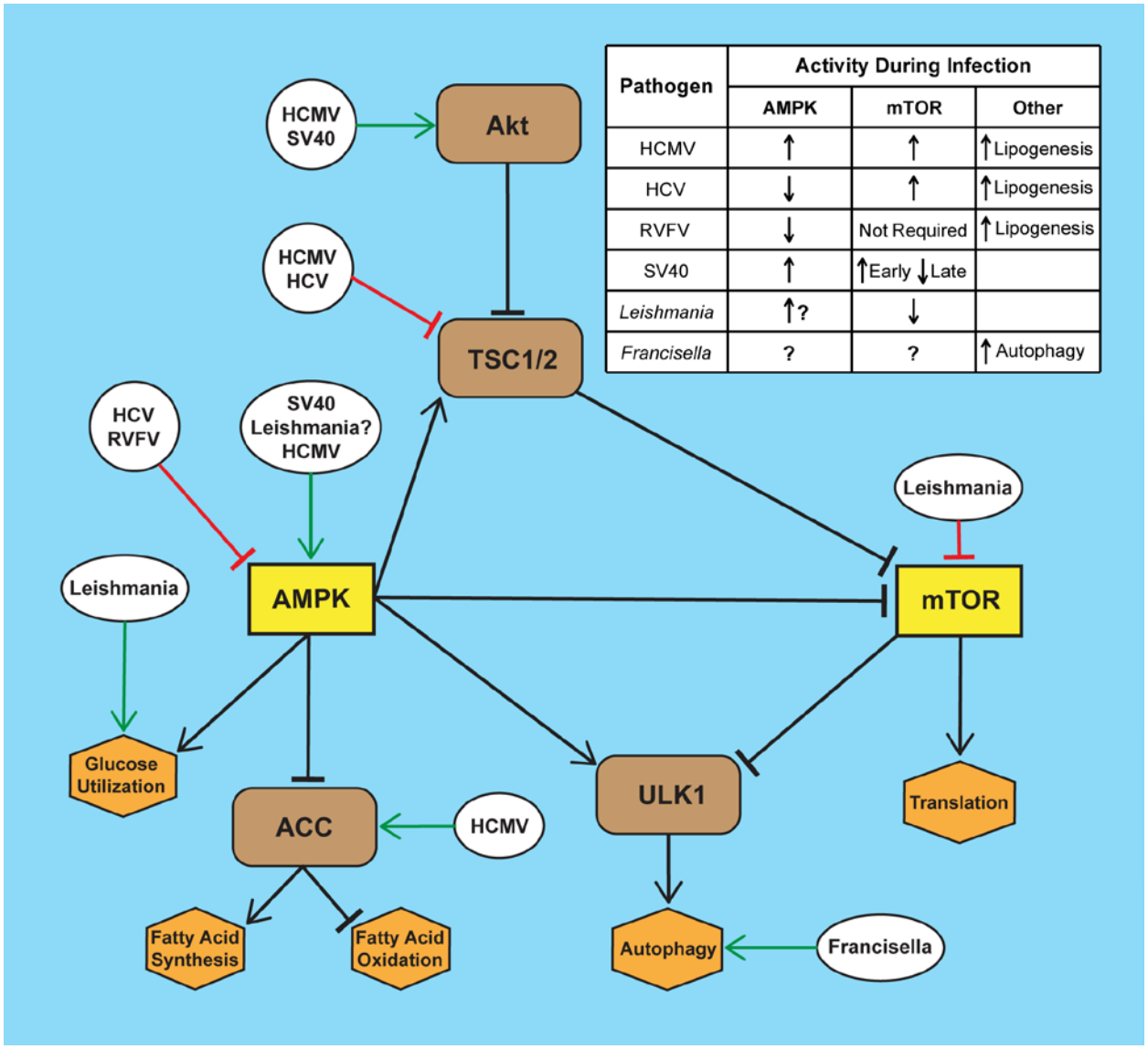

Pathogen	Activity During Infection		
	AMPK	mTOR	Other
HCMV	↑	↑	↑Lipogenesis
HCV	↓	↑	↑Lipogenesis
RVFV	↓	Not Required	↑Lipogenesis
SV40	↑	↑Early ↓Late	
Leishmania	↑?	↓	
Francisella	?	?	↑Autophagy

Figure A1. 1: Infection by Diverse Pathogens Impacts AMPK and mTOR Signaling.

Several intracellular pathogens manipulate the AMPK/mTOR pathway during infection through either directly targeting AMPK or mTOR or by targeting the upstream or downstream pathways. Depicted here are specific points of manipulation in the mTOR/AMPK pathway by human cytomegalovirus (HCMV), hepatitis C virus (HCV), Rift Valley fever virus (RVFV), simian virus 40 (SV40), *Leishmania*, and *Francisella* species. The table summarizes the resulting effects on the activities of mTOR and AMPK from infection by the specific pathogen.

APPENDIX 2: THE ROLE OF AUTOPHAGY IN INTRACELLULAR PATHOGEN NUTRIENT ACQUISITION[4]

Overview

Following entry into host cells intracellular pathogens must simultaneously evade innate host defense mechanisms and acquire energy and anabolic substrates from the nutrient-limited intracellular environment. Most of the potential intracellular nutrient sources are stored within complex macromolecules that are not immediately accessible by intracellular pathogens. To obtain nutrients for proliferation, intracellular pathogens must compete with the host cell for newly-imported simple nutrients or degrade host nutrient storage structures into their constituent components (fatty acids, carbohydrates and amino acids). It is becoming increasingly evident that intracellular pathogens have evolved a wide variety of strategies to accomplish this task. One recurrent microbial strategy is to exploit host degradative processes to break down host macromolecules into simple nutrients that the microbe can use. Herein we focus on how a subset of bacterial, viral and eukaryotic pathogens leverage the host process of autophagy to acquire nutrients that support their growth within infected cells.

Introduction

Food and reproduction are basic necessities for life. Intracellular pathogens infect host cells and are dependent on them for nutrients to propagate. While there is an abundance of food inside host cells, molecules are mostly sequestered in complex compounds or structures such as glycogen, lipid droplets, and proteins; forms that are not readily usable by microbial intruders.

[4] This chapter was previously published as an article in Frontiers Cellular and Infection Microbiology. The citation is: Steele S, Brunton J, Kawula T. The role of autophagy in intracellular pathogen nutrient acquisition. *Front. Cell. Infect. Microbiol.* 2015 Jun 9;5:51. doi: 10.3389/fcimb.2015.00051

Therefore, simply gaining access to the interior of a host cell and avoiding potent innate antimicrobial host defenses is not sufficient to guarantee successful occupation and growth. Once inside, pathogens must either stimulate host cell import of metabolites or degrade intracellular storage molecules into compounds that can be transported and metabolized. There are multiple mechanisms by which intracellular pathogens accomplish this goal. For example, *Mycobacterium tuberculosis* encodes proteins to degrade host-derived lipids, such as cholesterol, for a carbon source [168]. Pathogens can also take advantage of host signaling pathways to acquire nutrients. Both *Brucella abortus* and *Salmonella enterica* thrive on the increased glucose that is imported upon activation of various peroxisome proliferation-activated receptors (PPARs) in alternatively activated monocytes [214,215]. Recently, several pathogens have been demonstrated to exploit host cell macroautophagy, hereafter autophagy, for nutrients. Autophagy is a critical mechanism that host cells use to increase nutrient availability when stressed. Since infection should exert a wide range of stresses on cells, it is not surprising that a diverse range of microbes exploit autophagy.

Autophagy is a highly conserved, multi-faceted eukaryotic process that maintains cellular homeostasis by degrading cytosolic material. Autophagy was noted as early as 1957 during the characterization of kidney cells by transmission electron microscopy [216,217]. In 1964, autophagy was identified as a mechanism to degrade cytosolic components and mitochondria under starvation conditions [166]. Since then, autophagy has been linked to a wide range of functions including antigen presentation through major histocompatibility complex II (MHC-II), unconventional secretion of inflammatory mediators, and cell viability [50,164,165].

Autophagy is divided into several subsets based on the components being degraded. Bulk autophagy refers to non-specific cytoplasmic turnover while selective autophagy refers to

autophagic degradation of specific structures. There are several distinct types of selective autophagy, which target specific cellular components such as mitochondria (mitophagy) or lipids (lipophagy). During infections, intracellular microbes are recognized, targeted, and degraded through a form of selective autophagy termed xenophagy. Although xenophagy is efficient at destroying microbes that enter the cytosol, intracellular pathogens have developed numerous evasion strategies to avoid destruction by xenophagy, including the degradation or inhibition of autophagy components, camouflaging itself in host proteins, or blocking autophagosome maturation (Table B.1).

Several pathogens that evade xenophagic killing have incorporated autophagy into their intracellular life cycle. These microbes exploit autophagy to sustain host cell viability, increase nutrient production, and/or for non-lytic exocytosis (Table B.1). Viruses also use autophagy or autophagy components for viral assembly and maturation (Table B.1). In this review, we will focus on how pathogens avoid destruction by xenophagy while harvesting nutrients from autophagic degradation of host components.

What is Autophagy?

Autophagy is a constitutive process that degrades long lived-proteins, organelles, and aggregates. In mouse embryonic fibroblasts (MEFs), a common cell line used for autophagy research, the basal rate of autophagy is approximately 1-2% of the cytosolic volume of the cell [17]. A wide range of stimuli increase autophagy over the basal rate. Two major autophagy signaling nodes are the activation of the energy sensing protein AMP-activated protein kinase (AMPK) and inhibition of the mammalian target of rapamycin (mTOR). AMPK is activated in response to a low ATP to AMP ratio, such as during glucose deprivation [18,19]. AMPK induces

autophagy directly by phosphorylating ULK1 or indirectly through mTOR inhibition [20]. mTOR is inhibited by several other stress factors besides AMPK, such as amino acid starvation or hypoxia [21].

For an in-depth review of canonical autophagy signaling, see the following reviews [218-220]. Briefly, AMPK activation or mTOR inhibition result in ULK1 activation [20]. ULK1 phosphorylates Beclin-1 and activates the kinase VPS34. ULK1, Beclin-1, and VPS34 as well as their associated complexes localize to an open, double membrane structure termed the phagophore. The phagophore is elongated by the ATG5-ATG12-ATG16L complex [22]. The phagophore expands to engulf cytoplasmic material while forming a double membrane vacuole termed the autophagosome. Unprocessed LC3 is cytosolic (LC3-I), but LC3 is cleaved, lipidated with phosphatidylethanolamine (LC3-II), and embedded into the autophagic membrane upon autophagy initiation [23]. Molecules targeted for autophagic degradation are polyubiquitinated and adaptor proteins including p62, OPTINEURIN, or NDP52 bind to both LC3-II and ubiquitinated molecules [24-26]. The autophagosome then fuse with a lysosome to become an autolysosome. The adaptor molecule NDP52 was recently shown to also regulate the fusion of a subset of bacteria containing autophagosomes to lysosomes by mediating binding between LC3 (which is embedded in the autophagosome), Myosin VI (a myosin motor protein that moves toward the minus end of actin) and Tom-1 (which associates with lysosomes) [27]. The contents within the autolysosome are degraded into their components and exported to the cytosol.

Canonical autophagy is the best characterized form of autophagy, but there are several forms of non-canonical autophagy. These non-canonical forms also generate double membrane, degradative vacuoles with the same basic maturation process (phagophore to autophagosome to autolysosome). However, these non-canonical autophagosomes are initiated through different

mechanisms and do not use all of the proteins or protein complexes required for canonical autophagy. One recurrent form of non-canonical autophagy in pathogenesis is ATG5-independent autophagy. ATG5-independent autophagy uses some of the same machinery as canonical autophagy, such as ULK1 and Beclin-1, but does not require ATG5, ATG7, or LC3 [17]. LC3 cleavage and ATG5 knockouts are commonly used to assay for xenophagy; pathogens may preferentially induce ATG5-independent autophagy to avoid xenophagy.

ATG5-independent autophagy is induced by starvation and correlates with mTOR inhibition, but mTOR inhibition alone is not sufficient to induce this form of autophagy [5,17]. ATG5-independent autophagy is critical for *Francisella tularensis* replication and the ability of *B. abortus* to infect neighboring cells [5,28]. *Mycobacterium marinum* enters autophagosome-like vacuoles in an ATG5-independent manner although the function of this vacuole is unknown [29]. It is unclear how ATG5-independent autophagy is preferentially induced over canonical autophagy during these infections.

Pathogens Induce Xenophagy

Inhibition of mTOR induces xenophagy in response to extracellular or phagocytosed microbes through Toll-like receptors (TLRs). TLRs recognize conserved microbial factors and initiate several anti-microbial processes, including xenophagy via Myd88 and TRIF interacting with Beclin-1 [33,34]. Cell to cell signaling can also induce autophagy. Interferon gamma (IFN-γ) activates autophagy through IRGM1 in human cells while CD40 ligation stimulates autophagy through PI3K and Rab7; priming cells to resist microbes [54,55].

After phagocytosis, many pathogens escape the phagosome to replicate within the cytosol. The host cell mounts a xenophagic response to the membrane damage that occurs during

phagosomal escape [56]. Once microbes reach the cytosol, they can be targeted for xenophagy through immune surveillance or by causing cell stress. Several molecules identify microbial components within the cytosol to target microbes for xenophagy, such as Nod-1 and Nod-2. Nod-1 and Nod-2 induce xenophagy and microbial antigen processing in response to bacterial peptidoglycan [57,58]. Microbes can also induce xenophagy through a number of cell stress mechanisms. *B. abortus* secreted TcpB to induce endoplasmic reticulum stress via the unfolded protein response (UPR) pathway while *Toxoplasma gondii* increases intracellular calcium levels to induce autophagy [59-61].

Lastly, xenophagy can also be directly induced by microbial proteins (Table B.1). For example, *Shigella flexneri* exports VirG to polymerize actin and propel the bacteria through the cytosol [62]. ATG5 binds to VirG and initiates autophagosome formation without upstream autophagy signaling [63]. To prevent xenophagy from targeting *S. flexneri*, *S. flexneri* produces IcsB to block ATG5 from binding to VirG [63]. Likewise, the viral protein NS4B in Hepatitis C virus (HCV) induces autophagy by interacting with a Rab5/ Beclin-1/ VPS34 complex [221].

Pathogens have evolved complex xenophagy evasion mechanisms

Xenophagy is typically extremely effective at destroying microbes that enter the cytosol. For example, some serotypes of Group A Streptococcus (GAS) invade host cells, escape into the cytosol, and are then destroyed by xenophagy [51,52]. Xenophagy effectively blocks these serotypes from using the cytosol as a replicative niche. To defend themselves from xenophagy, most intracellular pathogens have evolved mechanisms to either inhibit or evade xenophagy (Table B.1). Some GAS serotypes encode SpeB, which degrades the xenophagy adaptor proteins p62

and NRB1 [53]. GAS serotypes that are normally destroyed by xenophagy can be functionally complemented for xenophagy evasion and intracellular replication by expressing SpeB [53].

To inhibit autophagy, pathogens frequently impair the function of xenophagy machinery. The RavZ protein secreted by *Legionella pneumophila* inactivates LC3, effectively blocking autophagy in infected cells [222]. Human Cytomegalovirus (HCMV), Herpes Simplex virus, and Kaposis sarcoma herpesvirus inactivate Beclin-1 to inhibit autophagy at specific points in their life cycle (Table B.1). Many viruses, such as Coxsackievirus, Hepatitis B virus, and HIV, inhibit autophagosome-lysosome fusion, functionally inhibiting xenophagy (Table B.1). The exact mechanism by which these viruses block autophagosome maturation is unknown, but many different RNA viruses encode proteins that interact with LC3, p62, NDP52, or NRB1 [223,224]. These proteins have several roles in xenophagy, but microbes may alter autophagosome maturation by manipulating these proteins [27].

A few pathogens evade xenophagy without inhibiting autophagy. *Listeria monocytogenes* camouflages itself by binding to the host proteins ARP2/3, major vault protein (MVP), and ena/VASP [225,226]. Many bacterial and eukaryotic pathogens modify phagosomes and are likely hidden from xenophagy targeting by remaining within a modified vacuole. *M. tuberculosis* and *S. enterica* typically reside in modified phagosomes but bacteria that disrupt the phagosomal membrane are rapidly destroyed by xenophagy [56,227]. Vacuolar *M. tuberculosis* and *T. gondii are* degraded via autophagy when autophagy is stimulated by external sources, such as CD40 ligation or IFN-γ [54,55,228]. Certain pathogens evade xenophagy by altering or destroying the components that target the microbes for degradation. *S. enterica* de-ubiquitinates aggregates with the effector protein SseL to prevent the aggregates from being degraded via autophagy [229]. Likewise, *B. pseudomallei* encodes the de-ubiquitinase TssM which blocks several innate

immune signals including the NF-kB and type 1 IFN pathways and has been proposed as a potential autophagy evasion mechanism [230,231]. A few other cytosolic pathogens, such as *Orientia tsutsugamuchi* and *F. tularensis*, induce autophagy but the mechanisms of xenophagy evasion are not clear [5,232,233].

Pathogens harvest autophagy derived nutrients for replication

Intracellular microbes acquire nutrients from a range of sources, but generally rely on macromolecule degradation or nutrient import. Most basic nutrients within cells (amino acids, fatty acids, and carbohydrates) are incorporated into macromolecules (proteins, lipid droplets and glycogen respectively). In uninfected cells, these macromolecules are primarily degraded by autophagy to increase the amount of basic nutrients so the cell can build new structures. Thus, autophagy can increase the intracellular pool of nutrients that pathogens can access. Microbes can divert the nutrient by-products of autophagy toward microbial replication rather than for use by the cell. Dengue virus, *F. tularensis*, *Anaplasma phagocytophilum*, and *T. gondii* all induce autophagy, evade autophagic degradation, and harvest the autophagy derived nutrients for replication through different mechanisms [5,61,234,235]. Additionally, *B. pseudomallei*, *Coxiella burnetti*, and *Leishmania amazonensis* have impaired replication when autophagy is inhibited and nutrient acquisition has been implicated as a potential explanation for this phenotype.

Dengue virus requires the degradation of lipid droplets via autophagy for optimal replication [235]. Dengue virus infections increase cellular levels of autophagy and the resulting autophagosomes form around and degrade lipid droplets. The triglycerides derived from the lipid droplets are catabolized via mitochondrial β-oxidation, generating ATP. Thus, autophagy produces energy for the cell to indirectly enhance viral replication [235]. In addition to energy

production, Dengue modifies autophagosomes or amphisomes to form a replicative niche [236-238]. Rather than being degraded through xenophagy, autophagy contributes to the maturation of infectious particles [237].

F. tularensis replicates in the cytosol of infected cells and induces an ATG5-independent, non-canonical form of autophagy. *F. tularensis* harvests amino acids from ATG5-independent autophagy for optimal intracellular replication. The amino acids are used for protein synthesis and are also metabolized as a major carbon source. *F. tularensis* bacteria are frequently adjacent to autophagosomes [5], indicating that *F. tularensis* is in the optimal physical location to compete with the host for autophagy derived nutrients. Although *F. tularensis* bacteria are frequently adjacent to autophagosomes, live bacteria are rarely degraded by xenophagy [5,175]. O-antigen contributes to *F. tularensis* xenophagy evasion, but other effectors are also likely to be involved [66].

A. phagocytophilum replicates in a vacuolar compartment and recruits autophagosomes directly to its replicative inclusions. *A. phagocytophilum* induces autophagy with the type IV secretion system (T4SS) effector Ats-1. Ats-1 binds to Beclin-1 and induces autophagosome nucleation directly rather than signaling through mTOR. Ats-1 induced autophagosomes localize with the inclusion membrane, suggesting that autophagosomes fuse with the inclusion body so that the bacteria can acquire the by-products of autophagic degradation. Inhibition of autophagy decreases *A. phagocytophilum* replication due to amino acid deficiency [234,239]. Likewise, *C. burnetti* induces autophagy to enhance replication [173,174,240]. *C burnetti* enters cells upon phagocytosis and modifies the phagosome to form a *C. burnetti* containing vacuoles (CCV). CCVs promiscuously fuse with other CCVs, endosomes and autophagosomes using the T4SS effector Cig2 [174,240]. When autophagy is impaired, CCVs do not fuse with one another and there

is a severe replication defect [173,240]. The autophagosomes recruited to the CCV contain LC3, p62 and LAMP-1, suggesting that the autophagosomes that are recruited to CCVs have already fused with lysosomes [174,241]. Since artificially enhancing autophagy further increases *C. burnetti* replication, the fusion of autophagosomes with the CCV has been postulated as a nutrient and membrane acquisition mechanism [173,174].

T. gondii induces autophagy in infected host cells in a calcium dependent, mTOR independent manner [61]. Inhibiting autophagy decreases *T. gondii* replication and parasite replication is rescued by supplementing with additional amino acids. Unlike its bacterial counterparts, fusion of *T. gondii* containing parasitophorous vacuoles (PVs) with autophagosomes leads to parasite destruction [242]. *T. gondii* activates EGFR and AKT to inhibit PV-autophagosome fusion with EGF-MICs, primarily MIC3 and MIC6 [242].

Exploiting autophagy for nutrients is a recurrent theme in the pathogenesis of a diverse range of microbes. Several other microbes have enhanced replication when autophagy is induced and impaired intracellular replication when autophagy is inhibited, such as Chikungunya virus, *B. pseudomallei* and *L. amazonensis* [171,243,244]. *B. pseudomallei* encodes the protein BPSS0180, which induces autophagy and is required for optimal intracellular replication [171]. Similarly, *L. amazonensis* induces autophagy and has a replication defect when cells are deficient for autophagy [243]. The role of autophagy in enhancing replication of these pathogens is unknown, but nutrient acquisition is a likely explanation for these phenotypes.

Conclusions and Perspectives

Autophagy has been linked to both nutrient acquisition and pathogen destruction for decades and it has recently become clear that a diverse range of pathogens harvest autophagy

derived products to enhance replication [5,61,234,235]. Autophagy derived nutrient acquisition is relatively straightforward in bacterial pathogens. *F. tularensis* is adjacent to autophagosomes while *C. burnetti* and *A. phagocytophilum* recruit autophagosomes to their replicative vacuoles [5,173,234,240]. These pathogens likely harvest the autophagy derived nutrients immediately after macromolecules are degraded. *T. gondii* acquires nutrients via host cell autophagy, but it is unclear how the parasites out-compete the host for autophagy by-products [61].

In contrast, the role of autophagy in viral nutrient acquisition is difficult to discern. For example, Dengue virus does not directly incorporate the autophagy by-products into structural components. Instead, autophagy increases the amount of intracellular ATP [235]. Additionally, many viruses benefit from other facets of autophagy, such as enhanced cell viability or the maturation of infectious particles, further confounding the role of autophagy in viral nutrient acquisition (Table B.1). Viruses that induce autophagy are likely to benefit from the increase in intracellular nutrients, although this benefit may be indirect, as with Dengue virus. It is important to note that autophagy still degrades host macromolecules in cells infected with microbes that block autophagy, indicating that autophagy derived nutrients are available to microbes that can outcompete the host [245]. Further investigation is needed to determine if autophagy derived nutrients are incorporated into viral macromolecules.

Autophagy is one of many mechanisms that intracellular pathogens use to acquire nutrients. Intracellular pathogens must acquire nutrients from the host cell to survive and propagate. These pathogens can acquire nutrients either by altering eukaryotic cell metabolism to increase nutrient import or by degrading macromolecules within the host through processes such as autophagy. For example, HCMV increases the expression of GLUT4 to increase glucose import for replication while *L. pneumophila* co-opts proteosomal degradation for amino acids

[142,246]. Since intracellular microbes invade cells primarily for nutrients, microbes likely have multiple, additive mechanisms of nutrient acquisition. *F. tularensis* requires autophagy and *L. pneumophila* requires proteosomal degradation for optimal replication, but both of these pathogens also up-regulate the expression of the host amino acid transporter SLC1A5 in macrophages to further enhance replication [247,248]. Inhibiting macromolecule degradation or import for these bacteria impairs, but does not block, replication, suggesting that these different nutrient acquisition strategies are additive. This is likely a common theme for microbial nutrient acquisition.

Research into how pathogens acquire nutrients is still in its infancy, particularly in how microbes acquire nutrients via autophagy. There are several outstanding questions in how intracellular microbes harvest autophagy-derived by-products. Foremost is if other intracellular microbes harvest nutrients via autophagy, even if it supplements another nutrient acquisition strategy for that pathogen. Additionally, ATG22, Avt3, and Avt4 are responsible for amino acid efflux from autophagosomes in yeast, but the mechanism mammalian cells use for nutrient efflux from the autophagosome is unclear [249]. Other critical questions that are largely unanswered are which nutrients microbes acquire from autophagy and how much microbes rely on autophagy for nutrients. Either glucose or amino acids rescues *T. gondii* replication in autophagy deficient cells while *F. tularensis* and *A. phagocytophilum* acquire amino acids from autophagy, but may need other nutrients as well [5,61,234]. It is also not clear how much microbes depend on autophagy for nutrients compared to other sources, such as nutrient import. Autophagy constitutively degrades macromolecules to generate basic components such as amino acids. Even microbes that do not induce autophagy or inhibit autophagy can compete with the host for these nutrients. It is unclear

if the host attempts to sequester these nutrients or all intracellular pathogens use autophagy derived molecules to varying degrees.

Pathogen	Autophagy up-regulation	Mechanism of autophagy evasion	Pro-microbial effect of autophagy	Ref
Anaplasma phagocytophilum	Increases autophagy via the effector ATS-1	Converts replication vacuole to modified autophagosome	Nutrient source	234,239
Brucella abortus	Likely induces via unfolded protein response (UPR)	Converts replication vacuole to modified autophagosome	-Promotes subsequent infections -May increase intracellular replication (controversial)	28,60,250
Burkholderia pseudomallei	Increases LC3 puncta formed via the bacterial effector BPSS0180	-deaminates Gln40 of ubiquitin, potentially blocks polyubiquitination -TSSM may de-ubiquitinate autophagy targets -*B. cenocepacia* blocks autophagosome maturation	-Proposed as a nutrient acquisition mechanism (not explicitly tested)	171,172, 231,251
Chlamydia trachomatis	-Bacterial protein synthesis enhances LC3 cleavage -LC3 has autophagy independent pro-bacterial effects and may not indicate increased autophagy			252-255
Coxiella burnetti	LC3 lipidation increases, but not p62 turnover	Converts replication vacuole to modified autophagosome	- Autophagy induction enhances replication - Autophagy inhibition decreases replication	173,174, 240,256
Francisella tularensis	-Increases ATG5-independent autophagy - Canonical autophagy remains at basal rate	- O-antigen contributes to xenophagy evasion - Other factors likely involved	Nutrient source	5,66,175, 247
Group A *Streptococcus*	Infection increases xenophagy	-SpeB degrades the autophagy adaptor molecules p62 and NRB1 - Not all serotypes		51,53

		encode SpeB		
Legionella pneumophila	Irreversibly inactivates LC3 with the bacterial effector RavZ to inhibit autophagy	Inhibits autophagy		142,222, 248
Listeria monocytogenes	LLO enhances autophagy through rupture of phagosomal membrane	-Camouflage via major vault protein, ARP2/3, and Ena/VASP -PlcA/PlcB reduce autophagic flux		225,226, 257-259
Mycobacterium tuberculosis	-Targets bacteria when ESX-1 permeabilizes the phagosome -autophagy is anti-bacterial, particularly in a mouse model	Unknown, likely by remaining in a modified phagosome		168,227
Orientia tsutsugamuchi	Infection induces autophagy	Unknown, but requires live bacteria		260,261
Salmonella enterica serovar *typhimurium*	Increases autophagy when phagosome is damaged	-SseL deubiquitinates bacterial products -recruits autophagy components to the replicative vacuole		56,229
Shigella flexneri	Increases autophagy through amino acid starvation and mTOR inhibition	-IcsB through by blocking ATG5 from binding to VirG -VirA suppresses autophagy		56,63,262

Pathogen	**Autophagy up-regulation**	**Mechanism of autophagy evasion**	**Pro-microbial effect of autophagy**	**Ref**
Chikungunya virus	Increases autophagy through ER stress and unfolded protein response (UPR)		-Promotes viral replication -delays caspase-dependent cell death	244,263
Coxsackievirus	Increases LC3 cleavage, but not p62 degradation	Limits autophagosome and lysosome fusion	- Enhances viral replication - Autophagosomes used for replication	264-266

			complexes - Viral exocytosis	
Dengue Virus	-Increases autophagy -Increases lipophagy		-Autophagy-derived lipids increases ATP production - maturation of infectious particles - Autophagosomes used for replication complexes	235-238
Epstein Barr virus (EBV)	-Rta induces autophagy through extracellular signal regulated kinase (ERK) signaling - LMP1 induces autophagy, likely via UPR	Blocks autophagosome-lysosome fusion	-Autophagy enhances replication -Autophagosomes contribute to exocytosis	267-270
Hantavirus	The glycoprotein Gn induces autophagy		Enhances replication	271
Hepatitis B virus (HBV)	-small surface protein induces autophagy through the unfolded protein response, -X protein promotes Beclin-1 translation. Observed increase in autophagosomes may be due to decreased autophagic flux	Viral X protein impairs autophagosome maturation, leading to autophagosome accumulation	-Autophagosome formation enhances viral replication -Autophagy contributes to HBV envelopment	272-274
Hepatitis C virus (HCV)	-NS5A induces autophagy -NS4B induces autophagy, likely via interactions with Rab5, Beclin-1 and VPS34	-autophagosome maturation impaired - impaired long-lived protein degradation	-Enhances viral replication -Replication does not occur in autophagosomes	221,245, 275-277
Herpes Simplex Virus (HSV)	-ICP34.5 protein suppresses autophagy by binding to Beclin-1 -US11 inhibits autophagy through PKR		An AMPK/AKT/mTOR/ Beclin-1 independent form of autophagy has been proposed to enhance cell viability	278-280

Human Cytomegalovirus (HCMV)	-Induces autophagy early independent of viral protein synthesis -Inhibits autophagy late through the viral protein TRS1 interacting with Beclin-1			246,281
Human immunodeficiency virus (HIV)	-Infection increases the number of autophagosomes by electron microscopy -Infection results in fewer LC3 puncta and decreased Beclin-1 protein levels -Discrepancy may be due to maturation defects or cell types	-Nef inhibits autophagosome maturation through an interaction with Beclin-1 -Tat inhibits autophagy in bystander cells	-autophagy enhances the number of infectious virions - autophagy processes Gag	282-285
Human parvovirus	Infection increases LC3 cleavage		Increased infected cell survival	286
Influenza A virus	Infection increases LC3 cleavage	-Matrix 2 ion channel blocks autophagosome-lysosome fusion - Matrix 2 ion channel redistributes LC3 to the plasma membrane	-Increases cell survival - increases replication (controversial)	287-289
Kaposis sarcoma herpesvirus (KSHV)	Timing dependent: - Viral BCL-2 binds to Beclin-1 and inhibits autophagy -vFlip (K13) binds to ATG3 and prevents ATG3-LC3 interactions -RTA induces autophagy during lytic cycle		Autophagy enhances lytic reactivation	290-292
Rotavirus	NSP4 leads to increased cytoplasmic calcium levels, resulting in autophagy	blocks autophagosome maturation	enhances viral replication	293

Pathogen	Autophagy up-regulation	Mechanism of autophagy evasion	Pro-microbial effect of autophagy	Ref
Leishmania amazonensis	Infection increases LC3 cleavage		enhances parasite replication	294,295
Toxoplasma gondii	Autophagy increase is calcium dependent but independent of mTOR	T. gondii micronemal proteins (MICs) prevents parasitophorous vacuole-lysosome fusion via activation of EGFR-Akt signaling	enhances nutrient acquisition	61,242
Candida albicans	Increase in LC3 cleavage			296
Cryptococcus neoformans		Autophagosomes fuse to *C. neoformans* containing vacuole, but structure has a single membranes	Enhances non-lytic exocytosis	297

Table B. 1: A summary of the mechanisms employed by select pathogens to induce autophagy, evade destruction through xenophagy, and pro-microbial benefits of autophagy induction.

Bacterial, viral, and eukaryotic pathogens are separated into individual sections. This list is not necessarily comprehensive for what is currently known about how each pathogen interacts with autophagy.

APPENDIX 3: IDENTIFICATION OF EARLY INTERACTIONS BETWEEN *FRANCISELLA* AND THE HOST[5]

Overview

The adaptive immune response to *Francisella tularensis* is dependent on the route of inoculation. Intradermal inoculation with the *F. tularensis* live vaccine strain (LVS) results in a robust Th1 response in the lungs, whereas intranasal inoculation produces fewer Th1 cells and instead many Th17 cells. Interestingly, bacterial loads in the lungs are similar early after inoculation by these two routes. We hypothesize that the adaptive immune response is influenced by local events in the lungs, such as the type of cells that are first infected with *Francisella*. Using fluorescence-activated cell sorting, we identified alveolar macrophages as the first cell type infected in the lungs of mice intranasally inoculated with *F. novicida* U112, LVS, or *F. tularensis* Schu S4. Following bacterial dissemination from the skin to the lung, interstitial macrophages or neutrophils are infected. Overall, we identified the early interactions between *Francisella* and the host following two different routes of inoculation.

Introduction

Immune responses following bacterial infections are influenced by the route of infection [298-300]. Cytokines produced by the innate immune response are critical in shaping the adaptive immune response (reviewed in reference [301]). For example, if a naive $CD4^+$ T cell encounters antigen in the presence of interleukin 12 (IL-12), it will differentiate into a Th1 effector T cell, but if it encounters IL-6 and transforming growth factor β (TGF-β) during antigen presentation, it

[5]This appendix was previously published in Infection and Immunity. The first three authors share a co-first authorship. The citation is: Roberts LM, Tuladhar S, Steele SP, et al. Identification of early interactions between francisella and the host. *Infect Immun*. 2014;82(6):2504-2510. doi: 10.1128/IAI.01654-13

will differentiate into a Th17 effector T cell [301]. Our previous experiments with mice using intranasal or intradermal inoculation with *Francisella tularensis* subsp. *holarctica* live vaccine strain (LVS) demonstrated striking differences in the adaptive immune response in the lungs when these two inoculation routes were compared [300]. Upon either intradermal or intranasal inoculation with LVS, bacteria rapidly disseminate and are found in the spleen, liver, and lungs 24 h after inoculation [300]. After 3 days, equivalent bacterial burdens are found in the spleen and lungs of mice inoculated via either route [300]. Despite similar burdens early after inoculation, intradermally inoculated mice clear the infection more rapidly than intranasally inoculated mice and have an increased gamma interferon (IFN-γ) response. Intradermal inoculation leads to significantly more $CD4^+$ and $CD8^+$ T cells producing IFN-γ in both the spleen and lungs on day 7 post-inoculation than does intranasal inoculation [300]. Faster bacterial clearance in intradermally inoculated mice correlates with the increased IFN-γ-mediated immune response. IFN-γ is required for controlling *F. tularensis* infection, and administration of recombinant IFN-γ decreases bacterial burdens [302-304]. Intranasal infection leads to an expansion in the lungs of Th17 cells, a $CD4^+$ T cell population not found in intradermally inoculated mice [300,305,306]. We conclude that T cell effector function is influenced by the inoculation route. Thus, it is important to understand the initiation of the immune response and identify the earliest cells infected by *Francisella* in the lungs.

Francisella tularensis is a facultative intracellular, Gram-negative coccobacillus. Infection with *F. tularensis* causes the zoonotic disease tularemia, which is endemic in regions of the United States and Europe. Three strains of *Francisella* are commonly used by researchers. *Francisella tularensis* subsp. *tularensis* Schu S4 is a type A strain and highly pathogenic in humans and mice. *Francisella tularensis* subsp. *holarctica* live vaccine strain (LVS) is an

attenuated, type B strain and does not cause severe disease in humans [307]. Murine infection with LVS closely resembles human infection [308]. The 50% lethal dose (LD_{50}) for intranasal inoculations is approximately 10^3 CFU, and that for intradermal inoculation is approximately 10^6 [309,310]. *F. novicida* U112 does not cause disease in immunocompetent humans but causes severe disease in mice with a course similar to that in mice inoculated with Schu S4. Intranasal inoculation with U112 or Schu S4 is typically fatal in mice before an adaptive immune response can occur, but low-dose inoculations with LVS in mice allow for the observation of the adaptive immune response to *Francisella*.

Due to similar bacterial burdens early after inoculation but very different adaptive immune responses for these inoculation routes, we hypothesized that the adaptive immune response to *Francisella* was shaped by events early after inoculation, such as what type of cell was initially infected. We therefore sought to identify host cells infected with *F. tularensis* early after intranasal and intradermal inoculation. We examined three strains of *Francisella* to determine whether all strains exhibit similar tropisms or if different strains target different cell types. Previously, we found that alveolar macrophages comprised between 50 and 80% of cells infected with U112 or LVS 24 h after intranasal inoculation [2]. These experiments, however, identified more infected cells than the initial bacterial inoculum, suggesting that multiple rounds of infection had occurred. Therefore, we were interested in identifying the infected cells 4 h post-inoculation, before re-infection of new cell types occurred. We found that alveolar macrophages were the primary cell type infected after intranasal inoculation and that interstitial macrophages and neutrophils were the first lung cell types infected following intradermal inoculation and bacterial dissemination. Together, our data demonstrate that the cell types initially infected with

Francisella are dependent on the inoculation route and are common among the different strains of *Francisella*.

Materials and Methods

Bacteria.

Francisella novicida U112 was obtained from Colin Manoil (University of Washington). *F. tularensis* subsp. *holarctica* live vaccine strain (LVS; ATCC 29684) was obtained from the American Type Culture Collection (Manassas, VA). *F. tularensis* subsp. *tularensis* Schu S4 (NR-643) was obtained from BEI Resources (Manassas, VA). Bacteria were grown on chocolate agar supplemented with 1% IsoVitaleX (Becton, Dickinson) at 37°C. Bacterial inoculations were prepared by removing bacteria from a lawn grown on chocolate agar and resuspended in sterile phosphate-buffered saline (PBS) at an optical density at 600 nm (OD_{600}) of 1 (equivalent to 1×10^7 CFU/μl). To achieve the desired inoculation dose, appropriate dilutions were made using sterile PBS. Viable bacteria in each preparation were quantified by serial dilution and plating on chocolate agar. All experiments using Schu S4 were performed at the Duke University NIAID-Regional Biocontainment Laboratory (RBL) under biosafety level 3 (BSL3) containment.

Mice.

C57Bl/6J (B6) mice were obtained from The Jackson Laboratory (Bar Harbor, ME). All mice were housed under specific-pathogen-free conditions at the University of North Carolina at Chapel Hill, the RBL, or the University of Arizona in accordance with their respective Institutional Animal Care and Use committees. Female mice used for experiments were between 7 and 12 weeks of age.

Inoculation of mice.

For intranasal bacterial inoculations, mice were anesthetized with 575 mg/kg (of body weight) of tribromoethanol (Avertin; Sigma) administered intraperitoneally. Mice were then intranasally inoculated with 1×10^4 CFU of U112, LVS, or Schu S4 suspended in 50 μl of PBS. For intradermal inoculations, mice were inoculated with 5×10^5 CFU of U112 or LVS in 25 μl in the tail. The inoculum was divided between three injection sites along the tail.

Single-cell suspension of mouse lung.

Following humane euthanasia, lungs were aseptically removed after perfusion with PBS and digested into a single-cell suspension as previously described [311]. For intranasally inoculated mice, 50 μg/ml of gentamicin (Sigma) was added to the digestion mix to kill extracellular bacteria. Red blood cells were lysed using ammonium chloride-potassium lysis buffer (Gibco) and washed with RMPI 1640 supplemented with 10% fetal calf serum (Atlas), l-glutamine, sodium pyruvate, and β-mercaptoethanol. The total number of viable cells was determined using a hemocytometer by trypan blue exclusion.

Bead enrichment of CD45+ cells.

Lung single-cell suspensions were stained for 20 min on ice with CD45-allophycocyanin (CD45-APC; clone 30–F11; Biolegend). After washing the cells to remove unbound antibody, IMag anti-APC magnetic particles (BD) were used to enrich CD45-APC-positive cells according to the manufacturer's instructions. CD45 enrichment was determined by flow cytometry.

Enriched eukaryotic cells were directly plated on chocolate agar containing 10 μg/ml of ampicillin (Sigma), and the CFU were counted 72 h later.

Identification of infected lung populations.

Lung cells in a single-cell suspension after intranasal inoculation with *Francisella* had Fc receptors blocked with 2.4G2 to prevent nonspecific staining and were then stained with F4/80 phycoerythrin (PE; clone BM8; eBioscience), CD11b Pacific blue (clone M1/70; Biolegend), and CD11c APC (clone N418; eBioscience). Lung cells from intradermally inoculated mice had Fc receptors blocked with 2.4G2 and were then stained with F4/80 PE, CD11b Pacific blue, CD11c APC, and GR-1 Pacific orange (clone RB6-8C5; Invitrogen). The cells were sorted using a Reflection cell sorter (iCyt/Sony; UNC) or FACSAria II (Becton Dickinson Immunocytometry Systems [BDIS]; RBL and University of Arizona) into four populations based on surface marker expression (Table C.1) using the gating scheme shown in (Figure C.1). Sorted populations were plated directly on chocolate agar containing 10 μg/ml of ampicillin without lysis, and bacterial CFU were counted 24 to 72 h later to enumerate the infected cells.

Statistical analysis.

A Kruskal-Wallis test was used to determine whether the distribution of infected cells was significantly different and not due to random sampling. GraphPad Prism (v.5.04) was used for analysis.

Results

LVS infects myeloid cells after intranasal inoculation.

The adaptive immune response to LVS is influenced by the route of infection despite similar bacterial burdens, and therefore antigen load, early after inoculation [300]. We hypothesized that the adaptive immune response in the lungs was shaped by the cell type(s) infected immediately after intranasal inoculation or after bacterial dissemination to the lungs after intradermal inoculation. We therefore sought to identify which cell populations were infected following inoculation. A previous study reported that a variety of lung cell types are infected with *Francisella* 24 and 72 h after intranasal inoculation [312]. Although the majority of infected cells 24 h after intranasal inoculation with green fluorescent protein (GFP)-expressing *Francisella* strains were myeloid, alveolar type II epithelial cells were also identified as an infected cell type by flow cytometry [312]. Therefore, our initial investigation into identifying the first infected lung cells sought to determine whether cells initially targeted by LVS were of the myeloid or nonmyeloid lineage. We chose to use 4 h after inoculation so that *Francisella* had sufficient time to reach and infect the cells it initially targets but not time for multiple rounds of reinfection. An intranasal inoculum dose of 1×10^4 CFU yielded approximately 100 infected cells out of 1×10^7 host lung cells at 4 h post-inoculation for all strains, giving us confidence that we were identifying the initially infected cells.

B6 mice were intranasally inoculated with 1×10^4 CFU of LVS and euthanized 4 h later. Lung tissue was digested into a single-cell suspension in the presence of gentamicin to kill extracellular bacteria. Cells were then stained with anti-CD45-APC, and anti-APC magnetic beads were used to positively select for myeloid cells. Figure C.2 shows representative flow cytometry histograms of CD45 staining within the pre-enrichment, negative selection ($CD45^-$),

and positive selection ($CD45^+$) samples. Eukaryotic cells were directly plated on chocolate agar, and the colonies within the $CD45^-$ and $CD45^+$ pools were counted. A total of 99% of the resulting LVS colonies were on the $CD45^+$ plates, indicating that LVS initially targets myeloid cells for infection (Figure C.2B). Although we did not repeat these experiments using U112 or Schu S4, we predicted similar results between strains and indeed did observe that all strains targeted the same cell types after intranasal inoculation (see below).

Alveolar macrophages are the dominant infected cell type after intranasal inoculation in all *Francisella* strains.

Of the myeloid cells in the lungs, we predicted that alveolar macrophages, interstitial macrophages, and dendritic cells were the cell types most likely to be initially infected with *Francisella* after intranasal inoculation. To identify infected cells in the lung early after intranasal inoculation, B6 mice were intranasally inoculated with 1×10^4 CFU of U112, LVS, or Schu S4 and euthanized 4 h post-inoculation. Lung tissue was digested in the presence of gentamicin to kill extracellular bacteria. The lung single-cell suspensions were stained for F4/80, CD11c, and CD11b, and cell populations were sorted based on expression of these surface markers (Table C.1 and Figure C.1). Sorted eukaryotic cells were plated directly on chocolate agar without lysis of the cells, and the resulting colonies were counted. Data from multiple mice were combined for each *Francisella* strain, and a weighted average was used to identify which cell type made up the majority of infected cells (Figure C.3). Approximately 90% of infected cells were alveolar macrophages for each *Francisella* strain, indicating that these cells were initially targeted by *Francisella* after intranasal inoculation. The remaining 10% of infected cells consisted of a mixture of interstitial macrophages, dendritic cells, and others. The results were

consistent across individual mice, although more variability was observed in the minor infected cell populations (interstitial macrophages, dendritic cells, and others) (Table C.2). In individual mice, alveolar macrophages constituted 86 to 96% of infected cells after U112 inoculation, 71 to 93% of infected cells after LVS inoculation, and 93 to 96% of infected cells after Schu S4 inoculation (Table C.2). Furthermore, determination of number of LVS CFU per 10^5 sorted cells showed that the alveolar macrophage population contained at least 7-fold more CFU per 10^5 sorted cells than did interstitial macrophages, dendritic cells, or others (Figure C.4). Together, these data indicate that alveolar macrophages are the dominant first infected cell type immediately after intranasal inoculation with each of the three distinct strains of *Francisella*.

Interstitial macrophages and neutrophils are the dominant infected cell types in the lungs after intradermal inoculation.

We observed very different adaptive immune responses in the lungs after intranasal versus intradermal inoculation [300] and therefore hypothesized that different innate immune events occurred early after infection. One possibility was different infected cell types in the lungs depending on the route of infection, particularly since one inoculation route introduced bacteria directly into the lungs, whereas intradermal inoculation required bacteria to disseminate from the skin to the lungs. We therefore sought to identify the early infected cell type(s) in the lungs after intradermal inoculation and subsequent bacterial dissemination to the lungs. Mice were intradermally inoculated with 5×10^5 CFU of U112 or LVS. Pilot experiments determined that euthanizing mice 48 h post-inoculation allowed enough time for bacteria to disseminate from the skin to the lungs and that 48 h was the earliest time point that bacteria could be reproducibly found in the lungs. Lung single-cell suspensions were stained and sorted as previously described.

In contrast to the case with intranasal inoculation, interstitial macrophages and neutrophils together comprise >90% of all cells infected with *Francisella* after intradermal inoculation and bacterial dissemination to the lungs (Figure C.5 and Table C.3). Importantly, alveolar macrophages were not appreciably infected with *Francisella* in the lungs following bacterial dissemination from the skin (<2% of infected cells). Additionally, when we calculated the number of CFU per 10^5 sorted cells for each population, we found that interstitial macrophages and neutrophils were both infected at a rate over 30 times greater than alveolar macrophages for both LVS and U112 inoculation (Figure C.6). We detected less than 500 infected cells in the mice intradermally inoculated with LVS. Although we detected more infected cells (100 to 6,000) in the mice intradermally inoculated with U112, the percentage of each infected cell population was similar to findings for LVS, even with variability in the number of infected cells, allowing us to be confident that we were observing early infection events in the lungs following bacterial dissemination. These results indicate that pulmonary interstitial macrophages and neutrophils are infected with *Francisella* in the lungs after intradermal inoculation. Furthermore, these results indicate that different cell types are infected with *Francisella* in the lungs depending on the inoculation route and support our hypothesis that the differences observed in the adaptive immune response are a result of different infected cell types.

Discussion

Francisella is capable of infecting a variety of cell types upon inoculation [2,91,312,313]. The early interactions between the host and pathogen set the stage for the adaptive immune response. We and others have shown that the route of inoculation influences the type of adaptive immune response that develops [299,300]. We were particularly interested in the early interactions between

Francisella and the host following intranasal and intradermal inoculations because of differential adaptive immune responses in the lungs. Intranasal and intradermal inoculations with LVS lead to similar bacterial burdens early after inoculation, yet the adaptive immune responses are very different [300]. We hypothesized that the cell type infected with *Francisella* immediately after inoculation shaped the adaptive immune response. We therefore sought to identify the cells that were infected with *Francisella* after inoculation that were likely responsible for shaping subsequent adaptive immunity.

We identified infected cells by sorting individual populations using fluorescence-activated cell sorting. This technique only identified host cells infected with live *Francisella*, since our experimental readout was colonies grown on agar. We had to intranasally inoculate mice with 1×10^4 CFU to have detectable infected cells after sorting. This inoculum dose is 20-fold higher than our typical LVS intranasal inoculation dose. We believe that the higher dose increased the number of infected cells without altering the distribution of infected cell types because nearly all of the infected cells were alveolar macrophages.

All three strains of *Francisella* predominantly infected alveolar macrophages following intranasal inoculation. Alveolar macrophages are the resident macrophages of the airway and interact with inhaled antigens. It is therefore not surprising that inhalation of *Francisella* leads to infection of alveolar macrophages. Other pathogens, like *Mycobacterium tuberculosis*, *Mycoplasma pulmonis*, and *Legionella pneumophila*, target alveolar macrophages upon infection as well [314-317]. Experiments found that LVS infects pulmonary dendritic cells 1 h after intratracheal inoculation with 5×10^4 CFU using flow cytometry to detect carboxyfluorescein succinimidyl ester (CFSE)-labeled bacteria inside host cells [313]. A potential explanation for the seemingly disparate results between the two experiments is the use of different surface markers

to define airway dendritic cells and alveolar macrophages. Surface markers used to define lung cellular populations by our group and others are shown in Table C.1. The markers described by Bosio and Dow [313] for alveolar macrophages best fit with our definition of interstitial macrophages, and their definition for airway dendritic cells best fits with our definition of alveolar macrophages (Table C.1). More recently, Guth et al. reported that alveolar macrophages express middle levels of DEC-205 and CD11c, giving this macrophage cell subset a more dendritic-cell-like surface phenotype [318]. We also observed mid-level expression of DEC-205 of alveolar macrophages. Therefore, the cell populations are likely the same based on surface marker phenotype.

While we did not pursue experiments to determine the underlying mechanisms responsible for bacterial dissemination, we identified interstitial macrophages and neutrophils as the dominant infected cell types in the lungs after intradermal inoculation and bacterial dissemination. We carefully timed the lung harvest after intradermal inoculation so that we were identifying infected cells soon after bacteria disseminated to the lungs. These results indicate that not only does the route of infection shape the adaptive immune response but also two different types of innate cells are initially infected with *Francisella* in the lungs, which we predict helps shape the different downstream adaptive responses. In the lungs, the differences in infected cell types between the two different inoculation routes may simply be spatial. Alveolar macrophages are located primarily in the alveoli. This spatial location would put them in direct contact with *Francisella* after an intranasal inoculation but out of the way during bacterial dissemination from the skin.

Because alveolar macrophages were infected following intranasal inoculation with LVS, we sought to determine whether the disease course was altered in the absence of alveolar

macrophages. Alveolar macrophages express high levels of CD11c and can therefore be depleted in CD11c.DOG mice upon intranasal treatment with diphtheria toxin (DT). We chose to use CD11c.DOG mice instead of other depletion strategies so that alveolar macrophages were specifically depleted while other phagocytic cells remained untouched. Alveolar macrophages can also be depleted by intranasal administration of liposomal clodronate; however, this treatment is nonspecific and depletes >90% of lung and airway antigen-presenting cells [313]. Although we successfully depleted alveolar macrophages from the lungs of CD11c.DOG mice with intranasal inoculation of diphtheria toxin, this treatment caused changes to the cytokine and chemokine milieu prior to infection with LVS (unpublished data). Diphtheria toxin also changed the proportion and absolute number of lung cellular populations (unpublished data). Although we observed an increase in LVS lung bacterial burdens when CD11c.DOG mice were depleted of alveolar macrophages prior to LVS inoculation, the changes in the lungs' cytokine and chemokine milieu as well as cellular distribution made it impossible to ascribe increased bacterial burdens simply to the lack of alveolar macrophages.

Alveolar macrophages have been shown in other models to be both protective and detrimental during infection [313,314,319-321]. CBA/J mice succumb rapidly (day 3) to *Klebsiella pneumoniae* in the absence of alveolar macrophages and have significantly higher bacterial burdens in the plasma and lungs, suggesting that alveolar macrophages control bacterial replication in the lungs [319,321]. B6 mice, normally resistant to *Mycoplasma pulmonis*, were more susceptible to infection in the absence of alveolar macrophages, indicating that alveolar macrophages are important for host defense during *M. pulmonis* infection [320]. In contrast, during *Mycobacterium tuberculosis* infection, mice lacking alveolar macrophages were less susceptible to infection and had decreased mycobacterial burdens in the lungs and liver, suggesting that the

presence of alveolar macrophages is detrimental during infection [314]. Bosio and Dow found that depletion of alveolar macrophages with clodronate followed 18 h later by intratracheal inoculation with a lethal dose of LVS led to decreased bacterial burdens and an increase in mean time to death [313]. It is possible that the difference in bacterial burdens observed in untreated and clodronate-treated mice was due to the absence of cells to infect, because nearly all phagocytic cells were reported to be depleted, leaving few cells for LVS to infect [313]. While specific depletion of alveolar macrophages might address this possibility, selective depletion of alveolar macrophages without other changes in cellular composition has not been possible.

Several groups have reported that LVS vaccination prior to lethal challenge with a highly virulent, type A strain of *Francisella* must be administered intranasally and not intradermally in order to achieve protective immunity [322,323]. The failure of intradermally vaccinated mice to survive a lethal type A challenge suggests that the T cell response is not successfully primed via this route. We have demonstrated that the adaptive immune response is different depending on the route of LVS inoculation [300]. Herein, we have shown that different cell types are initially infected with LVS, again depending on the route of inoculation. Taken together, these data suggest that alveolar macrophages could play a role in successful T cell priming (via antigen presentation and/or cytokine milieu), leading to a T cell response that is protective after secondary challenge with virulent *Francisella*. Alternatively, when interstitial macrophages are among the cells initially infected, an environment is established in which the T cells successfully clear the primary infection but fail to protect upon secondary challenge.

Overall, we have shown that alveolar macrophages are initially infected with *Francisella* in the lungs after intranasal inoculation. We also determined that interstitial macrophages and neutrophils are infected with *Francisella* in the lungs following bacterial dissemination from

intradermal inoculation in the skin. We had previously observed a differential adaptive immune response following intranasal and intradermal inoculation, despite similar bacterial burdens early after inoculation. We predicted that there would be differences in the innate immune response in the lungs that contributed to the development of two distinct T cell responses, and this was the case; different types of cells were infected in the lungs following each inoculation route.

Figures

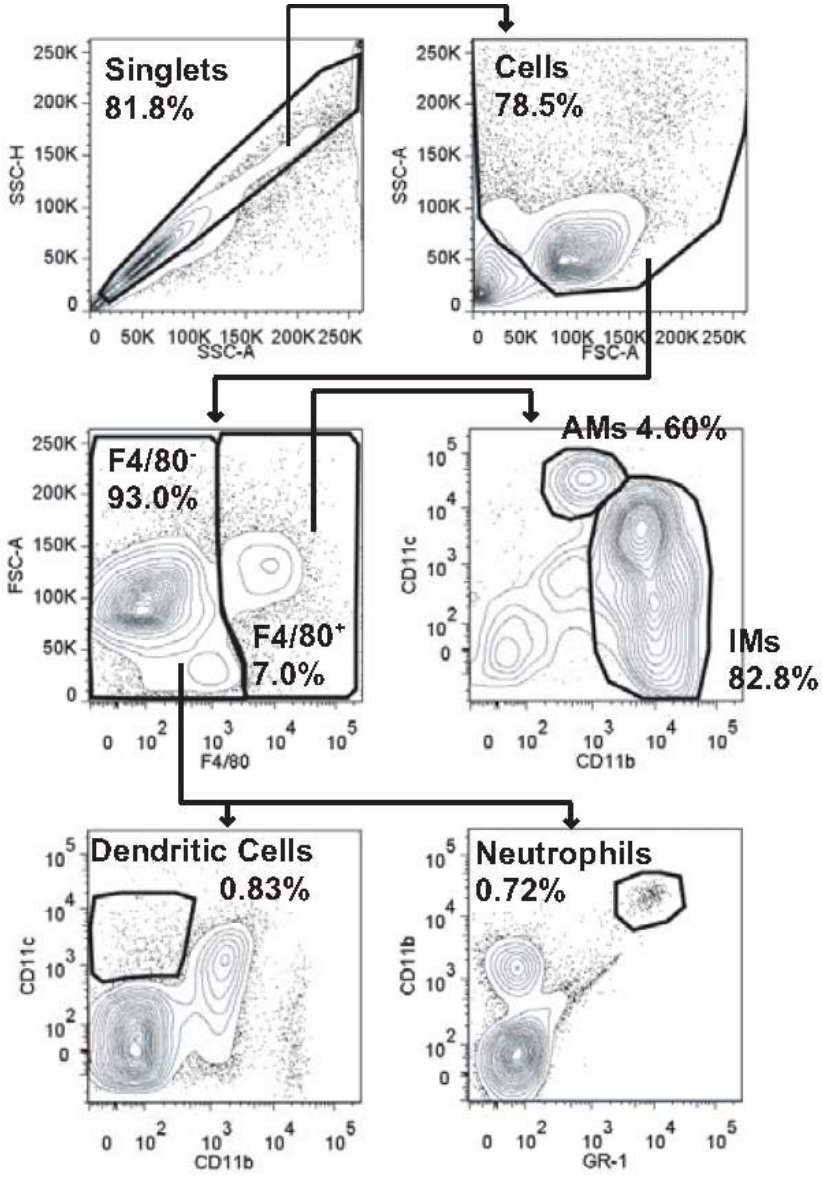

Figure C. 1: Lung gating scheme.

Single cells were discriminated from doublets by plotting side scatter height (SSC-H) versus side scatter area (SSC-A). Cells were selected by plotting SSC-A versus forward scatter area (FSC-A). $F4/80^-$ and $F4/80^+$ cells were gated on by plotting FSC-A versus F4/80. From the $F4/80^+$ gate, alveolar macrophages (AMs) were discriminated from interstitial macrophages (IMs) by

plotting CD11c versus CD11b. Of the F4/80$^-$ cells, dendritic cells were identified by plotting CD11c versus CD11b and neutrophils were identified by plotting CD11b versus GR-1. For each gate, the percent of the parent gate is indicated in bold (for example, AMs are 4.6% of the cells within the F4/80$^+$ gate).

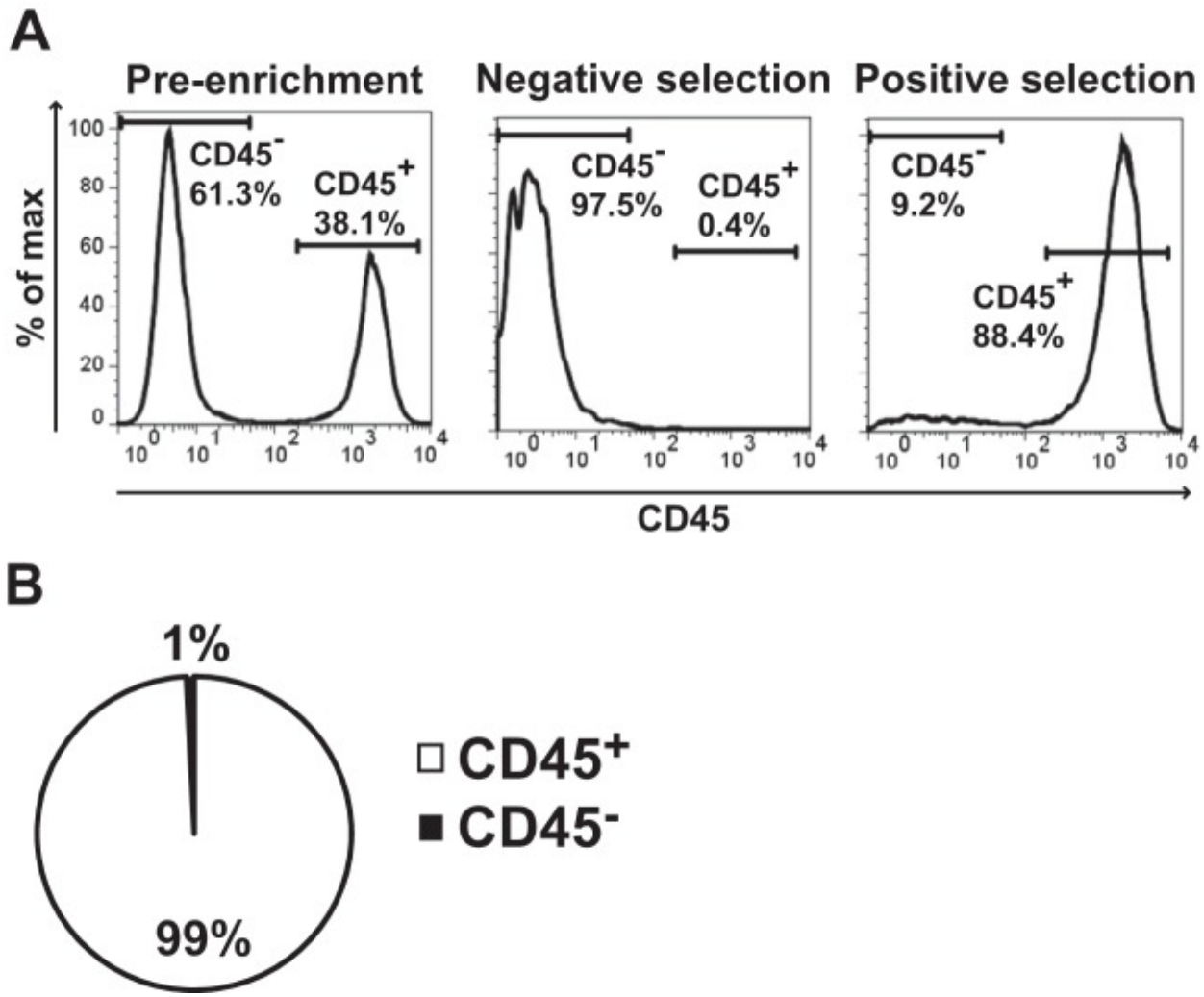

Figure C. 2: LVS infects myeloid-derived cells following intranasal inoculation.

B6 mice were intranasally inoculated with $1x10^4$ CFU LVS. 4 hours post-infection mice were sacrificed and lungs were removed and digested into a single cell suspension. Cells were stained with CD45 APC and then $CD45^+$ cells were enriched using magnetic beads. A) Representative flow cytometry analysis of CD45 enrichment. B) $CD45^+$ and $CD45^-$ populations were directly plated on chocolate agar and the number of colonies were counted 72 hours later. We counted 123 total CFU among 4 mice. Data are weighted by the total number of CFU and presented as the % of CFUs within a population from 4 infected mice in 2 independent experiments.

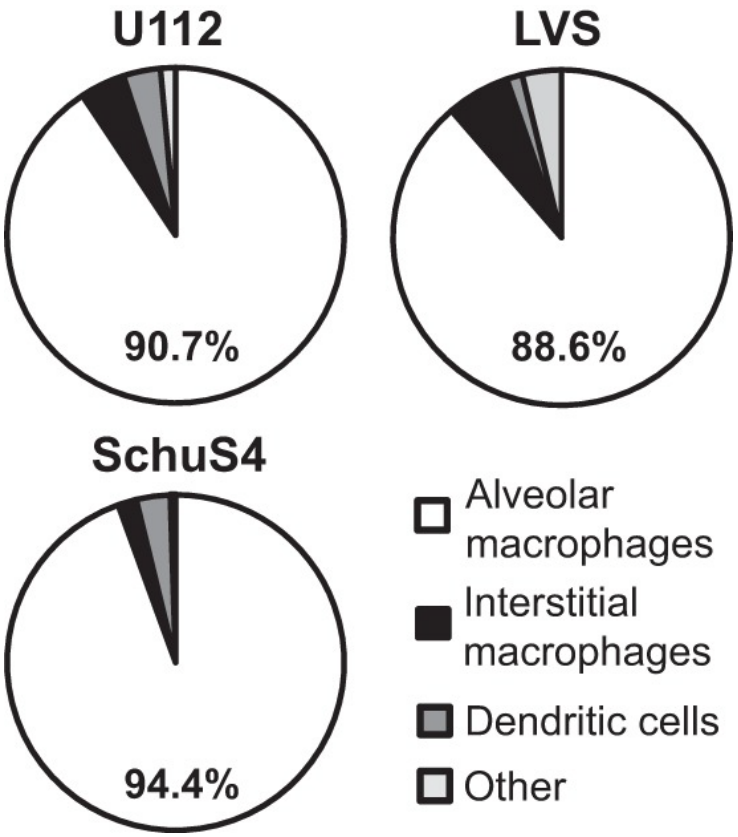

Figure C. 3: Alveolar macrophages are the primary infected cell type in the lung after intranasal inoculation with *Francisella*.

B6 mice were intranasally inoculated with ^{1x104} CFU U112, LVS, or Schu S4. 4 hours post-inoculation mice were sacrificed and lungs were removed and digested into a single cell suspension and stained for sorting. Alveolar macrophages, interstitial macrophages, dendritic cells, and other cell populations were sorted and directly plated on chocolate agar. Resulting colonies were counted 24-72 hours later. Data are weighted by the total number of CFU and presented as the % of CFUs within a population from 2 mice (U112; 139 total CFU), 6 mice (LVS; 132 total CFU), or 3 mice (SchuS4; 398 total CFU) from 1 (U112), 3 (LVS), or 2 (SchuS4) independent experiments. A Kruskal-Wallis test was used to determine whether the distribution of infected cells was significantly different. U112: ns (p=0.1767); LVS: **; Schu S4: *.

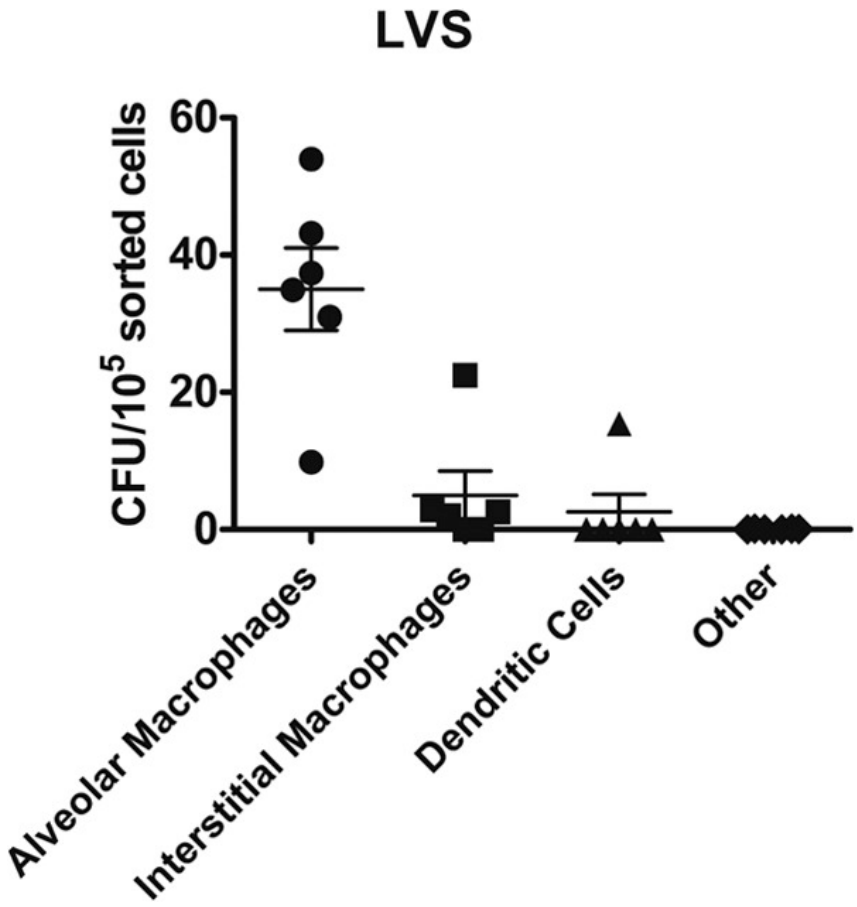

Figure C. 4: Alveolar macrophages are infected with LVS at the highest frequency.

B6 mice were intranasally inoculated with $1x10^4$ CFU LVS. 4 hours post-inoculation mice were sacrificed and lungs were removed and digested into a single cell suspension and stained for sorting. Alveolar macrophages, interstitial macrophages, dendritic cells, and other cell populations were sorted and directly plated on chocolate agar. The total number of sorted cells for each population was recorded during the sort. Resulting colonies were counted 72 hours later. Data are represented as the number of CFU per 10^5 sorted cells for each population from 6 mice in 3 independent experiments.

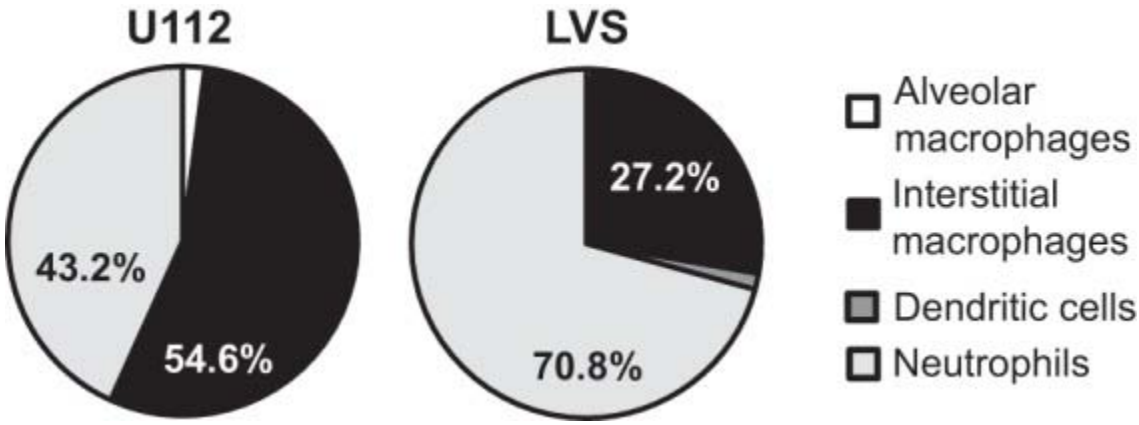

Figure C. 5: Interstitial macrophages and neutrophils are the primary cell types infected with U112 or LVS in the lung after intradermal inoculation.

B6 mice were intradermally inoculated with $5x10^5$ CFU U112 or LVS in 50 μL PBS at the base of the tail. 48 hours post-inoculation mice were sacrificed and lungs were removed and digested into a single cell suspension and stained for sorting. Alveolar macrophages, interstitial macrophages, dendritic cells, and neutrophil cell populations were sorted and directly plated on chocolate agar. Resulting colonies were counted 24-72 hours later. Data are weighted by the total number of CFU and presented as the % of CFUs within a population from 4 mice (U112; 9344 total CFU) or 2 mice (LVS; 537 total CFU) from 1 experiment per strain. A Kruskal-Wallis test was used to determine whether the distribution of infected cells was significantly different. U112: ns (p=0.1184); LVS: ns (p=0.1116).

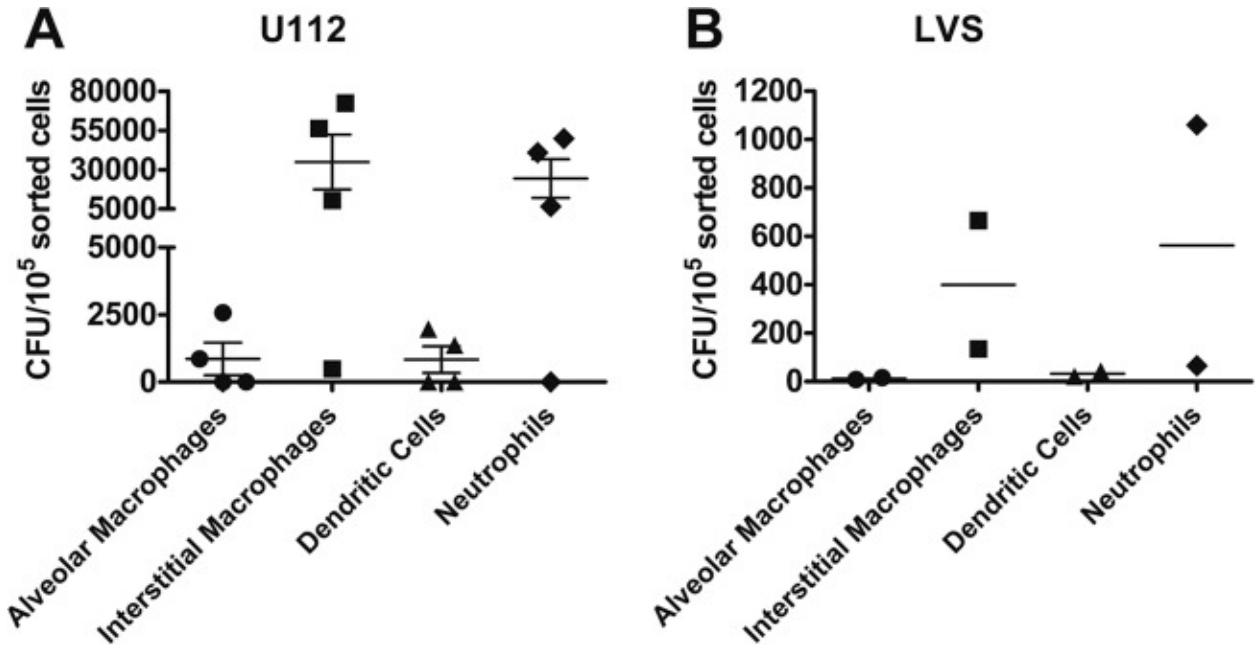

Figure C. 6: Interstitial macrophages and neutrophils are infected with U112 and LVS at the highest frequency.

B6 mice were intranasally inoculated with $1x10^4$ CFU U112 or LVS. 4 hours post-inoculation mice were sacrificed and lungs were removed and digested into a single cell suspension and stained for sorting. Alveolar macrophages, interstitial macrophages, dendritic cells, and other cell populations were sorted and directly plated on chocolate agar. The total number of sorted cells for each population was recorded during the sort. Resulting colonies were counted 24 or 72 hours later. Data are represented as the number of CFU per 10^5 sorted cells for each population from 4 (U112) or 2 (LVS) mice in 1 experiment per strain.

Cell type	Surface markers[a]
Alveolar macrophages	F4/80^{high}, CD11c^{high}, CD11b^{mid}, DEC-205^{mid}
Interstitial macrophages	F4/80^{high}, CD11c^{var}, CD11b^{high}
Dendritic cells	F4/80^{low}, CD11c^{high}, CD11b^{low}
Neutrophils	F4/80^{low},CD11b^{high}, GR-1^{high}
Other	F4/80low, CD11c^{low}, CD11b^{var}
Alveolar macrophages[304]	F4/80^{pos}, CD11c^{neg}, CD11b^{pos}, DEC-205^{neg}
Airway dendritic cells [304]	F4/80^{var}, CD11c^{pos}, CD11b^{var}, GR-1^{var}, DEC-205^{pos}
Alveolar macrophages [318]	F4/80l^{ow}, CD11c^{high}, CD11b^{neg}, DEC-205^{mid}

Table C.1: Identification of lung cell types.

[a]mid, medium level; var, variable level; pos, positive expression; neg, not expressed.

Bacterial Strain	Alveolar Macrophages	Interstitial Macrophages	Dendritic Cells	Other
F. novicida U112 (n=2)	90.82 ± 6.65% (86.11-95.52%)	4.32 ± 0.16% (4.17-4.48%)	3.51 ± 3.47% (0.0-6.94%)	1.41 ± 1.40% (0.0-2.78%)
F. tularensis LVS (n=6)	87.86 ± 7.72% (71.43-92.86%)	8.13 ± 10.6% (0.0-28.57%)	1.67 ± 4.08% (0.0-10%)	3.72 ± 4.81% (0.0-9.52%)
F. tularensis Schu S4 (n=3)	94.27 ± 1.27% (93.33-95.71%)	3.45 ± 2.96% (0.83-6.67%)	1.90 ± 2.69% (0.0-4.98%)	0.38 ± 0.36% (0.0-0.71%)

Table C.2: Mean percentage of infected cells in the lung 4 hours post intranasal inoculation.

Bacterial Strain	Alveolar Macrophages	Interstitial Macrophages	Dendritic Cells	Neutrophils
F. novicida U122 n=4	1.21 ± 1.84% (0.0-3.89%)	62.89 ± 26.82% (38.46-100%)	0.036 ± 0.044% (0.0-0.089%)	35.86 ± 26.75% (0.0-61.54%)
F. tularensis LVS n=2	1.26 ± 1.47% (0.22-2.30%)	32.91 ± 11.97% (24.44-41.38%)	4.13 ± 5.53% (0.22-8.05%)	61.69 ± 18.98% (48.28-75.11%)

Table C.3: Mean percentage of infected cells in the lung 48 hours post intradermal inoculation Mean ± standard deviation (range).

REFERENCES

1. Champion MD, Zeng Q, Nix EB, et al. Comparative genomic characterization of francisella tularensis strains belonging to low and high virulence subspecies. *PLoS Pathog*. 2009;5(5):e1000459. Epub 2009 May 29 doi:10.1371/journal.ppat.1000459. doi: 08-PLPA-RA-1475R3 [pii].

2. Hall JD, Woolard MD, Gunn BM, et al. Infected-host-cell repertoire and cellular response in the lung following inhalation of francisella tularensis schu S4, LVS, or U112. *Infect Immun*. 2008;76(12):5843-5852. doi: 10.1128/IAI.01176-08.

3. Roberts LM, Tuladhar S, Steele SP, et al. Identification of early interactions between francisella and the host. *Infect Immun*. 2014;82(6):2504-2510. doi: 10.1128/IAI.01654-13 [doi].

4. Bar-Haim E, Gat O, Markel G, Cohen H, Shafferman A, Velan B. Interrelationship between dendritic cell trafficking and francisella tularensis dissemination following airway infection. *PLoS Pathog*. 2008;4(11):e1000211. doi: 10.1371/journal.ppat.1000211 [doi].

5. Steele S, Brunton J, Ziehr B, Taft-Benz S, Moorman N, Kawula T. Francisella tularensis harvests nutrients derived via ATG5-independent autophagy to support intracellular growth. *PLoS Pathog*. 2013;9(8):e1003562. doi: 10.1371/journal.ppat.1003562; 10.1371/journal.ppat.1003562.

6. Leung KY, Finlay BB. Intracellular replication is essential for the virulence of salmonella typhimurium. *Proc Natl Acad Sci U S A*. 1991;88(24):11470-11474.

7. Portnoy DA, Jacks PS, Hinrichs DJ. Role of hemolysin for the intracellular growth of listeria monocytogenes. *J Exp Med*. 1988;167(4):1459-1471.

8. Chamberlain RE. Evaluation of live tularemia vaccine prepared in a chemically defined medium. *Appl Microbiol*. 1965;13:232-235.

9. Halmann M, Mager J. An endogenously produced substance essential for growth initiation of *Pasteurella tularensis*. . 1967;49:461-468.

10. Lindgren H, Honn M, Golovlev I, Kadzhaev K, Conlan W, Sjostedt A. The 58-kilodalton major virulence factor of francisella tularensis is required for efficient utilization of iron. *Infect Immun*. 2009;77(10):4429-4436. doi: 10.1128/IAI.00702-09 [doi].

11. Crosa LM, Crosa JH, Heffron F. Iron transport in francisella in the absence of a recognizable TonB protein still requires energy generated by the proton motive force. *Biometals*. 2009;22(2):337-344. doi: 10.1007/s10534-008-9170-7 [doi].

12. Barel M, Meibom K, Dubail I, Botella J, Charbit A. Francisella tularensis regulates the expression of the amino acid transporter SLC1A5 in infected THP-1 human monocytes. *Cell Microbiol*. 2012;14(11):1769-1783. doi: 10.1111/j.1462-5822.2012.01837.x [doi].

13. Alkhuder K, Meibom KL, Dubail I, Dupuis M, Charbit A. Glutathione provides a source of cysteine essential for intracellular multiplication of francisella tularensis. *PLoS Pathog*. 2009;5(1):e1000284. doi: 10.1371/journal.ppat.1000284 [doi].

14. Knapen MF, Zusterzeel PL, Peters WH, Steegers EA. Glutathione and glutathione-related enzymes in reproduction. A review. *Eur J Obstet Gynecol Reprod Biol*. 1999;82(2):171-184. doi: S0301211598002425 [pii].

15. Kaplowitz N, Aw TY, Ookhtens M. The regulation of hepatic glutathione. *Annu Rev Pharmacol Toxicol*. 1985;25:715-744. doi: 10.1146/annurev.pa.25.040185.003435 [doi].

16. Fuchs BC, Bode BP. Amino acid transporters ASCT2 and LAT1 in cancer: Partners in crime? *Semin Cancer Biol*. 2005;15(4):254-266. doi: S1044-579X(05)00022-2 [pii].

17. Nishida Y, Arakawa S, Fujitani K, et al. Discovery of Atg5/Atg7-independent alternative macroautophagy. *Nature*. 2009;461(7264):654-658. doi: 10.1038/nature08455.

18. Carling D, Zammit VA, Hardie DG. A common bicyclic protein kinase cascade inactivates the regulatory enzymes of fatty acid and cholesterol biosynthesis. *FEBS Lett*. 1987;223(2):217-222. doi: 0014-5793(87)80292-2 [pii].

19. Sato R, Goldstein JL, Brown MS. Replacement of serine-871 of hamster 3-hydroxy-3-methylglutaryl-CoA reductase prevents phosphorylation by AMP-activated kinase and blocks inhibition of sterol synthesis induced by ATP depletion. *Proc Natl Acad Sci U S A*. 1993;90(20):9261-9265.

20. Kim J, Kundu M, Viollet B, Guan KL. AMPK and mTOR regulate autophagy through direct phosphorylation of Ulk1. *Nat Cell Biol*. 2011;13(2):132-141. doi: 10.1038/ncb2152 [doi].

21. Jung CH, Ro SH, Cao J, Otto NM, Kim DH. mTOR regulation of autophagy. *FEBS Lett*. 2010;584(7):1287-1295. doi: 10.1016/j.febslet.2010.01.017 [doi].

22. Walczak M, Martens S. Dissecting the role of the Atg12-Atg5-Atg16 complex during autophagosome formation. *Autophagy*. 2013;9(3):424-425. doi: 10.4161/auto.22931 [doi].

23. Kabeya Y, Mizushima N, Ueno T, et al. LC3, a mammalian homologue of yeast Apg8p, is localized in autophagosome membranes after processing. *EMBO J*. 2000;19(21):5720-5728. doi: cdd565 [pii].

24. Thurston TL, Ryzhakov G, Bloor S, von Muhlinen N, Randow F. The TBK1 adaptor and autophagy receptor NDP52 restricts the proliferation of ubiquitin-coated bacteria. *Nat Immunol*. 2009;10(11):1215-1221. doi: 10.1038/ni.1800 [doi].

25. Zheng YT, Shahnazari S, Brech A, Lamark T, Johansen T, Brumell JH. The adaptor protein p62/SQSTM1 targets invading bacteria to the autophagy pathway. *J Immunol*. 2009;183(9):5909-5916. doi: 10.4049/jimmunol.0900441 [doi].

26. Wild P, Farhan H, McEwan DG, et al. Phosphorylation of the autophagy receptor optineurin restricts salmonella growth. *Science*. 2011;333(6039):228-233. doi: 10.1126/science.1205405 [doi].

27. Verlhac P, Gregoire IP, Azocar O, et al. Autophagy receptor NDP52 regulates pathogen-containing autophagosome maturation. *Cell Host Microbe*. 2015. doi: S1931-3128(15)00065-7 [pii].

28. Starr T, Child R, Wehrly TD, et al. Selective subversion of autophagy complexes facilitates completion of the brucella intracellular cycle. *Cell Host Microbe*. 2012;11(1):33-45. doi: 10.1016/j.chom.2011.12.002 [doi].

29. Collins CA, De Maziere A, van Dijk S, Carlsson F, Klumperman J, Brown EJ. Atg5-independent sequestration of ubiquitinated mycobacteria. *PLoS Pathog*. 2009;5(5):e1000430. doi: 10.1371/journal.ppat.1000430 [doi].

30. Miller CN, Steele SP, Brunton JC, et al. Extragenic suppressor mutations in inverted question mark ripA disrupt stability and function of LpxA. *BMC Microbiol*. 2014;14(1):2321. doi: s12866-014-0336-x [pii].

31. Peng K, Broz P, Jones J, Joubert LM, Monack D. Elevated AIM2-mediated pyroptosis triggered by hypercytotoxic francisella mutant strains is attributed to increased intracellular bacteriolysis. *Cell Microbiol*. 2011;13(10):1586-1600. doi: 10.1111/j.1462-5822.2011.01643.x [doi].

32. Kingry LC, Petersen JM. Comparative review of francisella tularensis and francisella novicida. *Front Cell Infect Microbiol*. 2014;4:35. doi: 10.3389/fcimb.2014.00035 [doi].

33. Shi CS, Kehrl JH. MyD88 and trif target beclin 1 to trigger autophagy in macrophages. *J Biol Chem*. 2008;283(48):33175-33182. doi: 10.1074/jbc.M804478200 [doi].

34. Delgado MA, Elmaoued RA, Davis AS, Kyei G, Deretic V. Toll-like receptors control autophagy. *EMBO J*. 2008;27(7):1110-1121. doi: 10.1038/emboj.2008.31 [doi].

35. Byrne BG, Dubuisson JF, Joshi AD, Persson JJ, Swanson MS. Inflammasome components coordinate autophagy and pyroptosis as macrophage responses to infection. *MBio*. 2013;4(1):e00620-12. doi: 10.1128/mBio.00620-12 [doi].

36. Kawai T, Akira S. Toll-like receptors and their crosstalk with other innate receptors in infection and immunity. *Immunity*. 2011;34(5):637-650. doi: 10.1016/j.immuni.2011.05.006 [doi].

37. Pyles RB, Jezek GE, Eaves-Pyles TD. Toll-like receptor 3 agonist protection against experimental francisella tularensis respiratory tract infection. *Infect Immun*. 2010;78(4):1700-1710. doi: 10.1128/IAI.00736-09 [doi].

38. Telepnev M, Golovliov I, Grundstrom T, Tarnvik A, Sjostedt A. Francisella tularensis inhibits toll-like receptor-mediated activation of intracellular signalling and secretion of TNF-alpha and IL-1 from murine macrophages. *Cell Microbiol*. 2003;5(1):41-51. doi: 251 [pii].

39. Barker JH, Weiss J, Apicella MA, Nauseef WM. Basis for the failure of francisella tularensis lipopolysaccharide to prime human polymorphonuclear leukocytes. *Infect Immun*. 2006;74(6):3277-3284. doi: 74/6/3277 [pii].

40. Cole LE, Shirey KA, Barry E, et al. Toll-like receptor 2-mediated signaling requirements for francisella tularensis live vaccine strain infection of murine macrophages. *Infect Immun*. 2007;75(8):4127-4137. doi: IAI.01868-06 [pii].

41. Crane DD, Ireland R, Alinger JB, Small P, Bosio CM. Lipids derived from virulent francisella tularensis broadly inhibit pulmonary inflammation via toll-like receptor 2 and peroxisome proliferator-activated receptor Î±. *Clin Vaccine Immunol*. 2013;20(10):1531-1540. doi: 00319-13 [pii].

42. Bosio CM, Bielefeldt-Ohmann H, Belisle JT. Active suppression of the pulmonary immune response by francisella tularensis Schu4. *J Immunol*. 2007;178(7):4538-4547. doi: 178/7/4538 [pii].

43. Latz E, Xiao TS, Stutz A. Activation and regulation of the inflammasomes. *Nat Rev Immunol*. 2013;13(6):397-411. doi: 10.1038/nri3452 [doi].

44. Thornberry NA, Bull HG, Calaycay JR, et al. A novel heterodimeric cysteine protease is required for interleukin-1 beta processing in monocytes. *Nature*. 1992;356(6372):768-774. doi: 10.1038/356768a0 [doi].

45. Dinarello CA. Immunological and inflammatory functions of the interleukin-1 family. *Annu Rev Immunol*. 2009;27:519-550. doi: 10.1146/annurev.immunol.021908.132612 [doi].

46. Crane DD, Bauler TJ, Wehrly TD, Bosio CM. Mitochondrial ROS potentiates indirect activation of the AIM2 inflammasome. *Front Microbiol*. 2014;5:10.3389/fmicb.2014.00438. doi: 10.3389/fmicb.2014.00438 [doi].

47. Hagar JA, Powell DA, Aachoui Y, Ernst RK, Miao EA. Cytoplasmic LPS activates caspase-11: Implications in TLR4-independent endotoxic shock. *Science*. 2013;341(6151):1250-1253. doi: 10.1126/science.1240988 [doi].

48. Chase JC, Celli J, Bosio CM. Direct and indirect impairment of human dendritic cell function by virulent francisella tularensis schu S4. *Infect Immun*. 2009;77(1):180-195. doi: 10.1128/IAI.00879-08 [doi].

49. Belhocine K, Monack DM. Francisella infection triggers activation of the AIM2 inflammasome in murine dendritic cells. *Cell Microbiol*. 2012;14(1):71-80. doi: 10.1111/j.1462-5822.2011.01700.x [doi].

50. Munz C. Enhancing immunity through autophagy. *Annu Rev Immunol*. 2009;27:423-449. doi: 10.1146/annurev.immunol.021908.132537 [doi].

51. Nakagawa I, Amano A, Mizushima N, et al. Autophagy defends cells against invading group A streptococcus. *Science*. 2004;306(5698):1037-1040. doi: 306/5698/1037 [pii].

52. Joubert PE, Meiffren G, Gregoire IP, et al. Autophagy induction by the pathogen receptor CD46. *Cell Host Microbe*. 2009;6(4):354-366. doi: 10.1016/j.chom.2009.09.006 [doi].

53. Barnett TC, Liebl D, Seymour LM, et al. The globally disseminated M1T1 clone of group A streptococcus evades autophagy for intracellular replication. *Cell Host Microbe*. 2013;14(6):675-682. doi: 10.1016/j.chom.2013.11.003 [doi].

54. Singh SB, Davis AS, Taylor GA, Deretic V. Human IRGM induces autophagy to eliminate intracellular mycobacteria. *Science*. 2006;313(5792):1438-1441. doi: 1129577 [pii].

55. Andrade RM, Wessendarp M, Gubbels MJ, Striepen B, Subauste CS. CD40 induces macrophage anti-toxoplasma gondii activity by triggering autophagy-dependent fusion of pathogen-containing vacuoles and lysosomes. *J Clin Invest*. 2006;116(9):2366-2377. doi: 10.1172/JCI28796 [doi].

56. Tattoli I, Sorbara MT, Vuckovic D, et al. Amino acid starvation induced by invasive bacterial pathogens triggers an innate host defense program. *Cell Host Microbe*. 2012;11(6):563-575. doi: 10.1016/j.chom.2012.04.012 [doi].

57. Cooney R, Baker J, Brain O, et al. NOD2 stimulation induces autophagy in dendritic cells influencing bacterial handling and antigen presentation. *Nat Med*. 2010;16(1):90-97. doi: 10.1038/nm.2069 [doi].

58. Travassos LH, Carneiro LA, Ramjeet M, et al. Nod1 and Nod2 direct autophagy by recruiting ATG16L1 to the plasma membrane at the site of bacterial entry. *Nat Immunol*. 2010;11(1):55-62. doi: 10.1038/ni.1823 [doi].

59. Qin QM, Pei J, Ancona V, Shaw BD, Ficht TA, de Figueiredo P. RNAi screen of endoplasmic reticulum-associated host factors reveals a role for IRE1alpha in supporting brucella replication. *PLoS Pathog*. 2008;4(7):e1000110. doi: 10.1371/journal.ppat.1000110 [doi].

60. Smith JA, Khan M, Magnani DD, et al. Brucella induces an unfolded protein response via TcpB that supports intracellular replication in macrophages. *PLoS Pathog*. 2013;9(12):e1003785. doi: 10.1371/journal.ppat.1003785 [doi].

61. Wang Y, Weiss LM, Orlofsky A. Host cell autophagy is induced by toxoplasma gondii and contributes to parasite growth. *J Biol Chem*. 2009;284(3):1694-1701. doi: 10.1074/jbc.M807890200 [doi].

62. Makino S, Sasakawa C, Kamata K, Kurata T, Yoshikawa M. A genetic determinant required for continuous reinfection of adjacent cells on large plasmid in S. flexneri 2a. *Cell*. 1986;46(4):551-555. doi: 0092-8674(86)90880-9 [pii].

63. Ogawa M, Yoshimori T, Suzuki T, Sagara H, Mizushima N, Sasakawa C. Escape of intracellular shigella from autophagy. *Science*. 2005;307(5710):727-731. doi: 1106036 [pii].

64. Eng CH, Yu K, Lucas J, White E, Abraham RT. Ammonia derived from glutaminolysis is a diffusible regulator of autophagy. *Sci Signal*. 2010;3(119):ra31. doi: 10.1126/scisignal.2000911 [doi].

65. Chong A, Wehrly TD, Child R, et al. Cytosolic clearance of replication-deficient mutants reveals francisella tularensis interactions with the autophagic pathway. *Autophagy*. 2012;8(9):1342-1356. doi: 10.4161/auto.20808 [doi].

66. Case ED, Chong A, Wehrly TD, et al. The francisella O-antigen mediates survival in the macrophage cytosol via autophagy avoidance. *Cell Microbiol*. 2014;16(6):862-877. doi: 10.1111/cmi.12246 [doi].

67. Domann E, Wehland J, Rohde M, et al. A novel bacterial virulence gene in listeria monocytogenes required for host cell microfilament interaction with homology to the proline-rich region of vinculin. *EMBO J*. 1992;11(5):1981-1990.

68. Kocks C, Gouin E, Tabouret M, Berche P, Ohayon H, Cossart P. L. monocytogenes-induced actin assembly requires the actA gene product, a surface protein. *Cell*. 1992;68(3):521-531. doi: 0092-8674(92)90188-I [pii].

69. Roberts LM, Tuladhar S, Steele SP, et al. Identification of early interactions between francisella and the host. *Infect Immun*. 2014;82(6):2504-2510. doi: 10.1128/IAI.01654-13 [doi].

70. Lindemann SR, Peng K, Long ME, et al. Francisella tularensis schu S4 O-antigen and capsule biosynthesis gene mutants induce early cell death in human macrophages. *Infect Immun*. 2011;79(2):581-594. doi: 10.1128/IAI.00863-10 [doi].

71. Rasmussen JA, Post DM, Gibson BW, et al. Francisella tularensis schu S4 lipopolysaccharide core sugar and O-antigen mutants are attenuated in a mouse model of tularemia. *Infect Immun*. 2014;82(4):1523-1539. doi: 10.1128/IAI.01640-13 [doi].

72. Doyle CR, Pan JA, Mena P, Zong WX, Thanassi DG. TolC-dependent modulation of host cell death by the francisella tularensis live vaccine strain. *Infect Immun*. 2014;82(5):2068-2078. doi: 10.1128/IAI.00044-14 [doi].

73. Platz GJ, Bublitz DAC, Mena P, Benach JL, Furie MB, Thanassi DG. A tolC mutant of francisella tularensis is hypercytotoxic compared to the wild type and elicits increased proinflammatory responses from host cells. *Infect Immun*. 2010;78(3):1022-1031. doi: 0992-09 [pii].

74. Checroun C, Wehrly TD, Fischer ER, Hayes SF, Celli J. Autophagy-mediated reentry of francisella tularensis into the endocytic compartment after cytoplasmic replication. *Proc Natl Acad Sci U S A*. 2006;103(39):14578-14583. doi: 10.1073/pnas.0601838103.

75. Saccheri F, Pozzi C, Avogadri F, et al. Bacteria-induced gap junctions in tumors favor antigen cross-presentation and antitumor immunity. *Sci Transl Med*. 2010;2(44):44ra57. doi: 10.1126/scitranslmed.3000739 [doi].

76. Blank F, Wehrli M, Lehmann A, et al. Macrophages and dendritic cells express tight junction proteins and exchange particles in an in vitro model of the human airway wall. *Immunobiology*. 2011;216(1-2):86-95. doi: 10.1016/j.imbio.2010.02.006 [doi].

77. Harshyne LA, Watkins SC, Gambotto A, Barratt-Boyes SM. Dendritic cells acquire antigens from live cells for cross-presentation to CTL. *J Immunol*. 2001;166(6):3717-3723.

78. Onfelt B, Nedvetzki S, Benninger RK, et al. Structurally distinct membrane nanotubes between human macrophages support long-distance vesicular traffic or surfing of bacteria. *J Immunol*. 2006;177(12):8476-8483. doi: 177/12/8476 [pii].

79. Sarvari AK, Doan-Xuan QM, Bacso Z, Csomos I, Balajthy Z, Fesus L. Interaction of differentiated human adipocytes with macrophages leads to trogocytosis and selective IL-6 secretion. *Cell Death Dis*. 2015;6:e1613. doi: 10.1038/cddis.2014.579 [doi].

80. Sowinski S, Jolly C, Berninghausen O, et al. Membrane nanotubes physically connect T cells over long distances presenting a novel route for HIV-1 transmission. *Nat Cell Biol*. 2008;10(2):211-219. doi: 10.1038/ncb1682 [doi].

81. Joly E, Hudrisier D. What is trogocytosis and what is its purpose? *Nat Immunol*. 2003;4(9):815. doi: 10.1038/ni0903-815 [doi].

82. Sattentau Q. Avoiding the void: Cell-to-cell spread of human viruses. *Nat Rev Microbiol*. 2008;6(11):815-826. doi: 10.1038/nrmicro1972; 10.1038/nrmicro1972.

83. Ahmed KA, Munegowda MA, Xie Y, Xiang J. Intercellular trogocytosis plays an important role in modulation of immune responses. *Cell Mol Immunol*. 2008;5(4):261-269. doi: 10.1038/cmi.2008.32 [doi].

84. Nudleman E, Wall D, Kaiser D. Cell-to-cell transfer of bacterial outer membrane lipoproteins. *Science*. 2005;309(5731):125-127. doi: 309/5731/125 [pii].

85. Machlenkin A, Uzana R, Frankenburg S, et al. Capture of tumor cell membranes by trogocytosis facilitates detection and isolation of tumor-specific functional CTLs. *Cancer Res*. 2008;68(6):2006-2013. doi: 10.1158/0008-5472.CAN-07-3119 [doi].

86. Wakim LM, Bevan MJ. Cross-dressed dendritic cells drive memory CD8+ T-cell activation after viral infection. *Nature*. 2011;471(7340):629-632. doi: 10.1038/nature09863 [doi].

87. Ralston KS, Solga MD, Mackey-Lawrence NM, Somlata, Bhattacharya A, Petri WA,Jr. Trogocytosis by entamoeba histolytica contributes to cell killing and tissue invasion. *Nature*. 2014;508(7497):526-530. doi: 10.1038/nature13242 [doi].

88. Broms JE, Sjostedt A, Lavander M. The role of the francisella tularensis pathogenicity island in type VI secretion, intracellular survival, and modulation of host cell signaling. *Front Microbiol*. 2010;1:10.3389/fmicb.2010.00136. doi: 10.3389/fmicb.2010.00136 [doi].

89. Clemens DL, Lee BY, Horwitz MA. Virulent and avirulent strains of francisella tularensis prevent acidification and maturation of their phagosomes and escape into the cytoplasm in human macrophages. *Infect Immun*. 2004;72(6):3204-3217. doi: 10.1128/IAI.72.6.3204-3217.2004.

90. Huang MT, Mortensen BL, Taxman DJ, et al. Deletion of ripA alleviates suppression of the inflammasome and MAPK by francisella tularensis. *J Immunol*. 2010;185(9):5476-5485. doi: 10.4049/jimmunol.1002154; 10.4049/jimmunol.1002154.

91. Bosio CM, Bielefeldt-Ohmann H, Belisle JT. Active suppression of the pulmonary immune response by francisella tularensis Schu4. *J Immunol*. 2007;178(7):4538-4547.

92. Hajjar AM, Harvey MD, Shaffer SA, et al. Lack of in vitro and in vivo recognition of francisella tularensis subspecies lipopolysaccharide by toll-like receptors. *Infect Immun*. 2006;74(12):6730-6738. doi: 10.1128/IAI.00934-06.

93. Lindgren M, Eneslatt K, Broms JE, Sjostedt A. Importance of PdpC, IglC, IglI, and IglG for modulation of a host cell death pathway induced by francisella tularensis LVS. *Infect Immun*. 2013. doi: 10.1128/IAI.00275-13.

94. Barker JR, Chong A, Wehrly TD, et al. The francisella tularensis pathogenicity island encodes a secretion system that is required for phagosome escape and virulence. *Mol Microbiol*. 2009;74(6):1459-1470.

95. Bonquist L, Lindgren H, Golovliov I, Guina T, Sjostedt A. MglA and igl proteins contribute to the modulation of francisella tularensis live vaccine strain-containing phagosomes in murine macrophages. *Infect Immun*. 2008;76(8):3502-3510. doi: 10.1128/IAI.00226-08; 10.1128/IAI.00226-08.

96. Broms JE, Lavander M, Sjostedt A. A conserved alpha-helix essential for a type VI secretion-like system of francisella tularensis. *J Bacteriol*. 2009;191(8):2431-2446. doi: 10.1128/JB.01759-08; 10.1128/JB.01759-08.

97. Broms JE, Lavander M, Meyer L, Sjostedt A. IglG and IglI of the francisella pathogenicity island are important virulence determinants of francisella tularensis LVS. *Infect Immun*. 2011;79(9):3683-3696. doi: 10.1128/IAI.01344-10; 10.1128/IAI.01344-10.

98. Lindgren H, Golovliov I, Baranov V, Ernst RK, Telepnev M, Sjostedt A. Factors affecting the escape of francisella tularensis from the phagolysosome. *J Med Microbiol*. 2004;53(Pt 10):953-958.

99. Schmerk CL, Duplantis BN, Wang D, et al. Characterization of the pathogenicity island protein PdpA and its role in the virulence of francisella novicida. *Microbiology*. 2009;155(Pt 5):1489-1497. doi: 10.1099/mic.0.025379-0; 10.1099/mic.0.025379-0.

100. Straskova A, Cerveny L, Spidlova P, et al. Deletion of IglH in virulent francisella tularensis subsp. holarctica FSC200 strain results in attenuation and provides protection against the

challenge with the parental strain. *Microbes Infect*. 2012;14(2):177-187. doi: 10.1016/j.micinf.2011.08.017; 10.1016/j.micinf.2011.08.017.

101. Long ME, Lindemann SR, Rasmussen JA, Jones BD, Allen LA. Disruption of francisella tularensis schu S4 iglI, iglJ, and pdpC genes results in attenuation for growth in human macrophages and in vivo virulence in mice and reveals a unique phenotype for pdpC. *Infect Immun*. 2013;81(3):850-861. doi: 10.1128/IAI.00822-12; 10.1128/IAI.00822-12.

102. Fuller JR, Craven RR, Hall JD, Kijek TM, Taft-Benz S, Kawula TH. RipA, a cytoplasmic membrane protein conserved among francisella species, is required for intracellular survival. *Infect Immun*. 2008;76(11):4934-4943. doi: 10.1128/IAI.00475-08; 10.1128/IAI.00475-08.

103. Fuller JR, Kijek TM, Taft-Benz S, Kawula TH. Environmental and intracellular regulation of francisella tularensis ripA. *BMC Microbiol*. 2009;9:216-2180-9-216. doi: 10.1186/1471-2180-9-216; 10.1186/1471-2180-9-216.

104. Bosio CM, Bielefeldt-Ohmann H, Belisle JT. Active suppression of the pulmonary immune response by francisella tularensis Schu4. *J Immunol*. 2007;178(7):4538-4547.

105. GREISMAN SE, HORNICK RB, CAROZZA FA,Jr, WOODWARD TE. The role of endotoxin during typhoid fever and tularemia in man. I. acquisition of tolerance to endotoxin. *J Clin Invest*. 1963;42:1064-1075. doi: 10.1172/JCI104792.

106. Kieffer TL, Cowley S, Nano FE, Elkins KL. Francisella novicida LPS has greater immunobiological activity in mice than F. tularensis LPS, and contributes to F. novicida murine pathogenesis. *Microbes Infect*. 2003;5(5):397-403.

107. Barker JR, Chong A, Wehrly TD, et al. The francisella tularensis pathogenicity island encodes a secretion system that is required for phagosome escape and virulence. *Mol Microbiol*. 2009;74(6):1459-1470.

108. Peng K, Broz P, Jones J, Joubert LM, Monack D. Elevated AIM2-mediated pyroptosis triggered by hypercytotoxic francisella mutant strains is attributed to increased intracellular bacteriolysis. *Cell Microbiol*. 2011;13(10):1586-1600. doi: 10.1111/j.1462-5822.2011.01643.x; 10.1111/j.1462-5822.2011.01643.x.

109. Chong A, Wehrly TD, Nair V, et al. The early phagosomal stage of francisella tularensis determines optimal phagosomal escape and francisella pathogenicity island protein expression. *Infect Immun*. 2008;76(12):5488-5499. doi: 10.1128/IAI.00682-08; 10.1128/IAI.00682-08.

110. LoVullo ED, Molins-Schneekloth CR, Schweizer HP, Pavelka MS,Jr. Single-copy chromosomal integration systems for francisella tularensis. *Microbiology*. 2009;155(Pt 4):1152-1163. doi: 10.1099/mic.0.022491-0; 10.1099/mic.0.022491-0.

111. LoVullo ED, Sherrill LA, Pavelka MS,Jr. Improved shuttle vectors for francisella tularensis genetics. *FEMS Microbiol Lett*. 2009;291(1):95-102. doi: 10.1111/j.1574-6968.2008.01440.x; 10.1111/j.1574-6968.2008.01440.x.

112. Fuller JR, Craven RR, Hall JD, Kijek TM, Taft-Benz S, Kawula TH. RipA, a cytoplasmic membrane protein conserved among francisella species, is required for intracellular survival. *Infect Immun*. 2008;76(11):4934-4943. doi: 10.1128/IAI.00475-08.

113. Mortensen BL, Fuller JR, Taft-Benz S, et al. Effects of the putative transcriptional regulator IclR on francisella tularensis pathogenesis. *Infect Immun*. 2010;78(12):5022-5032. doi: 10.1128/IAI.00544-10.

114. Schneider CA, Rasband WS, Eliceiri KW. NIH image to ImageJ: 25 years of image analysis. *Nat Meth*. 2012;9(7):671-675. http://dx.doi.org/10.1038/nmeth.2089.

115. Jung CH, Ro SH, Cao J, Otto NM, Kim DH. mTOR regulation of autophagy. *FEBS Lett*. 2010;584(7):1287-1295. doi: 10.1016/j.febslet.2010.01.017; 10.1016/j.febslet.2010.01.017.

116. Deretic V, Levine B. Autophagy, immunity, and microbial adaptations. *Cell Host Microbe*. 2009;5(6):527-549. doi: 10.1016/j.chom.2009.05.016.

117. Meijer AJ, Codogno P. Autophagy: Regulation by energy sensing. *Curr Biol*. 2011;21(6):R227-9. doi: 10.1016/j.cub.2011.02.007.

118. Levine B. Eating oneself and uninvited guests: Autophagy-related pathways in cellular defense. *Cell*. 2005;120(2):159-162. doi: 10.1016/j.cell.2005.01.005.

119. Deretic V. Autophagy: An emerging immunological paradigm. *J Immunol*. 2012;189(1):15-20. doi: 10.4049/jimmunol.1102108.

120. Ogawa M, Yoshikawa Y, Mimuro H, Hain T, Chakraborty T, Sasakawa C. Autophagy targeting of listeria monocytogenes and the bacterial countermeasure. *Autophagy*. 2011;7(3):310-314.

121. Knodler LA, Celli J. Eating the strangers within: Host control of intracellular bacteria via xenophagy. *Cell Microbiol*. 2011;13(9):1319-1327. doi: 10.1111/j.1462-5822.2011.01632.x; 10.1111/j.1462-5822.2011.01632.x.

122. Starr T, Child R, Wehrly TD, et al. Selective subversion of autophagy complexes facilitates completion of the brucella intracellular cycle. *Cell Host Microbe*. 2012;11(1):33-45. doi: 10.1016/j.chom.2011.12.002; 10.1016/j.chom.2011.12.002.

123. Niu H, Xiong Q, Yamamoto A, Hayashi-Nishino M, Rikihisa Y. Autophagosomes induced by a bacterial beclin 1 binding protein facilitate obligatory intracellular infection. *Proc Natl Acad Sci U S A*. 2012;109(51):20800-20807. doi: 10.1073/pnas.1218674109; 10.1073/pnas.1218674109.

124. Heaton NS, Randall G. Dengue virus-induced autophagy regulates lipid metabolism. *Cell Host Microbe*. 2010;8(5):422-432. doi: 10.1016/j.chom.2010.10.006.

125. Birmingham CL, Canadien V, Gouin E, et al. Listeria monocytogenes evades killing by autophagy during colonization of host cells. *Autophagy*. 2007;3(5):442-451.

126. Keim P, Johansson A, Wagner DM. Molecular epidemiology, evolution, and ecology of francisella. *Ann N Y Acad Sci*. 2007;1105:30-66. doi: 10.1196/annals.1409.011.

127. Saslaw S, Eigelsbach HT, Prior JA, Wilson HE, Carhart S. Tularemia vaccine study. II. respiratory challenge. *Arch Intern Med*. 1961;107:702-714.

128. Dennis DT, Inglesby TV, Henderson DA, et al. Tularemia as a biological weapon: Medical and public health management. *JAMA*. 2001;285(21):2763-2773.

129. Chong A, Wehrly TD, Child R, et al. Cytosolic clearance of replication-deficient mutants reveals francisella tularensis interactions with the autophagic pathway. *Autophagy*. 2012;8(9).

130. Fortier AH, Leiby DA, Narayanan RB, et al. Growth of francisella tularensis LVS in macrophages: The acidic intracellular compartment provides essential iron required for growth. *Infect Immun*. 1995;63(4):1478-1483.

131. Cheong H, Lindsten T, Wu J, Lu C, Thompson CB. Ammonia-induced autophagy is independent of ULK1/ULK2 kinases. *Proc Natl Acad Sci U S A*. 2011;108(27):11121-11126. doi: 10.1073/pnas.1107969108; 10.1073/pnas.1107969108.

132. Eng CH, Yu K, Lucas J, White E, Abraham RT. Ammonia derived from glutaminolysis is a diffusible regulator of autophagy. *Sci Signal*. 2010;3(119):ra31. doi: 10.1126/scisignal.2000911; 10.1126/scisignal.2000911.

133. Munafo DB, Colombo MI. A novel assay to study autophagy: Regulation of autophagosome vacuole size by amino acid deprivation. *J Cell Sci*. 2001;114(Pt 20):3619-3629.

134. Lovullo ED, Miller CN, Pavelka MS,Jr, Kawula TH. TetR-based gene regulation systems for francisella tularensis. *Appl Environ Microbiol*. 2012. doi: 10.1128/AEM.01679-12.

135. Kang R, Zeh HJ, Lotze MT, Tang D. The beclin 1 network regulates autophagy and apoptosis. *Cell Death Differ*. 2011;18(4):571-580. doi: 10.1038/cdd.2010.191; 10.1038/cdd.2010.191.

136. Hara K, Yonezawa K, Weng QP, Kozlowski MT, Belham C, Avruch J. Amino acid sufficiency and mTOR regulate p70 S6 kinase and eIF-4E BP1 through a common effector mechanism. *J Biol Chem*. 1998;273(23):14484-14494.

137. Kabeya Y, Mizushima N, Ueno T, et al. LC3, a mammalian homologue of yeast Apg8p, is localized in autophagosome membranes after processing. *EMBO J*. 2000;19(21):5720-5728. doi: 10.1093/emboj/19.21.5720.

138. Yoshikawa Y, Ogawa M, Hain T, et al. Listeria monocytogenes ActA-mediated escape from autophagic recognition. *Nat Cell Biol*. 2009;11(10):1233-1240. doi: 10.1038/ncb1967; 10.1038/ncb1967.

139. Zheng YT, Shahnazari S, Brech A, Lamark T, Johansen T, Brumell JH. The adaptor protein p62/SQSTM1 targets invading bacteria to the autophagy pathway. *J Immunol*. 2009;183(9):5909-5916. doi: 10.4049/jimmunol.0900441; 10.4049/jimmunol.0900441.

140. Orvedahl A, MacPherson S, Sumpter R,Jr, Talloczy Z, Zou Z, Levine B. Autophagy protects against sindbis virus infection of the central nervous system. *Cell Host Microbe*. 2010;7(2):115-127. doi: 10.1016/j.chom.2010.01.007; 10.1016/j.chom.2010.01.007.

141. Mesquita FS, Thomas M, Sachse M, Santos AJ, Figueira R, Holden DW. The salmonella deubiquitinase SseL inhibits selective autophagy of cytosolic aggregates. *PLoS Pathog*. 2012;8(6):e1002743. doi: 10.1371/journal.ppat.1002743; 10.1371/journal.ppat.1002743.

142. Price CT, Al-Quadan T, Santic M, Rosenshine I, Abu Kwaik Y. Host proteasomal degradation generates amino acids essential for intracellular bacterial growth. *Science*. 2011;334(6062):1553-1557. doi: 10.1126/science.1212868.

143. Barel M, Meibom K, Dubail I, Botella J, Charbit A. Francisella tularensis regulates the expression of the amino acid transporter SLC1A5 in infected THP-1 human monocytes. *Cell Microbiol*. 2012. doi: 10.1111/j.1462-5822.2012.01837.x; 10.1111/j.1462-5822.2012.01837.x.

144. McArdle J, Moorman NJ, Munger J. HCMV targets the metabolic stress response through activation of AMPK whose activity is important for viral replication. *PLoS Pathog*. 2012;8(1):e1002502. doi: 10.1371/journal.ppat.1002502.

145. Yang Z, Huang J, Geng J, Nair U, Klionsky DJ. Atg22 recycles amino acids to link the degradative and recycling functions of autophagy. *Mol Biol Cell*. 2006;17(12):5094-5104. doi: 10.1091/mbc.E06-06-0479.

146. Collins CA, De Maziere A, van Dijk S, Carlsson F, Klumperman J, Brown EJ. Atg5-independent sequestration of ubiquitinated mycobacteria. *PLoS Pathog*. 2009;5(5):e1000430. doi: 10.1371/journal.ppat.1000430; 10.1371/journal.ppat.1000430.

147. Jourdren L, Delaveau T, Marquenet E, Jacq C, Garcia M. CORSEN, a new software dedicated to microscope-based 3D distance measurements: mRNA-mitochondria distance, from single-cell to population analyses. *RNA*. 2010;16(7):1301-1307. doi: 10.1261/rna.1996810.

148. Klionsky DJ, Abdalla FC, Abeliovich H, et al. Guidelines for the use and interpretation of assays for monitoring autophagy. *Autophagy*. 2012;8(4):445-544.

149. Eskelinen EL. To be or not to be? examples of incorrect identification of autophagic compartments in conventional transmission electron microscopy of mammalian cells. *Autophagy*. 2008;4(2):257-260.

150. Yla-Anttila P, Vihinen H, Jokitalo E, Eskelinen EL. Monitoring autophagy by electron microscopy in mammalian cells. *Methods Enzymol*. 2009;452:143-164. doi: 10.1016/S0076-6879(08)03610-0; 10.1016/S0076-6879(08)03610-0.

151. Ramirez MC, Sigal LJ. Macrophages and dendritic cells use the cytosolic pathway to rapidly cross-present antigen from live, vaccinia-infected cells. *J Immunol*. 2002;169(12):6733-6742.

152. Rogers RS, Bhattacharya J. When cells become organelle donors. *Physiology (Bethesda)*. 2013;28(6):414-422. doi: 10.1152/physiol.00032.2013 [doi].

153. Tilney LG, Connelly PS, Portnoy DA. Actin filament nucleation by the bacterial pathogen, listeria monocytogenes. *J Cell Biol*. 1990;111(6 Pt 2):2979-2988.

154. Heinzen RA, Hayes SF, Peacock MG, Hackstadt T. Directional actin polymerization associated with spotted fever group rickettsia infection of vero cells. *Infect Immun*. 1993;61(5):1926-1935.

155. Reed SCO, Lamason RL, Risca VI, Abernathy E, Welch MD. Rickettsia actin-based motility occurs in distinct phases mediated by different actin nucleators. *Curr Biol*. 2014;24(1):98-103. doi: 10.1016/j.cub.2013.11.025 [doi].

156. Stinchcombe JC, Bossi G, Booth S, Griffiths GM. The immunological synapse of CTL contains a secretory domain and membrane bridges. *Immunity*. 2001;15(5):751-761. doi: S1074-7613(01)00234-5 [pii].

157. Smyth LA, Harker N, Turnbull W, et al. The relative efficiency of acquisition of MHC:Peptide complexes and cross-presentation depends on dendritic cell type. *J Immunol*. 2008;181(5):3212-3220. doi: 181/5/3212 [pii].

158. Chow T, Whiteley J, Li M, Rogers IM. The transfer of host MHC class I protein protects donor cells from NK cell and macrophage-mediated rejection during hematopoietic stem cell transplantation and engraftment in mice. *Stem Cells*. 2013;31(10):2242-2252. doi: 10.1002/stem.1458 [doi].

159. Zhang QJ, Li XL, Wang D, et al. Trogocytosis of MHC-I/peptide complexes derived from tumors and infected cells enhances dendritic cell cross-priming and promotes adaptive T cell responses. *PLoS One*. 2008;3(8):e3097. doi: 10.1371/journal.pone.0003097 [doi].

160. Li L, Kim S, Herndon JM, et al. Cross-dressed CD8alpha+/CD103+ dendritic cells prime CD8+ T cells following vaccination. *Proc Natl Acad Sci U S A*. 2012;109(31):12716-12721. doi: 10.1073/pnas.1203468109 [doi].

161. Gu P, Gao JF, D'Souza CA, Kowalczyk A, Chou KY, Zhang L. Trogocytosis of CD80 and CD86 by induced regulatory T cells. *Cell Mol Immunol*. 2012;9(2):136-146. doi: 10.1038/cmi.2011.62 [doi].

162. Dolan BP, Gibbs KD,Jr, Ostrand-Rosenberg S. Tumor-specific CD4+ T cells are activated by "cross-dressed" dendritic cells presenting peptide-MHC class II complexes acquired from cell-based cancer vaccines. *J Immunol*. 2006;176(3):1447-1455. doi: 176/3/1447 [pii].

163. Mortensen BL, Fuller JR, Taft-Benz S, et al. Effects of the putative transcriptional regulator IclR on francisella tularensis pathogenesis. *Infect Immun*. 2010;78(12):5022-5032. doi: 10.1128/IAI.00544-10.

164. Dupont N, Jiang S, Pilli M, Ornatowski W, Bhattacharya D, Deretic V. Autophagy-based unconventional secretory pathway for extracellular delivery of IL-1beta. *EMBO J*. 2011;30(23):4701-4711. doi: 10.1038/emboj.2011.398 [doi].

165. Ogata M, Hino S, Saito A, et al. Autophagy is activated for cell survival after endoplasmic reticulum stress. *Mol Cell Biol*. 2006;26(24):9220-9231. doi: MCB.01453-06 [pii].

166. Malkoff DB, Buetow DE. Ultrastructural changes during carbon starvation in euglena gracilis. *Exp Cell Res*. 1964;35:58-68.

167. Skaar EP. The battle for iron between bacterial pathogens and their vertebrate hosts. *PLoS Pathog*. 2010;6(8):e1000949. doi: 10.1371/journal.ppat.1000949 [doi].

168. Griffin JE, Pandey AK, Gilmore SA, et al. Cholesterol catabolism by mycobacterium tuberculosis requires transcriptional and metabolic adaptations. *Chem Biol*. 2012;19(2):218-227. doi: 10.1016/j.chembiol.2011.12.016 [doi].

169. Dierickx PJ, Almar MM, De Jonckheere JF. Glutathione transferase activity in some flagellates and amoebae, and purification of the soluble glutathione transferases from acanthamoeba. *Biochem Int*. 1990;22(4):593-600.

170. Abu Kwaik Y, Bumann D. Microbial quest for food in vivo: 'Nutritional virulence' as an emerging paradigm. *Cell Microbiol*. 2013;15(6):882-890. doi: 10.1111/cmi.12138 [doi].

171. Singh AP, Lai SC, Nandi T, et al. Evolutionary analysis of burkholderia pseudomallei identifies putative novel virulence genes, including a microbial regulator of host cell autophagy. *J Bacteriol*. 2013;195(24):5487-5498. doi: 10.1128/JB.00718-13 [doi].

172. Al-Khodor S, Marshall-Batty K, Nair V, Ding L, Greenberg DE, Fraser ID. Burkholderia cenocepacia J2315 escapes to the cytosol and actively subverts autophagy in human macrophages. *Cell Microbiol*. 2014;16(3):378-395. doi: 10.1111/cmi.12223 [doi].

173. Gutierrez MG, Vazquez CL, Munafo DB, et al. Autophagy induction favours the generation and maturation of the coxiella-replicative vacuoles. *Cell Microbiol*. 2005;7(7):981-993. doi: CMI527 [pii].

174. Winchell CG, Graham JG, Kurten RC, Voth DE. Coxiella burnetii type IV secretion-dependent recruitment of macrophage autophagosomes. *Infect Immun*. 2014;82(6):2229-2238. doi: 01236-13 [pii].

175. Chong A, Wehrly TD, Child R, et al. Cytosolic clearance of replication-deficient mutants reveals francisella tularensis interactions with the autophagic pathway. *Autophagy*. 2012;8(9):1342-1356. doi: 10.4161/auto.20808 [doi].

176. Duffy A, Le J, Sausville E, Emadi A. Autophagy modulation: A target for cancer treatment development. *Cancer Chemother Pharmacol*. 2015;75(3):439-447. doi: 10.1007/s00280-014-2637-z [doi].

177. Amaravadi RK, Lippincott-Schwartz J, Yin XM, et al. Principles and current strategies for targeting autophagy for cancer treatment. *Clin Cancer Res*. 2011;17(4):654-666. doi: 10.1158/1078-0432.CCR-10-2634 [doi].

178. Goodall ML, Wang T, Martin KR, et al. Development of potent autophagy inhibitors that sensitize oncogenic BRAF V600E mutant melanoma tumor cells to vemurafenib. *Autophagy*. 2014;10(6):1120-1136. doi: 10.4161/auto.28594 [doi].

179. Nakayama M. Antigen presentation by MHC-dressed cells. *Front Immunol*. 2014;5:10.3389/fimmu.2014.00672. doi: 10.3389/fimmu.2014.00672 [doi].

180. Zhang X, Wu J, Du F, et al. The cytosolic DNA sensor cGAS forms an oligomeric complex with DNA and undergoes switch-like conformational changes in the activation loop. *Cell Rep*. 2014;6(3):421-430. doi: 10.1016/j.celrep.2014.01.003 [doi].

181. Cai X, Chiu YH, Chen ZJ. The cGAS-cGAMP-STING pathway of cytosolic DNA sensing and signaling. *Mol Cell*. 2014;54(2):289-296. doi: 10.1016/j.molcel.2014.03.040 [doi].

182. Zhang QJ, Li XL, Wang D, et al. Trogocytosis of MHC-I/peptide complexes derived from tumors and infected cells enhances dendritic cell cross-priming and promotes adaptive T cell responses. *PLoS One*. 2008;3(8):e3097. doi: 10.1371/journal.pone.0003097 [doi].

183. Roberts NJ, Zhang L, Janku F, et al. Intratumoral injection of clostridium novyi-NT spores induces antitumor responses. *Sci Transl Med*. 2014;6(249):249ra111. doi: 10.1126/scitranslmed.3008982 [doi].

184. Coley WB. The treatment of inoperable sarcoma by bacterial toxins (the mixed toxins of the streptococcus erysipelas and the bacillus prodigiosus). *Proc R Soc Med*. 1910;3(Surg Sect):1-48.

185. Sinha G. Listeria vaccines join the checkpoint frenzy. *Nat Biotechnol*. 2014;32(12):1176-1177. doi: 10.1038/nbt1214-1176d [doi].

186. Schmitt CK, Meysick KC, O'Brien AD. Bacterial toxins: Friends or foes? *Emerg Infect Dis*. 1999;5(2):224-234.

187. Hood MI, Skaar EP. Nutritional immunity: Transition metals at the pathogen-host interface. *Nat Rev Microbiol*. 2012;10(8):525-537. doi: 10.1038/nrmicro2836 [doi].

188. Pechous RD, McCarthy TR, Zahrt TC. Working toward the future: Insights into francisella tularensis pathogenesis and vaccine development. *Microbiol Mol Biol Rev*. 2009;73(4):684-711. doi: 10.1128/MMBR.00028-09 [doi].

189. Terry LJ, Vastag L, Rabinowitz JD, Shenk T. Human kinome profiling identifies a requirement for AMP-activated protein kinase during human cytomegalovirus infection. *Proc Natl Acad Sci U S A*. 2012;109(8):3071-3076. doi: 10.1073/pnas.1200494109 [doi].

190. Inoki K, Kim J, Guan KL. AMPK and mTOR in cellular energy homeostasis and drug targets. *Annu Rev Pharmacol Toxicol*. 2012;52:381-400. doi: 10.1146/annurev-pharmtox-010611-134537 [doi].

191. Walsh D, Perez C, Notary J, Mohr I. Regulation of the translation initiation factor eIF4F by multiple mechanisms in human cytomegalovirus-infected cells. *J Virol*. 2005;79(13):8057-8064. doi: 79/13/8057 [pii].

192. McArdle J, Moorman NJ, Munger J. HCMV targets the metabolic stress response through activation of AMPK whose activity is important for viral replication. *PLoS Pathog*. 2012;8(1):e1002502. doi: 10.1371/journal.ppat.1002502 [doi].

193. Kudchodkar SB, Del Prete GQ, Maguire TG, Alwine JC. AMPK-mediated inhibition of mTOR kinase is circumvented during immediate-early times of human cytomegalovirus infection. *J Virol*. 2007;81(7):3649-3651. doi: JVI.02079-06 [pii].

194. Spencer CM, Schafer XL, Moorman NJ, Munger J. Human cytomegalovirus induces the activity and expression of acetyl-coenzyme A carboxylase, a fatty acid biosynthetic enzyme whose inhibition attenuates viral replication. *J Virol*. 2011;85(12):5814-5824. doi: 10.1128/JVI.02630-10 [doi].

195. Moorman NJ, Cristea IM, Terhune SS, Rout MP, Chait BT, Shenk T. Human cytomegalovirus protein UL38 inhibits host cell stress responses by antagonizing the tuberous sclerosis protein complex. *Cell Host Microbe*. 2008;3(4):253-262. doi: 10.1016/j.chom.2008.03.002 [doi].

196. Yu Y, Alwine JC. 19S late mRNAs of simian virus 40 have an internal ribosome entry site upstream of the virion structural protein 3 coding sequence. *J Virol*. 2006;80(13):6553-6558. doi: 80/13/6553 [pii].

197. Kumar SH, Rangarajan A. Simian virus 40 small T antigen activates AMPK and triggers autophagy to protect cancer cells from nutrient deprivation. *J Virol*. 2009;83(17):8565-8574. doi: 10.1128/JVI.00603-09 [doi].

198. Gastaminza P, Cheng G, Wieland S, Zhong J, Liao W, Chisari FV. Cellular determinants of hepatitis C virus assembly, maturation, degradation, and secretion. *J Virol*. 2008;82(5):2120-2129. doi: JVI.02053-07 [pii].

199. Diamond DL, Syder AJ, Jacobs JM, et al. Temporal proteome and lipidome profiles reveal hepatitis C virus-associated reprogramming of hepatocellular metabolism and bioenergetics. *PLoS Pathog*. 2010;6(1):e1000719. doi: 10.1371/journal.ppat.1000719 [doi].

200. Mankouri J, Tedbury PR, Gretton S, et al. Enhanced hepatitis C virus genome replication and lipid accumulation mediated by inhibition of AMP-activated protein kinase. *Proc Natl Acad Sci U S A*. 2010;107(25):11549-11554. doi: 10.1073/pnas.0912426107 [doi].

201. Bose SK, Shrivastava S, Meyer K, Ray RB, Ray R. Hepatitis C virus activates the mTOR/S6K1 signaling pathway in inhibiting IRS-1 function for insulin resistance. *J Virol*. 2012;86(11):6315-6322. doi: 10.1128/JVI.00050-12 [doi].

202. Nakashima K, Takeuchi K, Chihara K, Hotta H, Sada K. Inhibition of hepatitis C virus replication through adenosine monophosphate-activated protein kinase-dependent and -independent pathways. *Microbiol Immunol*. 2011;55(11):774-782. doi: 10.1111/j.1348-0421.2011.00382.x [doi].

203. Kasai D, Adachi T, Deng L, et al. HCV replication suppresses cellular glucose uptake through down-regulation of cell surface expression of glucose transporters. *J Hepatol*. 2009;50(5):883-894. doi: 10.1016/j.jhep.2008.12.029 [doi].

204. Daniel J, Maamar H, Deb C, Sirakova TD, Kolattukudy PE. Mycobacterium tuberculosis uses host triacylglycerol to accumulate lipid droplets and acquires a dormancy-like phenotype in lipid-loaded macrophages. *PLoS Pathog*. 2011;7(6):e1002093. doi: 10.1371/journal.ppat.1002093 [doi].

205. Cocchiaro JL, Kumar Y, Fischer ER, Hackstadt T, Valdivia RH. Cytoplasmic lipid droplets are translocated into the lumen of the chlamydia trachomatis parasitophorous vacuole. *Proc Natl Acad Sci U S A*. 2008;105(27):9379-9384. doi: 10.1073/pnas.0712241105 [doi].

206. Moser TS, Schieffer D, Cherry S. AMP-activated kinase restricts rift valley fever virus infection by inhibiting fatty acid synthesis. *PLoS Pathog*. 2012;8(4):e1002661. doi: 10.1371/journal.ppat.1002661 [doi].

207. Zhang HS, Wu MR. SIRT1 regulates tat-induced HIV-1 transactivation through activating AMP-activated protein kinase. *Virus Res*. 2009;146(1-2):51-57. doi: 10.1016/j.virusres.2009.08.005 [doi].

208. Mehla R, Bivalkar-Mehla S, Zhang R, et al. Bryostatin modulates latent HIV-1 infection via PKC and AMPK signaling but inhibits acute infection in a receptor independent manner. *PLoS One*. 2010;5(6):e11160. doi: 10.1371/journal.pone.0011160 [doi].

209. Rosenzweig D, Smith D, Opperdoes F, Stern S, Olafson RW, Zilberstein D. Retooling leishmania metabolism: From sand fly gut to human macrophage. *FASEB J*. 2008;22(2):590-602. doi: fj.07-9254com [pii].

210. Rabhi I, Rabhi S, Ben-Othman R, et al. Transcriptomic signature of leishmania infected mice macrophages: A metabolic point of view. *PLoS Negl Trop Dis*. 2012;6(8):e1763. doi: 10.1371/journal.pntd.0001763 [doi].

211. Jaramillo M, Gomez MA, Larsson O, et al. Leishmania repression of host translation through mTOR cleavage is required for parasite survival and infection. *Cell Host Microbe*. 2011;9(4):331-341. doi: 10.1016/j.chom.2011.03.008 [doi].

212. Takahashi M, Watari E, Shinya E, Shimizu T, Takahashi H. Suppression of virus replication via down-modulation of mitochondrial short chain enoyl-CoA hydratase in human glioblastoma cells. *Antiviral Res*. 2007;75(2):152-158. doi: S0166-3542(07)00217-3 [pii].

213. Deretic V, Levine B. Autophagy, immunity, and microbial adaptations. *Cell Host Microbe*. 2009;5(6):527-549. doi: 10.1016/j.chom.2009.05.016 [doi].

214. Xavier MN, Winter MG, Spees AM, et al. PPARgamma-mediated increase in glucose availability sustains chronic brucella abortus infection in alternatively activated macrophages. *Cell Host Microbe*. 2013;14(2):159-170. doi: 10.1016/j.chom.2013.07.009 [doi].

215. Eisele NA, Ruby T, Jacobson A, et al. Salmonella require the fatty acid regulator PPARÎ´ for the establishment of a metabolic environment essential for long term persistence. *Cell Host Microbe*. 2013;14(2):171-182. doi: 10.1016/j.chom.2013.07.010 [doi].

216. Clark SL,Jr. Cellular differentiation in the kidneys of newborn mice studies with the electron microscope. *J Biophys Biochem Cytol*. 1957;3(3):349-362.

217. Deter RL, de Duve C. Influence of glucagon, an inducer of cellular autophagy, on some physical properties of rat liver lysosomes. *J Cell Biol*. 1967;33(2):437-449.

218. Noda NN, Inagaki F. Mechanisms of autophagy. *Annu Rev Biophys*. 2015. doi: 10.1146/annurev-biophys-060414-034248 [doi].

219. Jewell JL, Russell RC, Guan KL. Amino acid signalling upstream of mTOR. *Nat Rev Mol Cell Biol*. 2013;14(3):133-139. doi: 10.1038/nrm3522 [doi].

220. Galluzzi L, Pietrocola F, Levine B, Kroemer G. Metabolic control of autophagy. *Cell*. 2014;159(6):1263-1276. doi: 10.1016/j.cell.2014.11.006 [doi].

221. Su WC, Chao TC, Huang YL, Weng SC, Jeng KS, Lai MM. Rab5 and class III phosphoinositide 3-kinase Vps34 are involved in hepatitis C virus NS4B-induced autophagy. *J Virol*. 2011;85(20):10561-10571. doi: 10.1128/JVI.00173-11 [doi].

222. Choy A, Dancourt J, Mugo B, et al. The legionella effector RavZ inhibits host autophagy through irreversible Atg8 deconjugation. *Science*. 2012;338(6110):1072-1076. doi: 10.1126/science.1227026 [doi].

223. Gregoire IP, Richetta C, Meyniel-Schicklin L, et al. IRGM is a common target of RNA viruses that subvert the autophagy network. *PLoS Pathog*. 2011;7(12):e1002422. doi: 10.1371/journal.ppat.1002422 [doi].

224. Judith D, Mostowy S, Bourai M, et al. Species-specific impact of the autophagy machinery on chikungunya virus infection. *EMBO Rep*. 2013;14(6):534-544. doi: 10.1038/embor.2013.51 [doi].

225. Yoshikawa Y, Ogawa M, Hain T, et al. Listeria monocytogenes ActA-mediated escape from autophagic recognition. *Nat Cell Biol*. 2009;11(10):1233-1240. doi: 10.1038/ncb1967 [doi].

226. Dortet L, Mostowy S, Samba-Louaka A, et al. Recruitment of the major vault protein by InlK: A listeria monocytogenes strategy to avoid autophagy. *PLoS Pathog*. 2011;7(8):e1002168. doi: 10.1371/journal.ppat.1002168 [doi].

227. Watson RO, Manzanillo PS, Cox JS. Extracellular M. tuberculosis DNA targets bacteria for autophagy by activating the host DNA-sensing pathway. *Cell*. 2012;150(4):803-815. doi: 10.1016/j.cell.2012.06.040 [doi].

228. Ling YM, Shaw MH, Ayala C, et al. Vacuolar and plasma membrane stripping and autophagic elimination of toxoplasma gondii in primed effector macrophages. *J Exp Med*. 2006;203(9):2063-2071. doi: jem.20061318 [pii].

229. Mesquita FS, Thomas M, Sachse M, Santos AJ, Figueira R, Holden DW. The salmonella deubiquitinase SseL inhibits selective autophagy of cytosolic aggregates. *PLoS Pathog*. 2012;8(6):e1002743. doi: 10.1371/journal.ppat.1002743 [doi].

230. Gong L, Cullinane M, Treerat P, et al. The burkholderia pseudomallei type III secretion system and BopA are required for evasion of LC3-associated phagocytosis. *PLoS One*. 2011;6(3):e17852. doi:10.1371/journal.pone.0017852. doi: PONE-D-11-00073 [pii].

231. Tan KS, Chen Y, Lim YC, et al. Suppression of host innate immune response by burkholderia pseudomallei through the virulence factor TssM. *J Immunol*. 2010;184(9):5160-5171. doi: 10.4049/jimmunol.0902663 [doi].

232. Choi JH, Cheong TC, Ha NY, et al. Orientia tsutsugamushi subverts dendritic cell functions by escaping from autophagy and impairing their migration. *PLoS Negl Trop Dis*. 2013;7(1):e1981. doi: 10.1371/journal.pntd.0001981 [doi].

233. Ko Y, Choi JH, Ha NY, Kim IS, Cho NH, Choi MS. Active escape of orientia tsutsugamushi from cellular autophagy. *Infect Immun*. 2013;81(2):552-559. doi: 10.1128/IAI.00861-12 [doi].

234. Niu H, Xiong Q, Yamamoto A, Hayashi-Nishino M, Rikihisa Y. Autophagosomes induced by a bacterial beclin 1 binding protein facilitate obligatory intracellular infection. *Proc Natl Acad Sci U S A*. 2012;109(51):20800-20807. doi: 10.1073/pnas.1218674109 [doi].

235. Heaton NS, Randall G. Dengue virus-induced autophagy regulates lipid metabolism. *Cell Host Microbe*. 2010;8(5):422-432. doi: 10.1016/j.chom.2010.10.006 [doi].

236. Panyasrivanit M, Khakpoor A, Wikan N, Smith DR. Co-localization of constituents of the dengue virus translation and replication machinery with amphisomes. *J Gen Virol*. 2009;90(Pt 2):448-456. doi: 10.1099/vir.0.005355-0 [doi].

237. Mateo R, Nagamine CM, Spagnolo J, et al. Inhibition of cellular autophagy deranges dengue virion maturation. *J Virol*. 2013;87(3):1312-1321. doi: 10.1128/JVI.02177-12 [doi].

238. Lee YR, Lei HY, Liu MT, et al. Autophagic machinery activated by dengue virus enhances virus replication. *Virology*. 2008;374(2):240-248. doi: 10.1016/j.virol.2008.02.016 [doi].

239. Niu H, Yamaguchi M, Rikihisa Y. Subversion of cellular autophagy by anaplasma phagocytophilum. *Cell Microbiol*. 2008;10(3):593-605. doi: CMI1068 [pii].

240. Newton HJ, Kohler LJ, McDonough JA, et al. A screen of coxiella burnetii mutants reveals important roles for dot/icm effectors and host autophagy in vacuole biogenesis. *PLoS Pathog*. 2014;10(7):e1004286. doi: 10.1371/journal.ppat.1004286 [doi].

241. Klionsky DJ, Abdalla FC, Abeliovich H, et al. Guidelines for the use and interpretation of assays for monitoring autophagy. *Autophagy*. 2012;8(4):445-544.

242. Muniz-Feliciano L, Van Grol J, Portillo JA, et al. Toxoplasma gondii-induced activation of EGFR prevents autophagy protein-mediated killing of the parasite. *PLoS Pathog*. 2013;9(12):e1003809. doi: 10.1371/journal.ppat.1003809 [doi].

243. Cyrino LT, Araujo AP, Joazeiro PP, Vicente CP, Giorgio S. In vivo and in vitro leishmania amazonensis infection induces autophagy in macrophages. *Tissue Cell*. 2012;44(6):401-408. doi: 10.1016/j.tice.2012.08.003 [doi].

244. Krejbich-Trotot P, Gay B, Li-Pat-Yuen G, et al. Chikungunya triggers an autophagic process which promotes viral replication. *Virol J*. 2011;8:432-422X-8-432. doi: 10.1186/1743-422X-8-432 [doi].

245. Sir D, Chen W, Choi J, Wakita T, Yen TSB, Ou JJ. Induction of incomplete autophagic response by hepatitis C virus via the unfolded protein response. *Hepatology*. 2008;48(4):1054-1061. doi: 10.1002/hep.22464 [doi].

246. Yu Y, Maguire TG, Alwine JC. Human cytomegalovirus activates glucose transporter 4 expression to increase glucose uptake during infection. *J Virol*. 2011;85(4):1573-1580. doi: 10.1128/JVI.01967-10 [doi].

247. Barel M, Meibom K, Dubail I, Botella J, Charbit A. Francisella tularensis regulates the expression of the amino acid transporter SLC1A5 in infected THP-1 human monocytes. *Cell Microbiol*. 2012;14(11):1769-1783. doi: 10.1111/j.1462-5822.2012.01837.x [doi].

248. Wieland H, Ullrich S, Lang F, Neumeister B. Intracellular multiplication of legionella pneumophila depends on host cell amino acid transporter SLC1A5. *Mol Microbiol*. 2005;55(5):1528-1537. doi: MMI4490 [pii].

249. Yang Z, Huang J, Geng J, Nair U, Klionsky DJ. Atg22 recycles amino acids to link the degradative and recycling functions of autophagy. *Mol Biol Cell*. 2006;17(12):5094-5104. doi: E06-06-0479 [pii].

250. Guo F, Zhang H, Chen C, et al. Autophagy favors brucella melitensis survival in infected macrophages. *Cell Mol Biol Lett*. 2012;17(2):249-257. doi: 10.2478/s11658-012-0009-4 [doi].

251. Cui J, Yao Q, Li S, et al. Glutamine deamidation and dysfunction of ubiquitin/NEDD8 induced by a bacterial effector family. *Science*. 2010;329(5996):1215-1218. doi: 10.1126/science.1193844 [doi].

252. Pachikara N, Zhang H, Pan Z, Jin S, Fan H. Productive chlamydia trachomatis lymphogranuloma venereum 434 infection in cells with augmented or inactivated autophagic activities. *FEMS Microbiol Lett*. 2009;292(2):240-249. doi: 10.1111/j.1574-6968.2009.01494.x [doi].

253. Al-Younes HM, Al-Zeer MA, Khalil H, et al. Autophagy-independent function of MAP-LC3 during intracellular propagation of chlamydia trachomatis. *Autophagy*. 2011;7(8):814-828. doi: 15597 [pii].

254. Cocchiaro JL, Kumar Y, Fischer ER, Hackstadt T, Valdivia RH. Cytoplasmic lipid droplets are translocated into the lumen of the chlamydia trachomatis parasitophorous vacuole. *Proc Natl Acad Sci U S A*. 2008;105(27):9379-9384. doi: 10.1073/pnas.0712241105 [doi].

255. Beatty WL. Trafficking from CD63-positive late endocytic multivesicular bodies is essential for intracellular development of chlamydia trachomatis. *J Cell Sci*. 2006;119(Pt 2):350-359. doi: 119/2/350 [pii].

256. Beron W, Gutierrez MG, Rabinovitch M, Colombo MI. Coxiella burnetii localizes in a Rab7-labeled compartment with autophagic characteristics. *Infect Immun*. 2002;70(10):5816-5821. doi: 0464 [pii].

257. Birmingham CL, Canadien V, Gouin E, et al. Listeria monocytogenes evades killing by autophagy during colonization of host cells. *Autophagy*. 2007;3(5):442-451. doi: 4450 [pii].

258. Py BF, Lipinski MM, Yuan J. Autophagy limits listeria monocytogenes intracellular growth in the early phase of primary infection. *Autophagy*. 2007;3(2):117-125. doi: 3618 [pii].

259. Tattoli I, Sorbara MT, Yang C, Tooze SA, Philpott DJ, Girardin SE. Listeria phospholipases subvert host autophagic defenses by stalling pre-autophagosomal structures. *EMBO J*. 2013;32(23):3066-3078. doi: 10.1038/emboj.2013.234 [doi].

260. Choi JH, Cheong TC, Ha NY, et al. Orientia tsutsugamushi subverts dendritic cell functions by escaping from autophagy and impairing their migration. *PLoS Negl Trop Dis*. 2013;7(1):e1981. doi: 10.1371/journal.pntd.0001981 [doi].

261. Ko Y, Choi JH, Ha NY, Kim IS, Cho NH, Choi MS. Active escape of orientia tsutsugamushi from cellular autophagy. *Infect Immun*. 2013;81(2):552-559. doi: 00861-12 [pii].

262. Dong N, Zhu Y, Lu Q, Hu L, Zheng Y, Shao F. Structurally distinct bacterial TBC-like GAPs link arf GTPase to Rab1 inactivation to counteract host defenses. *Cell*. 2012;150(5):1029-1041. doi: 10.1016/j.cell.2012.06.050 [doi].

263. Joubert PE, Werneke SW, de la Calle C, et al. Chikungunya virus-induced autophagy delays caspase-dependent cell death. *J Exp Med*. 2012;209(5):1029-1047. doi: 10.1084/jem.20110996 [doi].

264. Wong J, Zhang J, Si X, et al. Autophagosome supports coxsackievirus B3 replication in host cells. *J Virol*. 2008;82(18):9143-9153. doi: 10.1128/JVI.00641-08 [doi].

265. Kemball CC, Alirezaei M, Flynn CT, et al. Coxsackievirus infection induces autophagy-like vesicles and megaphagosomes in pancreatic acinar cells in vivo. *J Virol*. 2010;84(23):12110-12124. doi: 10.1128/JVI.01417-10 [doi].

266. Robinson SM, Tsueng G, Sin J, et al. Coxsackievirus B exits the host cell in shed microvesicles displaying autophagosomal markers. *PLoS Pathog*. 2014;10(4):e1004045. doi: 10.1371/journal.ppat.1004045 [doi].

267. Hung CH, Chen LW, Wang WH, et al. Regulation of autophagic activation by rta of epstein-barr virus via the extracellular signal-regulated kinase pathway. *J Virol*. 2014;88(20):12133-12145. doi: 10.1128/JVI.02033-14 [doi].

268. Lee DY, Sugden B. The LMP1 oncogene of EBV activates PERK and the unfolded protein response to drive its own synthesis. *Blood*. 2008;111(4):2280-2289. doi: blood-2007-07-100032 [pii].

269. Lee DY, Sugden B. The latent membrane protein 1 oncogene modifies B-cell physiology by regulating autophagy. *Oncogene*. 2008;27(20):2833-2842. doi: 1210946 [pii].

270. Granato M, Santarelli R, Farina A, et al. Epstein-barr virus blocks the autophagic flux and appropriates the autophagic machinery to enhance viral replication. *J Virol*. 2014;88(21):12715-12726. doi: 10.1128/JVI.02199-14 [doi].

271. Hussein IT, Cheng E, Ganaie SS, et al. Autophagic clearance of sin nombre hantavirus glycoprotein gn promotes virus replication in cells. *J Virol*. 2012;86(14):7520-7529. doi: 10.1128/JVI.07204-11 [doi].

272. Liu B, Fang M, Hu Y, et al. Hepatitis B virus X protein inhibits autophagic degradation by impairing lysosomal maturation. *Autophagy*. 2014;10(3):416-430. doi: 10.4161/auto.27286 [doi].

273. Li J, Liu Y, Wang Z, et al. Subversion of cellular autophagy machinery by hepatitis B virus for viral envelopment. *J Virol*. 2011;85(13):6319-6333. doi: 10.1128/JVI.02627-10 [doi].

274. Tang H, Da L, Mao Y, et al. Hepatitis B virus X protein sensitizes cells to starvation-induced autophagy via up-regulation of beclin 1 expression. *Hepatology*. 2009;49(1):60-71. doi: 10.1002/hep.22581 [doi].

275. Shrivastava S, Bhanja Chowdhury J, Steele R, Ray R, Ray RB. Hepatitis C virus upregulates Beclin1 for induction of autophagy and activates mTOR signaling. *J Virol*. 2012;86(16):8705-8712. doi: 10.1128/JVI.00616-12 [doi].

276. Mohl BP, Tedbury PR, Griffin S, Harris M. Hepatitis C virus-induced autophagy is independent of the unfolded protein response. *J Virol*. 2012;86(19):10724-10732. doi: 01667-12 [pii].

277. Shrivastava S, Raychoudhuri A, Steele R, Ray R, Ray RB. Knockdown of autophagy enhances the innate immune response in hepatitis C virus-infected hepatocytes. *Hepatology*. 2011;53(2):406-414. doi: 10.1002/hep.24073 [doi].

278. Orvedahl A, Alexander D, Talloczy Z, et al. HSV-1 ICP34.5 confers neurovirulence by targeting the beclin 1 autophagy protein. *Cell Host Microbe*. 2007;1(1):23-35. doi: S1931-3128(07)00002-9 [pii].

279. Lussignol M, Queval C, Bernet-Camard MF, et al. The herpes simplex virus 1 Us11 protein inhibits autophagy through its interaction with the protein kinase PKR. *J Virol*. 2013;87(2):859-871. doi: 10.1128/JVI.01158-12 [doi].

280. Tovilovic G, Ristic B, Siljic M, et al. mTOR-independent autophagy counteracts apoptosis in herpes simplex virus type 1-infected U251 glioma cells. *Microbes Infect*. 2013;15(8-9):615-624. doi: 10.1016/j.micinf.2013.04.012 [doi].

281. Chaumorcel M, Lussignol M, Mouna L, et al. The human cytomegalovirus protein TRS1 inhibits autophagy via its interaction with beclin 1. *J Virol*. 2012;86(5):2571-2584. doi: 10.1128/JVI.05746-11 [doi].

282. Kyei GB, Dinkins C, Davis AS, et al. Autophagy pathway intersects with HIV-1 biosynthesis and regulates viral yields in macrophages. *J Cell Biol*. 2009;186(2):255-268. doi: 10.1083/jcb.200903070 [doi].

283. Van Grol J, Subauste C, Andrade RM, Fujinaga K, Nelson J, Subauste CS. HIV-1 inhibits autophagy in bystander macrophage/monocytic cells through src-akt and STAT3. *PLoS One*. 2010;5(7):e11733. doi: 10.1371/journal.pone.0011733 [doi].

284. Wang X, Gao Y, Tan J, et al. HIV-1 and HIV-2 infections induce autophagy in jurkat and CD4+ T cells. *Cell Signal*. 2012;24(7):1414-1419. doi: 10.1016/j.cellsig.2012.02.016 [doi].

285. Zhou D, Spector SA. Human immunodeficiency virus type-1 infection inhibits autophagy. *AIDS*. 2008;22(6):695-699. doi: 10.1097/QAD.0b013e3282f4a836 [doi].

286. Nakashima A, Tanaka N, Tamai K, et al. Survival of parvovirus B19-infected cells by cellular autophagy. *Virology*. 2006;349(2):254-263. doi: S0042-6822(06)00201-7 [pii].

287. Beale R, Wise H, Stuart A, Ravenhill BJ, Digard P, Randow F. A LC3-interacting motif in the influenza A virus M2 protein is required to subvert autophagy and maintain virion stability. *Cell Host Microbe*. 2014;15(2):239-247. doi: 10.1016/j.chom.2014.01.006 [doi].

288. Gannage M, Dormann D, Albrecht R, et al. Matrix protein 2 of influenza A virus blocks autophagosome fusion with lysosomes. *Cell Host Microbe*. 2009;6(4):367-380. doi: 10.1016/j.chom.2009.09.005 [doi].

289. Zhou Z, Jiang X, Liu D, et al. Autophagy is involved in influenza A virus replication. *Autophagy*. 2009;5(3):321-328. doi: 7406 [pii].

290. Wen HJ, Yang Z, Zhou Y, Wood C. Enhancement of autophagy during lytic replication by the kaposi's sarcoma-associated herpesvirus replication and transcription activator. *J Virol*. 2010;84(15):7448-7458. doi: 0024-10 [pii].

291. Pattingre S, Tassa A, Qu X, et al. Bcl-2 antiapoptotic proteins inhibit beclin 1-dependent autophagy. *Cell*. 2005;122(6):927-939. doi: S0092-8674(05)00692-6 [pii].

292. Lee JS, Li Q, Lee JY, et al. FLIP-mediated autophagy regulation in cell death control. *Nat Cell Biol*. 2009;11(11):1355-1362. doi: 10.1038/ncb1980 [doi].

293. Crawford SE, Hyser JM, Utama B, Estes MK. Autophagy hijacked through viroporin-activated calcium/calmodulin-dependent kinase kinase-beta signaling is required for rotavirus replication. *Proc Natl Acad Sci U S A*. 2012;109(50):E3405-13. doi: 10.1073/pnas.1216539109 [doi].

294. Pinheiro RO, Nunes MP, Pinheiro CS, et al. Induction of autophagy correlates with increased parasite load of leishmania amazonensis in BALB/c but not C57BL/6 macrophages. *Microbes Infect*. 2009;11(2):181-190. doi: 10.1016/j.micinf.2008.11.006 [doi].

295. Cyrino LT, Araujo AP, Joazeiro PP, Vicente CP, Giorgio S. In vivo and in vitro leishmania amazonensis infection induces autophagy in macrophages. *Tissue Cell*. 2012;44(6):401-408. doi: 10.1016/j.tice.2012.08.003 [doi].

296. Smeekens SP, Malireddi RK, Plantinga TS, et al. Autophagy is redundant for the host defense against systemic candida albicans infections. *Eur J Clin Microbiol Infect Dis*. 2014;33(5):711-722. doi: 10.1007/s10096-013-2002-x [doi].

297. Nicola AM, Albuquerque P, Martinez LR, et al. Macrophage autophagy in immunity to cryptococcus neoformans and candida albicans. *Infect Immun*. 2012;80(9):3065-3076. doi: 10.1128/IAI.00358-12 [doi].

298. Moon JJ, Chu HH, Pepper M, et al. Naive CD4(+) T cell frequency varies for different epitopes and predicts repertoire diversity and response magnitude. *Immunity*. 2007;27(2):203-213. doi: S1074-7613(07)00366-4 [pii].

299. Pepper M, Linehan JL, Pagan AJ, et al. Different routes of bacterial infection induce long-lived TH1 memory cells and short-lived TH17 cells. *Nat Immunol*. 2010;11(1):83-89. doi: 10.1038/ni.1826 [doi].

300. Woolard MD, Hensley LL, Kawula TH, Frelinger JA. Respiratory francisella tularensis live vaccine strain infection induces Th17 cells and prostaglandin E2, which inhibits generation of gamma interferon-positive T cells. *Infect Immun*. 2008;76(6):2651-2659. doi: 10.1128/IAI.01412-07 [doi].

301. Nurieva RI, Chung Y. Understanding the development and function of T follicular helper cells. *Cell Mol Immunol*. 2010;7(3):190-197. doi: 10.1038/cmi.2010.24 [doi].

302. Anthony LS, Ghadirian E, Nestel FP, Kongshavn PA. The requirement for gamma interferon in resistance of mice to experimental tularemia. *Microb Pathog*. 1989;7(6):421-428.

303. Collazo CM, Sher A, Meierovics AI, Elkins KL. Myeloid differentiation factor-88 (MyD88) is essential for control of primary in vivo francisella tularensis LVS infection, but not for control of intra-macrophage bacterial replication. *Microbes Infect*. 2006;8(3):779-790. doi: S1286-4579(05)00364-3 [pii].

304. Leiby DA, Fortier AH, Crawford RM, Schreiber RD, Nacy CA. In vivo modulation of the murine immune response to francisella tularensis LVS by administration of anticytokine antibodies. *Infect Immun*. 1992;60(1):84-89.

305. Skyberg JA, Rollins MF, Samuel JW, Sutherland MD, Belisle JT, Pascual DW. Interleukin-17 protects against the francisella tularensis live vaccine strain but not against a virulent F. tularensis type A strain. *Infect Immun*. 2013;81(9):3099-3105. doi: 10.1128/IAI.00203-13 [doi].

306. Metzger DW, Salmon SL, Kirimanjeswara G. Differing effects of interleukin-10 on cutaneous and pulmonary francisella tularensis live vaccine strain infection. *Infect Immun*. 2013;81(6):2022-2027. doi: 10.1128/IAI.00024-13 [doi].

307. Oyston PC. Francisella tularensis vaccines. *Vaccine*. 2009;27 Suppl 4:D48-51. doi: 10.1016/j.vaccine.2009.07.090 [doi].

308. Fortier AH, Green SJ, Polsinelli T, et al. Life and death of an intracellular pathogen: Francisella tularensis and the macrophage. *Immunol Ser*. 1994;60:349-361.

309. Metzger DW, Bakshi CS, Kirimanjeswara G. Mucosal immunopathogenesis of francisella tularensis. *Ann N Y Acad Sci*. 2007;1105:266-283. doi: annals.1409.007 [pii].

310. Fortier AH, Slayter MV, Ziemba R, Meltzer MS, Nacy CA. Live vaccine strain of francisella tularensis: Infection and immunity in mice. *Infect Immun*. 1991;59(9):2922-2928.

311. Barrigan LM, Tuladhar S, Brunton JC, et al. Infection with francisella tularensis LVS clpB leads to an altered yet protective immune response. *Infect Immun*. 2013;81(6):2028-2042. doi: 10.1128/IAI.00207-13 [doi].

312. Hall JD, Craven RR, Fuller JR, Pickles RJ, Kawula TH. Francisella tularensis replicates within alveolar type II epithelial cells in vitro and in vivo following inhalation. *Infect Immun*. 2007;75(2):1034-1039. doi: IAI.01254-06 [pii].

313. Bosio CM, Dow SW. Francisella tularensis induces aberrant activation of pulmonary dendritic cells. *J Immunol*. 2005;175(10):6792-6801. doi: 175/10/6792 [pii].

314. Leemans JC, Juffermans NP, Florquin S, et al. Depletion of alveolar macrophages exerts protective effects in pulmonary tuberculosis in mice. *J Immunol*. 2001;166(7):4604-4611.

315. Davis JK, Davidson MK, Schoeb TR, Lindsey JR. Decreased intrapulmonary killing of mycoplasma pulmonis after short-term exposure to NO2 is associated with damaged alveolar macrophages. *Am Rev Respir Dis*. 1992;145(2 Pt 1):406-411. doi: 10.1164/ajrccm/145.2_Pt_1.406 [doi].

316. Gordon SB, Read RC. Macrophage defences against respiratory tract infections. *Br Med Bull*. 2002;61:45-61.

317. Nash TW, Libby DM, Horwitz MA. Interaction between the legionnaires' disease bacterium (legionella pneumophila) and human alveolar macrophages. influence of antibody, lymphokines, and hydrocortisone. *J Clin Invest*. 1984;74(3):771-782. doi: 10.1172/JCI111493 [doi].

318. Guth AM, Janssen WJ, Bosio CM, Crouch EC, Henson PM, Dow SW. Lung environment determines unique phenotype of alveolar macrophages. *Am J Physiol Lung Cell Mol Physiol*. 2009;296(6):L936-46. doi: 10.1152/ajplung.90625.2008 [doi].

319. Cheung DO, Halsey K, Speert DP. Role of pulmonary alveolar macrophages in defense of the lung against pseudomonas aeruginosa. *Infect Immun*. 2000;68(8):4585-4592.

320. Hickman-Davis JM, Michalek SM, Gibbs-Erwin J, Lindsey JR. Depletion of alveolar macrophages exacerbates respiratory mycoplasmosis in mycoplasma-resistant C57BL mice but not mycoplasma-susceptible C3H mice. *Infect Immun*. 1997;65(6):2278-2282.

321. Broug-Holub E, Toews GB, van Iwaarden JF, et al. Alveolar macrophages are required for protective pulmonary defenses in murine klebsiella pneumonia: Elimination of alveolar macrophages increases neutrophil recruitment but decreases bacterial clearance and survival. *Infect Immun*. 1997;65(4):1139-1146.

322. Wu TH, Hutt JA, Garrison KA, Berliba LS, Zhou Y, Lyons CR. Intranasal vaccination induces protective immunity against intranasal infection with virulent francisella tularensis biovar A. *Infect Immun*. 2005;73(5):2644-2654. doi: 73/5/2644 [pii].

323. Conlan WJ, Shen H, Kuolee R, Zhao X, Chen W. Aerosol-, but not intradermal-immunization with the live vaccine strain of francisella tularensis protects mice against subsequent aerosol challenge with a highly virulent type A strain of the pathogen by an alphabeta T cell- and interferon gamma- dependent mechanism. *Vaccine*. 2005;23(19):2477-2485. doi: S0264-410X(04)00853-9 [pii].